

See discussions, stats, and author profiles for this publication at: <https://www.researchgate.net/publication/36288580>

Optimal electrotactile stimulation waveforms for human information display /

Article · January 1991

Source: OAI

CITATIONS

9

READS

337

1 author:



[K.A. Kaczmarek](#)

University of Wisconsin-Madison

59 PUBLICATIONS 3,388 CITATIONS

SEE PROFILE

Optimal Electrotactile Stimulation Waveforms for Human Information Display

By

Kurt Alan Kaczmarek

August 1991

A thesis submitted in partial fulfillment of the requirement for the degree of Doctor of Philosophy (Electrical Engineering) at the University of Wisconsin-Madison

Chapters (with citation if published)

1. Introduction and summary: unpublished
2. Kaczmarek KA, Webster JG, Bach-y-Rita P, Tompkins WJ (1991) Electrotactile and vibrotactile displays for sensory substitution systems. *IEEE Trans Biomed Eng* 38:1-16.
3. Kaczmarek KA, Webster JG (1989) Voltage-current characteristics of the electrotactile skin-electrode interface. In: *Proc Annu Int Conf IEEE Eng Med Biol Soc*, vol. 11 (Kim, Y. and Spelman, F. A., eds), pp 1526-1527 Seattle, WA: IEEE.
4. Kaczmarek KA, Webster JG, Radwin RG (1990) Periodic variations in the electrotactile sensation threshold. In: *Proc Annu Int Conf IEEE Eng Med Biol Soc*, vol. 12 (Pedersen, P. C. and Onaral, B., eds), pp 1060-1061 Philadelphia, PA: IEEE.
5. Kaczmarek KA, Kramer KM, Webster JG, Radwin RG (1991) A 16-channel 8-parameter waveform electrotactile stimulation system. *IEEE Trans Biomed Eng* 38:933-943.
6. Kaczmarek KA, Webster JG, Radwin RG (1992) Maximal dynamic range electrotactile stimulation waveforms. *IEEE Trans Biomed Eng* 39:701-715.
7. Kaczmarek KA (2000) Electrotactile adaptation on the abdomen: Preliminary results. *IEEE Trans Rehab Eng* 8:499-505.
8. Electrotactile skin irritation: Intradermal dc current flow caused by asymmetrical stimulation waveforms and nonlinear electrode-skin voltage-current characteristics: unpublished

Many of these publications may be downloaded from <http://tcnl.bme.wisc.edu/library>

**OPTIMAL
ELECTROTACTILE STIMULATION WAVEFORMS
FOR
HUMAN INFORMATION DISPLAY**

by

KURT ALAN KACZMAREK

A thesis submitted in partial fulfillment of the
requirements for the degree of

Doctor of Philosophy
(Electrical Engineering)

at the
UNIVERSITY OF WISCONSIN-MADISON

1991

A dissertation entitled

Optimal
Electrotactile Stimulation
Waveforms
for
Human Information Display

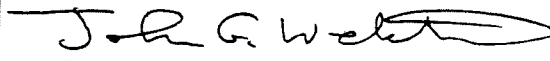
submitted to the Graduate School of the
University of Wisconsin-Madison
in partial fulfillment of the requirements for the
degree of Doctor of Philosophy

by

Kurt Alan Kaczmarek

Degree to be awarded: December 19__ May 19__ August 1991

Approved by Dissertation Readers:



Major Professor

August 7, 1991

Date of Examination





Dean, Graduate School

VITA SHEET

Title of thesis	Optimal Electrotactile Stimulation Waveforms for Human Information Display
Major professor	Professor John G. Webster
Major	Electrical Engineering
Minor	Mechanical Engineering
Name	Kurt Alan Kaczmarek
Place and date of birth	Arlington Heights, IL August 5, 1960
Colleges and universities: years attended and degrees	8/78-5/80 William Rainy Harper College A.S. 8/80-5/82 Univ. of Illinois-Urbana B.S.E.E. 8/82-5/84 Univ. Wisconsin-Madison M.S.E.E.
Memberships in learned or honorary societies	
Publications	continued on next page
Current date	August 20, 1991

PUBLICATIONS

- K. A. Kaczmarek, P. Bach-y-Rita, W. J. Tompkins and J. G. Webster, "A time-division multiplexed tactile vision substitution system," *Proc. Symp. Biosensors*, IEEE, pp. 101–106, 1984.
- K. Kaczmarek, P. Bach-y-Rita, W. J. Tompkins and J. G. Webster, "A tactile vision-substitution system for the blind: Computer-controlled partial image sequencing," *IEEE Trans. Biomed. Eng.*, vol. BME-32, pp. 602–608, 1985.
- K. A. Kaczmarek, "Interfacing flow sensors (thermal, mechanical, and differential-pressure)," in *Interfacing Sensors to the IBM PC*, W. J. Tompkins and J. G. Webster, Eds. Englewood Cliffs, NJ: Prentice-Hall, 1988, pp. 302–312.
- K. A. Kaczmarek, "Interfacing user input devices (digital camera)," in *Interfacing Sensors to the IBM PC*, W. J. Tompkins and J. G. Webster, Eds. Englewood Cliffs, NJ: Prentice-Hall, 1988, pp. 357–360.
- K. A. Kaczmarek and J. G. Webster, "Voltage–current characteristics of the electrotactile skin–electrode interface," *Proc. Annu. Int. Conf. IEEE Eng. Med. Biol. Soc.*, vol. 11, pp. 1526–1527, 1989.
- K. A. Kaczmarek, J. G. Webster and R. G. Radwin, "Periodic variations in the electrotactile sensation threshold," *Proc. Annu. Int. Conf. IEEE Eng. Med. Biol. Soc.*, vol. 12, pp. 1060–1061, 1990.
- K. A. Kaczmarek, J. G. Webster, P. Bach-y-Rita and W. J. Tompkins, "Electrotactile and vibrotactile displays for sensory substitution systems," *IEEE Trans. Biomed. Eng.*, vol. 38, pp. 1–16, 1991.
- K. A. Kaczmarek, K. M. Kramer, J. G. Webster and R. G. Radwin, "A 16-channel 8-parameter waveform electrotactile stimulation system," *IEEE Trans. Biomed. Eng.*, vol 38, no. 10, 1991 (in press).

ACKNOWLEDGEMENTS

At the risk of missing somebody...

I gratefully acknowledge the academic support received from many faculty members at the University of Wisconsin, especially Drs. Paul Bach-y-Rita, Murray Clayton, James Dannemiller, William Epstein, Donald Ermer, Robert Radwin, Willis Tompkins, and Steve Wiker. Most especially I thank my advisor John Webster for providing a friendly and creative academic environment in which I always felt entirely free to pursue by own ideas, and for over four years of financial support. Also in the University system I must thank Kurt Neuwirth at the academic computing center and Kathy Monroe in the ECE department office .

I credit my fifth-grade elementary-school teacher B. Abraham for fostering a creative spirit in the classroom that led to what was arguably my first experiment in electrotactile stimulation (p. iv).

I acknowledge financial support from the National Aeronautics and Space Administration through the Wisconsin Center for Space Automation and Robotics, from the Veterans Administration, and from the National Institutes of Health.

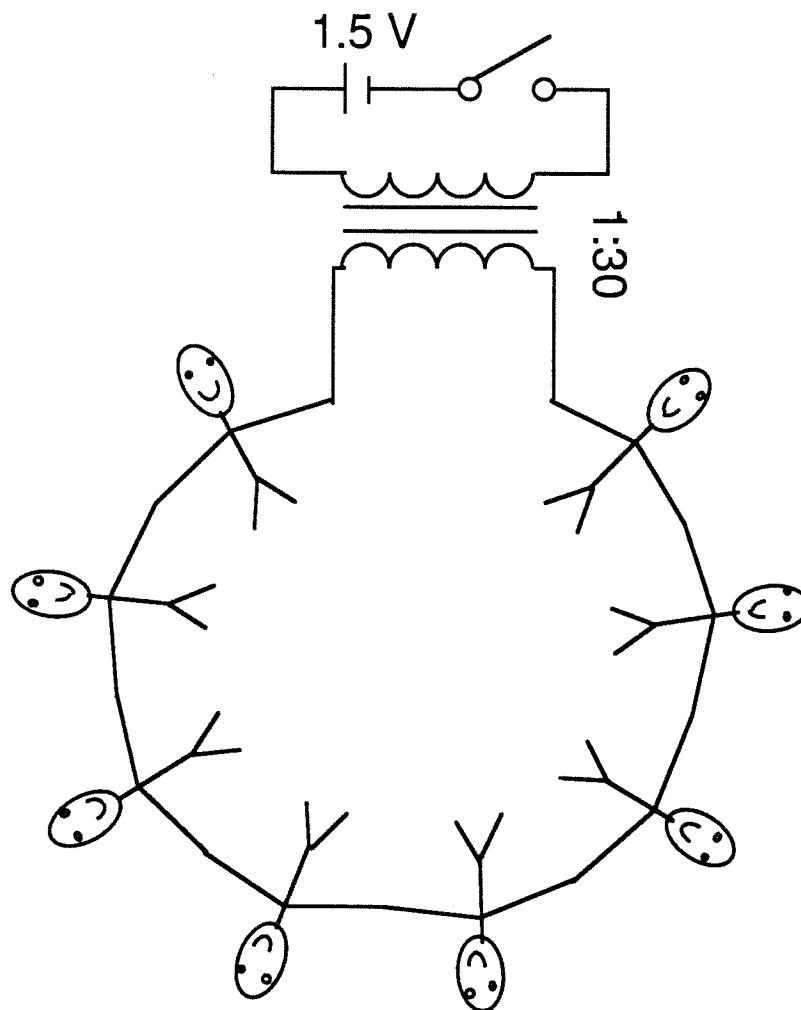
Many fellow students over the years provided friendship, diversions, and useful ideas, especially Dave Beebe, Bill Cumming, Dave Doak, Dave Hagner, Ping Hua, Shen Luo, Dorin Panescu, John Pfeffer, and Aparna Ramakrishnan. I especially thank Kevin Kramer for virtually all of the system programming and many useful software ideas.

Two of my longtime friends have provided me with constant encouragement through the peaks and valleys of my graduate studies: Renée Iverson and Dave Peters.

I thank most highly my father — to whom I dedicate this thesis — for instilling in me the spark of interest, the creative spirit, the critical mind, the freedom, and above all the confidence to pursue my own ideas — sometimes with reckless abandon. Just as highly I thank my mother who cares for him in his illness, whose example of selfless love never runs out, and who gave me the gift of determination to finish whatever I started — and to do it as well as possible.

Nancy, my wife, desired my completion of this work almost more than I did — and her emotional support made it possible — and worthwhile — for a lifetime.

And finally — to God be all the glory.



My first experiment in “electrotactile” stimulation, ca. 1971.

CONTENTS

	Acknowledgements	ii
	First experiment	iv
	Contents	v
	Abstract	vi
Chapter 1	Introduction and Summary	1
Chapter 2	Electrotactile and vibrotactile displays for sensory substitution systems	9
Chapter 3	Voltage–current characteristics of the electrotactile skin–electrode interface	76
Chapter 4	Periodic variations in the electrotactile sensation threshold	86
Chapter 5	A 16-channel 8-parameter waveform electrotactile stimulation system	97
Chapter 6	Maximal dynamic range electrotactile stimulation waveforms	142
Chapter 7	Electrotactile adaptation: Effect of stimulation waveform current, frequency, and number of pulses per burst	211
Chapter 8	Electrotactile skin irritation: Intradermal dc current flow caused by asymmetrical stimulation waveforms and nonlinear electrode–skin voltage–current characteristics	244

ABSTRACT

Electrotactile (electrocutaneous) stimulation can deliver visual, auditory, and remote tactile information to the skin by directly stimulating afferent touch nerve fibers in a localized region. We review sensory physiology, the mechanism of electrotactile stimulation and its limitations, and several applications.

A 16-channel custom electrotactile stimulation system produces rectangular current pulses with current 0 – 50 mA, interphase interval 0 – 1000 μ s, number of pulses/burst 1 – 100, pulse repetition rate 0.1 – 25 kHz, phase width 2 – 1000 μ s, and functionally-monophasic (zero dc current) or balanced-biphasic pulse type. Controlled by a command file and by analog inputs, the system automatically delivers the specified current waveform to each electrode through a high-performance transconductance amplifier, prompts the subject, and logs subject responses.

A new method to measure the electrotactile dynamic range determines the waveform variables that maximize the subjective magnitude (intensity) of the electrotactile percept at the maximal current without discomfort. The magnitude dynamic range is maximized with number of pulses/burst = 6, pulse repetition rate within a burst = 350 Hz, and phase width = 150 μ s. Six pulses/burst doubles the magnitude-based dynamic range compared with one pulse/burst but has little effect on the traditional dynamic range measure — the ratio of pain threshold to sensation threshold.

Intense electrotactile stimulation raises the sensation threshold current and reduces the perceived magnitude of stimulation (adaptation). The threshold elevation (recovery) follows an exponential function with a time constant of 0.3 – 1.2 min summed with a slower continuing rise (fall) for at least 15 min. The threshold rise in 15 min is approximately 0.43 times the difference between the adapting current and the initial threshold. Threshold elevation increases sevenfold as the frequency increases from 5 Hz to 45 Hz. Waveforms with 6 pulses/burst adapt twice as much as waveforms with 1 or 2 pulses/burst.

Poststimulation skin redness is often greater with asymmetric waveforms, even with zero dc current, possibly due to an intradermal circulating dc current. We present an electrical model which predicts this current and describes the voltage–current characteristics of the electrode–skin interface.

Chapter 1

INTRODUCTION AND SUMMARY

The title

Electrotactile (also known as electrocutaneous) *stimulation* produces tactile (touch) sensations by directly stimulating afferent touch nerve fibers with a localized electric current delivered to the skin by surface electrodes. Useful *information* can be presented to *humans* by an electrotactile *display*. Some stimulation waveforms are better suited than others for particular applications; an *optimal waveform* is the best waveform for a particular purpose.

Background

Scientific study of the sensations produced by controlled, localized electric stimulation of the skin dates back more than one century [1]. The prevalence of everyday experience with static discharges from carpets, clothing, etc. suggests that interest in this phenomenon surfaced much earlier, perhaps predating knowledge of electricity itself. However, the suggestion of *deliberately* applying an electric current to the skin with an electrode to produce some sensation is received with trepidation by most people. Even in recent years, some investigators continue to use the term “shock” to describe a stimulus which is not meant to be painful, or assume a priori that electric stimulation must be uncomfortable. This reputation is due partly to the use of electric stimulation as an aversive stimulus for behavioral conditioning [2]. Electric stimulation *is* painful at high levels or with some stimulation electrodes and waveforms. Moreover, the level of pain is difficult to control [3]. Numerous studies, however, including the experiments I shall describe, show that *well-controlled* electrotactile stimulation can produce touch sensations without excessive or even any discomfort [3], [4], [5], [6]. Out of the more than 45 paid and unpaid subjects that I have tested in four

years, only one refused to participate in further experiments — and that subject described the sensation as “threatening” rather than painful.

To my knowledge, electrotactile stimulation technology has found only one commercially-successful application — the Tacticon™ auditory aid for the deaf [7]. This device, which converts sound to patterns of electrotactile sensations on the abdomen, has been used mostly experimentally, where it has improved the speech clarity of deaf children [8]. Electrotactile stimulation has also seen much experimental use for conveying visual information to the skin of the blind [9], [10], [11] and for force and position feedback from prosthetic hands and arms [12], [13], [14].

To be used effectively to convey information, electrotactile stimulation needs to be well-controlled. In spite of the extensive research performed since approximately 1960, several aspects of electrotactile stimulation remain poorly characterized. This thesis attempts to fill in some of the larger information gaps.

Outline of thesis

I discuss three distinct topics in electrotactile stimulation along with sufficient background information to set each in perspective. These topics are dynamic range (Chapter 6), sensory adaptation (Chapter 7), and skin irritation (Chapter 8). The other chapters provide additional information on previous research, instrumentation, and preliminary experiments. Because they were written with publication as one objective, each of the chapters 2 – 8 is reasonably complete without reference to the other chapters. In the summary section of the present chapter, I discuss some of the practical implications of the combined results of chapters 2 – 8 on the design of electrotactile displays.

Chapter 2 is a literature review [5] which summarizes the major applications of sensory substitution including sensory prostheses for the deaf and blind. Electrotactile and vibrotactile (vibrating) displays are two practical types of information displays. I discuss electrotactile displays in detail.

Chapter 3 describes some preliminary experiments [15] to model the electrical characteristics of the electrode–skin system — necessary information for the instrumentation design. (Chapter 8 is largely an expansion on this topic.)

Chapter 4 describes preliminary experiments [16] that found periodic variations in the electrotactile sensation threshold. These fluctuations of undetermined origin were a source of noise for the adaptation studies (Chapter 7).

Chapter 5 describes the experimental instrumentation I developed [17] to perform most of the experiments in this thesis. It combines commercial hardware (where available) with custom computer-controlled waveform generators and electrode drivers to produce a flexible, automated electrotactile experimental system.

Chapter 6 presents a new method and original experiments conducted to measure and maximize the electrotactile dynamic range. Earlier methods relied entirely on electrical measurements like sensation and pain threshold. This method determines the stimulation waveform variables that can produce the strongest vibratory percept that is not uncomfortable.

Chapter 7 describes experiments that measure the elevation in electrotactile sensation threshold occurring during and after stimulation at levels above the initial sensation threshold. To date, electrotactile adaptation has received scant attention in the literature.

Chapter 8 expands on the electrical model developed in Chapter 3. The expanded model simultaneously explains three electrical characteristics of the electrode–skin interface that are normally treated separately. The skin redness produced by electrotactile stimulation may be related to this model.

Summary

The results of the experiments described in Chapter 6 are most important for the design of electrotactile displays. The use of bursts of stimulation pulses as opposed to single pulses greatly increases the maximal intensity of the vibratory percept produced by electrotactile stimulation, at least for the electrode configuration tested. Therefore, the range of electrotactile percept *intensities* (i.e., dynamic range) is maximized. A burst waveform, however, produces greater sensory adaptation (Chapter 7), requires more electric power, and probably produces more skin irritation. It also requires more complex waveform generation circuitry, and its increased duty cycle means that fewer multiplexed electrodes could be driven from a single current generator. In my opinion, the increase in stimulus comfort provided by bursts outweighs these disadvantages.

Because sensory adaptation is a normal characteristic of all human sensory systems, Chapter 7 does not claim an “optimal” waveform to minimize or maximize it. However, the high-frequency waveforms that maximize information transfer rate and the burst waveforms that maximize dynamic range both cause increased adaptation. Burst waveforms at 45 Hz adapt so quickly and completely that they have limited usefulness for a continuous display at high intensity, although they may be useful for an intermittent or very dynamic display. An engineering compromise based on a thorough knowledge of the intended application will be necessary when choosing a waveform if adaptation is an important design consideration.

Chapter 8 shows the superiority of the balanced-biphasic stimulation pulse shape over the functionally-monophasic (zero-dc) shape for reducing potential skin irritation. However, more complex circuitry is required to generate the balanced-biphasic pulses. In particular, bipolar electrode-driver and switching circuits are required, along with bipolar power supplies. (Functionally-monophasic pulses can rely on passive elements to generate the nonstimulating current phase.) Additionally, the duty cycle is increased, meaning fewer electrodes can be multiplexed from a single current source. Because the percepts are not too different, biphasic stimulation may not always be warranted unless lowest skin irritation is an important design objective.

In conclusion, it is clear that there is no unique “optimal” waveform, even for the three performance criteria measured by these experiments. A compromise will always be necessary, based on the electrotactile display system design and performance objectives.

REFERENCES

- [1] S. Tschiriew and A. d. Watteville, "On the electrical excitability of the skin," *Brain: A J. of Neurol.*, vol. 2, pp. 163–180, 1879.
- [2] E. A. Pfeiffer, "Electrical stimulation of sensory nerves with skin electrodes for research, diagnosis, communication and behavioral conditioning: A survey," *Med. Biol. Eng.*, vol. 6, pp. 637–651, 1968.
- [3] G. B. Rollman, "Electrocutaneous stimulation," in *Proc. Conf. Cutan. Comm. Sys. Dev.*, F. A. Geldard, Ed., Psychonomic Society, 1973, pp. 38–51.
- [4] R. H. Gibson, "Electrical stimulation of pain and touch," in *The Skin Senses*, D. R. Kenshalo, Ed. Springfield, IL: Charles C. Thomas, 1968, pp. 223–260.
- [5] K. A. Kaczmarek, J. G. Webster, P. Bach-y-Rita and W. J. Tompkins, "Electrotactile and vibrotactile displays for sensory substitution systems," *IEEE Trans. Biomed. Eng.*, vol. 38, pp. 1–16, 1991.
- [6] A. Y. J. Szeto and F. A. Saunders, "Electrocutaneous stimulation for sensory communication in rehabilitation engineering," *IEEE Trans. Biomed. Eng.*, vol. BME-29, pp. 300–308, 1982.
- [7] F. A. Saunders, *Tacticon 1600 Electrotactile Sensory Aid for the Deaf: User's Guide*. San Rafael, CA: Tacticon Corporation, 1986.
- [8] F. A. Saunders, W. A. Hill and B. Franklin, "A wearable tactile sensory aid for profoundly deaf children," *J. Med. Sys.*, vol. 5, pp. 265–270, 1981.
- [9] P. Bach-y-Rita, *Brain Mechanisms in Sensory Substitution*. New York: Academic, 1972.

- [10] C. C. Collins and F. A. Saunders, "Pictorial display by direct electrical stimulation of the skin," *J. Biomed. Sys.*, vol. 1, pp. 3–16, 1970.
- [11] C. C. Collins and M. F. Deering, "A microcomputer based blind mobility aid," in *Proc. IEEE Frontiers Eng. Comput. Health Care*, Los Angeles, 1984, pp. 52–56.
- [12] C. A. Phillips, "Sensory feedback control of upper- and lower-extremity motor prostheses," *CRC Crit. Rev. Biomed. Eng.*, vol. 16, pp. 105–140, 1988.
- [13] R. R. Riso, "Sensory augmentation for enhanced control of FNS systems," in *Ergonomics in Rehabilitation*, A. Mital, Ed. New York: Taylor and Francis, 1988, pp. 253–271.
- [14] A. Y. J. Szeto and R. R. Riso, "Sensory feedback using electrical stimulation of the tactile sense," in *Rehabilitation Engineering*, R. V. Smith and J. H. Leslie Jr., Eds. Boca Raton, FL: CRC Press, 1990, pp. 29–78.
- [15] K. A. Kaczmarek and J. G. Webster, "Voltage–current characteristics of the electrotactile skin–electrode interface," in *Proc. Annu. Int. Conf. IEEE Eng. Med. Biol. Soc.*, Seattle, WA, Y. Kim and F. A. Spelman, Eds., vol. 11, IEEE, 1989, pp. 1526–1527.
- [16] K. A. Kaczmarek, J. G. Webster and R. G. Radwin, "Periodic variations in the electrotactile sensation threshold," in *Proc. Annu. Int. Conf. IEEE Eng. Med. Biol. Soc.*, Philadelphia, PA, P. C. Pedersen and B. Onaral, Eds., vol. 12, IEEE, 1990, pp. 1060–1061.
- [17] K. A. Kaczmarek, K. M. Kramer, J. G. Webster and R. G. Radwin, "A 16-channel 8-parameter waveform electrotactile stimulation system," *IEEE Trans. Biomed. Eng.*, vol. 38, 1991 (in press).

Chapter 2

ELECTROTACTILE AND VIBROTACTILE DISPLAYS FOR SENSORY SUBSTITUTION SYSTEMS

Literature Review

Published as:

K. A. Kaczmarek, J. G. Webster, P. Bach-y-Rita and W. J. Tompkins,
"Electrotactile and vibrotactile displays for sensory substitution systems," *IEEE
Trans. Biomed. Eng.*, vol. 38, pp. 1–16, 1991.

ABSTRACT

Sensory substitution systems provide their users with environmental information through a human sensory channel (eye, ear, or skin) different from that normally used, or with the information processed in some useful way. We review the methods used to present visual, auditory, and modified tactile information to the skin.

First, we discuss present and potential future applications of sensory substitution, including tactile vision substitution (TVS), tactile auditory substitution, and remote tactile sensing or feedback (teletouch).

Next, we review the relevant sensory physiology of the skin, including both the mechanisms of normal touch and the mechanisms and sensations associated with electrical stimulation of the skin using surface electrodes (electrotactile (also called electrocutaneous) stimulation).

We briefly summarize the information-processing ability of the tactile sense and its relevance to sensory substitution.

Finally, we discuss the limitations of current tactile display technologies and suggest areas requiring further research for sensory substitution systems to become more practical.

INTRODUCTION

Purpose

In this paper, we summarize the technology developed by many investigators for presenting information to the skin by electrical and mechanical stimulation. We examine limitations of present displays for sensory substitution systems and propose topics for future research to overcome some of these limitations.

Definitions

A *biphasic* current pulse has a positive and a negative current phase of equal duration and magnitude for a zero net dc current. The literature is inconsistent in the use of the terms monophasic and biphasic. Biphasic is used elsewhere to refer to any waveform with positive and negative phases. We will use the restricted definition above.

A *Coaxial* (also called *concentric* or *annular*) electrode consists of an active center electrode insulated from a larger annular surrounding dispersive electrode for the return current path.

Electrotactile (also called *electrocutaneous*) stimulation evokes tactile (touch) sensations within the skin at the location of the electrode by passing a local electric current through the skin.

A *monophasic* current pulse has a single positive or negative current phase. A train of such pulses may or may not have a zero net dc current.

Sensory substitution is the use of one human sense to receive information normally received by another sense. For the sense of touch, sensory substitution may

also be the use of one area of skin to receive tactile information normally received at another location.

Spatial integration occurs when a skin tactile receptor or neuron sums a stimulus over some area of the skin.

Slowly-varying tactile stimulation is a slow local mechanical deformation of the skin that varies the deformation amplitude directly rather than the amplitude of a fixed frequency of vibration. This is “normal touch” for grasping objects, etc.

Telepresence consists primarily of visual, auditory, thermal, proprioceptive, and tactile feedback to a person from a remote location.

Teleproprioception is feedback of position and joint torques on a remote gripper to a human operator.

Teletouch is feedback of tactile (spatial force) patterns from a remotely grasped object to a person's skin.

Temporal integration occurs when a skin tactile receptor or neuron (or its CNS connection) sums a stimulus over time.

Vibrotactile stimulation evokes tactile sensations using mechanical vibration of the skin, typically at frequencies of 10 - 500 Hz.

TACTILE DISPLAY APPLICATIONS

This section provides some examples of the types of tactile displays used in experimental and commercial sensory substitution systems. For a broader overview of available devices, we refer the reader to reviews on systems for visual substitution [5],

[26], auditory substitution [93], [112], [123], and other applications [28], [89], [96], [106], [129], [128].

Single-element display

A single stimulation point can present information to the skin by variations in intensity, frequency, or both.

The source information could be temporally varying. For example, Leder et al. [73] describe the evaluation of an auditory prosthesis (sensory substitution system) in which the sound intensity as sensed by a microphone varies the vibration intensity of a vibrator strapped to the chest. Goldstein and Proctor [48] describe a similar device.

The source information might also vary spatially. Szeto et al. [127] discuss the evaluation of their system in which either the frequency or the amplitude of a single electrotactile stimulus could be controlled by the elbow angle in a below-the-shoulder arm prosthesis.

One-dimensional display

A row of two or more stimulation points presents spatial information more naturally (dimensionally more like normal touch) than a single-element display. For example, a variant of the prosthetic example above stimulates one of five electrodes in a line depending on the shoulder angle [97]. This voluntary shoulder position controls a functional neuromuscular stimulation orthosis for restoration of hand grasp to quadriplegic spinal-injured patients. Szeto and Chung [124] and Szeto and Lyman [125] earlier found that such a one-dimensional code was superior to frequency or intensity modulation of a single electrode when a subject was asked to position a joystick based on the electrotactile sensation. Mann and Reimers [79] describe a one-

dimensional vibrotactile display of the elbow angle of a prosthetic arm. Sandstrom [103] developed an ultrasonic ranging device for the blind which displays the distance to the nearest object on a linear array of vibrators along the finger. The compact vibrators are modified dot-matrix-printhead mechanisms.

Even the display of temporal information may be enhanced by spatially spreading it over several stimulators. Based on the early work of von Békésy [9], who discovered that the human ear performs a frequency analysis of incoming sounds at frequency-selective regions in the cochlea, Saunders et al. [108] developed an auditory prosthesis which adjusts the perceived intensity of 16 electrodes, each corresponding to the sound intensity in a given passband in the audio spectrum. This commercially-available device, the Tacticon, provides enough "auditory" feedback to improve the speech clarity of deaf children. Blamey and Clark [14] and Boothroyd et al. [19] describe similar 8-channel electrotactile devices. Brooks and Frost [21], [22] describe a similar 16-channel vibrotactile device.

Two-dimensional display

Tactile vision substitution (TVS): A two-dimensional matrix of stimulators can display spatial information to the skin similarly to the way the eye presents spatial information to its retina. The television-type camera in a TVS system receives a "visual" image and presents it to the user's skin with vibrotactile or electrotactile stimulators. Each stimulator's intensity (pulse width or amplitude) is controlled by the light intensity at a single camera receptive pixel. Following the initial report of successful laboratory use of a vision substitution device [7], Bach-y-Rita [5], Collins [25], Collins and Bach-y-Rita [27], Collins and Madey [28], Craig [30], White [148], and others used TVS systems extensively in the early 1970s to study the skin's ability

to interpret "visual" information. They found that subjects could immediately recognize vertical, horizontal, and diagonal lines. Experienced users could identify common objects and peoples' faces [5], and perform tasks such as electronic assembly under a microscope [6]. However, due partly to poor spatial resolution and dynamic range compared with the eye, TVS systems are not useful for acquiring information from "cluttered" visual environments such as hallways and are therefore not presently useful as navigation aids for the blind.

Similarly, Bliss et al. [17] developed the commercially-available Optacon (Optical to Tactile Converter). It converts the outline of printed letters recorded by a small, hand-held camera to vibrotactile letter outlines on the user's fingertip. Exceptional blind users can read ordinary printed text at up to 90 words per minute with the Optacon [58].

Tactile feedback: Performing detailed manual tasks is difficult for people with advanced cases of Hansen's disease (leprosy). They lack the sense of touch in the fingers and thus unknowingly injure their hands by grasping objects too tightly. Collins and Madey [28] developed a teletouch (tactile feedback) system in which strain gages mounted in a special glove measured the force (range 10 g to 5 kg) on each fingertip. Each of the 5 sensors controlled the electrotactile stimulation intensity of one forehead electrode. Subjects without sensation in the hands were able to distinguish smooth from rough surfaces, soft from hard objects, and by scanning were able to detect edges and corners, in spite of the low resolution of the display. It is likely that the large amount of perceived information from such a low-resolution display comes from (1) spatial information received by manually scanning complex objects (haptic exploration) with the few sensors (in effect, forming a "perceptual organ" [5]) and (2)

receiving texture information from surfaces by the minute frictional vibrations recorded by the sensors [64].

Astronauts in space face a similar lack of sensation. The gloves of their pressurized suits reduce touch sensation because they are thick and pressurized. Their hands tire rapidly because they tend to overgrasp objects which could slip out of their grasp. One way to make space activity safer for astronauts is to use remotely-controlled robots to perform extravehicular activity (EVA). However, current remote manipulators lack teletouch, so it is difficult for the operator to perceive if an object has been properly grasped.

At the University of Wisconsin, we are developing teletouch systems for space gloves and space telerobots [8], and people with insensate feet and hands (common complications of diabetes) [78], [146]. Pressure sensors on the glove surface, end effector (gripper), shoe insole, and fingers, respectively, control the electrotactile stimulation perceived intensity.

Auditory feedback: Sparks et al. [118], [119] use a 2-dimensional display of 288 electrodes (36 columns of 8 electrodes in a 1.3-cm-spacing square matrix on a belt [117]) to present auditory information to the abdomen. Each column corresponds to a certain band of frequencies, with the sound intensity in this passband controlling which electrodes in the column are active. Subjects could identify various segmental features of speech with 50% to 95% accuracy, depending on the particular set of sounds used. This performance is similar to that achieved with other auditory prostheses [93].

MECHANISM OF STIMULATION

Sensory physiology of the skin for normal touch

Skin anatomy: Human skin contains six types of tactile receptors that have been identified and characterized [37], [41], [110], [113]. Note that some receptors are found only in hairy or only in glabrous (hairless) skin. Table 2.1 lists several characteristics of these receptors, following the nomenclature of Schmidt [110] for hairy skin and Vallbo and Johansson [140] for glabrous skin. Some of the receptor characteristics in Table 2.1 are from primate studies [31], [132] where human data are not available.

Neural response of tactile receptors to a step change in skin displacement:

Phillips and Johnson [90] and Vallbo and Johansson [140] provide excellent reviews of the responses of the known receptor types.

Tactile receptors can be roughly classified by the speed of their adaptation to a step change in applied pressure to the skin. A receptor's response is measured by its ability to produce a change in the firing rate of action potentials on its corresponding afferent nerve fiber; an action potential is always an all-or-none event. Table 2.1 describes the step displacement response of the four traditional divisions of receptors in glabrous skin: (1) Fast adapting, broad-receptive-field FA II receptors, (2) Fast adapting, small-receptive-field (FA I) receptors, (3) Slowly adapting, large-field (SA II) receptors, and (4) Slowly-adapting, small-field (SA I) receptors. Note that in the literature, FA II is also called PC (Pacinian corpuscle), and FA is also called RA (rapidly adapting) or QA (quickly adapting). Finally, FA (without a I or II designation) sometimes refers specifically to FA I receptors, and sometimes it refers to both FA I and FA II receptors.

Sensory psychophysics: The sensation produced by mechanical stimulation of the skin is determined by both mechanoreceptor properties and central neural mechanisms [140].

Weinstein [145] conducted an extensive study to determine the detectable static force applied by a fine wire to most body locations. For men, the lips were the most sensitive, needing 0.05 g for sensation, the fingertips and belly 0.63 g, and the sole of the foot 3.5 g. The thresholds for women were 2 - 3 times lower for the least sensitive locations. The fingertip threshold corresponds to a skin indentation of about 10 μm . Both peripheral (tactile receptors) and central mechanisms determine sensation thresholds [139].

Geldard [41] summarizes the sensation threshold for vibrotactile stimulation with a 1- cm^2 vibrator at most body locations. The fingertips are more sensitive than most body locations by at least one order of magnitude. The abdomen, in particular, is 60 times less sensitive than the fingertips to 200-Hz vibration.

In a comprehensive review paper, Verrillo [144] discusses the mechanisms influencing the sensation threshold of the (glabrous) palm to vibrating stimuli. The skin's sensation threshold is 5 μm peak amplitude from 25 to 650 Hz for stimulation areas less than 0.05 cm^2 . For larger areas, the threshold is frequency dependent, achieving best sensitivity (0.16 μm) at 250 Hz with a stimulation area of 5 cm^2 . He explains this characteristic with the "duplex model" which states that at least two functional types of receptors (Pacinian and non-Pacinian) are present. The Pacinian (FA II) system integrates stimuli spatially and therefore is responsible for the threshold curve at stimulator areas larger than 0.05 cm^2 , while the non-Pacinian system does not, and accounts for the response to small-area stimulators. Further psychophysical

studies by Gescheider et al. [44] and Bolanowski et al. [18] suggest that three and four, respectively, receptor populations may mediate touch in glabrous skin, likely corresponding to the four known glabrous receptors.

The threshold amplitude for vibrotactile stimulation increases after a strong conditioning stimulus. Gescheider and Verrillo [45] found that a 10-min stimulus 6 dB over threshold raises the sensation threshold amplitude by 2 dB, while a 40-dB stimulus raises the threshold by 20 dB. This adaptation occurs at least for frequencies from 10 to 250 Hz. Hahn [54], [55] reports that a 7 to 25-min conditioning vibrotactile stimulus results in full adaptation, i.e., the sensation threshold does not further increase at longer conditioning stimuli durations. Full recovery from adaptation occurs in approximately 2 min. Furthermore, a conditioning stimulus has more influence on the sensation threshold than on the suprathreshold perceived intensity.

Finally, the perception due to stimulation of only the FA II (PC) receptors summates over time. The vibrotactile threshold to a 250-Hz, 2.9-cm² stimulus falls by 12 dB as stimulus time increases from 10 ms to 1 s, whereas no threshold shift appears for a 0.02-cm² stimulator [143]. Because the FA II receptors themselves do not show temporal summation in electrophysiological recordings [132], higher neural mechanisms must be responsible for the perceived summation.

Spatial resolution: Several experimental methods attempt to measure the spatial resolution of the tactile sense. Table 2.2 summarizes the simultaneous two-point-discrimination-threshold (TPDT) for static, vibratory, and electrotactile stimuli on several body locations. The TPDT (the oldest and simplest measure of tactile spatial acuity) is usually defined as the minimal distance at which two simultaneous stimuli are distinguishable from a single stimulus. The numbers in Table 2.2 should be used only

as a guide to the TPDT; comparisons of absolute numbers between static, vibratory, and electrotactile stimuli may be inaccurate due to the differing methodologies of different investigators. Note that the TPDT is smaller if the stimuli are presented sequentially rather than simultaneously.

Other methods used to measure tactile spatial resolution include the determination of the minimum width of a deep groove which can just be detected on an otherwise smooth surface (0.87 mm on the fingertip) and the minimum width of parallel grooves in a square-wave grating that allows subjects to discriminate the orientation of the grating (0.84 mm on the fingertip) [65].

Furthermore, the skin can identify a frictionless position shift of a stimulus 10 times smaller than the TPDT [77], indicating that the skin's spatial resolution is much better for certain tasks than the TPDT suggests. Indeed, different grades of sandpaper (with very fine spatial features) are readily discriminated by touch. Clearly, "spatial resolution" is not a uniquely defined quantity, but depends on the particular type of stimulus and task to be performed [32]; temporal and intensive cues also provide spatial information at the perceptual level [66]. Gardner [35] discusses cortical mechanisms which may be responsible for resolving spatio-temporal information (such as from a moving stimulus).

A further illustration of the complexity of spatial processing is the phenomenon of "funneling," which is the perception of several spatially-separated tactile stimuli as one stimulus in between the actual stimulation points [11], [12]. The neural mechanisms to account for funneling are higher than the peripheral afferent nerves [36].

Slowly-varying tactile displays

Due to the rapid adaptation of the tactile sense to static stimuli and the high stimulus levels required, slowly-varying tactile displays are not generally used in sensory substitution systems, unless the user actively scans the display with the fingers (haptic exploration).

Vibrotactile displays

It is tempting to tailor the frequency of a vibrotactile display to activate the low-temporal-frequency FA I receptors (most sensitive frequency 20-40 Hz) with their restricted receptor fields to achieve a display that responds to high spatial frequencies. However, Rogers [101] showed that the skin actually receives spatial information from an Optacon best at 250 Hz in spite of the spatially diffuse receptive fields of the FA II (PC). One explanation for this is that the spatial frequency of touch is not limited by the spacing of receptors or their receptive fields [77]. More likely is that even if the FA II are recruited, the fine spatial information is still provided by the smaller-field (FA I or more likely SA I) receptors [90]. The complex central mechanisms responsible for integrating information from all of these receptor types into useful percepts are only slowly being unraveled.

The above remarks only hold for very small stimulators; the optimal stimulation frequency may not be 250 Hz for stimulators over 0.05 cm^2 because the FA II will be increasingly recruited, possibly reducing the display's effective resolution.

Finally, the skin is particularly sensitive to make-and-break contact of a vibrotactor. For example, the vibrating pins in the Optacon's finger display contact the skin for only 20% of their vibrational period [17].

Electrotactile stimulation

Stimulation mechanism: Most investigators believe that an electric current passing through the skin directly stimulates afferent nerve fibers [23], [102], [129], although Pfeiffer [88] suggests that small electrodes (1 mm^2) stimulate receptors directly. Blamey and Clark [14], [15] intentionally chose electrode locations to stimulate entire nerve bundles in the finger for their auditory prosthesis. The sensation resulting from nerve bundle stimulation is not necessarily confined to a small skin region.

Subjects describe electrotactile sensations qualitatively as a tingle, itch, vibration, buzz, touch, pressure, pinch, and sharp and burning pain, depending on the stimulating voltage, current, and waveform, and the electrode size, material, and contact force, and the skin location, thickness, and hydration [29], [46], [80], [81], [88], [105], [129], [133]. The technique of single-afferent-fiber stimulation with microelectrodes is revealing the sensation qualities associated with activation of the different fiber types [135], [138].

Fine wire electrodes inserted in the skin also give rise to tactile sensations. Several investigators [3], [99], [98], [100] propose (invasive) subcutaneous stimulation as an alternative to surface electrodes. Among the advantages claimed are a reduction in the change in pulse repetition rate required for subject perception of the change (lower just-noticeable difference), high consistency over time of the sensations evoked, mechanical stability of the electrode interface, and elimination of the need to mount and remove skin electrodes.

Stimulation of a hair follicle with a needle electrode produces sensations of vibration or sharp pain depending on the insertion depth [109].

Finally, if a dry patch of skin moves over the electrode surface during 50-Hz stimulation, a weak vibrating sensation may be felt at currents as low as $2\text{ }\mu\text{A}$. Grimnes [50] calls this sensation electrovibration and shows that it is probably due to electrostatically-generated mechanical deformation of the skin, not electrical stimulation of neurons. Strong and Troxel [121] describe a manually-scanned fingertip display based on this principle.

Electrochemistry of electrode-skin interface: Because current flow through the skin is ionic, a transducer (electrode) is needed to convert electron flow in the lead wire to ionic flow (although it has been shown that a nerve may also be stimulated magnetically [94]). To reduce skin irritation and possible damage, the electrode should not introduce non-native ions into the skin. The electrode must also not react chemically so as to produce an insulating layer between the electrode and the skin. Most sensory substitution systems use metal electrodes; the most common are gold, platinum, silver, and stainless steel. Greatbatch [49] and Mortimer [83] review the electrochemistry of implantable metal electrodes; the same general principles apply to skin electrodes.

Current distribution under electrodes: Electrode-skin reactions under an electrode increase with the current density J , which should be kept as low and uniform as possible. Unfortunately, the distribution of J is not well-understood. Figure 2.1 shows a cross section of the current density for a circular electrode contacting an "infinite" homogeneous volume conductor. Even in this homogeneous case, J is much higher at the edge of the electrode than at the center.

The conductive path through the skin, however, is not uniform at the microscopic level for any electrode type. Grimnes [52] and Saunders [104] show that

current flows through small regions of low resistance (probably sweat ducts, sebaceous glands, and minute epithelial breaks, 1 to 6 per mm^2 skin area). Presently there is no adequate model of current distribution under a stimulation electrode which includes these nonuniformities.

Under large ($>100 \text{ mm}^2$) metal electrodes on dry skin, one of the skin's conductive paths will occasionally drop suddenly in resistance, shunting much of the electrode current through that pathway [46], [106]. The resulting high current density causes a sudden sharp sting and a red spot on the skin. The sting is most likely to occur with negatively-pulsed electrodes. Grimnes [51] proposes that a mechanism called electro-osmosis draws water through pores toward a negative electrode. Within about 1 s this considerably increases a pore's conductance and thereby might cause a positive feedback runaway condition in one pore as it rapidly becomes hydrated. Lin [74] found that coating 12-mm^2 metal electrodes with a conductive adhesive eliminates these sharp stings. The resistance of the adhesive may serve to equalize the current in several pathways, even if one has lower resistance than the others, or the adhesive may absorb excess water from the pore [53]. The exact mechanism is unclear.

Electrode impedance: The resistive part of the impedance of the electrode-skin interface (R in Figure 2.2) drops sharply with increased current [20], [46], [67]. The change in R is localized in the stratum corneum [20]. Because of this change, electrodes are usually stimulated with constant current rather than constant voltage. One disadvantage of constant current stimulation is that if an electrode makes poor skin contact, the reduced effective area results in a higher current density and a much stronger sensation. Saunders [104] suggests that a constant-power output circuit might be more suitable for electrodes prone to poor contact.

Figure 2.3 shows the voltage of a 12-mm² active electrode on the forearm relative to a large indifferent electrode when stimulated with monophasic, 10-mA, 10- μ s duration constant current pulses [105]. Figure 2.2 shows the classical model of the electrode-skin interface which explains this waveform. The electrochemical half-cell potential and series resistive components are omitted because they are insignificant considering the high voltages used for stimulation. Note that the first part of the voltage curve (a) rises exponentially with a time constant of approximately 10 μ s, as the capacitor charges. An extrapolation of this curve for long pulse durations (b) shows a constant voltage. We can calculate $R = 8 \text{ k}\Omega$ and $C = 1.25 \text{ nF}$. Normalized to the 12-mm² area electrode, these values can be expressed as approximately $0.1 \text{ M}\Omega\text{-mm}^2$ and 0.1 nF/mm^2 . Pfeiffer [88] summarizes the findings of several investigators, who found that R varies from 0.25 to $40 \text{ M}\Omega\text{-mm}^2$ and C from 0.031 to 0.4 nF/mm^2 for sinusoidal excitation at various frequencies and electrode sizes. R varies widely with skin condition and it decreases markedly at high stimulation currents. Indeed, Gibson [46] found that for a 330-mm² electrode R drops from 32 to $3 \text{ M}\Omega\text{-mm}^2$ as the stimulation current increases from 0.1 to 5 mA. The related time constant RC drops from 1.2 to 0.13 ms over this current range, showing that $C = 40 \text{ pF/mm}^2$ varies little over this current range. Boxtel [20] discusses in some detail the change in R with current.

Thresholds of sensation and pain: The useful intensity dynamic range of an electrotactile stimulator is the ratio (Threshold of Pain):(Threshold of Sensation) or P/S. Table 2.3 shows that the P/S ratio varies from under 2 (6 dB) to about 10 (20 dB) at best. This range is limited compared to other senses; the ear has a dynamic range of 120 dB and the eye 70 dB. If we assume a maximal comfortable vibratory stimulus

amplitude of 0.5 mm for a 0.78-mm² stimulator [25], the vibrotactile range of the skin is about 40 dB.

Table 2.3 summarizes the results of several investigators who determined the current required to elicit electrotactile sensation and pain. A model predicting the thresholds as functions of electrode size, material, waveform, etc. is difficult to formulate owing to the great variations in methodology between investigators.

At least four factors account for the disparities in results among investigators in determining P/S. (1) There is no uniform definition of "pain;" it could be defined as mild discomfort to intolerable. (2) The psychological condition and training modify the threshold of pain; experienced subjects tolerate at least twice the stimulation levels of naive subjects [104]. (3) At least for thermally-induced pain, noxious stimuli may raise or lower the pain threshold [134]. (4) The P/S ratio is a function of electrode size, material, and placement as well as by the parameters of the stimulation waveform; all of the relevant factors are rarely reported.

Furthermore, skin condition has a profound influence on the dynamic range and comfort of stimulation; dry skin has a high impedance and a prickly sensation (likely due to nonuniform current distribution). Effective skin preparation ranges from applying electrodes 20 min prior to stimulation to allow sweat to build up [80], to premoistening the skin with water [129] or saline [104] before applying the electrodes. Once stimulation starts, sweat production increases and provides sufficient moisture. While commercial conductive electrode gels provide a low skin resistance, they can short-circuit adjacent electrodes in a closely-spaced array and increase the required current levels. Furthermore, the gel can dry out and require reapplication after several hours of operation.

Finally, the sensation and pain thresholds can change significantly with small (1 mm) changes in electrode position.

Mechanism of sensation and pain thresholds: Figure 2.4 shows that the required sensation threshold current increases with decreasing pulse width, suggesting that the threshold of sensation is determined by the pulse charge (current \times duration). Figure 2.4 also shows that for pulse durations longer than 100 μ s, the threshold charge increases, leading Rollman [102] and Girvin et al. [47] to conclude that temporal integration of electric charge leading to electrotactile sensation occurs only partially above 100 μ s and not at all above 5 ms. At least 2 mechanisms may be responsible for this temporal integration. (1) The electrode-skin interface temporally summates charge. The electrode-skin model in Figure 2.2 has a time constant that varies approximately from 10 μ s to 1 ms depending on skin condition and stimulus current [46]. (2) The afferent nerve fiber membrane temporally summates charge. Butikofer and Lawrence [23] used the Frankenhauser-Huxley model [34] to predict the threshold charge across the membrane of a peripheral afferent myelinated nerve necessary to produce an action potential. Their model showed temporal integration up to only 50 μ s.

Geddes and Baker [38] and Mouchawar et al. [84] review several competing mathematical descriptions of this strength-duration relationship.

Because of the limited electrotactile temporal integration of the skin and the reduction of dynamic range with longer durations, current pulses with duration less than 0.5 ms are the most appropriate. In fact, Saunders and Collins [107] use very short pulses (5 - 20 μ s).

Finally, for pulse durations longer than 500 μs , the pain threshold drops more quickly than the sensation threshold [46], indicating that different integration mechanisms may determine the sensation and pain thresholds.

The P/S ratio increases with electrode size as long as sudden stings do not occur. Saunders [104], [106] found that 10-15 mm^2 is the optimal area of metal electrodes on the (hairy) abdomen; this is a compromise between larger electrodes (higher P/S) and smaller electrodes (less possibility of sudden stings). Gibson [46] specified 175 to 700- mm^2 area for hairy skin and 50 mm^2 for glabrous skin. However, Gibson used longer pulses (500 vs. 10 μs) and may have used conductive gel (possibly equalizing current flow in the current pathways) under electrodes while Saunders did not.

Solomonow and Preziosi [116] determined sensation and pain thresholds for a gelled 8.4- mm^2 coaxial stainless steel electrode pulsed for 100 μs on several body locations. They found that the sensation threshold was about 2 mA on most trunk sites and about 7 mA on the palmar and plantar surfaces.

Several mathematical models have recently appeared which predict the stimulation of afferent nerve fibers in response to an external electric field such as that produced by an electrode [72], [91], [92], [95], [94], [141], [142]. Of these models, only Larkin and Reilly [72] and Rattay [91] deal with surface stimulation (the others deal with invasive electrodes). Rattay [91] does not consider capacitance; his model is a static model. Larkin and Reilly [72] use an arc discharge (point) stimulation. We are not yet aware of any unified dynamic model which adequately explains the sensation and pain thresholds of electrotactile stimulation using surface electrodes, although great strides have been made in this area.

Subjective magnitude of electrotactile stimulation: The subjective intensity of a train of pulses is increased by raising the pulse current, width, or, to a lesser extent, pulse rate (frequency). Rollman [102] summarizes the results of several investigators who fit electrotactile data to Stevens' power law [120]

$$\psi = (\phi - \phi_0)^n$$

where ψ is the subjective magnitude, ϕ_0 is the sensation threshold (which is sometimes set arbitrarily to zero), and ϕ is the stimulus level (in this case, current). Only Rollman's data was taken from a localized cutaneous sensation (electrode away from nerve bundles); his value for n increased from 2.3 to 3.0 (with ϕ_0 set to 0) as the number of pulses in a burst increased from 1 to 30. The value n (rate of subjective magnitude growth) is high compared to other sensory modalities such as pressure on the palm of the hand ($n = 1.5$) and loudness of a 1-kHz tone ($n = 0.3$) [120]. This result indicates that the stimulation current must be carefully controlled to avoid unpleasantly strong sensations. Furthermore, if current is to be modulated to convey information, a careful mapping must be made from the sensed variable (e.g. pressure) to the stimulation current.

Because electrode impedance decreases with increasing current but is not affected by pulse duration, Saunders [104] does not recommend current modulation. Both pulse duration [29] and frequency [14] modulation have been used for sensory substitution. Szeto [122] found that subjects perceive a constant stimulation level (but varying "quality") if pulse duration and rate are varied according to the relationship

$$\log PW = 2.82 - 0.412 * (\log PR)$$

where PW is the pulse width in microseconds and PR is the pulse rate in Hz. Finally, Saunders [104] describes a technique using the 10-kHz pulse bursts in Fig. 2.5(c) in which the number of pulses in each burst varies from 0 to 40. For clarity, Fig. 2.5(c) only shows monophasic pulses; Saunders actually used biphasic pulse pairs.

The subjective intensity of a continuous train of pulses [Fig. 2.5(a)] decreases with time due to adaptation. The adaptation rate varies with frequency; while little adaptation occurs at 10 Hz, the sensation produced by a 1000-Hz pulse train decreases within seconds [129]. As with vibrotactile stimulation, electrotactile adaptation has more effect at the sensation threshold than at suprathreshold levels. A modulated pulse train [Fig. 2.5(b)] reduces the adaptation [29]. With bursts of 500-Hz pulses gated at a 25-Hz rate, this waveform elicits a "buzz" sensation.

Subjective description of sensation: In 1943 Bishop [13] found that electrically stimulating the skin in very small areas with spark discharges caused two distinct sensations depending on the location: prick and touch, with the prick locations being more numerous. Moving the stimulus location by as little as 0.1 mm changed the sensation. Therefore, on most skin loci, electrodes of about 1-mm² area give a prickly, uncomfortable sensation which becomes painful at levels just above threshold [106]. Larger electrodes result in a more comfortable stimulation described as touch or vibration, probably because: (1) both touch and pain (prick) fibers are stimulated, and the touch sensation can partially mask the pain [23], and/or (2) the large-diameter touch fibers are stimulated at lower current densities than the pain fibers [141]. However, even 1-mm position shifts of larger electrodes can change the subjective sensation as

well as the sensation and pain thresholds. Because of the great variations in experimental methods and the vagueness of sensation descriptions, it is difficult to predict which stimulation waveforms, body locations, etc. give rise to which types of sensations, much less determine the underlying neural mechanisms. Nevertheless, some investigators have proposed mechanisms [23], [24], [56], [80], [102], [121].

Pain: Pain sensations are the major disadvantage of electrotactile stimulation, although comfortable stimulation is normally assured if several design recommendations are adhered to. The three most common types of pain or discomfort are: (1) prickly sensations at all stimulation levels, (2) sudden stings at low-to-moderate stimulation levels, and (3) burning sensations at high stimulation levels [80]. Prickly sensations are best avoided by using electrodes of 10-mm² area and allowing sweat to build up [106]. Partial loss of electrode contact reduces the effective electrode area and must therefore be prevented to avoid prickly, painful sensations. Mason and Mackay [80] propose that the sudden sting phenomenon is due to pinpoints of corneal burning due to high current density. The stings are largely avoided by using electrodes smaller than 100 mm² [106] or by using conductive polymer coatings on the electrodes [74]. Burning sensations represent the upper limit of electrotactile stimulation intensity. Note that we distinguish a burning sensation from true thermal damage to the skin.

HUMAN TACTILE INFORMATION PROCESSING

Sherrick [111] lamented that as a communication channel, the tactile sense is often considered inferior to sight and hearing. However, the tactile system possesses some of the same attributes as both of the "primary" senses [5]. With over 10,000

parallel channels (receptors) [29] capable of responding to stimulus interruptions as short as 10 ms [5], the tactile system may be capable of processing a great deal of information if it is properly presented.

What information is important?

We introduce this section with simple yet representative human information-processing task. Suppose a person is shown 10 pictures of people and is asked to simply identify whether each picture is of a man or a woman. Unless considerable effort is expended to choose ambiguous pictures, this task could probably be accomplished in about 10 s. According to the classical definition of information rate

$$\text{rate (bits/s)} = (\text{decisions/s}) \times \log_2 (\text{number of choices in decision})$$

the information rate of the subject's response is $(1 \text{ decision/s}) \times \log_2(2 \text{ choices}) = 1 \text{ bit/s}$. Yet the pictures contain far more information than 1 bit each. Indeed, such a pattern recognition task would be formidable for a personal computer (which can perform approximately 10^6 operations/s).

This admittedly trivial example illustrates the difficulty of defining a useful information-transfer rate for any of the human senses, including the tactile sense. The key issue is deciding what information is important. Then, formal information theory can be applied meaningfully to predict the usefulness of specific sensory feedback codes.

Clearly, "information" is not a uniquely-defined quantity in a system. Biological systems, in particular, exhibit a great deal of divergence (one stimulus may activate hundreds of sensors) and convergence (a single CNS decision may be made on

the basis of thousands of neural inputs). As a further illustration, Lindblom [76] notes that a vibratory stimulus of up to 200 Hz results in synchronized firing of afferent nerve fibers, showing that the tactile sensing units are capable of great physiological information flow. However, we perceive only a smooth vibration. A loose description would be that the higher neural centers treat this data stream as highly redundant or trivial. Indeed, J. J. Gibson's definition of information (reviewed in Epstein [33]) implies some behavioral significance to the information carried in a stimulus. An alternative interpretation is that the volume of neural information from the simple vibrating stimulus is placed into one "chunk" with the redundant, useless information being discarded [82]. Information theory would state that the information in the afferent fibers has a low variance; it is somewhat predictable with a simple vibratory stimulus.

Estimates of tactile information flow

Table 2.4 shows the results of several investigators who calculated the rate at which humans process vibrotactile and electrotactile information at the perceptual level (2 - 56 bits/s). Although there are large differences in methodology, we may loosely compare these rates with those quoted by Schmidt [110] for understanding spoken speech (40 bits/s) and reading (30 bits/s). The approximate maximal rates of information flow at the receptor level (based on the number of receptors and their afferent nerve fibers) for the eye, skin, and ear are 10^7 , 10^6 , and 10^5 bits/s, respectively [110].

Not included in Table 2.4 are the numerous studies which determined not the information rate, but only the number of discernible levels of stimulation (Just-Noticeable Differences or JNDs). Table 2.5 summarizes these studies; the number of

JNDs has been estimated at from 6 to 59 levels for electrotactile stimulation and 15 levels for vibrotactile stimulation [39], [40]. The wide electrotactile variations are due in part to the different waveform quantity being manipulated to change the "level." In particular, it is possible that increasing the current by small steps at a slow rate will yield a large number of steps because at each step, some of the perceptual level increase will be lost due to adaptation. Table 2.5 reflects this effect with the number of JNDs for current being higher than the number of JNDs for frequency.

The JND itself is a measure of channel sensitivity. Table 2.6 summarizes the results of investigators who reported the JND for electrotactile and vibrotactile stimulation. The JND is expressed as a percentage because it is roughly proportional to stimulus level or frequency.

Note that the number of JNDs is not the same as the number of absolute levels which can be reliably classified. For example, only 4 or 5 levels of vibrotactile stimulation duration [39], [40] and 6 levels of electrotactile stimulation frequency [98] can be reliably classified. This is not likely a limitation of the tactile sense, however. Miller [82] found that subjects classifying pitch and loudness of tones, counting dots presented on a screen, identifying locations of tactile stimuli, recall of spoken words and numbers, and similar tasks could typically "process" from 5 to 9 discrete pieces of information...which averages to his magical number seven.

Spatial information processing

The skin appears to thrive on a flood of information for "visual" pattern recognition tasks, suggesting that system spatial processing should not reduce the amount of information delivered to the skin [148]. However, edge-enhancement of TVS images often improves subject performance, as edges appear to carry the most

important information for pattern recognition [5]. Curiously, scrambling the columns in a TVS system does not significantly impair the performance of subjects identifying letters by touch, although training time is longer than with a spatially-corresponding TVS system, i.e., one with object shapes preserved [30]. This finding illustrates the remarkable adaptability of the human sensory system.

Temporal information processing

In spite of the slowness of the CNS to react to tactile input (200 ms) [102], the perceived stimulation can vary significantly with small (< 1 ms) variations in the timing of successive stimulations. For example, von Békésy [10] and Gescheider [43] note that if two square-wave mechanical tactile stimulators spaced about 5 cm apart or even on different fingertips are simultaneously pulsed for 1 ms, a single sensation will be felt midway between the stimulators. However, if the pulses are staggered by as little as 0.2 ms, the perceived position of this "phantom" stimulus moves toward the earlier stimulus. An even larger shift in apparent position occurs when the amplitudes of the two stimuli are unequal, with the sensation appearing closer to the stronger stimulus [2], [43], [46], [79]. Mann and Reimers [79] use the position of a phantom sensation to display the angle of a prosthetic arm. Furthermore, Verrillo [143] showed that the threshold for vibrotactile stimulation drops as the stimulus time increases to one second, i.e., the skin exhibits temporal summation over one second.

Finally, while we have presented spatial and temporal information separately, they do in fact strongly interact [42].

These results suggest that different types of temporal processing with "time constants" ranging over at least 0.2 ms to greater than 1 min occur in the human somatosensory system. Therefore, the precise effects of such real system

characteristics as time delay, time skew between elements, and phase shift are difficult to predict and might need to be determined empirically for a specific system.

Integration of information from tactile receptors

Although some correlation between tactile receptor activity and the quality of the perceived sensation is known, for complex (and even many simple) stimuli the percept depends on input from several receptor types [18].

Ramifications for sensory substitution systems

Clearly, a sensory substitution system must accommodate the unique sensory characteristics of the skin, particularly if cross-modality (visual-to-tactile or auditory-to-tactile) substitution is attempted. For example, an auditory prosthesis cannot simply use the microphone signal to directly control electrode current because the skin has insufficient high-frequency response. The auditory information must be processed to match the properties of the tactile sense.

The dynamic range (ratio of maximal to minimal signal level) of a given sensor usually does not match the dynamic range of a given tactile display. For example, in a TVS system the range of light input to a camera is much higher than the typically 6-20 dB range of electrotactile stimulation. Some form of amplitude compression or scaling may be desired. For a teletouch system, one approach might be to implement a transfer function from the pressure sensor to the tactile display so that the perceived stimulation magnitude closely matches the perceived magnitude of the same pressure stimulus on normal skin.

Based on Miller's [82] absolute-level identification conclusion (above), is it useful to optimize tactile display parameters to maximize the number of absolute-level identifications? Perhaps the parameter choice need only guarantee some (as yet

unspecified) minimum number of levels n . Furthermore, whether the information channel to the tactile display may be quantized to n levels without loss of end-application system performance remains an open question. Another open question is the relationship between the JND of a display stimulus and the end-application system performance.

Finally, an electrotactile display undoubtedly stimulates afferent fiber types in different proportions than normal touch, and not much control is presently available over which fiber types are stimulated. Such differential excitation may be necessary to produce more effective sensory substitution displays [18], [138]. A similar situation exists with a vibrotactile display, where a constant (dc) level is presented as a sinusoidal stimulus.

PRACTICAL CONSIDERATIONS

Safety

Burns: Electrodes and vibrators can both generate sufficient heat to cause painful sensation of heat as well as burns. LaMotte [71], in a review of thermally-induced pain, reports that for a 3-s application of radiant heat to a 7.5-mm diameter patch of glabrous skin on the hand the average threshold temperatures for perception of warmth and pain without tissue damage are 40°C and 47°C, respectively. Three minutes of exposure at 49°C are required to cause a minor burn. In terms of radiant energy, the pain and burn thresholds are 0.92 W/cm² and 2.0 W/cm², respectively, for 3-s exposures [41]. However, Taige [131] found that 12-mm-diameter vibrotactile transducers are uncomfortably warm at continuous average power levels above only 62

mW (55 mW/cm^2). This lower power is likely due to the fact that the transducers (and mounting hardware) are in physical contact with the skin, trapping heat, in contrast with the radiant heat studies.

Burns under electrodes are of at least 3 types. (1) Electrochemical burns and irritation due to a net flow of ions are largely prevented by ensuring that the net dc current flow at an electrode is zero. However, Szeto and Saunders [129] recommend biphasic pulse pairs to prevent the net electrochemical reactions that occur even with capacitively-coupled (no net dc flow) monophasic pulses. (2) Large thermal burns are not likely to occur at the frequencies of interest in sensory substitution systems ($< 1 \text{ kHz}$) unless the stimulation level is driven well into the pain region. For example, from the data in Table 2.3, a 15.9-mm^2 electrode requires $20 \text{ mA} \times 8 = 160 \text{ mA}$ for $2\text{-}\mu\text{s}$ pulses at a 200-Hz rate to cause pain [107]. If we assume the maximal voltage to be 100 V , the average power density at the electrode is 40 mW/cm^2 , well below the burn level. (3) Tiny black marks (0.25 mm diameter) are visible on the skin under magnification after sudden stings from an electrode. Mason and Mackay [80] propose that the marks are burns caused by high power density in a single conductive pathway. However, their calculations assume that the dynamics of the electrode voltage and current are measurable during a sting with a stripchart recorder and that most of the current flows through one pathway.

Electric shock: To prevent the possibility of cardiac fibrillation, the stimulator output circuit should be designed so that the maximal current flow across the user's torso is under 0.1 mA at any time [87], even if there is a circuit fault or if a body part contacts another metal object, grounded or otherwise.

Comfort

Electrotactile: The maximal level of comfortable electrotactile stimulation varies between individuals and even varies with one individual. The user must have a simple means of adjusting the stimulation level and quickly turning it off completely if necessary.

Vibrotactile stimulation is comfortable with amplitudes up to 0.5 mm for a 1-mm diameter stimulator [25] unless the heat generated at the stimulator is greater than 62 mW/cm^2 [131].

General: The mechanical comfort of any tactile display is heavily influenced by the method used to hold the display to the skin. A compromise must often be made between performance and comfort. For example, the sensation produced by electrotactile stimulation is most comfortable when the electrode-skin interface is wet with perspiration and the electrodes are held firmly against the skin.

Repeatability and spatial uniformity

Because of the high variations in thresholds of electrotactile sensation and pain between subjects, a fixed relationship between the desired information (e.g. force) and the stimulation parameter (e.g. current) is not practical or desirable. The system user must be free to adjust the stimulation intensity and dynamic range as desired. Tursky and O'Connell [137] showed that for a single subject, suprathreshold levels are more repeatable than the sensation threshold.

We are not aware of any studies for electrotactile or vibrotactile stimulation which report the amount of variation of sensation or pain thresholds over an array of stimulators on one body surface.

Power consumption

Low system power consumption is desirable in portable sensory substitution systems. This section comments on the power consumed by example tactile displays.

Electrotactile: A 3-mm diameter electrode consumes 1.2 mW/pixel at a comfortable continuous stimulation level of 6 mA, based on the waveform in Fig. 2.5(b) used by Collins [25]. However, in a practical system, only a fraction of the stimulators are active at a given time, leading to an average power dissipation as low as 1 μ W/pixel [29].

Vibrotactile: Kovach [70] used the mechanical properties of the skin to estimate the mechanical power dissipated in abdominal skin for a 250-Hz, 4-mm-diameter vibrotactile stimulator. The threshold power is 0.4 mW, with an "adequate" continuous stimulation level 8 dB higher requiring 2.5 mW, close to Collins' [25] estimate of 10 mW for a 1-mm-diameter stimulator. The electrical power consumption of the actual 4-mm vibrator (Star Micronics QMB-105 audio transducer) is considerably higher (138 mW for sine waves at threshold) due to conversion inefficiency and coupling losses. The resulting energy-conversion efficiency of 0.29% is too low for practical use of this transducer. To work around this problem, Nunziata et al. [86] and Taige [131] developed a special driving waveform for this transducer so that it dissipates only 0.05 mW average power. However, this power was attained by using 40-ms bursts of 250-Hz stimulation and 2-s rest periods between bursts, creating a very small duty cycle. The 2-s time between bursts would make the system slow to respond to changes in the desired stimulus level.

Finally, as with electrotactile stimulation, only a small percentage of the stimulators will be active at any given time, reducing considerably the average power consumption.

Static tactile arrays using electromechanical solenoids require at least 1 W/pixel to produce forces well above threshold, making them impractical for limited-power applications. They also suffer from severe adaptation to constant stimuli lasting longer than 1 s.

Electrotactile skin irritation

Szeto and Saunders [129] present informal comments on skin irritation as well as report on a 10 h/day, 2-week trial in which 5 subjects wore stimulators driving silver coaxial electrodes on the upper arm. They found that while a biphasic waveform caused the least long-term skin irritation, a monophasic waveform caused less transient skin reddening. They concluded that either waveform is suitable.

Riso et al. [98] report that long-term use of subcutaneous electrodes does not cause skin infection if the electrode site is cleaned daily with alcohol.

More research is necessary to determine the long-term effects of electrotactile stimulation as functions of electrode types and waveforms.

PERFORMANCE EVALUATION

Developing an optimal display for sensory substitution requires some objective method to evaluate the performance of the display. Preferably numerical performance criteria should be established regarding issues such as information transfer and practicality. Each of the performance criteria can then be optimized by varying the parameters of the display (waveforms, signal processing, etc.). A possible list of performance criteria is:

- (1) Minimal power consumption
- (2) Maximal stimulation comfort
- (3) Minimal poststimulation skin irritation
- (4) Minimal sensory adaptation
- (5) Maximal information transfer measured by:
 - (a) Minimal just-noticeable difference (JND) of the modulation parameters Current, Width, Frequency, and Number of pulses per burst
 - (b) Minimal error in identifying the absolute stimulation level of a randomly stimulated electrode
 - (c) Minimal error in manually tracking a randomly varying target stimulus [60], [97], [124], [125], [127], [136]
- (6) Maximal dynamic range: Max. Comfort Level / Sensory Threshold
- (7) Minimal variation of Sensory Threshold and Max. Comfort Level with the precise electrode location on a given skin region

Performance criteria should be chosen carefully with the final system application in mind. Does the chosen evaluation method criteria mimic (at least in theory) the final task? For example, if the final application is a sensory prosthesis for the insensate hand, are small changes in the JND (system gain) really meaningful? In light of Miller's [82] conclusion that the absolute identification of stimuli levels is a high-level process largely independent of the sensory modality, it may be meaningful to optimize a cutaneous display for the greatest number of discriminable levels only if the end task requires absolute judgements. Furthermore, such absolute judgements might

be better provided by a warning-signal approach where some appropriate circuit or microprocessor algorithm makes the judgements. We do not believe that traditional psychophysical measures should be applied simply because they are available. Where practical, final task measures (such as word discrimination with an auditory prosthesis) are preferable to more abstract criteria.

Finally, with multiple performance measures for a system there may be no unique set of optimal parameters; engineering judgement will determine which performance measures are most important.

TRAINING

In order to effectively use information from a sensory substitution system, the brain must form new functional neural pathways by means of "unmasking" of previously underused pathways [5]. Our normal senses were developed over a period of years; the ability to use sensory substitution information will also take time.

For example, users of tactile vision substitution systems such as the Optacon can immediately recognize vertical, horizontal, and diagonal lines presented to the display. Forty hours of training enable tactile reading rates of 10 words/min [17]; further training typically raises the rate to about 28 wpm [59]. For the exceptional reading rate of 90 wpm, over 100 h of experience are required. Some users of TVS systems can recognize familiar objects after 20 h of training [4].

FUTURE RESEARCH

Sensory substitution systems currently enjoy little use partly because of (1) Uncomfortable or impractical displays and (2) A lack of understanding of how displays can efficiently transfer useful information to the tactile sense. Further research is therefore needed in the following areas.

Electrodes and stimulation waveforms

The waveform and electrode parameters determine the mode of information transfer to the user, the qualitative sensation, and the level of skin irritation.

The current distribution under stimulation electrodes of various sizes and geometries must be accurately modeled. Investigation needs to continue into the coupling of skin-electrode-induced cutaneous electric fields with afferent nerve fibers in the time domain to supplement existing models. Because it may be necessary to differentially excite different afferent fiber types to achieve the desired information transfer [18], a model is needed to predict which fibers are preferentially excited by different waveform and electrode parameters.

The subjective level of stimulation (including the definitions of thresholds of sensation and pain) is not sufficiently characterized, although it has been extensively studied. The varying methodologies of different investigators make it impossible to write down a single magnitude-estimation function of all the relevant variables:

$$\text{Subjective intensity} = f(\text{electrode and waveform variables})$$

or even

Threshold of sensation = $f(\text{electrode and waveform variables})$

The qualitative sensation (vibration, tingle, sting, etc.) is clearly a function of the electrode material, size, geometry, skin preparation, and stimulus waveform, but the relationships are reported largely anecdotally in the literature. Systematic study of this area is necessary because uncomfortable sensations are the primary disadvantage of electrotactile stimulation. This area will also benefit from knowledge of differential excitation of afferent fiber types.

Present electrodes and waveforms may cause skin irritation after several hours of stimulation. Electrode and waveform parameters need to be optimized to minimize the irritation level.

Finally, uniform skin contact for each electrode in an array is difficult to achieve. Improved electrodes and mounting methods are needed.

Vibrators and driving waveforms

Although the mechanical properties of the skin and the psychophysical response to vibrating stimuli are largely understood, few practical vibrator arrays have been developed. Off-the-shelf transducers will likely never prove practical due to low energy-conversion efficiency. An optimal vibrator will likely need to be a custom design (such as that in the Optacon) to meet the simultaneous practical constraints of small size, low noise, low power consumption, and an adequately large dynamic range. Only a careful electromechanical design will achieve the efficient coupling of stimulation energy to the skin necessary to meet the above constraints.

Tactile Information processing

Much effort has been expended characterizing tactile display technologies with specific psychophysical performance measures such as JND, number of discernible levels, absolute level identification, two-point discrimination thresholds, and tracking of varying stimuli. What is needed to complement this extensive body of knowledge is some correlation between these standardized measures and the performance of complete sensory substitution systems in their end applications.

REFERENCES

- [1] G. L. Aiello and M. A. Valenza, "Psychophysical response to electrocutaneous stimulation," *IEEE Trans. Biomed. Eng.*, vol. BME-31, pp. 558–560, 1984.
- [2] D. S. Alles, "Information Transmission by Phantom Sensations," *IEEE Trans. Man-Mach. Sys.*, vol. MMS-11, pp. 85–91, 1970.
- [3] A. B. Anani, K. Ikelda and L. M. Korner, "Human ability to discriminate various parameters in afferent electrical nerve stimulation with particular reference to prostheses sensory feedback," *Med. Biol. Eng. Comput.*, vol. 15, pp. 363–372, 1977.
- [4] P. Bach-y-Rita, "A tactile vision substitution system based on sensory plasticity," in *Visual Prosthesis: The Interdisciplinary Dialogue*, T. D. Sterling, J. E. A. Bering, S. V. Pollack and J. H. G. Vaughan, Eds. New York: Academic Press, 1971, pp. 281–290.
- [5] P. Bach-y-Rita, *Brain Mechanisms in Sensory Substitution*. New York: Academic, 1972.
- [6] P. Bach-y-Rita, "Visual information through the skin- A tactile vision substitution system," *Trans. Am. Acad. Ophthalmology and Otolaryngology*, vol. 78, pp. OP-729–OP-739, 1974.
- [7] P. Bach-y-Rita, C. C. Collins, F. A. Saunders, B. White and L. Scadden, "Vision substitution by tactile image projection," *Nature*, vol. 221, pp. 963–964, 1969.

- [8] P. Bach-y-Rita, J. G. Webster, W. J. Tompkins and T. Crabb, "Sensory substitution for space gloves and for space robots," in *Proc. Workshop on Space Telerobotics*, vol. 2, Jet Propulsion Laboratory, 1987, pp. 51–57.
- [9] G. v. Bekesy, "Human skin perception of traveling waves similar to those of the cochlea," *J. Acoust. Soc. Am.*, vol. 27, pp. 830–841, 1955.
- [10] G. v. Bekesy, "Sensations on the skin similar to directional hearing, beats, and harmonics of the ear," *J. Acoust. Soc. Am.*, vol. 29, pp. 489–501, 1957.
- [11] G. v. Bekesy, *Experiments in Hearing*. New York: McGraw-Hill, 1960.
- [12] G. v. Bekesy, *Sensory inhibition*. Princeton: Princeton Univ. Press, 1967.
- [13] G. H. Bishop, "Responses to electrical stimulation of single sensory units of skin," *J. Neurophysiol.*, vol. 6, pp. 361–382, 1943.
- [14] P. J. Blamey and G. M. Clark, "A wearable multiple-electrode electrotactile speech processor for the profoundly deaf," *J. Acoust. Soc. Am.*, vol. 77, pp. 1619–1621, 1985.
- [15] P. J. Blamey and G. M. Clark, "Psychophysical studies relevant to the design of a digital electrotactile speech processor," *J. Acoust. Soc. Am.*, vol. 82, pp. 116–125, 1987.
- [16] J. C. Bliss, "Summary of three Optacon-related cutaneous experiments," in *Proc. Conf. Cutan. Comm. Sys. Dev.*, F. A. Geldard, Ed., Psychonomic Society, 1973, pp. 84–94.
- [17] J. C. Bliss, M. H. Katcher, C. H. Rogers and R. P. Shepard, "Optical-to-tactile image conversion for the blind," *IEEE Trans. Man-Mach. Sys.*, vol. MMS-11, pp. 58–65, 1970.

- [18] S. J. Bolanowski, G. A. Gescheider, R. T. Verrillo and C. M. Checkosky, "Four channels mediate the mechanical aspects of touch," *J. Acoust. Soc. Am.*, vol. 84, pp. 1680–1694, 1988.
- [19] A. Boothroyd and T. Hnath-Chisolm, "Spatial, tactile presentation of voice fundamental frequency as a supplement to lipreading: Results of extended training with a single subject," *J. Rehab. Res. Dev.*, vol. 25, no. 3, pp. 51–56, 1988.
- [20] A. v. Boxtel, "Skin resistance during square-wave electrical pulses of 1 to 10 mA," *Med. Biol. Eng. Comput.*, vol. 15, pp. 679–687, 1977.
- [21] P. L. Brooks and B. J. Frost, "The development and evaluation of a tactile vocoder for the profoundly deaf," *Can. J. Pub. Health*, vol. 77, pp. 108–113, 1986.
- [22] P. L. Brooks, B. J. Frost, J. L. Mason and D. M. Gibson, "Continuing evaluation of the Queen's University tactile vocoder I: Identification of open set words," *J. Rehab. Res. Dev.*, vol. 23, no. 1, pp. 119–128, 1986.
- [23] R. Butikofer and P. D. Lawrence, "Electrocutaneous nerve stimulation - I: Model and experiment," *IEEE Trans. Biomed. Eng.*, vol. BME-25, pp. 526–531, 1978.
- [24] R. Butikofer and P. D. Lawrence, "Electrocutaneous nerve stimulation - II: stimulus waveform selection," *IEEE Trans. Biomed. Eng.*, vol. BME-26, pp. 69–75, 1979.
- [25] C. C. Collins, "Tactile television — mechanical and electrical image projection," *IEEE Trans. Man-Mach. Sys.*, vol. MMS-11, pp. 65–71, 1970.

- [26] C. C. Collins, "On mobility aids for the blind," in *Electronic Spatial Sensing for the Blind*, D. H. Warren and E. R. Strelow, Eds. Dordrecht, The Netherlands: Martinus Nijhoff, 1985, pp. 35–64.
- [27] C. C. Collins and P. Bach-y-Rita, "Transmission of pictorial information through the skin," *Adv. Biol. Med. Phys.*, vol. 14, pp. 285–315, 1973.
- [28] C. C. Collins and J. M. J. Madey, "Tactile sensory replacement," in *Proc. San Diego Biomed. Symp.*, vol. 13, 1974, pp. 15–26.
- [29] C. C. Collins and F. A. Saunders, "Pictorial display by direct electrical stimulation of the skin," *J. Biomed. Sys.*, vol. 1, pp. 3–16, 1970.
- [30] J. C. Craig, "Pictorial and abstract cutaneous displays," in *Proc. Conf. Cutan. Comm. Sys. Dev.*, F. A. Geldard, Ed., Psychonomic Society, 1973, pp. 78–83.
- [31] I. Darian-Smith and L. E. Oke, "Peripheral neural representation of the spatial frequency of a grating moving across the monkey's finger pad," *J. Physiol.*, vol. 309, pp. 117–133, 1980.
- [32] A. L. Dellon, *Evaluation of Sensibility and Re-Education of Sensation in the Hand*. Baltimore, MD: Williams and Wilkins, 1981.
- [33] W. Epstein, "Amodal information and transmodal perception," in *Electronic Spatial Sensing for the Blind*, D. H. Warren and E. R. Strelow, Eds. Dordrecht, The Netherlands: Martinus Nijhoff, 1985, pp. 421–430.
- [34] B. Frankenhauser and A. F. Huxley, "The action potential in the myelinated nerve fiber of *Xenopus Laevis* as computed on the basis of voltage clamp data," *J. Physiol. (London)*, vol. 171, pp. 302–315, 1964.

- [35] E. P. Gardner, "Cortical neuronal mechanisms underlying the perception of motion across the skin," in *Somatosensory Mechanisms*, C. v. Euler, O. Franzen, U. Lindblom and D. Ottoson, Eds. London: MacMillan Press, 1984, pp. 93–112.
- [36] E. P. Gardner and W. A. Spencer, "Sensory Funneling. I. Psychophysical observations of human subjects and responses of cutaneous mechanoreceptive afferents in the cat to patterned skin stimuli," *J. Neurophysiol.*, vol. 35, pp. 925–953, 1972.
- [37] L. A. Geddes, *Electrodes and the Measurement of Bioelectric Events*. New York: Wiley, 1972.
- [38] L. A. Geddes and L. E. Baker, *Principles of Applied Biomedical Instrumentation*, 3rd ed. New York: Wiley, 1989.
- [39] F. A. Geldard, "Some neglected possibilities of communication," *Science*, vol. 131, pp. 1583–1588, 1960.
- [40] F. A. Geldard, "Body English," *Psych. Today*, vol. 2, pp. 43–47, 1968.
- [41] F. A. Geldard, *The Human Senses*. New York: Wiley, 1972.
- [42] F. A. Geldard, "The mutability of time and space on the skin," *J. Acoust. Soc. Am.*, vol. 77, pp. 233–237, 1985.
- [43] G. A. Gescheider, "Some comparisons between touch and hearing," *IEEE Trans. Man-Mach. Sys.*, vol. MMS-11, pp. 28–35, 1970.
- [44] G. A. Gescheider, B. F. Sklar, C. L. V. Doren and R. T. Verrillo, "Vibrotactile forward masking: Psychophysical evidence for a triplex theory of cutaneous mechanoreception," *J. Acoust. Soc. Am.*, vol. 78, pp. 534–543, 1985.

- [45] G. A. Gescheider and R. T. Verrillo, "Vibrotactile frequency characteristics as determined by adaptation and masking procedures," in *Sensory Functions of the Skin of Humans*, D. R. Kenshalo, Ed. New York: Plenum Press, 1978, pp. 183–203.
- [46] R. H. Gibson, "Electrical stimulation of pain and touch," in *The Skin Senses*, D. R. Kenshalo, Ed. Springfield, IL: Charles C. Thomas, 1968, pp. 223–260.
- [47] J. P. Girvin, L. E. Marks, J. L. Antunes, D. O. Quest, M. D. O'Keefe, P. Ning and W. H. Dobelle, "Electrocutaneous stimulation I. The effects of stimulus parameters on absolute threshold," *Percept. Psychophys.*, vol. 32, pp. 524–528, 1982.
- [48] M. H. Goldstein and A. Proctor, "Tactile aids for profoundly deaf children," *J. Acoust. Soc. Am.*, vol. 77, pp. 258–265, 1985.
- [49] W. Greatbatch, "Metal electrodes in bioengineering," *CRC Crit. Rev. Biomed. Eng.*, vol. 5, pp. 1–36, 1981.
- [50] S. Grimnes, "Electrovibration, cutaneous sensation of microampere current," *Acta. Physiol. Scand.*, vol. 118, pp. 19–25, 1983.
- [51] S. Grimnes, "Skin impedance and electro-osmosis in the human epidermis," *Med. & Biol. Eng. & Comput.*, vol. 21, pp. 739–749, 1983.
- [52] S. Grimnes, "Pathways of ionic flow through human skin in vivo," *Acta. Derm. Venerol. (Stockh)*, vol. 64, pp. 93–98, 1984.
- [53] S. Grimnes, Personal Communication, May, 1988.
- [54] J. F. Hahn, "Tactile adaptation," in *The Skin Senses*, D. R. Kenshalo, Ed. Springfield, IL: Charles C. Thomas, 1968, pp. 322–326.

- [55] J. F. Hahn, "Vibratory adaptation," in *Proc. Conf. Cutan. Comm. Sys. Dev.*, F. A. Geldard, Ed., Psychonomic Society, 1973, pp. 6–8.
- [56] R. G. Hallin and H. E. Torebjork, "Electrically induced A and C fiber responses in intact human skin nerves," *Exp. Brain Res.*, vol. 16, pp. 309–320, 1973.
- [57] A. Higashiyama and T. Tashiro, "Temporal and spatial integration for electrocutaneous stimulation," *Percept. Psychophys.*, vol. 33, pp. 437–442, 1983.
- [58] J. W. Hill, "Limited field of view in reading lettershapes with the fingers," in *Proc. Conf. Cutan. Comm. Sys. Dev.*, F. A. Geldard, Ed., Psychonomic Society, 1973, pp. 95–105.
- [59] D. W. Hislop, "Characteristics of reading rate and manual scanning patterns of blind Optacon readers," *Hum. Fact.*, vol. 25, pp. 379–389, 1983.
- [60] G. Jansson, "Tactile guidance of movement," *Int. J. Neurosci.*, vol. 19, pp. 37–46, 1983.
- [61] R. J. Johansson, "Tactile afferent units with small and well demarcated receptive receptive fields in the glabrous skin area of the human hand," in *Sensory Functions of the Skin of Humans*, D. R. Kenshalo, Ed. New York: Plenum Press, 1978, pp. 129–145.
- [62] R. S. Johansson and A. B. Vallbo, "Detection of tactile stimuli. Thresholds of afferent units related to psychophysical thresholds in the human hand," *J. Physiol.*, vol. 297, pp. 405–422, 1979.

- [63] R. S. Johansson, A. B. Vallbo and G. Westling, "Thresholds of mechanosensitive afferents in the human hand as measured with von Frey hairs," *Brain Res.*, vol. 184, pp. 343–351, 1980.
- [64] R. S. Johansson and G. Westling, "Signals in tactile afferents from the fingers eliciting adaptive motor responses during precision grip," *Exp. Brain Res.*, vol. 66, pp. 141–154, 1987.
- [65] K. O. Johnson and J. R. Phillips, "Tactile spatial resolution. I. Two-point discrimination, gap detection, grating resolution, and letter recognition," *J. Neurophys.*, vol. 46, pp. 1177–1191, 1981.
- [66] K. O. Johnson and J. R. Phillips, "Spatial and nonspatial neural mechanisms underlying tactile spatial discrimination," in *Somatosensory mechanisms*, C. v. Euler, O. Franzen, U. Lindblom and D. Ottoson, Eds. London: Macmillan Press, 1984, pp. 237–248.
- [67] K. A. Kaczmarek and J. G. Webster, "Voltage-current characteristics of the electrotactile skin-electrode interface," in *Proc. Annu. Int. Conf. IEEE Eng. Med. Biol. Soc.*, Seattle, WA, Y. Kim and F. A. Spelman, Eds., vol. 11, IEEE, 1989, pp. 1526–1527.
- [68] W. F. Keidel, "The cochlear model in skin stimulation," in *Proc. Conf. Cutan. Comm. Sys. Dev.*, F. A. Geldard, Ed., Psychonomic Society, 1973, pp. 27–32.
- [69] K. J. Kokjer, "The information capacity of the human fingertip," *IEEE Trans. Sys. Man. Cybern.*, vol. SMC-17, pp. 100–102, 1987.
- [70] M. W. Kovach, "Design considerations for the construction of a vibrotactile array," M.S. Thesis, Biomed. Eng., Ohio State Univ., Columbus, 1985.

- [71] R. H. LaMotte, "Intensive and temporal determinants of thermal pain," in *Sensory Functions of the Skin of Humans*, D. R. Kenshalo, Ed. New York: Plenum Press, 1978, pp. 327–358.
- [72] W. D. Larkin and J. P. Reilly, "Strength/duration relationships for electrocutaneous sensitivity: Stimulation by capacitive discharges," *Percept. Psychophys.*, vol. 36, pp. 68–78, 1984.
- [73] S. B. Leder, J. B. Spitzer, P. Milner, C. Flevaris-Phillips and F. Richardson, "Vibrotactile stimulation for the adventitiously deaf: An alternative to cochlear implantation," *Arch. Physical Med. Rehabil.*, vol. 67, pp. 754–758, 1986.
- [74] C. Lin, "Electrodes for Sensory Substitution," M. S. Thesis, Electrical Engineering, Univ. of Wisconsin-Madison, 1984.
- [75] U. Lindblom, "Properties of touch receptors in distal glabrous skin of the monkey," *J. Neurophysiol.*, vol. 28, pp. 966–985, 1965.
- [76] U. Lindblom, "The afferent discharge elicited by vibrotactile stimulation," *IEEE Trans. Man-Mach. Sys.*, vol. MMS-11, pp. 2–5, 1970.
- [77] J. M. Loomis and C. C. Collins, "Sensitivity to shifts of a point stimulus: An instance of tactile hyperacuity," *Percept. Psychophys.*, vol. 24, pp. 487–492, 1978.
- [78] N. Maalej and J. G. Webster, "A miniature electrooptical force transducer," *IEEE Trans. Biomed. Eng.*, vol. 35, pp. 93–98, 1988.
- [79] R. W. Mann and S. D. Reimers, "Kinesthetic sensing for the EMG controlled "Boston Arm"," *IEEE Trans. Man-Mach. Sys.*, vol. MMS-11, pp. 110–115, 1970.

- [80] J. L. Mason and N. A. M. Mackay, "Pain sensations associated with electrocutaneous stimulation," *IEEE Trans. Biomed. Eng.*, vol. BME-23, pp. 405–409, 1976.
- [81] R. D. Melen and J. D. Meindl, "Electrocutaneous stimulation in a reading aid for the blind," *IEEE Trans. Biomed. Eng.*, vol. BME-18, pp. 1–3, 1971.
- [82] G. A. Miller, "The magical number seven, plus or minus two: Some limits on our capacity for processing information," *Psychol. Rev.*, vol. 63, pp. 81–97, 1956.
- [83] J. T. Mortimer, "Motor Prostheses," in *Handbook of Physiology, section I, The Nervous System*, V. B. Brooks, Ed. Bethesda, MD: American Physiological Society, 1981, pp. 155–187.
- [84] G. A. Mouchawar, L. A. Geddes, J. D. Bourland and J. A. Pearch, "Ability of the Lapicque and Blair strength-duration curves to fit experimentally obtained data from the dog heart," *IEEE Trans. Biomed. Eng.*, vol. 36, pp. 971–974, 1989.
- [85] M. R. Neuman, "Artificial Sensory Transducers: Quarterly Progress Report", Applied Neural Control Laboratory, Electronics Design Center, and Department of Obstetrics and Gynecology, Case Western Reserve University, Feb. 11, 1987.
- [86] E. Nunziata, C. Perez, E. Jarmul, L. E. Lipetz and H. R. Weed, "Effect of tactile stimulation pulse characteristics on sensation threshold and power consumption," *Ann. Biomed. Eng.*, vol. 17, pp. 423–435, 1989.
- [87] W. H. Olsen, "Electrical safety," in *Medical Instrumentation: Application and Design*, J. G. Webster, Ed. Boston: Houghton Mifflin, 1978, pp. 667–707.

- [88] E. A. Pfeiffer, "Electrical stimulation of sensory nerves with skin electrodes for research, diagnosis, communication and behavioral conditioning: A survey," *Med. & Biol. Eng.*, vol. 6, pp. 637–651, 1968.
- [89] C. A. Phillips, "Sensory feedback control of upper- and lower-extremity motor prostheses," *CRC Crit. Rev. Biomed. Eng.*, vol. 16, pp. 105–140, 1988.
- [90] J. R. Phillips and K. O. Johnson, "Neural mechanisms of scanned and stationary touch," *J. Acoust. Soc. Am.*, vol. 77, pp. 220–224, 1985.
- [91] F. Rattay, "Modeling the excitation of fibers under surface electrodes," *IEEE Trans. Biomed. Eng.*, vol. 35, pp. 199–202, 1988.
- [92] F. Rattay, "Analysis of models for extracellular fiber stimulation," *IEEE Trans. Biomed. Eng.*, vol. 36, pp. 676–682, 1989.
- [93] C. M. Reed, N. I. Durlach and L. D. Bradia, "Research on tactile communication of speech: A review," *AHSA Monographs*, vol. 20, pp. 1–23, 1982.
- [94] J. P. Reilly, "Peripheral nerve stimulation by induced electric currents: exposure to time-varying magnetic fields," *Med. Biol. Eng. Comput.*, vol. 27, pp. 101–110, 1989.
- [95] J. P. Reilly and R. H. Bauer, "Application of a neuroelectric model to electrocutaneous sensory sensitivity: Parameter variation study," *IEEE Trans. Biomed. Eng.*, vol. BME-34, pp. 752–754, 1987.
- [96] R. R. Riso, "Sensory augmentation for enhanced control of FNS systems," in *Ergonomics in rehabilitation*, A. Mital, Ed. New York: Taylor and Francis, 1988, pp. 253–271.

- [97] R. R. Riso and A. R. Ignagni, "Electrocutaneous sensory augmentation affords more precise shoulder position command for control of FNS orthoses," in *Proc. RESNA 8th Annu. Conf.*, Memphis, TN, 1985, pp. 228–230.
- [98] R. R. Riso, A. R. Ignagni and M. W. Keith, "Electrocutaneous sensations elicited using subdermally located electrodes," *Automedica*, vol. 11, pp. 25–42, 1989.
- [99] R. R. Riso, M. W. Keith, K. R. Gates and A. R. Ignagni, "Subdermal stimulation for electrocutaneous communication," in *Proc. Sixth Annu. Conf. Rehab. Eng.*, San Diego, 1983, pp. 321–323.
- [100] R. R. Riso, A. Y. J. Szeto and M. W. Keith, "Comparison of subdermal versus surface electrocutaneous stimulation," in *Proc. IEEE Frontiers of Engineering in Health Care Conf.*, IEEE, 1982, pp. 343–347.
- [101] C. H. Rogers, "Choice of stimulator frequency for tactile arrays," *IEEE Trans. Man-Mach. Sys.*, vol. MMS-11, pp. 5–11, 1970.
- [102] G. B. Rollman, "Electrocutaneous stimulation," in *Proc. Conf. Cutan. Comm. Sys. Dev.*, F. A. Geldard, Ed., Psychonomic Society, 1973, pp. 38–51.
- [103] P. Sandstrom, Personal Communication, May, 1988.
- [104] F. A. Saunders, "Electrocutaneous displays," in *Proc. Conf. Cutan. Comm. Sys. Dev.*, F. A. Geldard, Ed., Psychonomic Society, 1973, pp. 20–26.
- [105] F. A. Saunders, "Recommended procedures for electrocutaneous displays," in *Functional Electrical Stimulation: Applications in Neural Prostheses*, F. T. Hambrecht and J. B. Reswick, Eds. New York: Marcel Dekker, 1977, pp. 303–309.

- [106] F. A. Saunders, "Information transmission across the skin: High-resolution tactile sensory aids for the deaf and the blind," *Intern. J. Neurosci.*, vol. 19, pp. 21–28, 1983.
- [107] F. A. Saunders and C. C. Collins, "Electrical stimulation of the sense of touch," *J. Biomed. Sys.*, vol. 2, pp. 27–37, 1971.
- [108] F. A. Saunders, W. A. Hill and B. Franklin, "A wearable tactile sensory aid for profoundly deaf children," *J. Med. Sys.*, vol. 5, pp. 265–270, 1981.
- [109] B. Scharf, J. Hyvarinen, A. Poranen and M. M. Merzenich, "Electrical stimulation of human hair follicles via microelectrodes," *Percept. Psychophys.*, vol. 14, pp. 273–276, 1973.
- [110] R. F. Schmidt, "Somatovisceral sensibility," in *Fundamentals of Sensory Physiology*, R. F. Schmidt, Ed. New York: Springer-Verlag, 1986, pp. 30–67.
- [111] C. E. Sherrick, "Current prospects for cutaneous communication," in *Proc. Conf. Cutan. Comm. Sys. Dev.*, F. A. Geldard, Ed., Psychonomic Society, 1973, pp. 106–109.
- [112] C. E. Sherrick, "Basic and applied research on tactile aids for deaf people: Progress and prospects," *J. Acoust. Soc. Am.*, vol. 75, pp. 1325–1342, 1984.
- [113] D. Sinclair, *Mechanisms of Cutaneous Sensation*. New York: Oxford Univ. Press, 1981.
- [114] M. Solomonow and C. Conaway, "Plasticity in electrotactile frequency discrimination," in *Proc. IEEE Frontiers Eng. Comput. Health Care Conf.*, IEEE, 1983, pp. 570–574.

- [115] M. Solomonow, J. Lyman and A. Freedy, "Electrotactile two-point discrimination as a function of frequency, body site, laterality, and stimulation codes," *Ann. Biomed. Eng.*, vol. 5, pp. 47–60, 1977.
- [116] M. Solomonow and M. Preziosi, "Electrotactile sensation and pain thresholds and ranges as a function of body site, laterality and sex," in *Proc. IEEE Frontiers Eng. Health Care Conf.*, IEEE, 1982, pp. 329–331.
- [117] D. W. Sparks, "The identification of the direction of electrocutaneous stimulation along lineal multistimulator arrays," *Percept. Psychophys.*, vol. 25, pp. 80–87, 1979.
- [118] D. W. Sparks, L. A. Ardell, M. Bourgeois, B. Wiedmer and P. K. Kuhl, "Investigating the MESA (Multipoint Electrotactile Speech Aid): The transmission of connected discourse," *J. Acoust. Soc. Am.*, vol. 65, pp. 810–815, 1979.
- [119] D. W. Sparks, P. K. Kuhl, A. E. Edmonds and G. P. Gray, "Investigating the MESA (Multipoint Electrotactile Speech Aid): The transmission of segmental features of speech," *J. Acoust. Soc. Am.*, vol. 63, pp. 246–257, 1978.
- [120] S. S. Stevens, "The psychophysics of sensory function," in *Sensory Communication*, W. Rosenblith, Ed. Cambridge: M.I.T. Press, 1962, pp. 1–33.
- [121] R. M. Strong and D. E. Troxel, "An electrotactile display," *IEEE Trans. Man-Mach. Sys.*, vol. MMS-11, pp. 72–79, 1970.
- [122] A. Y. J. Szeto, "Relationship between pulse rate and pulse width for a constant-intensity level of electrocutaneous stimulation," *Ann. Biomed. Eng.*, vol. 13, pp. 373–383, 1985.

- [123] A. Y. J. Szeto, "Technological devices for deaf-blind children: Needs and potential impact," *IEEE Eng. Med. Biol. Mag.*, vol. 7, no. 3, pp. 25–29, 1988.
- [124] A. Y. J. Szeto and Y. Chung, "Effects of training on human tracking of electrocutaneous signals," *Ann. Biomed. Eng.*, vol. 14, pp. 369–381, 1986.
- [125] A. Y. J. Szeto and J. Lyman, "Comparison of codes for sensory feedback using electrocutaneous tracking," *Ann. Biomed. Eng.*, vol. 5, pp. 367–383, 1977.
- [126] A. Y. J. Szeto, J. Lyman and R. E. Prior, "Electrocutaneous pulse rate and pulse width psychometric functions for sensory communications," *Hum. Fact.*, vol. 21, pp. 241–249, 1979.
- [127] A. Y. J. Szeto, R. E. Prior and J. Lyman, "Electrocutaneous tracking: A methodology for evaluating sensory feedback codes," *IEEE Trans. Biomed. Eng.*, vol. BME-26, pp. 47–49, 1979.
- [128] A. Y. J. Szeto and R. R. Riso, "Sensory feedback using electrical stimulation of the tactile sense," in *Rehabilitation Engineering*, R. V. Smith and J. H. Leslie Jr., Eds. Boca Raton, FL: CRC Press, 1990, pp. 29–78.
- [129] A. Y. J. Szeto and F. A. Saunders, "Electrocutaneous stimulation for sensory communication in rehabilitation engineering," *IEEE Trans. Biomed. Eng.*, vol. BME-29, pp. 300–308, 1982.
- [130] S. Tachi, K. Tanie, K. Komoriya and M. Abe, "Electrocutaneous communication in seeing-eye robot (MELDOG)," in *Proc. IEEE Frontiers of Eng. in Health Care Conf.*, IEEE, 1982, pp. 356–361.

- [131] P. Taige, "A power minimizing stimulus for electromechanical vibrators used in a portable tactile vision substitution system," M.S. Thesis, Bio-Medical Engineering, Ohio State Univ., 1986.
- [132] W. H. Talbot, I. Darian-Smith, H. H. Kornhuber and V. B. Mountcastle, "The sense of flutter-vibration: Comparison of the human capacity with response patterns of mechanoreceptive afferents from the monkey hand," *J. Neurophys.*, vol. 31, pp. 301–334, 1968.
- [133] T. Tashiro and A. Higashiyama, "The perceptual properties of electrocutaneous stimulation: Sensory quality, subjective intensity, and intensity-duration relation," *Percept. Psychophys.*, vol. 30, pp. 579–586, 1981.
- [134] H. E. Torebjork, R. H. LaMotte and C. J. Robinson, "Peripheral neural correlates of magnitude of cutaneous pain and hyperalgesia: Simultaneous recordings in humans of sensory judgements of pain and evoked responses in nociceptors with C-fibers," *J. Neurophysiol.*, vol. 51, pp. 325–339, 1984.
- [135] H. E. Torebjork, W. Schady and J. Ochoa, "Sensory correlates of somatic afferent fibre activation," *Human Neurobiol.*, vol. 3, pp. 15–20, 1984.
- [136] T. J. Triggs, W. H. Levison and R. Sanneman, "Some experience with flight-related electrocutaneous and vibrotactile displays," in *Proc. Conf. Cutan. Comm. Sys. Dev.*, F. A. Geldard, Ed., Psychonomic Society, 1973, pp. 57–64.
- [137] B. Tursky and D. O'Connell, "Reliability and interjudgement predictability of subjective judgements of electrocutaneous stimulation," *Psychophysiol.*, vol. 9, pp. 290–295, 1972.

- [138] A. B. Vallbo, "Sensations evoked from the glabrous skin of the human hand by electrical stimulation of unitary mechanosensitive afferents," *Brain Res.*, vol. 215, pp. 359–363, 1981.
- [139] A. B. Vallbo, "Tactile sensation related to activity in primary afferents with special reference to detection problems.," in *Somatosensory Mechanisms*, C. v. Euler, O. Franzen, U. Lindblom and D. Ottoson, Eds. London: Macmillan Press, 1984, pp. 163–172.
- [140] A. B. Vallbo and R. S. Johansson, "Properties of cutaneous mechanoreceptors in the human hand related to touch sensation," *Human Neurobiol.*, vol. 3, pp. 3–14, 1984.
- [141] P. H. Veltink, J. A. v. Alste and H. B. K. Boom, "Influences of stimulation conditions on recruitment of myelinated nerve fibers: A model study," *IEEE Trans. Biomed Eng.*, vol. 35, pp. 917–924, 1988.
- [142] P. H. Veltink, B. K. v. Veen, J. J. Struijk, J. Holsheimer and H. B. K. Boom, "A modeling study of nerve fascicle stimulation," *IEEE Trans. Biomed. Eng.*, vol. 36, pp. 683–692, 1989.
- [143] R. T. Verrillo, "Temporal summation in vibrotactile sensitivity," *J. Acoust. Soc. Am.*, vol. 37, pp. 843–846, 1965.
- [144] R. T. Verrillo, "Psychophysics of vibrotactile stimulation," *J. Acoust. Soc. Am.*, vol. 77, pp. 225–232, 1985.
- [145] S. Weinstein, "Intensive and extensive aspects of tactile sensitivity as a function of body part, sex and laterality," in *The Skin Senses*, D. R. Kenshalo, Ed. Springfield, IL: Charles C. Thomas, 1968, pp. 195–218.

- [146] J. J. Wertsch, P. Bach-y-Rita, M. B. Price, J. Harris and J. Loftsgaarden, "Development of a sensory substitution system for the insensate foot," *J. Rehab. Res. Dev.*, vol. 25, no. 1, pp. 269–270, 1988.
- [147] G. K. Westling, "Sensori-motor mechanisms during precision grip in man," Ph. D. Thesis, Umea University, Sweden, 1986.
- [148] B. W. White, "Perceptual findings with the vision-substitution system," *IEEE Trans. Man-Mac. Sys.*, vol. MMS-11, pp. 54–58, 1970.
- [149] C. T. White and P. G. Cheatham, "Temporal numerosity: IV. A comparison of the major senses," *J. Exp. Psych.*, vol. 58, pp. 441–444, 1959.
- [150] J. D. Wiley and J. G. Webster, "Analysis and control of the current distribution under circular dispersive electrodes," *IEEE Trans. Biomed. Eng.*, vol. BME-29, pp. 381–385, 1982.

Table 2.2

Static Simultaneous Two-point
Discrimination Thresholds
(mm)

Body location	Static touch (a)	Vibro-tactile	Electro-tactile (d)
Fingertip	3	2 (b)	<7 (*)
Palm	10	?	8
Forehead	17	?	?
Abdomen	36	?	10
Forearm	38	?	9
Back	39	11-18(c)	5(e)-10
Thigh	43	?	10
Upper arm	44	?	9
Calf	46	?	9
Refs: a:[145], b:[16], c:[5], d:[115], e:[28]			
(*): 7mm was smallest distance which apparatus in [115] could measure.			

Table 2.4

Estimates of Perceptual Information
Flow from Tactile Stimuli

Ref. []	Method	Number of channels	Information rate (bits/s)
110	?	?	5
102	Reaction time	1	5
69	Fusion freq. of vibratory bursts	1	2-56
69	Optacon reading	144	5-10
149	Counting stimuli	1	12

Table 2.5

Discernible levels of Subjective
Intensity of Electrotactile and
Vibrotactile (*) Stimulation
(Number of JNDs)

Ref. []	Location	Variable	Number of levels
107	Abdomen	Current	59
1	Abdomen	Current	32
114	Palm	Frequency	13
130	Arm	Energy	8-16
130	Arm	Frequency	6-8
39	? (*)	Amplitude	15

Table 2.6

Just-Noticeable Differences of
Electrotactile and Vibrotactile (*)
Stimulation

Ref. []	Location	Variable	JND %
28	Abdomen	Width	> 6
85	Arm	Current	9-29
	Arm (Sub)	Current	8-42
88	?	Current	2-6
	?	Frequency	> 2
100	Arm	Frequency	15-30
	Arm (Sub)	Frequency	10-25
104	Abdomen	Current	3.5
	Abdomen	# Pulses	10
114	Palm	Frequency	19-24
126	Arm	Frequency	16-38
	Arm	Width	37-46
129	Several	Width	8-10
	Several	Current	8-10
68	? (*)	Frequency	5-10

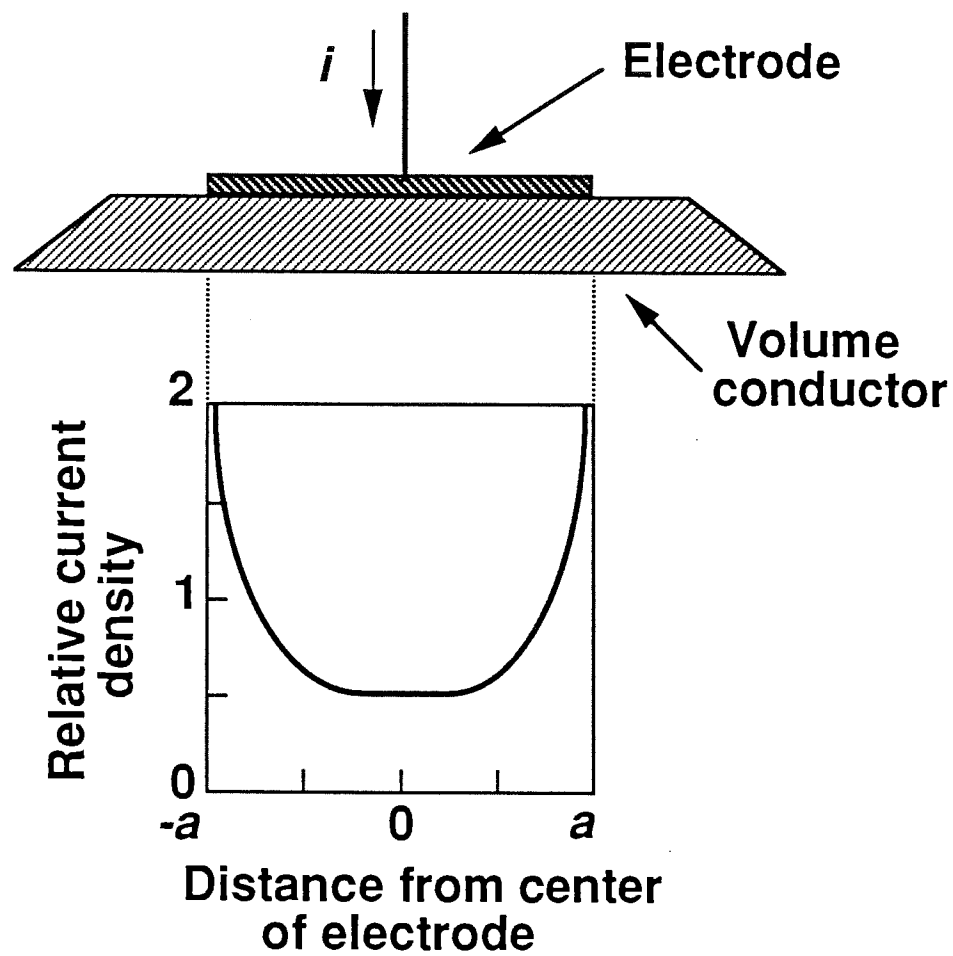


Fig. 2.1. Current density at the surface of a homogeneous volume conductor as a function of distance from the center of a circular stimulation electrode of radius a . Adapted from [150].

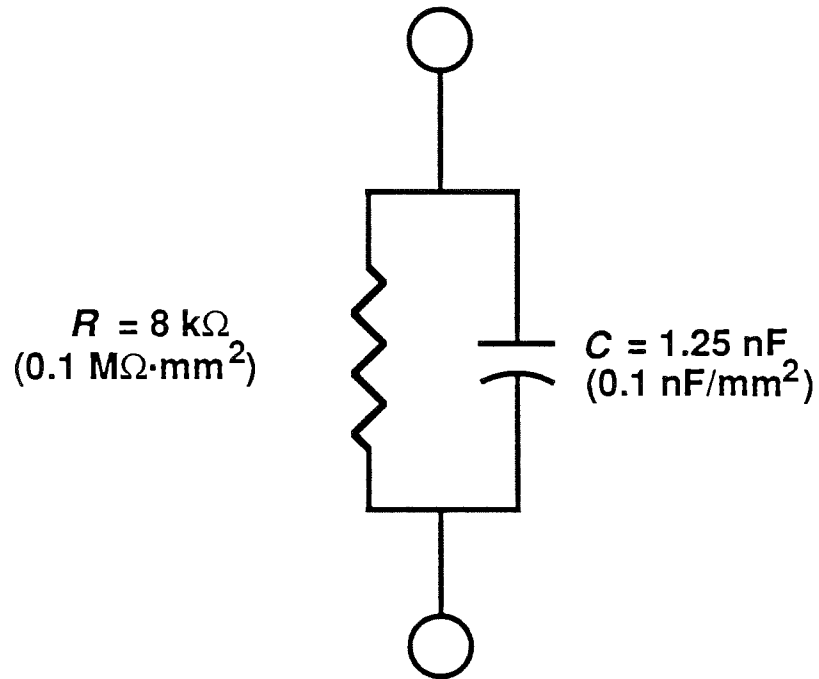


Fig. 2.2. Simplified electrical model of the electrode-skin interface. The resistance R and capacitance C shown are for a 12-mm^2 area metal electrode on the abdomen [105]. Values in parentheses are normalized to the electrode area. R and C vary with electrode type and skin condition.

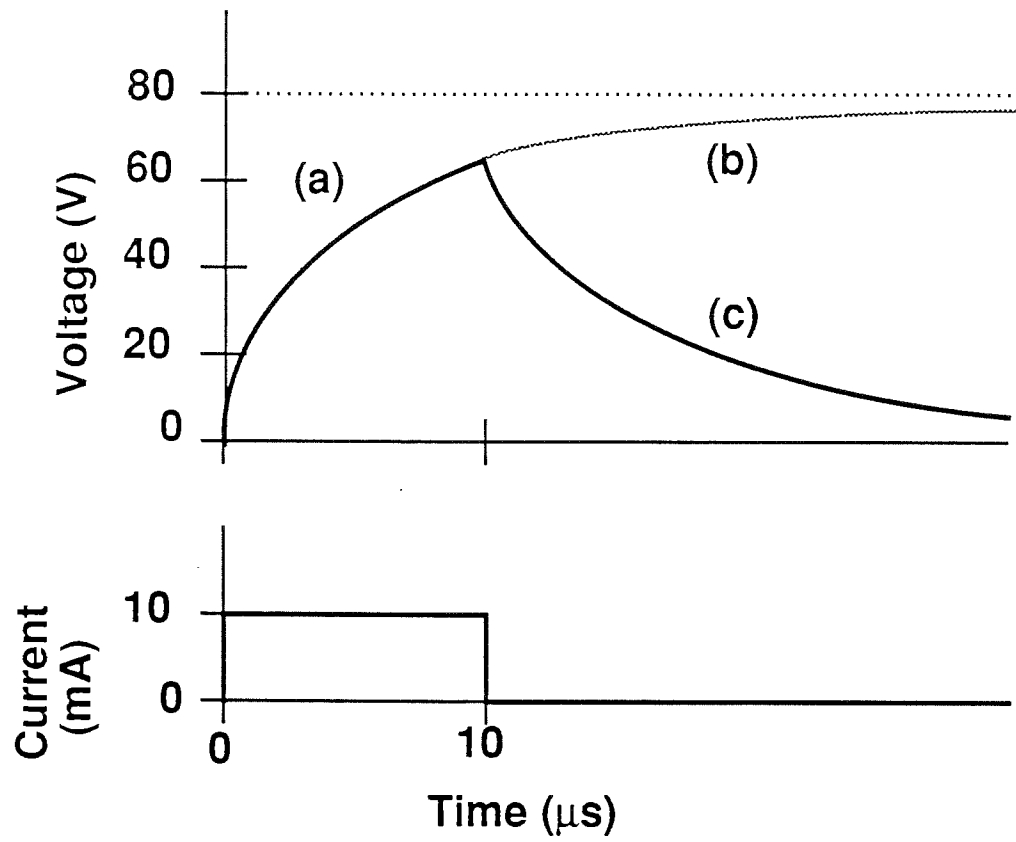


Fig. 2.3. Voltage on the 12-mm² area active center with respect to the outer ring of a coaxial electrode stimulated with 10-mA, 10- μs constant current pulses. (a) Charging region; (b) Resistive heating region; (c) Discharge region. Adapted from [105].

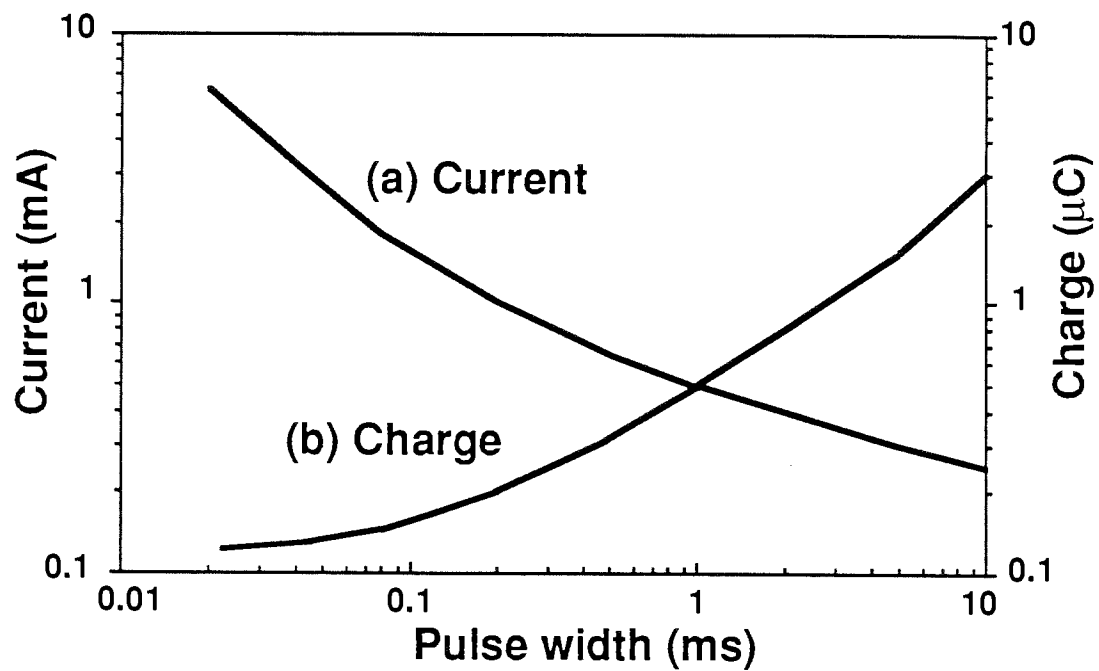


Fig. 2.4. Electrotactile sensation threshold (a) current and (b) charge as a function of monophasic pulse duration. Data from [102].

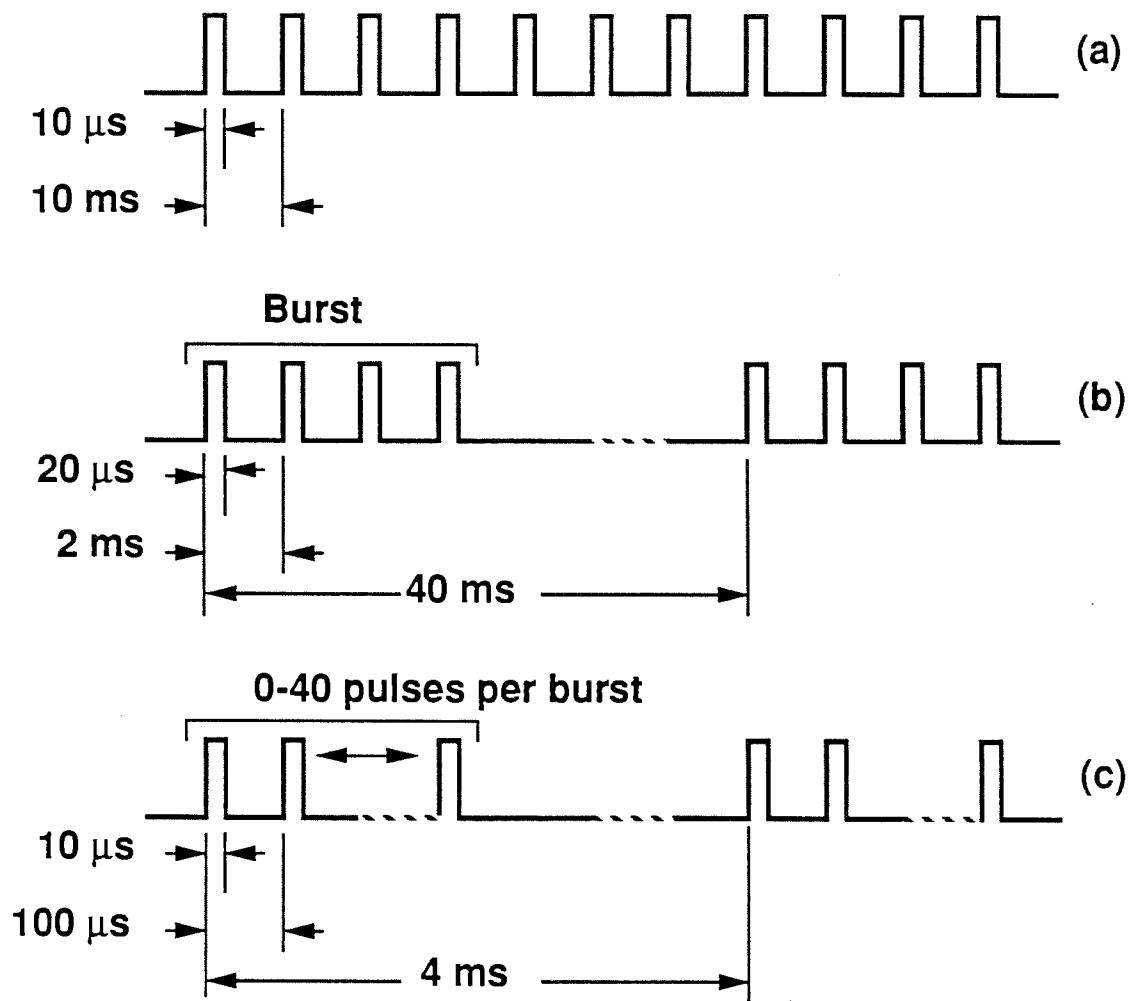


Fig. 2.5. Electrotactile stimulation waveforms. (a) Continuous 100-Hz pulse train, subject to adaptation; (b) 500-Hz bursts of pulses at a 25-Hz rate, less subject to adaptation; (c) 10-kHz bursts of pulses, the subjective intensity increases with the number of pulses per burst.

Chapter 3

VOLTAGE-CURRENT CHARACTERISTICS OF THE ELECTROTACTILE SKIN-ELECTRODE INTERFACE

Original Experiments and Model

Published as:

K. A. Kaczmarek and J. G. Webster, "Voltage-current characteristics of the electrotactile skin-electrode interface," in *Proc. Annu. Int. Conf. IEEE Eng. Med. Biol. Soc.*, Seattle, WA, Y. Kim and F. A. Spelman, Eds., vol. 11, IEEE, 1989, pp. 1526–1527.

ABSTRACT

During electric stimulation of the sense of touch the static skin-electrode resistance decreases nonlinearly with increasing stimulation current. We present a mathematical model which fits these data and has a possible physical explanation. We also model the voltage vs. time response of an electrode stimulated with constant-current pulses. We provide two possible explanations for this characteristic.

INTRODUCTION

Localized tactile sensations ranging from tingle to vibration to stinging are produced when pulses of current (10–500 μ s, 1–20 mA, 1–100 Hz) are passed into the skin through 1–10-mm skin electrodes. Szeto and Saunders [1] review applications of electrotactile stimulation including sensory prostheses for the deaf and blind.

We can use the electrical properties of stimulated electrodes to design a practical stimulator circuit and to provide insight into the nature of the skin-electrode interface. We have used pulsatile stimulation because sinusoidal excitation obscures the fundamental nonlinearities of the skin-electrode interface. The term "impedance" is therefore only properly used to describe the small-signal (e.g. biopotential recording) properties of the nonlinear skin-electrode system.

We used balanced biphasic current waveforms (zero net dc current) but show data only for the positive phase. The negative phase gives similar results.

The electrodes used are those of the Tacticon (Concord, CA) model 1600 auditory prosthesis. Sixteen 5.5-mm gold-plated electrodes are mounted on a belt which encircles the abdomen. All of the electrodes share a common reference plane which is the conductive rubber base material of the belt. The skin and belt were

moistened with tap water before the experiment to facilitate proper electrical contact [1].

STATIC V-I CHARACTERISTIC AND MODEL

Figure 3.1 shows the voltage recorded across an electrode stimulated with 1-mA, 400- μ s pulses at a rate of 10 pulses/s. Consider now only the steady-state electrode voltage V_m near the end of the current pulse. Figure 3.2 shows that this voltage increases nonlinearly with stimulation current. Figure 3.3 shows the same data plotted as static resistance ($R = V_m/I$) vs. current.

A mathematical model which fits the data in Figs. 3.2 and 3.3 is

$$R(i) = R_0 + R_p R_v(i) / (R_p + R_w(i)) \quad (1)$$

$$R_v(i) = R_p I_0 / i \quad (2)$$

where R_0 , R_p , and I_0 are empirically-determined constants. Figure 3.4(a) shows a simple physical realization of (1) and (2). The exact correspondence (if any) of the elements of Fig. 3.4(a) to the skin-electrode interface is not known. Szeto and Saunders [1] and Grimnes [2] propose that the sweat ducts carry most of the current across the skin, so the current density in these ducts may be high enough to heat the sweat. However, the conductance of 0.017-0.051 mM NaCl solution (the approximate ionic content of sweat) only increases 100% from 40°C to 100°C. Therefore, heating of sweat in the sweat ducts cannot account for the 30-fold change in $R(i)$. Grimnes [3] discusses other possible mechanisms including electrically-driven filling of sweat ducts.

A least-squares nonlinear regression using the SYSTAT software package determined the following values for the constants in (1) and (2) using the data in Fig. 3.2: $R_0 = 0.895 \text{ k}\Omega$, $R_p = 60.1 \text{ k}\Omega$ and $I_0 = 0.585 \text{ mA}$.

Boxtel [4] and Gibson [5] further discuss the nonlinear characteristic of the skin-electrode interface.

DYNAMIC VOLTAGE CHARACTERISTIC WITH CONSTANT CURRENT STIMULATION

A casual glance at Fig. 3.1 suggests that the voltage response to a constant current pulse is a simple exponential rise and fall modeled by the classical electrode model Fig. 3.4(b). The Fig. 3.4(b) skin-electrode voltage is:

$$\text{Rise: } v(t) = V_m(1 - e^{-t/\tau}) \quad (3)$$

$$\text{Fall: } v(t) = V_m e^{-t/\tau} \quad (4)$$

where $\tau = RC$ and $V_m = IR$. Note that t in the fall phase is normalized so that $t = 0$ corresponds to the end of the current pulse. We also ignore the series resistor in Fig. 3.4(b); its value of 200–900 Ω is small compared to the total electrode resistance. It likely represents the electrolyte-electrode resistance. We measured a resistance of 565–625 Ω for the electrode applied to a saline-soaked (34 mM) paper towel at currents of 0.1, 1, and 10 mA.

Figure 3.1 shows the voltage predicted by (3) and (4) where V_m and τ are chosen for a least-squares fit. ($V_m = 27.7 \text{ V}$ and $\tau = 46.7 \text{ }\mu\text{s}$.) While the rise phase is

modeled quite well by (3), the fall phase is not modeled by (4). Not only are the model parameters changing between the rise and fall phases, but the model itself is changing or is inadequate.

Since the skin is a multilayer structure, we might assume the double exponential model in Fig. 3.4(c), which is described by:

$$\text{Rise: } v(t) = V_{m1}(1 - e^{-t/\tau_1}) + V_{m2}(1 - e^{-t/\tau_2}) \quad (5)$$

$$\text{Fall: } v(t) = V_{m1}e^{-t/\tau_1} + V_{m2}e^{-t/\tau_2} \quad (6)$$

We were not able to find parameters for (5) using the data in Fig. 3.1; V_{m1} and τ_1 tended toward V_m and τ in the simple model (1) and τ_2 tended to infinity.

We conclude that for the rise phase, a double exponential model is not necessary.

However, Fig. 3.1 shows that (6) models the falling phase much better than (4). ($V_{m1} = 19.6$ V, $V_{m2} = 7.8$ V, $\tau_1 = 52.8$ μ s and $\tau_2 = 642.6$ μ s.

Using two different models for rise and fall seems unphysiological. It is likely that a better model might have time-varying parameters.

REFERENCES

- [1] A. Y. J. Szeto and F. Saunders, "Electrocutaneous stimulation for sensory communication in rehabilitation engineering," *IEEE Trans. Biomed. Eng.*, Vol. BME-29, pp. 300–308: 1982.
- [2] S. Grimnes, "Pathways of ionic flow through human skin in vivo," *Acta Derm. Venerol. (Stockh.)*, Vol. 64, pp. 93–98: 1984.
- [3] S. Grimnes, "Skin impedance and electro-osmosis in the human epidermis," *Med. Biol. Eng. Comput.* Vol. 21, pp. 739–749: 1983.
- [4] A. v. Boxtel, "Skin resistance during square-wave electrical pulses of 1 to 10 mA," *Med. Biol. Eng. Comput.*, vol. 15, pp. 679–687, 1977.
- [5] R. H. Gibson, "Electrical stimulation of pain and touch," in *The Skin Senses*, D. R. Kenshalo, Ed. Springfield, IL: Charles C. Thomas, 1968, pp. 223–260.

This work was supported by NIH grant NS26328.

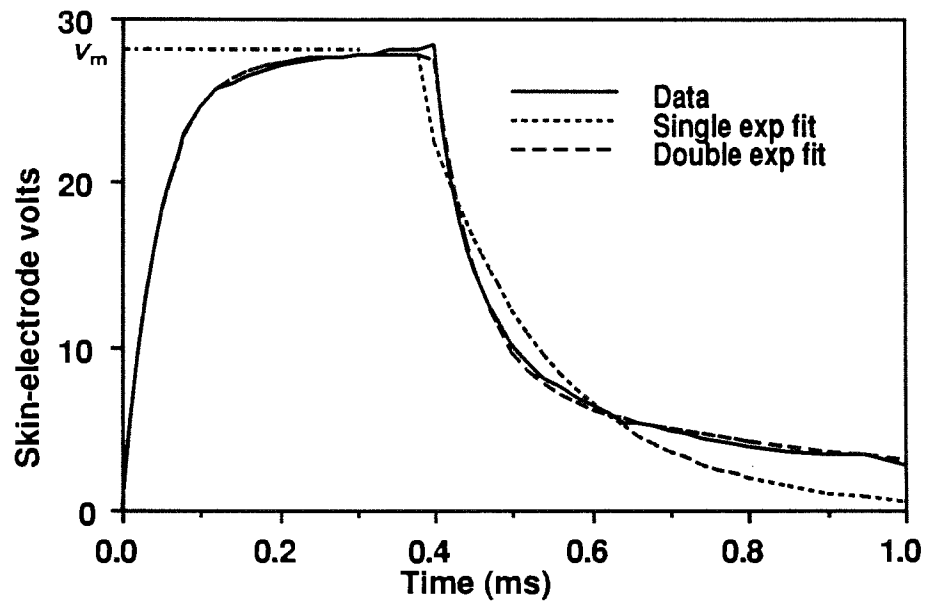


Fig. 3.1. Electrode voltage from a 400- μ s current pulse; two exponential models.

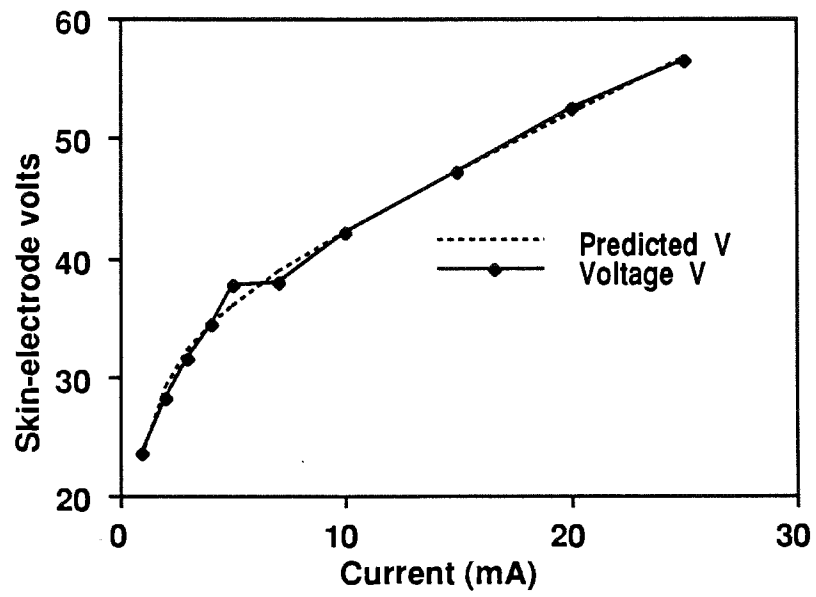


Fig. 3.2. Voltage across the skin–electrode interface as a function of stimulation current.

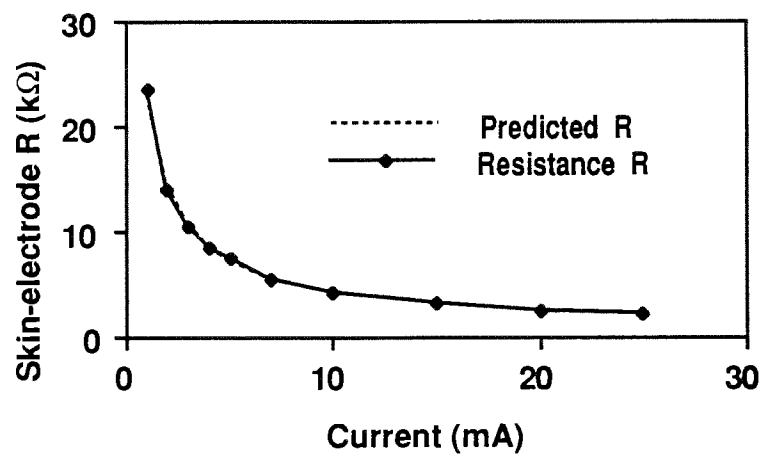


Fig. 3.3. Resistance of skin–electrode interface as a function of stimulation current.

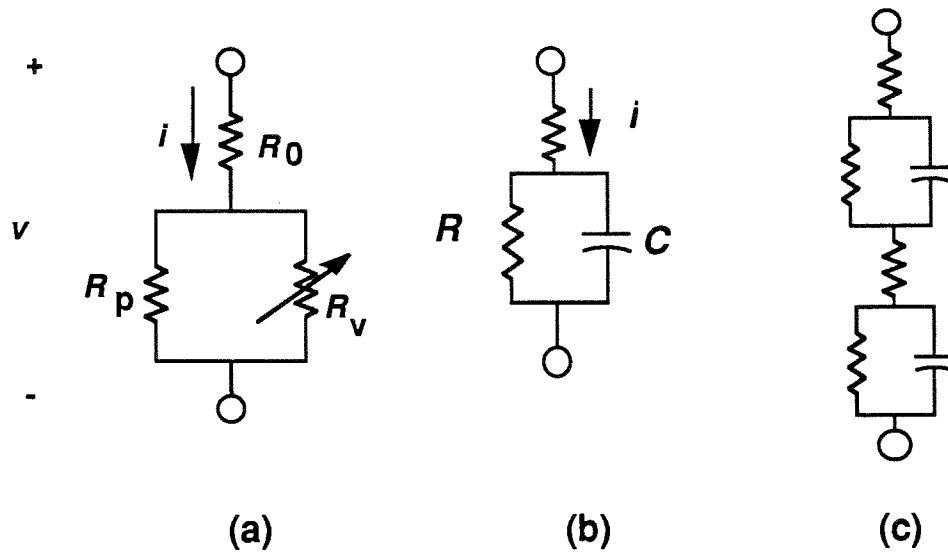


Fig. 3.4. Electrode-skin models.

- (a) Nonlinear static resistance model.
- (b) Single exponential dynamic model.
- (c) Double exponential dynamic model.

Chapter 4

PERIODIC VARIATIONS IN THE ELECTROTACTILE SENSATION THRESHOLD

Original Experiments

Published as:

K. A. Kaczmarek, J. G. Webster and R. G. Radwin, "Periodic variations in the electrotactile sensation threshold," in *Proc. Annu. Int. Conf. IEEE Eng. Med. Biol. Soc.*, Philadelphia, PA, P. C. Pedersen and B. Onaral, Eds., vol. 12, IEEE, 1990, pp. 1060-1061.

ABSTRACT

The sensation threshold current for electrotactile (electrocutaneous) stimulation increases and decreases over time with a period of 3–10 min. The magnitude of these variations ranges from unmeasurably small to 25% of the average sensation threshold. The thresholds of two electrodes separated on the skin by 11 cm are loosely correlated in time. These periodic variations do not appear to be related to changes in the static electrode–skin resistance, to respiration, cutaneous blood flow, or to the periodic sampling process used in measurement.

INTRODUCTION

Localized tactile sensations ranging from tingle to vibration to stinging are produced when pulses of current (10–500 μ s, 1–20 mA, 1–100 Hz) are passed into the skin through 1–10-mm diameter skin electrodes. Electrotactile stimulation may be useful for tactile displays as part of sensory prostheses for the deaf and blind [1], [2].

It has long been known that the sensation threshold, strength, and "quality" of electrotactile stimulation vary with the stimulation waveform, and with the location, size, and geometry of the electrode on the skin. However, we do not believe that periodic time variations have been previously reported, perhaps because they have been dismissed as random noise.

MATERIALS

An automated electrotactile stimulation system (ETSS) provides stimuli and response logging for all experiments. A custom waveform generation (WG) circuit

controlled by an IBM PC produces balanced-biphasic pulses (100- μ s positive phase, 100- μ s interphase interval, 100- μ s negative phase) at a repetition rate of 10 Hz.

A custom voltage-to-current converter (VIC) circuit converts the voltage waveforms from the WG into current waveforms for the stimulation electrodes. The VIC has an maximal voltage compliance of 100 V and an output resistance of 2–5 M Ω so that the stimulation current is independent of electrode impedance over the expected range of approximately 1–25 k Ω [3]. The pulse rise and fall times are less than 1 μ s.

The electrodes used are those of the Tacticon (Concord, CA) model 1600 auditory prosthesis. Sixteen 5.5-mm gold-plated electrodes are mounted on a belt which encircles the abdomen. All of the electrodes share a common reference plane which is the conductive rubber base material of the belt. The skin and belt are moistened with tap water before the experiment to facilitate proper electrical contact [2]. The belt is mounted 15 min before the experiment.

For the few experiments using vibrotactile (vibrating) simulation, 600- μ s current pulses drive miniature audio transducers (Star Micronics QMB-105) at a pulse repetition rate of 10 Hz. Because these transducers are highly nonlinear, the mechanical waveform at the abdominal skin is unknown. White noise from headphones worn by the subject masks the noise from the transducers to prevent aural cues.

A potentiometer connected to the PC via an analog-to-digital converter allows the subject to control the stimulation current (or vibration amplitude) when prompted. The PC records stimulation current with an accuracy of $\pm 5\%$ and a linearity of $\pm 2\%$ over the ETSS operating range 1–40 mA.

To prevent the subject from using potentiometer position as a cue for determining sensation thresholds, the relationship between potentiometer rotation and stimulation current is different for each experimental trial. The function is

$$i = 7.5(x - RND/2) \quad \text{subject to } i \geq 0$$

where i is the stimulation current in mA; x is the potentiometer position and 0 is fully counter-clockwise (CCW) and 1 is fully clockwise (CW); and RND is a random number between 0 and 1.

METHODS

Every 15 or 30 s as requested, the subject sequentially determined the sensation threshold for two electrodes "A" and "B" separated by 11 cm on the electrode belt (5 electrodes in from the left and right ends of the belt, respectively).

A modified method of limits provided rapid determination of the sensation thresholds (15 s for both determinations). At the appropriate instant, we instructed the subject to turn the potentiometer CW from zero until he could just feel the stimulus. Frequently, the subject would overshoot the threshold position because of the randomization function. The subject then readjusted the knob CCW (and CW again if required) until the stimulus was just perceptible. The subject always determined how many such readjustments were required to find the threshold before entering the response by pressing a button. With 5 min of practice this tweaking process became second-nature.

Approximately 32 min of data collection provided either 128 or 64 threshold determinations for each electrode, depending on whether the sampling interval was 15 s or 30 s. The sequential nature of the threshold determinations causes the electrode B data to be approximately 10 s behind electrode A data (not shown on graphs).

All of the data in the graphs were collected with the first author as the (best-trained) subject. Data from two other subjects show a bit more scatter, but otherwise similar results. All three subjects were 25–30-year old male university graduate students.

RESULTS AND DISCUSSION

Figure 4.1 shows a typical plot of the electrotactile sensation threshold vs. time for the 32-min experiment with a 30-s sampling interval. The cyclical nature of the sensation thresholds is evident above the scatter, but the period repetition and general shape of the data over time are not clear. In this plot, for example, the period for electrode B seems to change from 9 min to 4 min over the course of the experiment. Replications of this experiment showed more and less data scatter and more and less uniformity of the cyclical variations. In some cases, the variations seem entirely random. In other cases, the peak-to-peak amplitude of the fluctuations was as much as 25% of the average threshold.

To illustrate whether the sensation thresholds for the two electrodes are correlated in time, Fig. 4.2 shows a scatterplot of the same data as in Fig. 4.1. A positive correlation is evident from visual inspection; the correlation coefficient $r = 0.52$. Three replications of this experiment showed less correlation: 0.22, 0.28,

and 0.28. All, however, were positive, indicating that there is likely some common mechanism affecting the sensation threshold at both skin sites. This mechanism may or may not be the same one responsible for the periodicity.

We chose 64 and 128-point samples so that a fast-Fourier transform (FFT) could provide frequency domain information not visible in the time plots. However, the power spectra of most of the data were too noisy to identify frequency peaks relating to periodic behavior. To improve the signal-to-noise ratio in this analysis, we averaged the power spectra for 4 replications of the above experiment (a total of 8 spectra, because each experiment produces two time series). Figure 4.3 shows that a clear peak of periodic activity occurs at 0.16 cycles/min, or a period of 6.4 min.

Visual inspection of time plots of these and other similar experiments reveals periods of 3–10 min. Note the vertical axis scaling; the dc component is at 10000, well off the scale. The low-frequency peak at 0.031 cycles/min (32-min period) represents the slow upward drift of sensation thresholds during the experiments. This drift was not always evident and not always positive.

Other experiments attempted to determine the source of the periodic threshold variations. A 15-s sampling period showed similar results to a 30-s period, indicating that 30 s is not special in any way. Further proof of this was provided by an experiment with random sampling times; the period between samples varied randomly from 10 s – 60 s. This method of data collection did not eliminate the periodicity.

To determine if respiration (which causes mechanical stretch on abdominal skin) could be involved, we had the subject determine sensation thresholds only at peak expiration in quiet tidal breathing, with the breath gently held during the

threshold determination. No differences were apparent between these data and data taken with normal breathing.

We found that the periodic activity occurred for electrotactile stimulation on the thigh as well as the abdomen, ruling out the possible influence of gastric and intestinal smooth muscle activity.

Because the static resistance [3] of the electrode-skin interface did not change during a 30-min period with periodic application of a 1-mA test stimulus, changes in the electrode-skin interface are not likely responsible for the periodicity.

Cutaneous blood flow varies with time, alertness, and other factors. Using the thermal blood flow transducer described by Dittmar [4], we found no correlation between sensation threshold and cutaneous blood flow in the vicinity of the stimulation electrode.

Finally, the sensation threshold for vibrotactile stimulation on the abdomen showed similar periodic behavior, further suggesting that the mechanism is not related to the electrical properties of the electrode-skin interface. Although not mentioned in the article, data from the vibrotactile adaptation study by Hahn [5] show periodic behavior.

REFERENCES

- [1] K. A. Kaczmarek, J. G. Webster, P. Bach-y-Rita and W. J. Tompkins, "Electrotactile and vibrotactile displays for sensory substitution," *IEEE Trans. Biomed. Eng.*, vol. 38, pp. 1–16, 1991.
- [2] A. Y. J. Szeto and F. Saunders, "Electrocutaneous stimulation for sensory communication in rehabilitation engineering," *IEEE Trans. Biomed. Eng.*, vol. BME-29, pp. 300–308, 1982.
- [3] K. A. Kaczmarek, "Voltage-current characteristics of the electrotactile skin-electrode interface," *Proc. Annu. Int. Conf. IEEE Eng. Med. Biol. Soc.*, vol. 11, pp. 1526–1527, 1989.
- [4] A. Dittmar, "Skin thermal conductivity," in *Cutaneous Investigation in Health and Disease*, J.-L. Leveque, Ed. New York: Marcel Dekker, 1989, pp. 323–358.
- [5] J. F. Hahn, "Vibrotactile adaptation and recovery measured by two methods," *J. Exp. Psychol.*, vol. 71, pp. 655–658, 1966.

This work was supported by NIH grant NS26328.

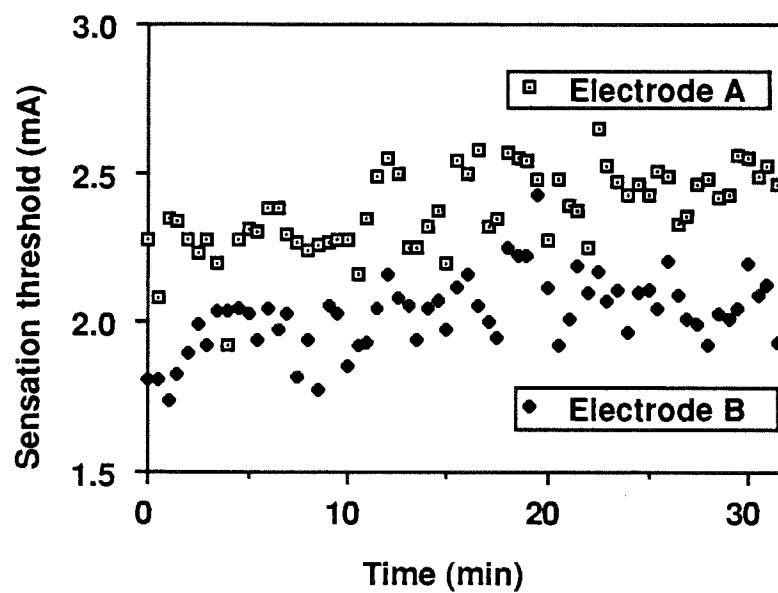


Fig. 4.1. The electrotactile sensation threshold varies periodically with time.

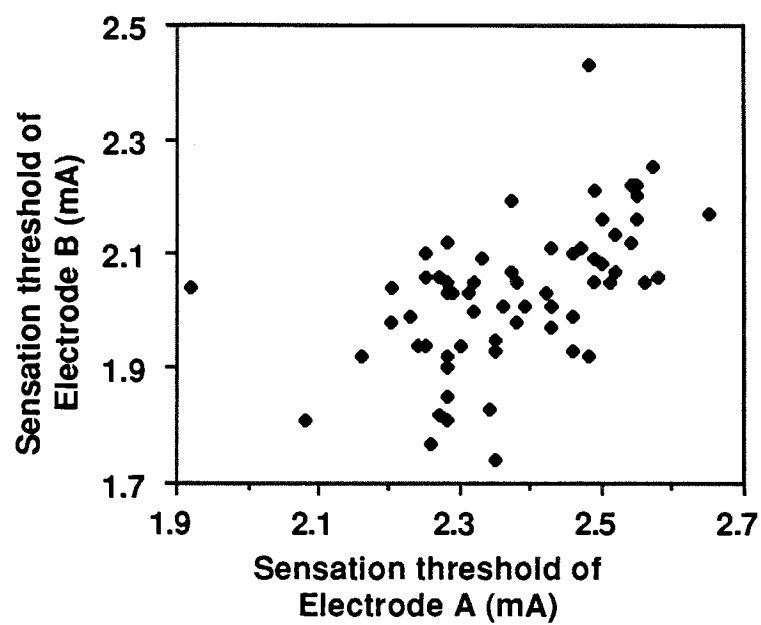


Fig. 4.2. The electrotactile sensation thresholds of two electrodes are loosely correlated in time.

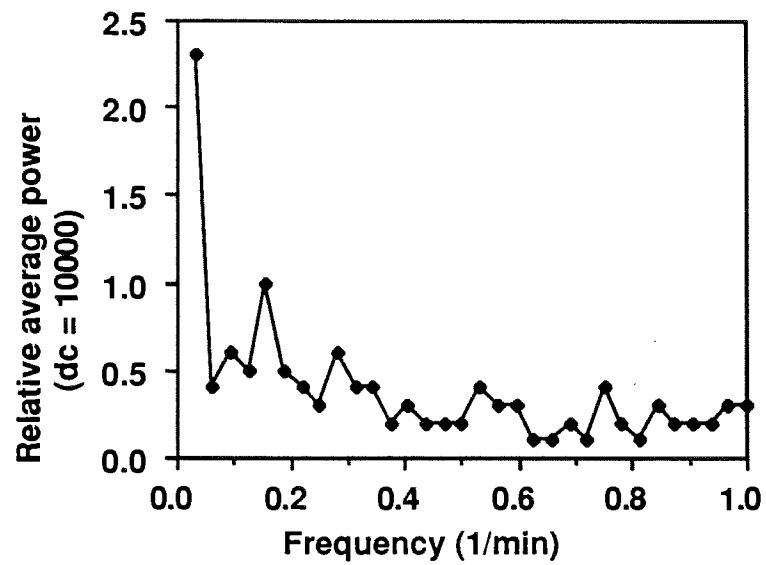


Fig. 4.3. The average power spectrum of the sensation threshold for eight electrodes shows a peak at a period of 1 cycle/6.4 min.

Chapter 5

A 16-CHANNEL 8-PARAMETER WAVEFORM ELECTROTACTILE STIMULATION SYSTEM

Experimental Instrumentation

Published as:

K. A. Kaczmarek, K. M. Kramer, J. G. Webster and R. G. Radwin, "A 16-channel 8-parameter waveform electrotactile stimulation system," *IEEE Trans. Biomed. Eng.*, vol. 38, no. 10, 1991 (in press).

ABSTRACT

We have developed a general-purpose electrotactile (electrocutaneous) stimulation system as a research tool for studying psychophysiological performance associated with various stimulation waveforms. An experimenter-defined command file specifies the stimulation current and waveform of each of the 16 channels. The system provides burst onset delay of 0 – 20 ms, phase current of 0 – 50 mA, interphase interval of 0 – 1000 μ s, number of pulses per burst from 1 – 100, pulse repetition rate of 0.1 – 25 kHz, phase width of 2 – 1000 μ s, and functionally-monophasic pulses (with zero dc current) or balanced-biphasic pulses (with equal positive and negative phases). The system automatically delivers the desired stimulation, prompts the subject for responses, and then logs subject responses. Key features of the system are (1) very flexible choice of bursts of pulsatile waveforms, (2) real-time control of all of the waveform parameters as mathematical functions of external analog inputs, and (3) high-performance electrode-driver circuitry.

INTRODUCTION

Electrotactile stimulation evokes tactile (touch) sensations within the skin at the location of the electrode by passing a local electric current through the skin. Sensory substitution is the use of one human sense (in this case, touch) to receive environmental information normally received by another sense (often vision or hearing). For the sense of touch, sensory substitution is the use of one area of skin to receive tactile information normally received at another location. Several articles review technology and devices for electrotactile stimulation [1], [2], visual substitution [3], [4], auditory substitution [5], [6], [7], and other applications [2], [8], [9], [10], [11], [12].

Limitations Of Present Electrotactile Displays

Insufficient Dynamic Range: A substantial limitation of present electrotactile displays is that they lack sufficient intensity dynamic range. Our normal senses of vision, hearing, and touch can mediate stimuli which we perceive as strong or intense without being painful. Electrotactile stimulation, on the other hand, can develop an uncomfortable stinging quality even at moderate stimulation levels if improper stimulation waveforms or electrodes are used. The traditional measure of intensity dynamic range is the ratio of the stimulation currents required to produce sensation threshold I_S and pain threshold I_P . I_P/I_S typically ranges from 2 – 4 for unexperienced subjects and 6 – 8 for experienced subjects [13]. This range is a limitation for intensity-modulated stimulation codes but not necessarily for frequency or spatially-modulated codes.

Interpretation of Unfamiliar Sensations: Electrotactile stimulation produces sensations that are often unfamiliar and not comparable to normal touch sensations. In particular, the relationship between the stimulus intensity (current) and the perceived sensation is quite different than that for normal touch. Research using this instrumentation will provide information to assist in the design of appropriate information processing schemes for electrotactile displays [1].

Required Instrumentation

To determine optimal stimulation waveforms, we require a system which independently controls all eight waveform parameters (defined below) for several channels of electrotactile stimulation. For independent channel control, the output circuit should simultaneously drive several electrodes without interchannel interaction due to output circuit multiplexing such as that used in the Tacticon auditory prosthesis [7], [11]. Finally, the system should be capable of administering predefined experiments to subjects and automatically recording their responses with minimal experimenter intervention during the session. We therefore developed this custom electrotactile stimulation system (ETSS).

Waveform And Electrode Definitions

All eight of the waveform parameters in Table 5.1 and all seven of the electrode parameters in Table 5.2 influence the electrotactile sensation. Figure 5.1 shows the pulse timing relationships; Figure 5.2 shows the four pulse types. Figure 5.3 defines

the generalized single-electrode parameters. The eight waveform parameters define a generalized stimulation waveform; proper choice of parameters can describe any rectangular electrotactile stimulation waveform previously described in the literature.

The literature contains inconsistent waveform terminology. Frequently, M+ and M− waveforms as shown in Fig. 5.2 (with zero net dc current and nonzero baseline) are called "biphasic" because they have positive and negative parts. B+ and B− are sometimes called "biphasic with equal positive and negative parts." A zero-baseline monophasic waveform (with a net dc current) is never used for electrotactile stimulation due to rapid skin irritation resulting from electrochemical reactions at the electrode–skin interface [11]. Therefore, we use the terms "functionally-monophasic" for M+ and M− and "balanced-biphasic" for B+ and B− to avoid ambiguity.

Finally, the two *phases* of a *balanced-biphasic* waveform pulse (Fig. 5.1) are often called *pulses* (with the result that interphase interval is called "interpulse interval"). Introducing the term "phase" avoids the above ambiguity, and uniquely specifies the interpulse and interphase timing relationships.

ETSS SYSTEM FUNCTIONS

Waveform Parameter Control

Each of the 16 independently-controllable stimulation channels can deliver waveforms within the parameter limits in Table 5.1. Parameter changes in one channel do not affect the waveform in any other channel. The Hardware-Performance section elaborates on the parameter control tolerances.

All of the waveform parameters can be controlled in real time by mathematical functions of time or external analog inputs from subject-controlled knobs or sensors. Furthermore, the stimulation parameters for one experimental trial may be functions of earlier subject responses in the experiment.

Automated Experiments

An experimenter-defined command file controls the following functions:

1. Fixed waveform parameters for each channel.
2. Source of dynamic variation of waveform parameters (time or an external analog input).
3. Order of stimulus presentation (randomization available).
4. Timing of stimulus presentation.
5. Subject instructions and prompts.
6. Output file format.

HARDWARE

Figure 5.4 shows that the ETSS consists of four major parts. The waveform generator (WG) produces repetitive rectangular voltage pulse trains which the voltage-to-current converter (VIC) converts to constant-current pulses; these pulses stimulate the subject through skin electrodes. The analog system receives analog control signals from a user interface such as a potentiometer, or from force or pressure sensors, and

provides signals which control the current of each of the 16 stimulation channels. The IBM personal computer (PC) directly controls the WG through the PC bus and through the analog system. It receives status information from the WG and receives external analog data from the analog system. Finally, the PC logs subject responses and system status information in an output file.

Waveform Generator

The WG consists of a PC bus interface (Fig. 5.5), sixteen programmable timer circuits (Fig. 5.6) and a waveshaping circuit (Fig. 5.7). Figure 5.8 shows the interconnections between Figures 5.6 and 5.7 for the 16-channel WG. Figure 5.9 shows the common 5-MHz clock for the timers.

Bus Interface: Each of the Am9513 timer circuits (Fig. 5.6) is controlled by two bidirectional input/output (I/O) ports. The bus interface maps each of the timers consecutively into the PC I/O space B00 – B1F hex. Only one 9513 timer is accessible at a time.

Timer Selection: Advanced Micro Devices (Sunnyvale, CA) Am9513 programmable timer integrated circuits perform all of the timing functions in generating the pulsatile stimulation waveforms. They are controllable in real time by an extensive set of software commands and are easily interfaced to the PC bus. A separate timer IC for each channel controls the seven waveform timing parameters for each channel.

Timer Description: One off-chip master crystal-controlled 5-MHz clock (Fig. 5.9) provides the time base for all 16 timer ICs. Each 9513 timer IC has five

independently-controllable counters, each with programmable clock rate and source, start/stop trigger conditions, numeric preload, and reset capability.

Counter Functions: Figure 5.10(a) shows the functional counter interconnections for one channel of waveform generation. Using the waveform definitions in Table 5.1, Fig. 5.10(b) shows that counters 1 and 2 produce the positive and negative phases, respectively, of the stimulation waveform. These counters function as hardware-triggered delayed-pulse one-shot generators and control phase width W , interphase interval IPI , and *Type* (monophasic, biphasic) waveform parameters via software commands. Counter 3 operates as a rate generator with level gating, thereby controlling the pulse-repetition rate PRR . While counter 3 is on, counters 1 and 2 produce pulses at a constant rate. Counter 3 may be gated off by either counter 4 or 5. Counter 4 controls the burst-onset delay D by gating counters 3 and 5 off. It is a software-triggered strobe with no gating. Finally, counter 5 is a variable duty cycle rate generator with level gating. While its output is high, counter 3 is active which causes counters 1 and 2 to produce pulses. If the output of counter 5 is low, counter 3 is gated off and no pulses are produced. Counter 5 controls the burst repetition frequency F and the number of pulses per burst NPB via software commands.

Waveshaping: Figures 5.7 and 5.10(b) show how the output from the 9513 counters 1 and 2 control the timing of a B+ stimulation waveform. When the output from counter 1 is high, an analog multiplier gates the analog signal from the analog section directly to the WG output, producing the positive phase of the stimulation waveform. A high counter 2 output similarly produces a negative phase by gating an inverted version of the analog control signal. In all other cases the WG output is zero.

By controlling counters 1 and 2 with software, the waveshaping circuit can produce all of the four pulse types: M+, M−, B+, and B−. The analog control signal sets the stimulation current.

Part Selection: The National Semiconductor 74HC4052 analog multiplexer is a single IC that can perform the conversion of counter output pulses to the desired WG output waveform. This IC has a maximal supply voltage of ± 7.5 V, necessitating a separate power supply of ± 6 V.

Trimming of \pm Phases: Because the voltage-to-current converter (VIC) gain is typically different for positive and negative phases, adding R_a or R_b in Figure 5.7 allows the negative phase amplitude to be trimmed upward and downward, respectively, with respect to the positive phase. For example, selecting $R_a = 1\text{ M}\Omega$ will make the negative phase amplitude approximately 1% larger than the positive phase amplitude.

Analog Ground: To prevent a ground loop which could cause a common-mode noise signal to appear on the ground lead from the analog section to the WG, the signal ground is isolated from the PC chassis ground (Figs. 5.7, 5.8).

Voltage-To-Current Converter – Simplified Circuit

Figure 5.11 shows a simplified form of the VIC which converts only positive voltage pulses to positive current pulses.

Current Control Loop: The voltage-to-current function is performed by the loop consisting of U_1 and Q_3 . The high gain of U_1 forces v_{E3} to be very close to v_1 , the input voltage. Therefore,

$$i_{E3} = \frac{v_{E3}}{R_5} \quad (1)$$

and

$$i_{C3} = \frac{\beta}{\beta + 1} i_{E3} \quad (2)$$

Therefore, the input voltage is converted into a current.

Current Mirror: Q_5 and Q_7 form a Wilson current mirror [14], which reflects i_{C3} to the load current i_L and allows the load to be grounded. This also allows multiple electrodes to share a common return path. We chose a Wilson mirror for three reasons. (1) It has better matching of input and output current, (2) it is less dependent on transistor β variations than a conventional mirror, and (3) it does not require the β of Q_7 to be matched to Q_{5a} or Q_{5b} . Therefore, we were able to use a high-voltage transistor for Q_7 as required. A conventional mirror would have required matched-pair transistors which could withstand 240 V and these were not readily available.

If all of the transistors in Figure 5.11 have similar current gain β and Q_{5a} and Q_{5b} are matched,

$$i_L = \frac{1}{1 + 2/(\beta^2 + \beta)} i_{C3} \quad (3)$$

Static Transfer Function: Combining Equations (1), (2), and (3), and noting that $\beta \approx 100$ for these transistors and $R_5 = 100 \Omega$, the overall static transfer function (transconductance) for the V-I converter is

$$\frac{i_L}{v_1} = \frac{0.99}{R_5} = g_m \quad (4)$$

or approximately 10 mA/V. Finally, g_m is relatively independent of temperature, load resistance, and power supply voltage.

Voltage-to-Current Converter – Full Circuit

This section describes the additional circuitry which improves the performance and safety of the circuit in Figure 5.11. Figure 5.12 shows one complete channel for the VIC (less power supply, common-mode buffer, and switching).

Differential Input: To provide rejection of common-mode noise which develops on the long input ground lead, the VIC has a differential input. The current feedback loop consisting of C_5 and C_6 causes the voltage at the junction of R_3 and R_5 to be nearly equal to v_1 , so

$$i_{E3} = \frac{v_1 - v_2}{R_5 \parallel R_6} \quad (5)$$

where

$$R_5 \parallel R_6 = \frac{R_5 R_6}{R_5 + R_6} \quad (6)$$

Therefore, i_L is dependent on $v_1 - v_2$ rather than on v_1 only.

Common-Mode Buffer: A wideband, high-current buffer circuit (Fig. 5.13) provides the necessary current (up to 50 mA per channel) to drive the (–) input of the VIC in Fig. 5.12.

Decoupling and Bypassing: In Figure 5.12, C_1 and C_2 provide bypassing for the low-voltage supply to prevent cross-channel interference. R_{10} and R_{11} decouple each channel from the high-voltage supply. Without these resistors, high-frequency current transients which occur when the Q_5 , Q_6 , Q_7 , and Q_8 switch on and off in one channel will distort the output waveform from physically-adjacent channels. No value of bypass capacitor was sufficient to provide this decoupling without R_{10} and R_{11} .

Rejection of dc: Figure 5.12 shows that the current feedback loop is capacitively-coupled. C_5 and C_6 pass stimulation pulses with widths (W) up to approximately 10 ms with minimal distortion, effecting current control as in the simplified circuit. R_9 , however, provides a dc negative-feedback path from the circuit output. The high overall circuit voltage gain forces the dc component of v_{C7} to track the dc component of v_1 , which is < 0.5 V for any reasonable functionally-monophasic stimulation waveform (for balanced-biphasic waveforms, it is zero). The resulting net dc load current is < 25 nA for a linear load. Because an electrode load is nonlinear [15], an *additional* net dc voltage source of up to 1.25 V (for strong stimulation by a 5.5-mm diameter metal electrode) can appear due to rectification of the asymmetrical functionally-monophasic waveform. The resulting maximal net dc electrode current is $(1.25 \text{ V} + 0.5 \text{ V})/20 \text{ M}\Omega = 87.5 \text{ nA}$.

One result of this dc rejection is that the output current pulse amplitude is lower than expected because the input waveform is dc-shifted. For functionally-monophasic pulses we must therefore modify Eq. (4):

$$\frac{i_L}{v_1} = \frac{0.99}{R_5} (1 - DUTY) = g_m \quad (7)$$

because $I = (1 - DUTY) \cdot I'$ in Fig. 5.2 where $DUTY = NPB \cdot W/T$ is the duty cycle for functionally-monophasic stimulation. To compensate, the software multiplies the desired functionally-monophasic current by $1/(1 - DUTY)$.

Output ac Coupling: To prevent the dangerous flow of dc current from the 120-V supply to the subject should one of the output transistors fail, C₃ and C₄ couple the electrode to the output transistors Q₇ and Q₈. R₇ and R₈ serve to equally distribute any residual dc drop that may develop across these capacitors.

Bias Point Stabilization: The quiescent current through Q₃ and Q₄, and hence, Q₅, Q₆, Q₇, and Q₈, is maintained at approximately 0.5 – 1 mA by R₁, R₂, R₃, and R₄. Q₁ and Q₂ are diode-wired and thermally-coupled to Q₃ and Q₄, respectively, to prevent temperature changes from adversely affecting the bias point.

Output Stray Capacitance Compensation: Because the output circuit is a current source, stray capacitance between the output and ground creates a first-order lag (low-pass filter), distorting the current waveform i_L at the electrode load Z_L . The stray capacitance to ground (C_{ST} in Fig. 5.12) is approximately 55 pF in the output circuit, 155 pF in the 2-m output cable, and 45 pF in the electrode array. Because the resistive part of the electrode load varies more than an order of magnitude with current [15],

[16], a simple lead-compensation network would not correct this effect. Instead, C_7 provides a differentiated positive-feedback path from the circuit output to its input, so that in Fig. 5.12

$$\begin{aligned} I_L(s) &= I_O(s) - sC_{ST}V_O(s) \\ &= g_m[V_1(s) - V_2(s) + sKC_7V_O] - sC_{ST}V_O(s) \end{aligned} \quad (8)$$

where K is a constant determined by the input circuit characteristics of U_1 . Noting that $V_O(s) = I_L(s)Z_L(s)$, the overall transfer function of this circuit then becomes (assuming an otherwise ideal voltage-to-current converter)

$$\frac{I_L(s)}{V_1(s) - V_2(s)} = \frac{g_m}{1 - sZ_L(KC_7 - C_{ST})} \quad (9)$$

Proper choice of C_7 will therefore cancel the effect of stray output capacitance C_{ST} , independent of the load impedance Z_L (see "Performance," below). The value of C_7 is dependent on the output cable length. For a 2-m output cable, 4 pF is appropriate and is small enough to provide a nearly-ideal differentiated feedback.

One of the dc-offset-correction terminals on U_1 is used as an additional input to avoid using a second op-amp as a summer. This unconventional usage requires National LF351 circuits with a date code of 8906 or later. Earlier units have a much lower "input" resistance at pin 1 (160 Ω vs. 14 k Ω), preventing proper operation of this circuit.

Gain Adjustment: Since the circuit gain in Eq. (4) is slightly less than 10 mA/V in the simplified circuit, variable R_6 is added which allows g_m to be trimmed to 10 mA/V. This is shown in Eqs. (5) and (6).

Physical Layout: Because this is a high-gain, wideband circuit with a high output impedance, stray capacitance between input and output must be minimized to prevent undesired oscillations due to capacitive coupling. While a single-channel prototype never oscillated, we experienced difficulty preventing high-frequency oscillations (≈ 3 MHz) when two or more channels were operated in close proximity. Power-supply bypassing at each LF351 was helpful. Most of the cross-channel coupling, however, occurred in the output cable to the electrodes. A flat ribbon cable with a grounded lead between each pair of output leads provided sufficient interchannel isolation while avoiding the bulk and high capacitance to ground of 16 individually-shielded leads. When this cable configuration connected the output circuit board to the electrode array, the oscillations disappeared.

Semiconductor Selection: Q_3 and Q_4 need to withstand 120 V; Q_7 and Q_8 need to withstand 240 V, yet all must operate at low currents of 0.1 to 50 mA. Otherwise their characteristics are not critical. Power consumption is low (< 600 mW, usually much lower) because the driving waveform duty cycle never exceeds 10%. We chose 300-V, 600-mW units. Selection of Q_5 and Q_6 proved more difficult. Few matched-pair devices exist in complementary (NPN and PNP) forms with flat β and matched characteristics from 0.1 to 50 mA. We chose the best available and correct for their nonlinearity in software and correct for NPN–PNP mismatch in the waveform generator circuit.

Power Supplies: The VIC requires two power supplies: low-voltage (± 15 V) and high-voltage (± 120 V). The 15-V supply must be energized first and de-energized last to minimize output transients. A three-position power switch (off, standby, operate) provides this function. An optional subject-operated footswitch can also disable the 120-V supply for emergency shutdown of stimulation.

Furthermore, a current surge which occurs upon application of the 120-V supply requires that this supply (Acopian 120GT05D) receive ac line power before connection to the VIC circuit (also provided by the three-position power switch). Failure to follow this procedure results in automatic supply shutdown.

Analog System

We chose an analog data acquisition and control system from Analog Devices (Norwood, MA) because of its flexibility and software support. Its model RTI-820 circuit board which resides in the PC contains one analog-to-digital converter (ADC) and one digital-to-analog converter (DAC), in addition to three 8-bit parallel ports. Four peripheral model STB-HL02 interface boards containing analog multiplexers provide a total of 64 channels of analog input to the PC and 16 channels of analog output from the PC. The analog inputs receive signals from subject-controlled potentiometers or from force or pressure sensors. The analog output signals control the current of the 16 stimulation channels.

IBM Personal Computer

An IBM PC controls the ETSS. The PC is equipped with 640 kbytes of RAM, one 360-kbyte floppy disk drive, a 10-Mbyte hard disk drive, an 8087 numeric coprocessor, a serial port to communicate with a Diablo 630 printer, and a real-time clock (MIO-100 Multi-I/O card). Although not required for ETSS operation, the Microway (Kingston, MA) Number Smasher/ECM and Motherboard Accelerator speed up data logging and waveform updating on the system by (1) substituting an 8086 processor for the PC's 8088 and (2) increasing the PC clock speed from 4.77 to 12 MHz. An upgraded (150-W) power supply and an extra cooling fan support the custom WG circuit board which plugs into the PC backplane and draws 4 A from the +5-V PC power supply.

Safety Features

The following features protect the subject from electrical injury even with multiple system faults:

Redundancy: Figure 5.12 shows that at least three faults are required to connect the output to a dangerous voltage (the ± 120 -V dc supply). A combination of any two faults (for example, shorted Q₇ and shorted C₃) will allow a maximum of 1.2 mA to flow into the electrode. While 1.2 mA dc is painful, it is not dangerous.

Power-Line Protection: The subject return electrode is connected directly to the equipment ground. Therefore, a ground-fault circuit interrupter (GFCI) in the 120-V ac power line to the entire experimental apparatus protects the subject from receiving a dangerous shock if a major power-distribution fault occurs. The GFCI will also

disconnect the ac power in the unlikely event that the subject touches a 120-V ac conductor in the ETSS .

Physical Layout: Circuitry with an electrical path to the subject is oriented or mounted so that broken or abraded wires, bent mountings, etc. are not able to contact dangerous voltages (120 V ac or ± 120 V dc).

Footswitch: A footswitch which interrupts the ± 120 V dc supply allows the subject to quickly turn off the stimulation if the stimulation intensity becomes painfully high due to software failure.

Charge-Limiting Output Coupling: The value of the output coupling capacitors ensures that insufficient charge ($24 \mu\text{C}$) can flow into a single electrode to cause ventricular fibrillation ($560 \mu\text{C}$ – see below) in the subject, even with software failure or two circuit failures.

Consider the worst-case scenario in which C_4 in Figure 5.12 is shorted and C_3 is initially charged with the circuit terminal +120 V with respect to the load. Then suppose that Q_8 shorts, temporarily placing -120 V on the electrode load. Current will flow through the load (subject) to reverse the polarity of charge on C_3 . The required charge is $q = C\Delta v = (0.1 \mu\text{F})(240 \text{ V}) = 24 \mu\text{C}$. This is the maximal charge that can flow into the subject with two system faults.

We arrive at the fibrillation charge of $560 \mu\text{C}$ as follows. The accepted lower limit of ventricular fibrillation for whole-body, arm-to-arm 60-Hz current flow in humans is 75 mA rms [17]. Roy et al. [18] show that electrical stimulation (extrasystole) of isolated rabbit hearts (using large electrodes to simulate whole-body current flow) occurs within the first half-cycle of ac stimulation at 500 Hz. We assume that this is also true at 60 Hz, because the period is longer and because the time constant

for stimulation of the human myocardium is 0.6 – 1.1 ms [19]. Furthermore, the required average pulse current for external defibrillation of dog hearts is independent of pulse shape from 2 – 20 ms [20]. Therefore, the required human fibrillation charge in the first half-cycle of 75-mA 60-Hz stimulation is (68 mA ave)(8.3 ms) = 560 μ C.

Electrode Design: Finally, coaxial electrodes (an active center electrode surrounded by a grounded ring) restrict the current flow to the vicinity of the electrode. To cause fibrillation, the ground lead would have to break and the subject would have to touch a grounded object to provide a current path through the heart, in addition to the faults discussed above.

Performance

Operational Limits: Due to the limited supply voltage of ± 120 V, the output coupling circuit (C_3 , C_4 , R_7 , R_8) imposes limits on the maximal output current into various loads with various waveforms. These are hard limits; minimal waveform distortion occurs before the limits are reached.

For functionally-monophasic pulses driving a 0- Ω load, the maximal available current I_{MAX} (mA) is approximately ($\pm 15\%$)

$$I_{MAX} = \frac{k [1 + (a/W)] [1 + c \ln(F)] [1 - d(NPB - 1) \ln(PRR)]}{b + (NPB - 1) IBI \cdot F} \quad (10)$$

where the inter-burst interval $IBI = T - (10^{-3})NPB \cdot P - (10^{-6})W$. Experimental determination of the empirical constants for a least-squares fit yields $k=0.98$, $a=4800$, $b=1.08$, $c=0.31$, and $d=0.0057$. The unit for IBI is s; the other waveform parameter units are defined in Table 5.1.

For balanced-biphasic pulses, the maximal current into $0\ \Omega$ is approximately ($\pm 10\%$)

$$I_{\text{MAX}} = \frac{(100\ \text{V}) \cdot C}{W} \quad (11)$$

where $C = 50\ \text{nF}$ (the equivalent of C_3 and C_4).

The exact analytical expressions for (10) and (11) are very complex. Equation (10) is an empirical model which applies over the physiologically-useful range of stimulation waveforms. Equation (11) determines the current which will cause 100 V to appear across the C_3 , C_4 network during the first phase of a balanced-biphasic pulse.

A typical electrode requires 25 – 60 V depending on the stimulation current [15]. This reduces the maximal output current of the circuit into an electrode to approximately $I_{\text{MAX}}/2$. For the electrodes used in most of our studies (5.5-mm diameter) the drive capability of this circuit for balanced-biphasic pulses is sufficient to produce painful stimulation if desired. Some functionally-monophasic pulse trains with $NPB > 1$ are not capable of delivering very strong stimulations due to the delimiting in (10).

Output Impedance: An ideal current source has an infinite output impedance. This circuit has a primarily resistive output impedance of $2\ \text{M}\Omega$, which results in $< 1\%$ change in current over the range of electrode impedances (approximately $2\ \text{nF}$ capacitance in parallel with $1 - 20\ \text{k}\Omega$ resistance [15]).

Linearity: The transconductance of $10\ \text{mA/V}$ varies $+1\%$ to -4% over the useful operating range of $1 - 50\ \text{mA}$ ($+1\%$ to -2% for $2 - 30\ \text{mA}$). Since this nonlinearity is somewhat predictable with current, the software corrects the linearity to $\pm 2\%$ over $1 - 50\ \text{mA}$. Also, since the VIC gain for positive and negative phases is

often different, the WG has a provision for trimming the amplitude of the negative phase.

Dynamics: With a rectangular pulse at the input, the output current into $100\ \Omega$ or into an electrode settles to its final value in $< 1\ \mu\text{s}$ with a maximal overshoot of 2%. The pulse flatness is $\pm 0.5\%$ for a relatively long (1-ms) pulse.

Timing: All of the waveform parameters except current are derived from the 5-MHz crystal and hence their accuracy is limited only by the resolution of discrete frequency division in the Am9513 timer circuits (Table 5.1).

SOFTWARE

The entire ETSS is controlled by the IBM PC through its bus. A custom software package translates a user input file containing commands for all of the waveform parameters for each of the 16 output channels into hardware commands for (1) the WG timers (which control all parameters except current) and (2) the analog section (which controls stimulation current). The PC bus interface uses I/O hex addresses B00 – B1F for the waveform generator and I/O hex addresses 220 – 22F for the analog system.

The software performs the following functions:

1. Read the input file containing the experiment control commands.
2. Check the input file for errors.
3. Randomize the order of stimulus presentations if specified.
4. Provide the specified subject instructions and prompts.
5. Present the stimuli to the subject as defined in the input file.

6. Record the subject's responses, relevant parameters, and system error and status messages.
7. Sort the recorded data in the same order as the input file.
8. Generate an output file with recorded data.

Development Tools

We wrote most of the source code in Borland (Scotts Valley, CA) Turbo C version 2.0 along with with the Turbo Assembler 1.0 and Turbo Debugger 1.0. Several time-critical functions use 8086 assembly code. Compiled drivers (Analog Devices model AC1527-A) simplify communication with the analog system.

Software Features

Command Language: The ETSS software conducts experiments written in the ETSS command file language. This language supports directives and operation codes that enable the experimenter to control every feature of the system.

The command file consists of a header section and a body section. The programmer must define all variables, mathematical function, blocks of text, and output file format commands in the header section. The body contains the data and commands that produce stimulations. The body is divided into groups of trials which are further divided into parts. In addition, each trial is assigned a design number. This structure allows the system to randomize the execution order of experiments as well as sort result files in a consistent fashion.

Waveform Parameter Control: Every waveform parameter except for Type and D may be updated in real-time (during an experimental trial) via mathematical functions. ETSS functions accept from one to three arguments and support operators such as logarithms, exponentiation, powers, roots, multiplication, division, addition, and subtraction. Arguments may be a combination of analog inputs (e.g. knobs connected to potentiometers), time, user-defined variables, or constants. A range-checking routine reports out-of-range parameters to the experimenter and prevents subsequent system malfunctions.

The command language provides user-defined variables, waveform parameter soft-limits, and analog "jitter". A variable such as an experimentally-determined sensation threshold may be defined and used in a later trial. For example, the stimulation current for one trial can be a function of an earlier subject response.

The operational limits of the waveform parameters may be limited via a software command; thus, the system programmer can set the minimal and maximal operating value of a parameter. Furthermore, the programmer may specify the scope of this feature to affect any particular trial or the entire file.

The optional analog jitter function adds a random number to any desired analog input to prevent the subject from memorizing a particular potentiometer position for a repeated response.

Subject-Experimenter Interface: The ETSS software supports numerous methods of acquiring data from a test subject and displaying information to the subject. The subject may either enter data from the keyboard or from an analog input (eg. by adjusting a potentiometer). The system always prompts the user when data inputs are required. At the end of each trial, the subject's responses are logged to an output result

file for further processing. Long experiments may be saved and resumed at a later time. A group of experimental trials may be repeated if the subject makes a procedural error. At any time, the experimenter can append a comment to the output file.

Error Detection and Trapping: Experiments may run in either the normal mode or the debug mode. Normal mode operation displays only the information necessary for the subject to interact with the system. The debug mode displays the above information as well as information useful to the system programmer when debugging a command file, such as a real-time display of waveform parameters.

The ETSS system supports extensive error trapping, generating over one hundred error messages for conditions like out-of-range parameters and errors in command file syntax.

Executable Modules

The ETSS software consists of three executable files: (1) the command file preparer and randomizer, (2) the command file parser and interpreter, and (3) the result file organizer. An intelligent batch file sequentially invokes each file, aborting the process when necessary.

Preparser: If the experimenter specifies a randomized experiment, the command file preparer randomizes the execution order of the specified part of an experiment and creates a temporary reordered command file.

Parser and Interpreter: The command file parser and interpreter executes command files line by line. To optimize system performance, each part in the command file body is compiled prior to execution.

In addition, the system translates mathematical functions into Intel 8087 coprocessor machine code. Mathematical translation is accomplished as follows. First the function is formatted and operators are distinguished from variables and constants. Then the mathematical function is converted from infix to postfix notation. The conversion is necessitated by the 8087 coprocessor stack-based structure. Finally, each operator is translated into a sequence of Intel 8087 machine-language instructions.

Result File Organizer: The result file organizer sorts and formats the output files generated by the parser and interpreter and sorts the output file according to the design numbers associated with each trial. Thus, data from a randomized experiment are logged to a result file in a convenient order for analysis.

Unusual Software Solutions

IBM-PC Timer Interrupt: The ETSS system utilizes the IBM PC TIMER interrupt (interrupt zero) to conduct many of its time-dependent functions. The ETSS software changes the timer frequency to 20.0 Hz by reprogramming the 8253-5 programmable interval timer and installs a new interrupt service routine for the duration of the experiment. The original interrupt routine which updates the IBM PC system clock is not called by the new interrupt service routine, so upon exiting the system, the system clock must be reset from the hardware time-of-day clock. During the parsing of command file lines, the TIMER interrupt is disabled by masking the appropriate bit of the

8259A programmable interrupt controller. The PC will function as expected with the TIMER interrupt disabled except when calling some DOS interrupt functions, for example, subfunction 08H of the DOS interrupt 21H (retrieve a character from the keyboard).

Real-Time Update of Am9513A Registers: The ETSS software updates the Am9513A system timing controllers in real-time. This may be accomplished without losing waveform integrity as long as one does not write to a counter during its terminal count. (During terminal count, the counter reloads itself from internal registers.) To avoid this situation, updating is synchronized with the 9513 oscillator via its FOUT (frequency out) pin. The ETSS software configures the FOUT pin to produce a 50-kHz signal derived by frequency division of the master oscillator. The software updates registers only after a level transition of FOUT to ensure terminal count does not occur during the update process (which lasts approximately 8 μ s).

Complete schematic diagrams and software are available by contacting the third author.

CONCLUSIONS

The system described above is fully operational; it rapidly and automatically delivers a wide variety of electrotactile stimuli to subjects. Using this flexibility, we hope to determine (1) which waveforms can maximize dynamic range and comfort, (2) minimize error in identification of waveform parameter changes for information display, and (3) minimize skin irritation.

The ability to rapidly record large amounts of data has already yielded an interesting observation on the time variations in the electrotactile sensation threshold [21]. Ongoing experiments include (1) the determination of how accurately a subject can control hand grasp force using electrotactile force feedback, (2) maximization of the perceived intensity of stimulation without discomfort, and (3) characterization of sensory adaptation to electrotactile stimulation.

REFERENCES

- [1] K. A. Kaczmarek, J. G. Webster, P. Bach-y-Rita and W. J. Tompkins, "Electrotactile and vibrotactile displays for sensory substitution systems," *IEEE Trans. Biomed. Eng.*, vol. 38, pp. 1–16, 1991.
- [2] A. Y. J. Szeto and F. A. Saunders, "Electrocutaneous stimulation for sensory communication in rehabilitation engineering," *IEEE Trans. Biomed. Eng.*, vol. BME-29, pp. 300–308, 1982.
- [3] P. Bach-y-Rita, *Brain Mechanisms in Sensory Substitution*. New York: Academic, 1972.
- [4] C. C. Collins, "On mobility aids for the blind," in *Electronic Spatial Sensing for the Blind*, D. H. Warren and E. R. Strelow, Eds. Dordrecht, The Netherlands: Martinus Nijhoff, 1985, pp. 35–64.
- [5] C. M. Reed, N. I. Durlach and L. D. Bradia, "Research on tactile communication of speech: A review," *AHSA Monographs*, vol. 20, pp. 1–23, 1982.
- [6] C. E. Sherrick, "Basic and applied research on tactile aids for deaf people: Progress and prospects," *J. Acoust. Soc. Am.*, vol. 75, pp. 1325–1342, 1984.
- [7] A. Y. J. Szeto and K. M. Christensen, "Technological devices for deaf-blind children: Needs and potential impact," *IEEE Eng. Med. Biol. Mag.*, vol. 7, no. 3, pp. 25–29, 1988.
- [8] C. C. Collins and J. M. J. Madey, "Tactile sensory replacement," in *Proc. San Diego Biomed. Symp.*, vol. 13, 1974, pp. 15–26.

- [9] C. A. Phillips, "Sensory feedback control of upper- and lower-extremity motor prostheses," *CRC Crit. Rev. Biomed. Eng.*, vol. 16, pp. 105–140, 1988.
- [10] R. R. Riso, "Sensory augmentation for enhanced control of FNS systems," in *Ergonomics in Rehabilitation*, A. Mital, Ed. New York: Taylor and Francis, 1988, pp. 253–271.
- [11] F. A. Saunders, "Information transmission across the skin: High-resolution tactile sensory aids for the deaf and the blind," *Int. J. Neurosci.*, vol. 19, pp. 21–28, 1983.
- [12] A. Y. J. Szeto and R. R. Riso, "Sensory feedback using electrical stimulation of the tactile sense," in *Rehabilitation Engineering*, R. V. Smith and J. H. Leslie Jr., Eds. Boca Raton, FL: CRC Press, 1990, pp. 29–78.
- [13] F. A. Saunders, "Electrocutaneous displays," in *Proc. Conf. Cutan. Comm. Sys. Dev.*, F. A. Geldard, Ed., Psychonomic Society, 1973, pp. 20–26.
- [14] A. S. Sedra and K. C. Smith, *Microelectronic Circuits*, 2nd ed. New York: CBS College Publishing, 1987.
- [15] K. A. Kaczmarek and J. G. Webster, "Voltage–current characteristics of the electrotactile skin–electrode interface," in *Proc. Annu. Int. Conf. IEEE Eng. Med. Biol. Soc.*, Seattle, WA, Y. Kim and F. A. Spelman, Eds., vol. 11, IEEE, 1989, pp. 1526–1527.
- [16] A. v. Boxtel, "Skin resistance during square-wave electrical pulses of 1 to 10 mA," *Med. Biol. Eng. Comput.*, vol. 15, pp. 679–687, 1977.
- [17] W. H. Olsen, "Electrical safety," in *Medical Instrumentation: Application and Design*, J. G. Webster, Ed. Boston: Houghton Mifflin, 1978, pp. 667–707.

- [18] O. Z. Roy, A. J. Mortimer, B. J. Trollope and E. J. Villeneuve, "Effects of short-duration transients on cardiac rhythm," *Med. Biol. Eng. Comput.*, vol. 22, pp. 225–228, 1984.
- [19] J. A. Pearce, J. D. Bourland, W. Nielsen, L. A. Geddes and M. Voelz, "Myocardial stimulation with ultrashort duration current pulses," *PACE*, vol. 5, pp. 52–58, 1982.
- [20] C. F. Babbs and J. D. Bourland, "Defibrillators," in *Therapeutic Medical Devices: Application and Design*, A. M. Cook and J. G. Webster, Eds. Englewood Cliffs, NJ: Prentice-Hall, 1982, pp. 66–85.
- [21] K. A. Kaczmarek, J. G. Webster and R. G. Radwin, "Periodic variations in the electrotactile sensation threshold," in *Proc. Annu. Int. Conf. IEEE Eng. Med. Biol. Soc.*, Philadelphia, PA, P. C. Pedersen and B. Onaral, Eds., vol. 12, IEEE, 1990, pp. 1060–1061.

Table 5.1

Electrotactile Waveform Parameters

Parameter	Symbol	ETSS Range	Resolution	Unit
Burst onset delay	D	0 – 120	0.002	ms
Burst rate	F	1 – 1000	#	Hz
Phase current	I	0 – 50	0.00122	mA
Interphase interval	IPI	0 – 1000	0.2	μ s
Pulses/burst	NPB	1 – 100	1	pulses
Pulse rate	PRR	0.1 – 25	#	kHz
Phase width	W	2 – 1000	0.2	μ s
Pulse type	Type	M+, M–, B+, B–	N/A	
Pulse repeat period	$P^* = 1/PRR$	0.04 – 10	0.002	ms
Time between bursts	$T^* = 1/F$	1 – 1000	0.02	ms

*P and T are redundant parameters, being derived directly from PRR and F, respectively.

#The resolution of F and PRR vary over the operating range to correspond with the resolutions of T and P, respectively.

Table 5.2

Electrotactile Electrode Parameters

Parameter	Symbol
Active electrode diameter	D _A
Insulating ring diameter	D _I
Dispersive electrode diameter	D _D
Body location	Loc
Electrode separation	Sep
Electrode material	Mat
Skin preparation technique	Prep

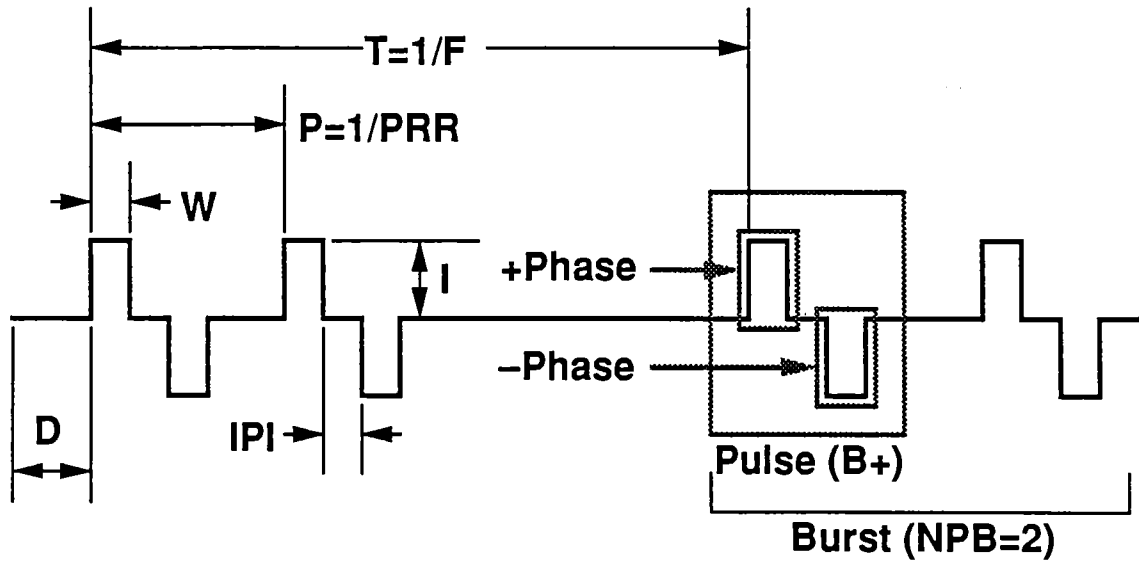


Fig. 5.1. Electrotactile waveform parameters: D , delay; W , width; IPI , interphase interval; I , current; T , time between bursts; F , frequency of burst repetition; P , period of pulse repetition; PRR , pulse repetition rate; NPB , number of pulses per burst.

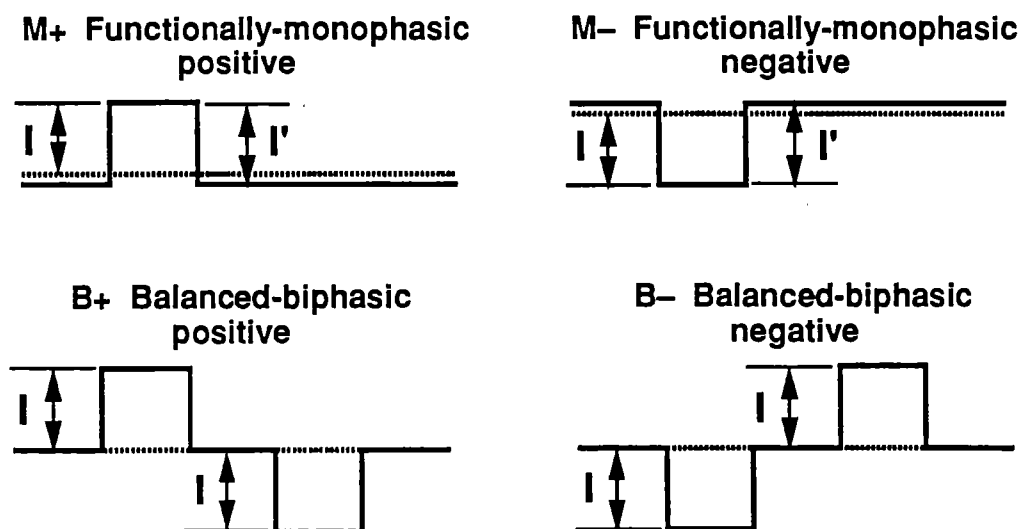


Fig. 5.2. Electrotactile waveform pulse types. Average current is zero for all types.

The dotted line is the zero-current reference.

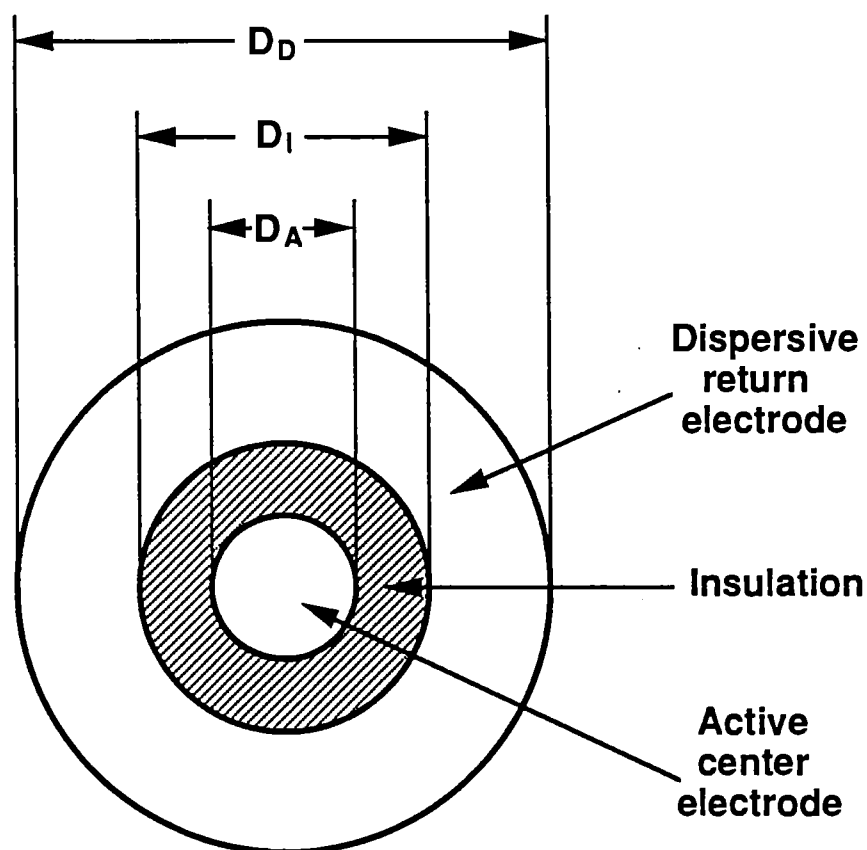


Fig. 5.3. In electrotactile electrodes, current enters through the active center electrode and returns through the annular dispersive return electrode. This focuses the region of highest current density to the skin region directly beneath the active electrode to provide well-localized sensations. Typical electrode dimensions are 2–10 mm for D_A , 1–4 mm for $D_I - D_A$, and 4–100 mm for D_D .

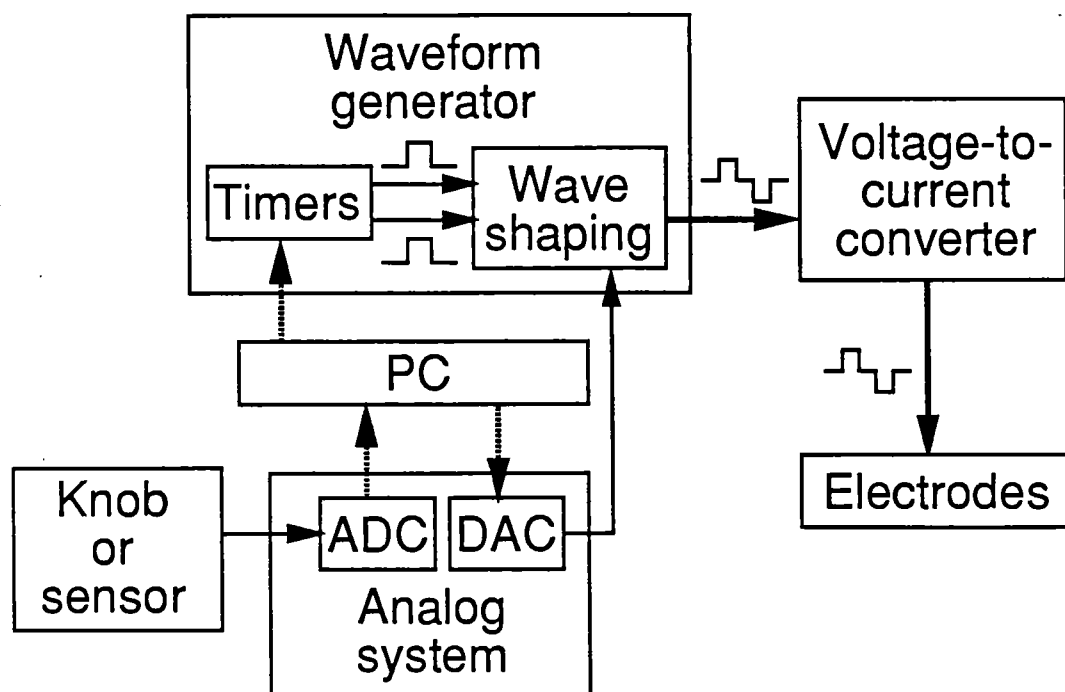


Fig. 5.4. Electrotactile stimulation system. Dashed lines represent PC bus interface connections. Solid lines are steady or slowly-varying analog signals. Heavy solid lines are pulsatile waveforms.

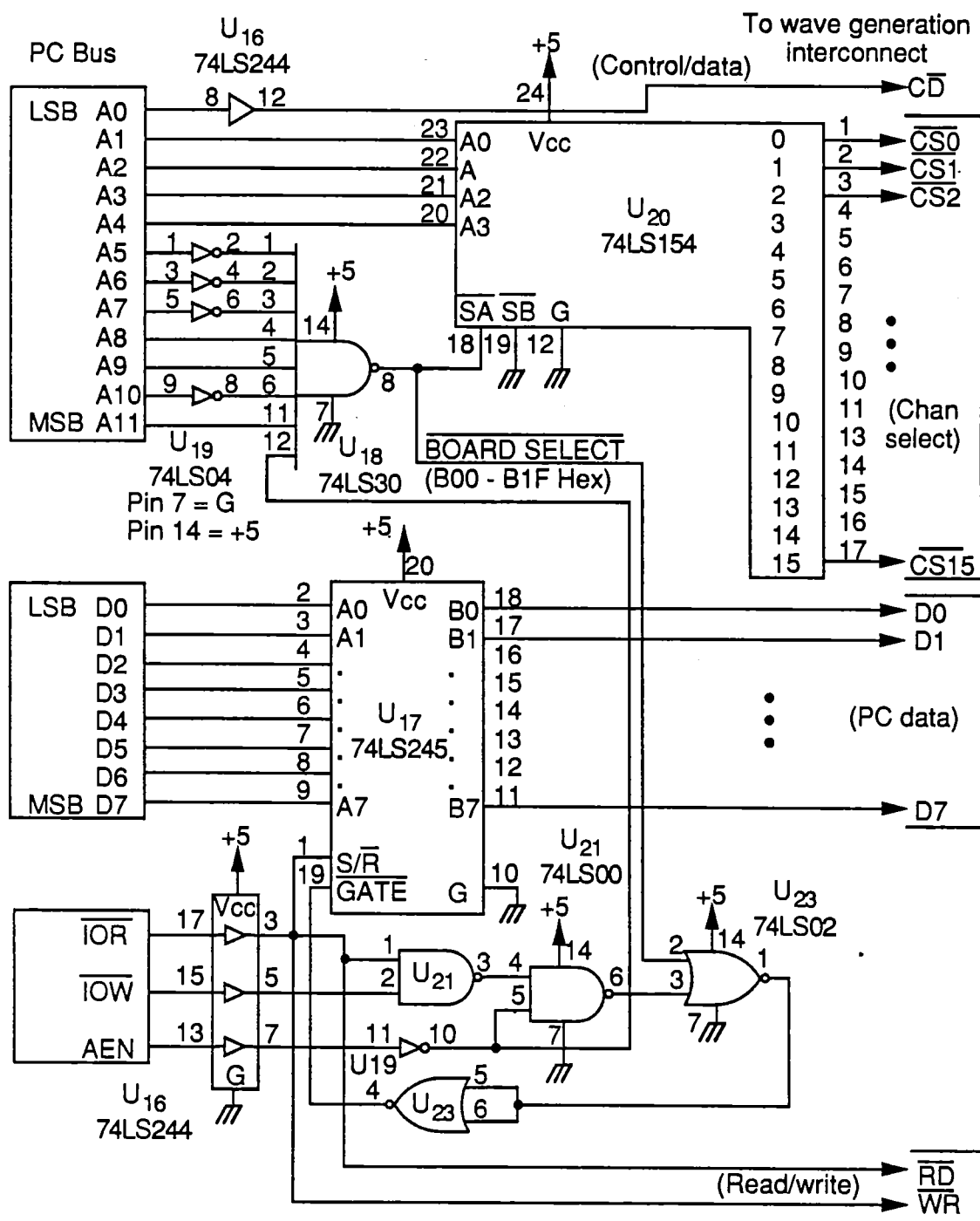


Fig. 5.5. The PC bus interface decodes software-generated signals which set the timers in the waveform generator.

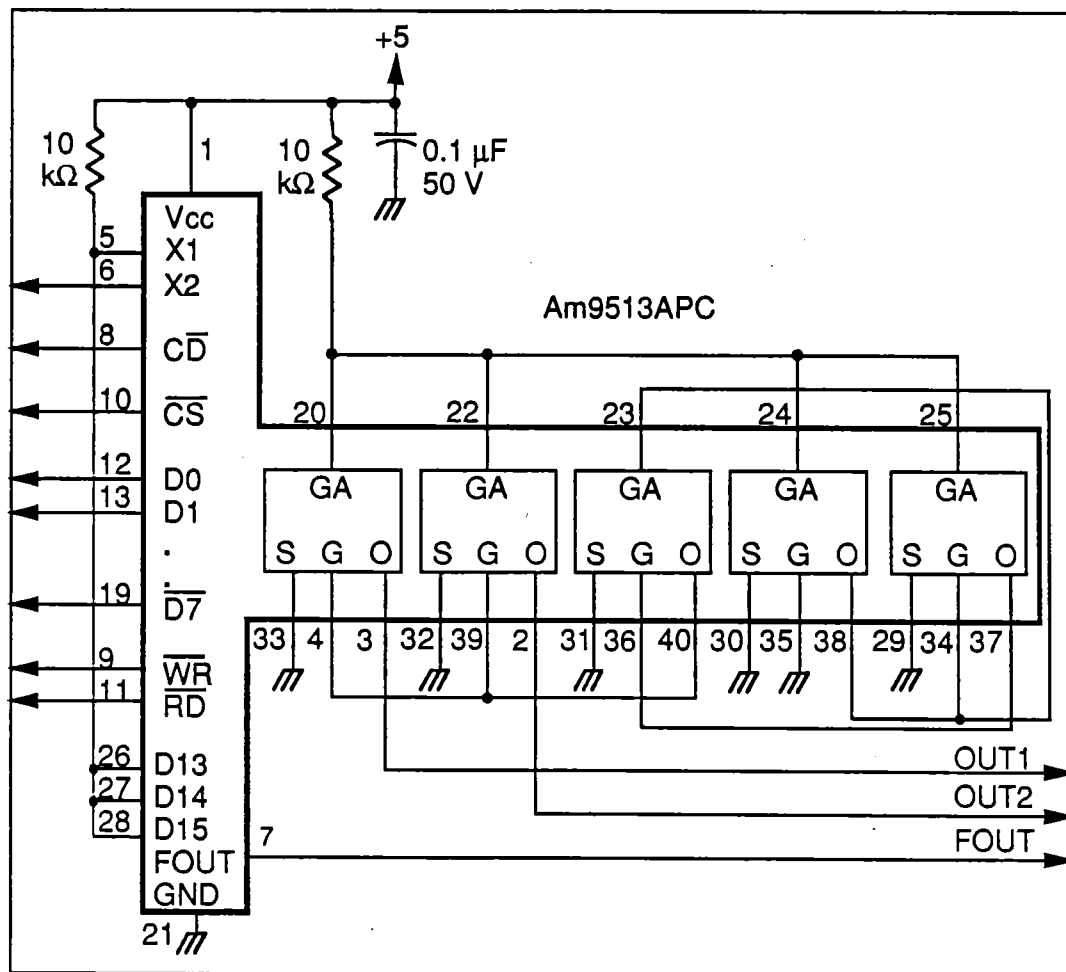


Fig. 5.6. One channel of programmable timers, which are set to generate the waveform.

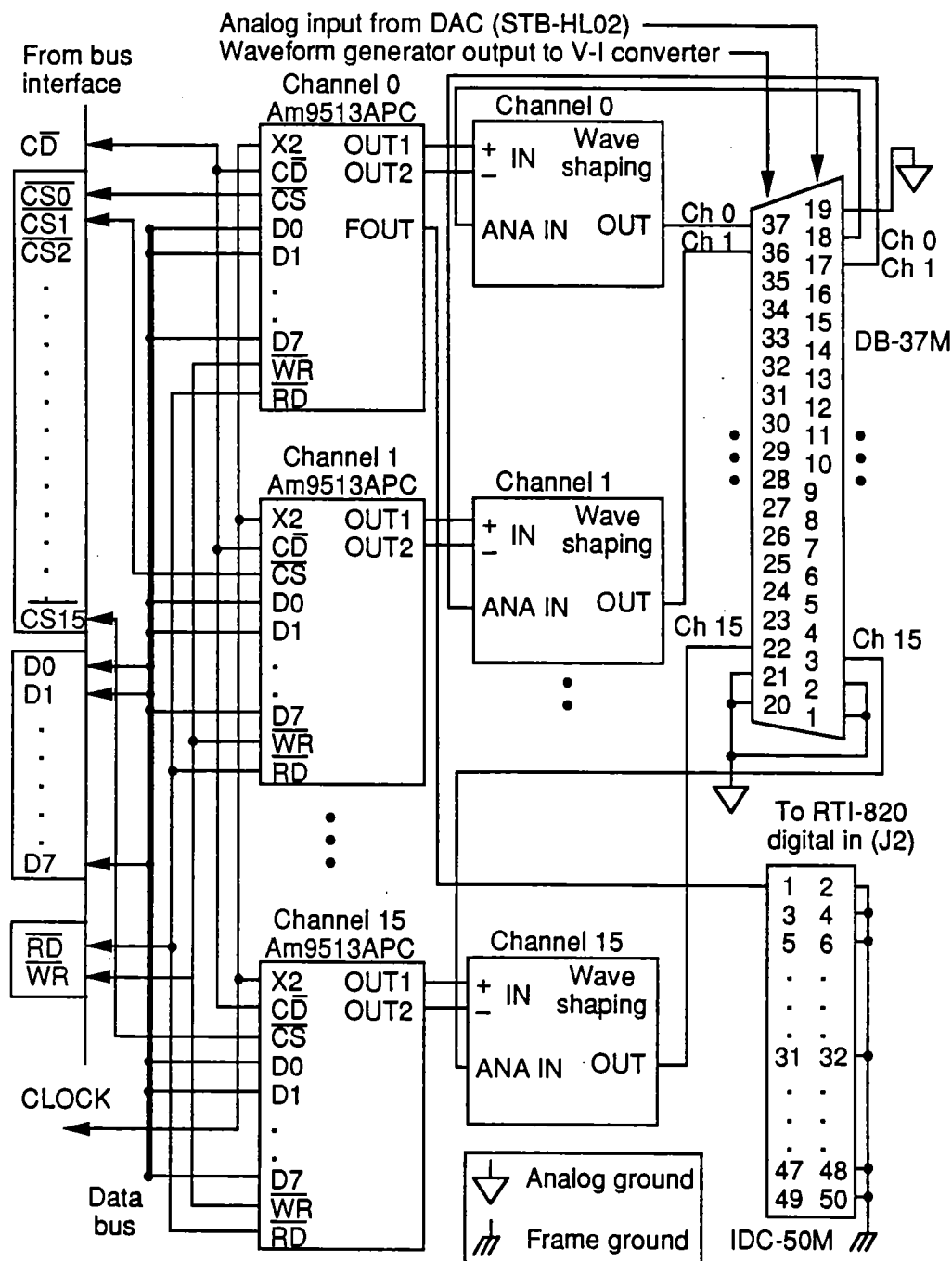


Fig. 5.8. Waveform generator interconnect: Timer outputs and DAC analog outputs combine in the waveshaping circuit to provide waveform generator output to the voltage-to-current converter.

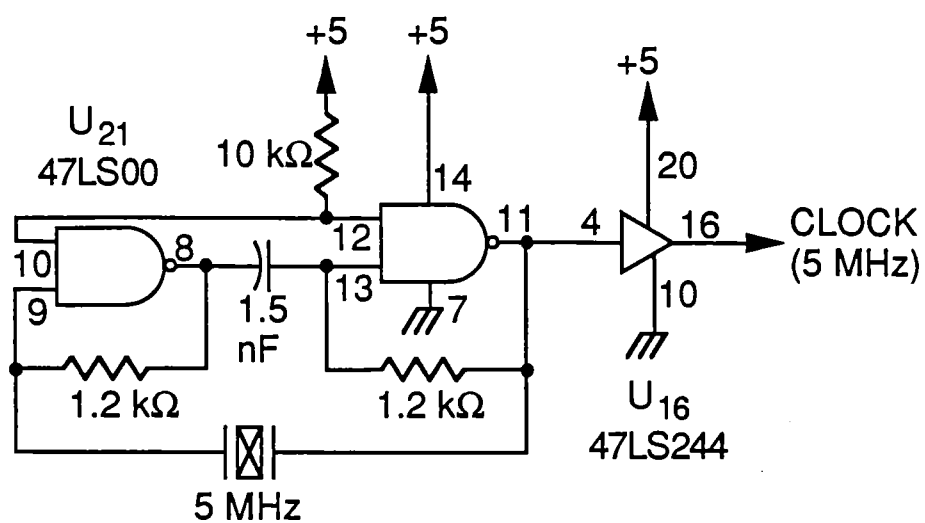


Fig. 5.9. Two NAND gates and a 5-MHz crystal form the common clock for all sixteen channels.

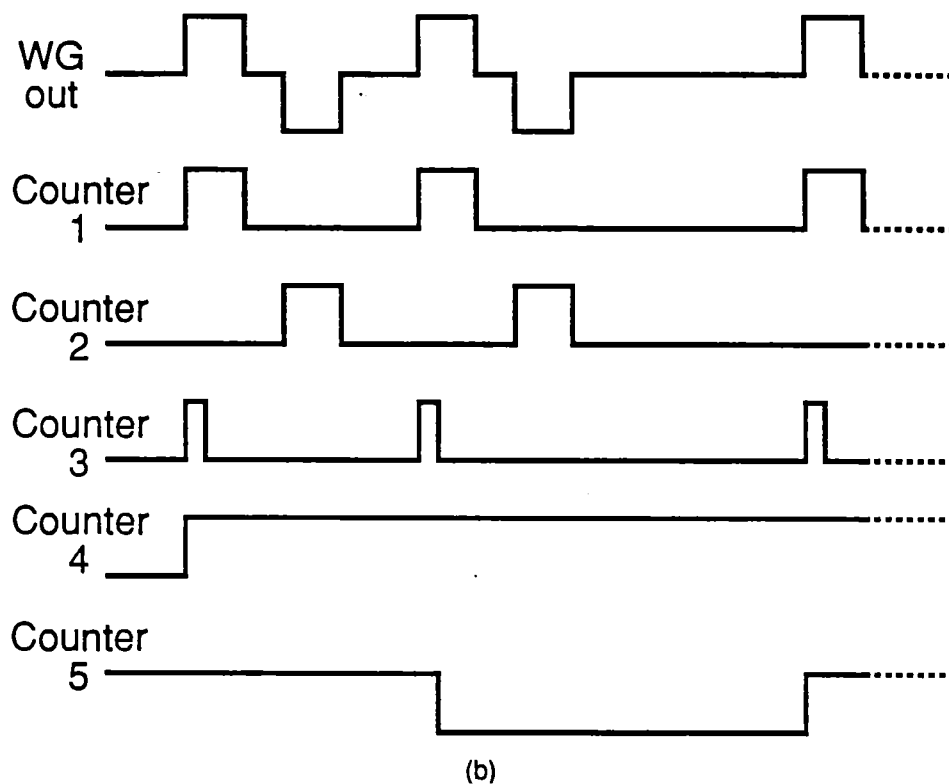
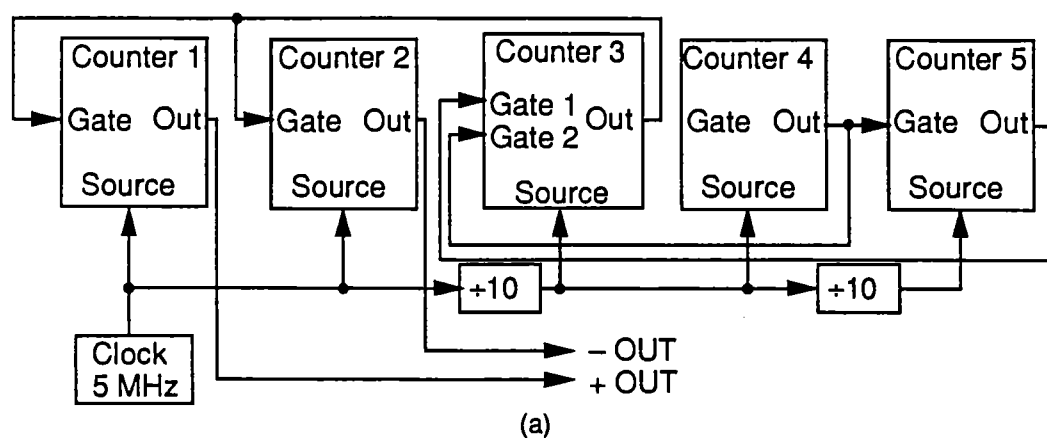


Fig. 5.10. (a) Some of the counter interconnections for Am9513 timer circuit are internally controlled via software. (b) Timer counters 1 and 2 control *W*, *IPI*, and *Type* waveform parameters via software commands. Counter 3 controls *PRR*, counter 4 controls *D*, and counter 5 controls *F* and *NPB* via software commands.

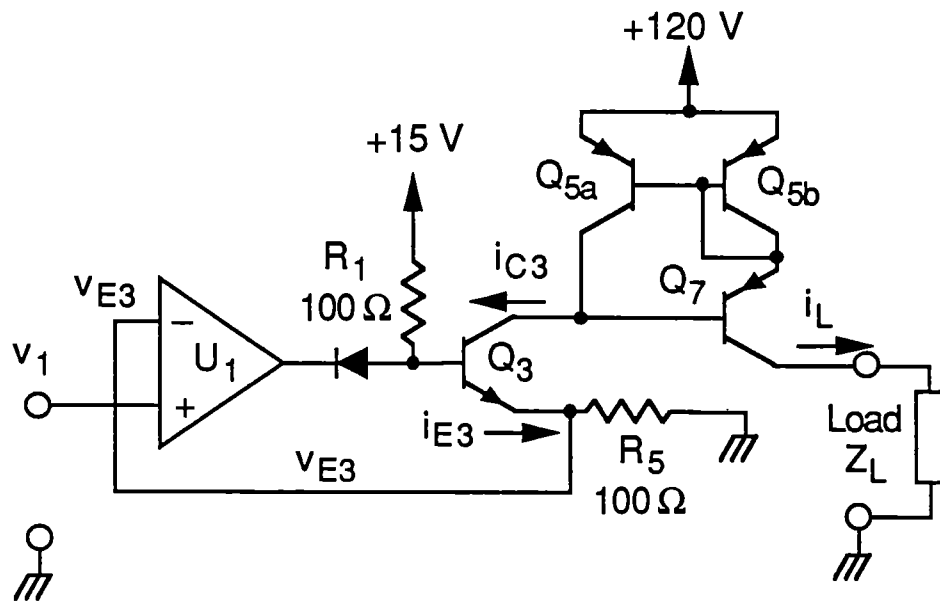


Fig. 5.11. Simplified voltage-to-current converter. V_1 appears across R_5 . The resulting current is reflected by the current mirror (Q_5 , Q_7) and flows through the load.

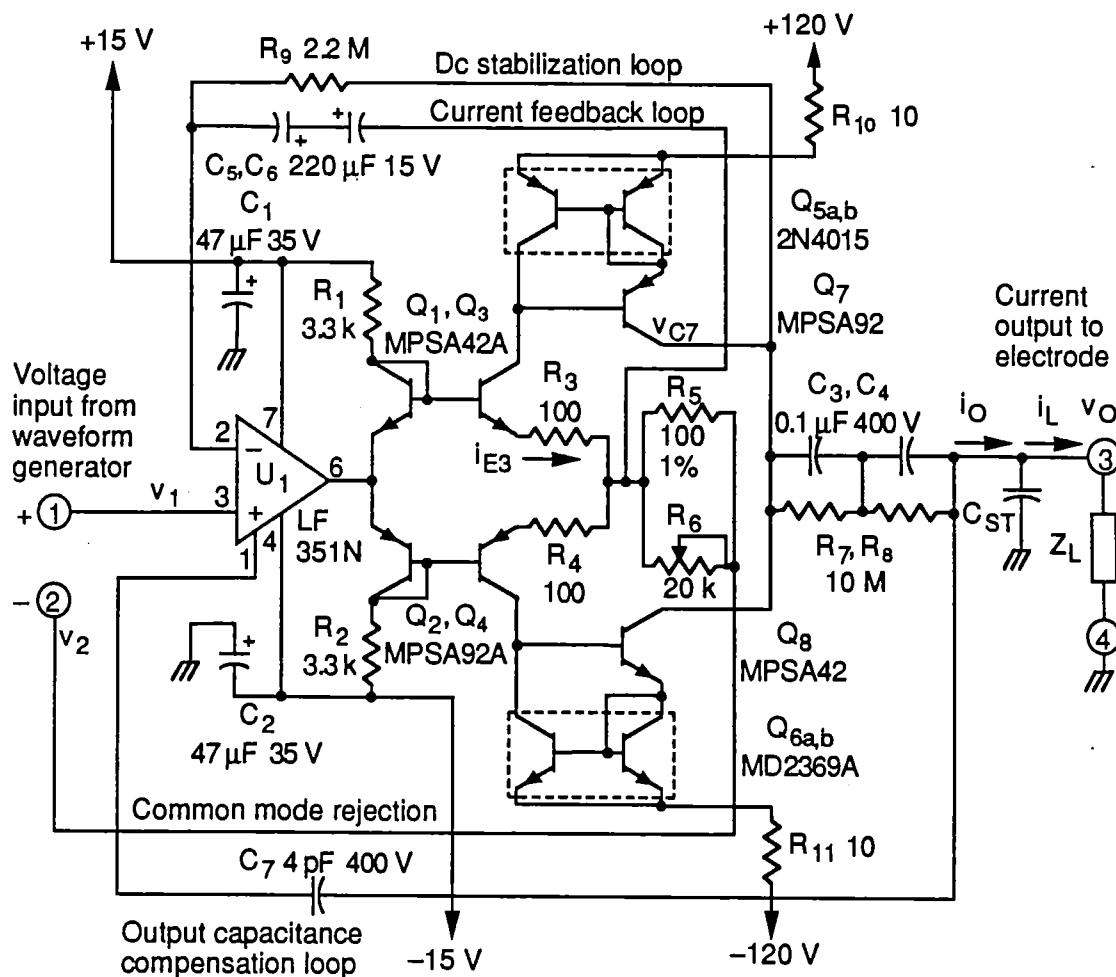


Fig. 5.12. Bipolar voltage-to-current converter has feedback loops to stabilize the dc operating point and compensate for output cable capacitance. Some of the special part requirements are: C_3, C_4 are metal film polyester; C_7 is ceramic; all transistors are Motorola; Q_1 and Q_3 are thermally coupled; Q_2 and Q_4 are thermally coupled; Q_5 sub is RCA SK9115; Q_6 sub is RCA SK9114; all resistors 1/4 W 5% carbon. U_1 is National date code 8906 or later. Resistance in Ω unless noted; adjust R_6 for circuit transconductance $g_m = 10$ mA/V. C_{ST} is the stray capacitance from the output terminal to ground.

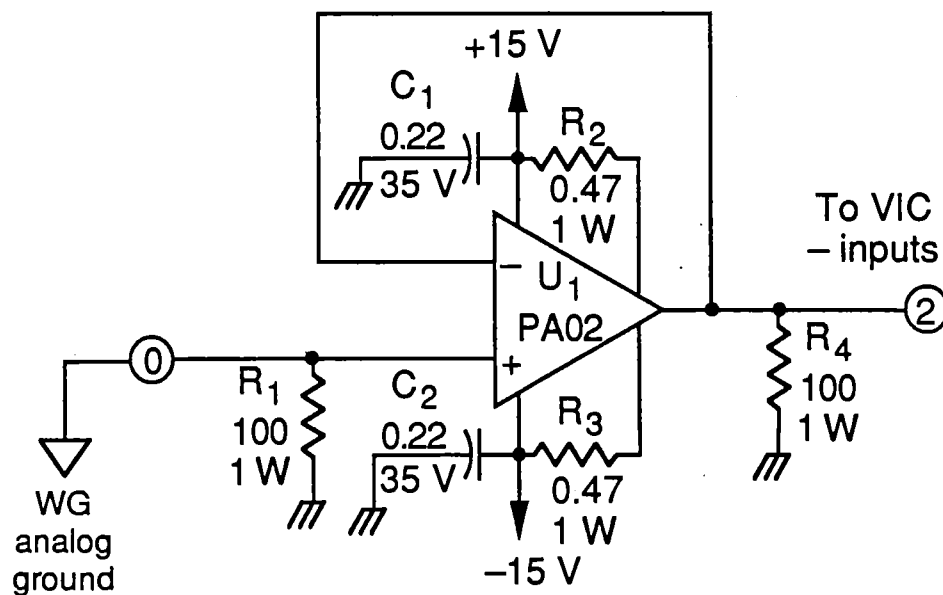


Fig. 5.13. A high-current buffer provides up to 50 mA to drive the negative input of all 16 voltage-to-current converter circuits to reduce common-mode interference. U_1 is Apex Microtechnology (Tucson, AZ) type PA02. All R in Ω , all C in μF .

Chapter 6

MAXIMAL DYNAMIC RANGE ELECTROTACTILE STIMULATION WAVEFORMS

Original Experiments

A slightly shorter version of this chapter coauthored by K. A. Kaczmarek, J. G. Webster, and R. G. Radwin is submitted to *IEEE Transactions on Biomedical Engineering*.

ABSTRACT

A new method to measure the dynamic range of electrotactile (electrocutaneous) stimulation uses both steepest ascent (gradient) and one-variable-at-a-time methods to determine the waveform variables that maximize the subjective magnitude (intensity) of the electrotactile percept at the maximal current without discomfort for balanced-biphasic pulse bursts presented at a 15-Hz rate. The magnitude at the maximal current without discomfort is maximized by the following waveform: Number of pulses/burst = 6, Pulse repetition rate within a burst = 350 Hz, and Phase width = 150 μ s. The interphase interval (separation between positive and negative phases in a biphasic pulse) does not affect dynamic range from 0 – 500 μ s, although it does affect the sensation threshold current and the maximal current without discomfort.

The number of pulses/burst has a large effect on the magnitude-based dynamic range, whereas it has little effect on the traditional dynamic range measure of (maximal current without discomfort)/(sensation threshold current). The stimulation magnitude at the maximal current without discomfort is approximately twice as strong with 6 pulses/burst as it is with 1 pulse/burst (a frequently-used waveform).

INTRODUCTION

Background

Electrotactile stimulation evokes tactile (touch) sensations within the skin at the location of the electrode by passing a local electric current through the skin. Sensory substitution is the use of one human sense (in this case, touch) to receive environmental information normally received by another sense (often vision or hearing). For the sense of touch, sensory substitution is the use of one area of skin to receive tactile

information normally received at another location. Several articles review technology and devices for electrotactile stimulation [1], [2], visual substitution [3], [4], auditory substitution [5], [6], [7], and other applications [2], [8], [9], [10], [11], [12].

Dynamic range

A substantial limitation of present electrotactile displays is that they lack sufficient magnitude dynamic range. Our normal senses of vision, hearing, and touch can mediate stimuli which we perceive as strong or intense without being painful. Electrotactile stimulation, on the other hand, can develop an uncomfortable stinging quality even at moderate stimulation levels if improper stimulation waveforms or electrodes are used.

The traditional measure of magnitude dynamic range is the ratio of the stimulation *currents* required to produce sensation threshold S and pain threshold P . The ratio P/S typically ranges from 2 – 4 for unexperienced observers (Os) and 6 – 8 for experienced Os [13]. (This range is a limitation for magnitude (intensity)-modulated stimulation codes but not necessarily for frequency or spatially-modulated codes.) However, P , S , and by extension P/S are *electrical* measures that give little information about the *percept* produced by stimulation. Choosing a stimulation waveform which maximizes P/S does not guarantee a usefully-strong or comfortable sensation.

We propose that a better measure of the dynamic range of a tactile display is the range of *perceived* stimulation magnitudes that are both perceptible and comfortable, from the magnitude at the sensation threshold current $\psi(S)$ to the magnitude at the maximal current without discomfort $\Psi = \psi(M)$. (We chose M instead of the pain threshold P to avoid any stimulations described as uncomfortable or painful because

eventual users of a practical sensory substitution system would not likely accept such sensations. For five Os, P/M varied from 1.1 to 1.6, with a mean value of 1.3.

The actual stimulus percept is a psychophysical function of all of the waveform and electrode variables, including the current I . One aspect of the stimulus percept is its strength or magnitude, typically designated by ψ . It can be described by Stevens' power law [14], [15]:

$$\psi = (I - S)^n$$

where ψ is the subjective magnitude, S is the sensation threshold current (which is sometimes set arbitrarily to zero — inappropriate in our view for electrotactile stimulation in which S is not small compared with I), and I is the stimulus current. Note that by this definition, the magnitude at sensation threshold $\psi(S) = 0$. The exponent n has been reported to range from 0.9 — 3.5 [16], [17]. The range of n values is due to several factors. (1) Stimulation of nerve bundles (e.g. the median nerve at the wrist) produces a much different nonlocalized percept than stimulation of localized areas of skin (our method), which produces a percept similar to normal touch. (2) Some studies assume *a priori* that electrotactile stimulation is uncomfortable by using such terms as "shock," and ask the observer to rate discomfort magnitude rather than tactile magnitude. Studies measuring tactile magnitude and discomfort magnitude cannot be directly compared because the dependent variables are different. (3) The calculated value of n varies depending on the overall range of stimulation intensities and other experimental biases [16]. (4) A power function may not provide the best

description of the relationship between ψ and I [18]. The present studies do not intrinsically depend on any particular function.

Furthermore, we distinguish between the (vibratory) tactile magnitude ψ and another aspect of the stimulus percept: its degree of "unpleasantness" or "sting." Figure 6.1 qualitatively shows that at one set of stimulation waveform variables (condition 2) the ratio $\mathcal{R}_2 = M_2/S$ is high but the magnitude Ψ_2 is low. Condition 1 represents a potentially better operating range; while \mathcal{R}_1 is smaller, Ψ_1 is higher than for condition 2, i.e. the range of perceived stimulation intensities $\Psi - \psi(S) = \Psi$ is larger. Therefore, we believe that Ψ is a better measure of dynamic range than \mathcal{R} . If Ψ is maximized, the entire range of stimulation intensities is maximally comfortable. The purpose of this study is to determine the set of waveform variables which maximize Ψ . Note that while ψ is dependent on the stimulus current I , Ψ is not. By definition, Ψ is defined at the maximal I that is not uncomfortable.

MATERIALS AND METHODS

Nomenclature

Waveforms: Eight stimulation waveform variables influence the electrotactile sensation. Figure 6.2 defines the pulse timing relationships; Figure 6.3 defines the four pulse types. The eight waveform variables define a generalized stimulation waveform; proper choice of these variables can describe any rectangular electrotactile stimulation waveform previously described.

The literature contains inconsistent waveform terminology [19]. Frequently, M+ and M- waveforms are called "biphasic" because they have positive and negative parts. We will use the terms "functionally-monophasic" for M+ and M- and "balanced-biphasic" for B+ and B- to avoid ambiguity. The two *phases* of a *balanced-biphasic*

waveform pulse (Fig. 6.2) are often called *pulses* (with the result that interphase interval *IPI* is called "interpulse interval"). Introducing the term "phase" avoids the above ambiguity, and uniquely specifies the waveform timing relationships.

Numerical notation: Many experimental measurements are repeated and averaged to improve precision and assess repeatability. A quantity $x_{rj}(\boldsymbol{w})$ is measured with the stimulation waveform \boldsymbol{w} . (Boldface notation distinguishes between the general waveform vector quantity \boldsymbol{w} , which is the set of all applicable waveform variables, and W , the phase width.) In several experiments, most of the waveform variables are held fixed and only one is varied, in which case \boldsymbol{w} becomes the scalar k .

The measurements are taken in sets or replications r where $r = 1, 2 \dots R$. Within each replication, the trial number j indicates the actual (random) order of measurements where $j = 1 \dots J$. Therefore, an individual measurement x can be uniquely specified with either x_{rj} — the j th trial in the r th replication, or with $x_r(\boldsymbol{w})$ — the waveform \boldsymbol{w} in the r th replication. When data are averaged, an overbar specifies the variable that is an average and a dot replaces the variable that is averaged over. For example

$$\overline{x.}(\boldsymbol{w}) = \frac{1}{R} \sum_{r=1}^R x_r(\boldsymbol{w})$$

specifies the mean of all R replications of x with waveform \boldsymbol{w} .

The actual measured quantities (dependent variables) in this set of experiments are (1) the sensation threshold current S , (2) the maximal current without discomfort M , (3) the estimated magnitude (intensity, strength) ψ , and (4) the estimated magnitude at the maximal current without discomfort $\Psi(\boldsymbol{w}) = \psi[\boldsymbol{w}, M(\boldsymbol{w})]$. We emphasize that

the upper-case Ψ is the magnitude *at the predetermined* current M , and that it is a function of w . Because some experiments measure S , M , and Ψ , we respectively use U , V , and R to denote the number of replications u , v , and r for each.

Where data from more than one O combine in one expression, a second comma-separated subscript o denotes the observer; e.g. $S_{rj,o}(w)$ is the sensation threshold for the r th replication on the o th observer for waveform w ; j is the trial corresponding to waveform w . Finally, nonnumeric subscripts denote a specific stimulation condition (independent variable) rather than a replication or trial number. For example, NPB_{REF} is the value of NPB for a reference stimulus REF. The small caps notation denotes a specific stimulation condition. Measured quantities (dependent variables) do not use this notation.

Instrumentation

Waveform generator: A computer-controlled electrotactile stimulation system (ETSS) [19] automatically delivered the desired stimulation, prompted the observer for responses, and then logged O's responses. For determination of the sensation threshold current S and the maximal current without discomfort M , a knob manipulated by O's left hand controlled the stimulation current according to:

$$I = (x - rnd)A$$

where I is the stimulation current in mA (clamped so that $I \geq 0$), x is the knob rotation where 0 is fully counter-clockwise (CCW) and 1 is fully clockwise (CW) (approximately 355° rotation from zero), rnd is a random number between 0 and 0.2 and A is a scaling factor which causes $0.2 < x < 0.8$ for all S and M determinations.

Subtracting the knob offset rnd prevents O from using the knob rotation x as a cue for determining S and M .

Electrode: The current-controlled pulses were delivered to O's tapwater-premoistened abdomen by the twelfth electrode from the left (cable side) in the elasticized-belt linear electrode array from a Tacticon™ auditory prosthesis for the deaf [11], [20], [21]. The 5.5-mm-diameter gold-plated electrodes are surrounded by the conductive rubber base material of the belt, which serves as a ground plane. The electrode site was approximately 2 cm above and 7 cm right of the navel. For Os with dense hair or bony protuberances at this location which prevented proper electrode contact (as evidenced by sharp, prickly electrotactile sensations), we relocated the electrode laterally to a smoother location. Occasionally the chosen site would yield prickly sensations or muscle contractions for no apparent reason; this was readily corrected by moving the electrode a few mm in any direction and re-wetting the skin. On particularly dry winter days with indoor relative humidity $RH < 30\%$, a steam humidifier under the experiment station desk maintained sufficient abdominal skin hydration by keeping RH between 20% and 40% near O. Insufficient skin hydration causes prickly sensations, probably because of nonuniform current density at the electrode-skin interface [1].

Observers

Ten Os (3 female and 7 male, aged 19 – 30 with varied ethnic backgrounds) initially participated in this study. Three were later dismissed due to unrepeatable results. Os received \$5.00/h payment, and were recruited by personal contact and posters in University buildings.

Optimization scheme

The objective of the following set of experiments, identified by boldface names, was to refine an initial guess *Baseline 1* of the optimal waveform w which maximizes Ψ . Several types of experiments gathered information for screening Os and systematically maximizing the dynamic range Ψ . **Scale 1**, **Scale 2**, and **Scale 3**, using slightly different procedures, determined the relationship between the stimulation current I and the subjective magnitude ψ . **MagNPBscreen** measured the relative intensity $\Psi(NPB)$ at the maximal current without discomfort M as a function of NPB . Because preliminary data established a strong dependency of Ψ on NPB , **MagNPBscreen** and **Scale 1** screened observers by testing their ability to consistently identify M , ψ , and Ψ at a number of waveforms w with subjectively different percept "qualities."

Figure 6.4 illustrates in two dimensions the procedure used to maximize Ψ in the four-dimensional space (NPB , PRR , W , IPD). With 7 suitable Os, **Gradient** determined $\nabla\Psi(w)$ at the first guess of $w = \textit{Baseline 1}$. (Preliminary unpublished experiments provided the value of *Baseline 1*.) $\nabla\Psi(w)$ is a vector in the space (NPB , PRR , W , IPD) which points in the direction of maximal Ψ . Then **Search** varied w in the direction of $\nabla\Psi(w)$, starting at *Baseline 1*, to estimate the value of w which maximized $\Psi(w)$. This value of w is *Baseline 2*. **Gradient** also supplied information on how the effects of NPB , PRR , W , and IPD interacted, i.e., how the value of one of these variables influenced the effect of the others on Ψ .

Finally, **MagNPB**, **MagPRR**, **MagW** and **MagIPD** varied each of these four variables separately around *Baseline 2* to investigate the detailed response of $\Psi(w)$. A final adjustment in w based on these four experiments determined the best approximation of the optimal w .

Order of experiments

A set of 7 Os completed all of the following four experimental sessions in the following order:

- | | |
|-----------------|--|
| First session: | Scale 1 and MagNPBscreen |
| Second session: | Scale 2, Gradient, and Search |
| Third session: | Scale 3 and two of the following: MagNPB, MagPRR, MagW and MagIPI |
| Fourth session: | Scale 3 and the remaining two of the following: MagNPB, MagPRR, MagW and MagIPI |

The **Scale 1 – 3** experiments served to (1) train or retrain Os on the basic procedure of magnitude estimation and (2) investigate the nature of the ψ vs I relationship over different current ranges. The third and fourth sessions were structured so that each of the experiments **MagIPI**, **MagNPB**, **MagPRR**, and **MagW** had an equal chance of appearing as the second or third experiment in the third or fourth session. Three of the ten Os were dismissed after session 1 due to unrepeatable results. Finally, one of the 7 remaining Os (O1) did not complete session 4.

Scale 1: Magnitude scale

At the beginning of each experimental session, O waited 5 min for the electrode-skin interface to stabilize after placing the electrode belt on moistened skin. O then performed a magnitude estimation experiment to determine the magnitude scale at that electrode site (perceived stimulation magnitude ψ vs. stimulation current I).

Choice of stimulation waveform and current: Based on preliminary data from four Os, the waveform variables for **Scale 1** were fixed at *Baseline 1* ($Type = B+$, $F = 15$ Hz, $PRR = 400$ Hz, $W = IPI = 100$ μ s, and $NPB = 6$), which was the first approximation of the waveform w which maximizes $\Psi(w)$. O first determined the sensation threshold current S by a modified method of limits. Upon prompt by the ETSS, O turned a knob CW, starting at the zero (fully CCW) position, until s/he perceived a distinct but very weak tingling sensation at the electrode site. We instructed O to readjust the knob CW and CCW until s/he could just barely feel the stimulus, and then press the ENTER (RETURN) key on the keyboard, causing S to be logged to a result file and saved in memory for future use. Then O returned the knob to zero. This procedure was then repeated two more times. The computer averaged the three results to obtain:

$$\bar{S} = (S_1 + S_2 + S_3)/3$$

Next, O determined the maximal current without discomfort M . Starting at zero, O turned the knob CW until the stimulus was as strong as possible without feeling uncomfortable as manifest by sharp, prickly, or burning sensations. O logged the response by pressing ENTER and then returned the knob to zero. As for the sensation threshold, the computer calculated the mean \bar{M} of three trials. A 10-s separation between M trials allowed O's somatosensory system to partially recover from adaptation.

Finally, the computer calculated the set of 11 test stimulus currents (independent variable) for magnitude estimation, as well as a reference stimulus current:

$$I_0 = \bar{S}. + 0.00(\bar{M}. - \bar{S}.) = \bar{S}.$$

$$I_1 = \bar{S}. + 0.10(\bar{M}. - \bar{S}.)$$

$$I_2 = \bar{S}. + 0.20(\bar{M}. - \bar{S}.)$$

.

.

$$I_{10} = \bar{S}. + 1.00(\bar{M}. - \bar{S}.) = \bar{M}.$$

$$I_{\text{REF}} = I_{10}$$

Magnitude estimation: We then asked O to rate these eleven stimulus currents numerically on an magnitude scale where:

Level 0 = Cannot feel test stimulus.

Level 1 = Can barely feel test stimulus.

Level 20 = Test stimulus same magnitude as reference REF.

Open-ended upper scale; assign numbers as appropriate.

This is not a "pure" magnitude scale because standard levels are defined. We chose this method in spite of its limitations [22], [23] because in later experiments we require O to make fine distinctions in magnitude ψ near a reference magnitude $\psi(\text{REF}) = 20$. While inflating error in other regions of the magnitude scale, presenting the reference stimulus REF reduces the error near $\psi(\text{REF})$.

The ETSS presented the reference stimulus before each test stimulus so that O did not need to remember the REF magnitude for more than 2 s. Earlier experiments

with the reference presented less frequently (e.g. once every 10 trials) showed that O's magnitude estimations ψ tended to drift substantially upward or downward (sometimes even reversing direction midway) between reference presentations.

The computer reviewed on-screen for O the above instructions for the magnitude estimation trials (previously given verbally). The ETSS then presented five sets (replications) of eleven magnitude estimation trials at the levels $I_0 - I_{10}$. Each replication r presented the trials in a different computer-generated random order [19]. Each trial consisted of these actions:

1. ETSS gives Beep sound, gives message on screen that next stimulus is coming, then pauses for 6 s.
2. Beep, message READY!, then a 1-s pause.
3. Beep, ETSS delivers a 1-s reference stimulus I_{REF} (level 20).
4. Beep, ETSS delivers a 1-s test stimulus at one of the eleven currents $I_0 - I_{10}$.
5. Beep-Beep, ETSS prompts O to type in a number representing the magnitude $\psi_{rj}(I)$ of the test stimulus.

Scale 2: Magnitude scale

Scale 2 was similar to **Scale 1** except that the reference waveform current and the range of test waveform currents were:

$$I_0 = \bar{S} + 0.50(\bar{M} - \bar{S}) = \bar{S}.$$

$$I_1 = \bar{S} + 0.55(\bar{M} - \bar{S})$$

$$I_2 = \bar{S}. + 0.60(\bar{M}. - \bar{S}.)$$

•

•

$$I_{10} = \bar{S}. + 1.00(\bar{M}. - \bar{S}.) = \bar{M}.$$

$$I_{\text{REF}} = I_8$$

Scale 3: Magnitude scale

Scale 3 was similar to Scale 1 except that the reference waveform current and the range of test waveform currents were

$$I_0 = \bar{S}. + 0.00(\bar{M}. - \bar{S}.) = \bar{S}.$$

$$I_1 = \bar{S}. + 0.10(\bar{M}. - \bar{S}.)$$

$$I_2 = \bar{S}. + 0.20(\bar{M}. - \bar{S}.)$$

•

•

$$I_{10} = \bar{S}. + 1.00(\bar{M}. - \bar{S}.) = \bar{M}.$$

$$I_{\text{REF}} = I_8$$

and the waveforms were at *Baseline 2* (*Type* = B+, *F* = 15 Hz, *PRR* = 400 Hz, *W* = 120 μ s, *IPI* = 100 μ s, and *NPB* = 7).

MagNPBscreen: Effect of NPB

Earlier unpublished results showed a large predictable increase in Ψ as *NPB* increased from 1 to 10. This is consistent with others' recommendations to deliver repeating bursts of stimulation pulses: (*Type* = M+, *F* = 25 Hz, *NPB* = 4, *PRR* = 500 Hz, *W* = 20 μ s) in [24], [25]; (*Type* = B+, *F* = 200 Hz, *NPB* = 1 – 32, *PRR* = 10

kHz, $W = 10 \mu\text{s}$, $IPI = 40 \mu\text{s}$) in [11]; ($Type = B+$, $F = 30 \text{ Hz}$, $NPB = 1 - 150$, $PRR = 10 \text{ kHz}$, $W = 4.5 - 9 \mu\text{s}$, $IPI = 41 - 45.5 \mu\text{s}$) in [17]. We therefore screened O's ability to discern this change. All waveform variables were fixed at *Baseline 1* except for the independent variable NPB , which had values $NPB_1, NPB_2, \dots, NPB_{10}$ of 1, 2, 3, 4, 5, 6, 8, 10, 15, and 20.

Sensation threshold current: First, O determined the sensation threshold current $S_{uj}(NPB)$ using the **Scale 1** procedure for each of the ten values of NPB . Three replications u of these 10 trials were performed in different random orders. The index j specifies the actual run order (trial) within each replication.

Maximal current without discomfort: Next O determined the maximal current without discomfort $M_{vj}(NPB)$ using the **Scale 1** procedure for each of the ten values of NPB (three replications v). Possibly because the 10-s interval between M trials provides insufficient time for the skin to completely recover from sensory adaptation, the 30 values of M usually show a distinct upward trend (Fig. 6.5). (In rare cases, it is downward, usually indicating insufficient skin hydration or poor electrode-skin contact.) This drift averaged 19% over the 30 trials, lying between 0.3% and 30% for 80% of the experiments (Table 6.1). The drift systematically increases the replication variance

$$\frac{1}{V-1} \sum_{v=1}^V \left[M_{vj}(w) - \bar{M}_{.j}(w) \right]^2$$

in determining M at each level of NPB ($V = 3$). Because the drift is monotonic and

approximately linear, we compensate by subtracting a correction factor from each logged current M :

$$\begin{aligned} M'_{vj}(w) &= M_{vj}(w) - b(j' - 15) && \text{where} && (1) \\ j' &= j + 10(v - 1) && \text{and} \\ b &= [\bar{M}_3.(w) - \bar{M}_1.(w)]/20 && \text{and} \end{aligned}$$

M' is the corrected current M , v is the replication (1... $V = 3$), j is the trial in each replication (1...10 corresponding to the 10 values of NPB in random order), j' is the sequence of all trials in the three replications (monotonic with time), $\bar{M}_3.$ and $\bar{M}_1.$ are the means of all maximal currents in replications 3 and 1, respectively, and b is the estimated slope of the drift (mA/trial). The method of using the replication means $\bar{M}_3.$ and $\bar{M}_1.$ results in a slope b similar to that obtained by a linear regression of M_{vj} vs. j' , but it has less bias due to the effect of NPB on M because $\bar{M}_3.$ and $\bar{M}_1.$ are means over all ten values of NPB .

The computer then calculated the mean drift-corrected currents $\bar{M}'.(1)$, $\bar{M}'.(2)$,... $\bar{M}'.(10)$ for presentation to O. (Recall that $\bar{M}'.(1)$ corresponds to the waveform with $NPB = 1$, $\bar{M}'.(2)$ corresponds to $NPB = 2$, etc.) Furthermore, $NPB_{REF} = NPB_5 = 6$ with associated current $I(REF) = \bar{M}'.(5)$ was also used as the reference stimulus. Finally, a lower-current stimulus

$$I_{LOW} = \bar{S}.(REF) + 0.75[\bar{M}'.(REF) - \bar{S}.(REF)]$$

provided a scale relating a change in current ΔI to a change in magnitude $\Delta\psi$ so that error in determining M could be related to the resulting error in ψ .

Magnitude estimation: We then asked O to rate these ten waveforms numerically on a magnitude scale using the procedure for **Scale 1**. The ETSS presented five replications of 10 magnitude estimation trials. Each replication r presented the 10 trials $\Psi_r(NPB_1) - \Psi_r(NPB_{10})$ in a different random order. Interspersed in each replication were two magnitude estimations of the REF current $\psi_r(11)$, $\psi_r(12)$ and two magnitude estimations of the LOW current $\psi_r(13)$, $\psi_r(14)$.

Observer screening

We reviewed data from the session 1 (**Scale 1** and **MagNPBscreen** experiments) before proceeding with sessions 2 – 4 to make sure that O understood the procedures. Three of the ten Os initially contacted were dismissed at this point because their magnitude estimates were very scattered and unrepeatable, although similar in trend to the results of the chosen Os. We speculate that this scatter was caused by lack of O's attention to the task.

Gradient: Determination of gradient and interactions

Independent variables: Earlier unpublished results suggested that the effects of the waveform variables F , IPI , NPB , PRR , and W strongly interacted, i.e. the effect of one variable depended on the values of one or more of the others [26]. Therefore, we conducted a full factorial experiment in NPB , PRR , W , and IPI to (1) evaluate the effects of such interactions, and (2) determine the gradient of the response surface $\nabla\Psi(NPB, PRR, W, IPI)$ i.e. the vector which points in the direction of increasing Ψ .

Knowing the gradient provides an efficient method to simultaneously vary (NPB , PRR , W , IPI) to search for the waveform variables which maximize Ψ .

Fixed variables: Because F has a direct effect on ψ [27], Os had a difficult time separating changes in Ψ from changes in the perceived frequency. Therefore, F remained constant at 15 Hz for these experiments. Higher frequencies cause increasingly rapid sensory adaptation; lower frequencies result in a low communication rate as evidenced by a noticeable lag between stimulus magnitude and attempted magnitude changes with the knob during determination of S and M . The waveform *Type* remained fixed at B+ because M+ and M- waveforms caused much more skin redness (in a 1 – 3-cm-diameter circular area centered on the stimulation electrode), even though they had a net-dc current of zero [2]. B- waveforms did not appear to be perceptually different from B+ [28].

Factorial structure: The ETSS administered the three-stage experiment (S , M , Ψ) as in **MagNPBscreen**, but with the variable settings in Table 6.2. These settings form an orthogonal experiment which simplifies calculation of the variable effects and the gradient [26]. Waveform conditions 17 and 18 are the reference REF waveform (defined as the *Baseline 1* stimulus) located in the center of the hyper-cube formed by the set of all sixteen points (NPB , PRR , W , IPI).

Threshold and maximal currents: To each of seven Os, the ETSS administered 3 replications u of sensation threshold current S and 3 replications v of maximal current without discomfort M determinations with the waveforms w in Table 6.2. As before, the computer corrected the M values for drift (Eq. 1) and then averaged three replications of M' .

Magnitude estimation: The Os then estimated the magnitude of the 16 waveforms $\Psi_r(1) - \Psi_r(16)$ plus two REF estimations $\psi_r(17) - \psi_r(18)$ plus two LOW estimations $\psi_r(19) - \psi_r(20)$. O performed five replications r of these 20 trials in different random orders.

Search: Find maximal Ψ along gradient path

The gradient search is based on the linear approximation in the vicinity of the *Baseline 1* waveform w_{REF}

$$\begin{aligned} \Psi(w) \approx & \Psi(w_{\text{REF}}) + a'_1(NPB - NPB_{\text{REF}}) + a'_2(PRR - PRR_{\text{REF}}) \\ & + a'_3(W - W_{\text{REF}}) + a'_4(IPI - IPI_{\text{REF}}) \end{aligned}$$

where the constants

$$a'_1 = \frac{\partial \Psi}{\partial NPB}(w_{\text{REF}})$$

$$a'_2 = \frac{\partial \Psi}{\partial PRR}(w_{\text{REF}})$$

$$a'_3 = \frac{\partial \Psi}{\partial W}(w_{\text{REF}})$$

$$a'_4 = \frac{\partial \Psi}{\partial IPI}(w_{\text{REF}})$$

define a least-squares regression. In practice, we estimated these coefficients by scaling the main (single-factor) effects $a_1 - a_4$ calculated in the effects analysis to follow in the *Results* section.

Before proceeding with each O, we calculated the gradient $\nabla \Psi(w)$ separately for each O based on the **Gradient** experiment:

$$\nabla \Psi(w) = \begin{bmatrix} a_1 \\ a_2 \\ a_3 \\ a_4 \end{bmatrix}$$

The path of steepest ascent (i.e. the direction in w which most quickly increases Ψ) is then (Fig. 6.4)

$$NPB(k) = NPB_{\text{REF}} + a_1 \cdot \text{scale} \cdot (k - 3) \quad (2)$$

$$PRR(k) = PRR_{\text{REF}} + a_2 \cdot \text{scale} \cdot (k - 3)$$

$$W(k) = W_{\text{REF}} + a_3 \cdot \text{scale} \cdot (k - 3)$$

$$IPI(k) = IPI_{\text{REF}} + a_4 \cdot \text{scale} \cdot (k - 3)$$

where k is a scalar index between 1 and 10 (e.g. the waveform w) and scale is an arbitrary constant which specifies the size of the steps for the gradient search (Table 6.3). To verify that the gradient direction was approximately correct, the gradient search was performed backwards ($k = 1 \dots 2$) from *Baseline 1* ($k = 3$) as well as forwards ($k = 4 \dots 10$). If the gradient direction is correct, Ψ should increase as $k > 3$ and decrease as $k < 3$, at least in the region near *Baseline 1* where a linear approximation of Ψ is valid. Eventually, as the linear approximation breaks down, Ψ should peak and then decrease as k continues to increase. The waveform w corresponding to the value of k which maximizes Ψ , where w is averaged over all 7 Os, became the new optimum, *Baseline 2*.

MagNPB, MagPRR, MagW, and MagIPI: Single-variable effects

The same seven Os then proceeded with a set of experiments which varied one-at-a-time each of the four waveform variables NPB , PRR , W , and IPI around *Baseline 2*. Ten levels of one variable (the independent variable IV) were presented for each experiment, using the three-step procedure in **MagNPBscreen** (sensation threshold current S , maximal current without discomfort M , and magnitude at maximal current without discomfort Ψ). The levels of IV were:

NPB: 1, 2, 4, 5, 6, **7**, 8, 10, 15, 20 pulses/burst

PRR: 200, 250, 300, 350, **400**, 450, 500, 700, 1000, 1500 Hz

W: 40, 60, 90, **120**, 150, 180, 220, 260, 300, 350 μ s

IPI: 0, 25, 50, 75, **100**, 130, 160, 200, 300, 500 μ s

The boldface numbers along with the fixed values $F = 15$ Hz and $Type = B+$ define the *Baseline 2* waveform, i.e., values for the waveform variables which were *not* varied in a particular experiment. *Baseline 2* was also used for w_{REF} . As above, the S and M determinations consisted of three replications of 10 values of IV , while the ψ determinations consisted of five replications of 10 values of IV $\Psi_{rj}(1) - \Psi_{rj}(10)$ plus two REF stimuli $\Psi_{rj}(11) - \Psi_{rj}(12)$ plus two LOW stimuli $\Psi_{rj}(13) - \Psi_{rj}(14)$ (all in different random orders).

RESULTS AND DISCUSSION

Data analysis

Data correction: The tedious nature of these experiments caused some Os to lapse in concentration or enter magnitude estimates incorrectly, e.g. entering 9 instead of 19 on the keyboard. We manually scanned the data for each experiment for errors by comparing the five replications r of the magnitude estimation $\psi_1(w) - \psi_5(w)$ for each waveform w . If one entry was far different from the other four, we attempted to correct the assumed error under the following conditions: (1) The error must be obvious. For example, for a set of five replicated ψ values (19, 20, 10, 20, 20), the value 10 is very likely a misentry, whereas the data set (4, 16, 8, 13, 9) indicates genuine nonrepeatability, not simply careless entry. (2) There must be only one assumed errant entry in the five replicates. If the assumed error was attributable to a missed, extra, or adjacent keystroke we corrected the single keystroke. In the above

example, we replaced 10 with 20. If the error appeared to be due to lapse of concentration, we replaced the assumed error with the closest integer mean of the other four points; e.g. (20, 6, 4, 9, 4) was changed to (6, 6, 4, 9, 4). We did not attempt to correct data which did not meet both conditions; doubtful data were unaltered. No single experiment required more than two corrections; 53 of the 67 experiments required no corrections.

Error analysis: The calculations of variance and standard error of the mean (SE) for S and M are straightforward, as these measurements are replicated $U = V = 3$ times:

$$\text{Var}[M'_{\nu}(w)] = \frac{1}{V-1} \sum_{\nu=1}^V [M'_{\nu}(w) - \overline{M}'(w)]^2$$

$$\text{SE}[\overline{M}'(w)] = \sqrt{\frac{1}{V} \text{Var}[M'_{\nu}(w)]}$$

where M'_{ν} is the drift-corrected M from Eq. (1), ν is the replicate, $\overline{M}'(w)$ is the mean of three replicates, and w is the waveform. (The calculations are identical for S).

The variance of $\overline{\mathcal{R}}(w)$ is approximated by the variance of the first term of its Taylor Series expansion [29]:

$$\text{Var}[\overline{\mathcal{R}}(w)] = \left(\frac{\overline{\mathcal{R}}(w)}{\overline{M}'(w)} \right)^2 \text{Var}[\overline{M}'(w)] + \left(\frac{\overline{\mathcal{R}}(w)}{\overline{S}'(w)} \right)^2 \text{Var}[\overline{S}'(w)] \quad (3)$$

where

$$\text{Var}[\overline{M}'(w)] = \frac{1}{V} \text{Var}[M'_{\nu}(w)] \quad (4)$$

(similar for S). Note that $\text{Var}[\mathfrak{R}_u(\mathbf{w})]$ does not exist because $\mathfrak{R}_u(\mathbf{w})$ does not exist; the measurements of $S_u(\mathbf{w})$ and $M_v(\mathbf{w})$ were not paired.

For analysis of variance (ANOVA) to test the significance of the effect of waveform k on \mathfrak{R} , the mean-square of the treatment (waveform) $MSTr$ is calculated in the usual way (we replace the waveform vector \mathbf{w} with the scalar index k):

$$MSTr = \frac{U}{K-1} \sum_{k=1}^K \left[\overline{\mathfrak{R}}_{\cdot}(k) - \overline{\mathfrak{R}}_{\cdot}(\cdot) \right]^2 \quad (5)$$

where $K = 10$ is the number of waveforms. Because $\mathfrak{R}_u(\mathbf{w})$ does not exist, the mean-square error MSE cannot be calculated in the usual way:

$$MSE = \frac{1}{K(U-1)} \sum_{k=1}^K \sum_{u=1}^U \left[\mathfrak{R}_u(k) - \overline{\mathfrak{R}}_{\cdot}(k) \right]^2$$

However, if we note that MSE is the mean of the variance of all K waveforms

$$MSE = \frac{1}{K} \sum_{k=1}^K \text{Var}[\mathfrak{R}_{\cdot}(k)]$$

and that $\text{Var}[\overline{\mathfrak{R}}_{\cdot}(k)] = \text{Var}[\mathfrak{R}_u(k)]/U$ if $\mathfrak{R}_u(k)$ did exist (assuming the independence of the replicates r), we can calculate the error as

$$MSE = \frac{U}{K} \sum_{k=1}^K \text{Var}[\overline{\mathfrak{R}}_{\cdot}(k)]$$

where $\text{Var}[\overline{\mathfrak{R}}_{\cdot}(k)]$ is given by Eq. (3). The ANOVA test then proceeds with $f =$

$MSTr/MSE$ with $K - 1 = 9$ degrees of freedom (dof) in the numerator and $K(U - 1) = 20$ dof in the denominator.

Figure 6.6 shows that the magnitude estimates $\Psi_r(w)$ contain two sources of experimental error: (1) error in determining $M_v(w)$ and (2) error in estimating Ψ when $\bar{M}'(w)$ is re-presented to O. (In the following discussion we will drop the prime notation for clarity so that $\bar{M}(w)$ means $\bar{M}'(w)$, the mean of the 3 drift-corrected replications v of maximal current without discomfort $M_v(w)$ for waveform w). These two error sources are independent; each is the result of measurement replication in different random orders. The total variance in $\Psi_r(w)$ is therefore the sum of the component variances, with appropriate scaling. We model the **MAG** experiments as follows:

$$\begin{aligned} M_v(w) &= f(w) + \alpha_v \\ \Psi_r &= g[w, \bar{M}(w)] + \beta_r \end{aligned} \tag{6}$$

where

$$\bar{M}(w) = \frac{1}{V} \sum_{v=1}^V M_v(w)$$

and α and β are normal random variables with mean 0 and variance σ_f^2 and σ_g^2 , respectively, f and g are the "true" functions for M and Ψ in the absence of experimental error, and v ($1 \dots V = 3$) and r ($1 \dots R = 5$) are the replicates of the M and Ψ experimental trials. Because α and β are independent,

$$\text{Var}(\Psi_r) = \text{Var}[g(w, \bar{M})] + \text{Var}(\beta_r)$$

where $\bar{M}.$ is assumed to mean $\bar{M}.(w)$ for clarity. Because the relationship between Ψ and M is approximately linear in the region of interest near $\psi = \psi(\text{REF}) = 20$,

$$\text{Var}(\Psi_n) = \left(\frac{\partial \psi}{\partial w} \right)^2 \text{Var}(w) + \left(\frac{\partial \psi}{\partial \bar{M}.} \right)^2 \text{Var}(\bar{M}.) + \sigma_g^2$$

but because w is constant and because of Eq. (6),

$$\text{Var}(\Psi_n) = \frac{1}{U} \left(\frac{\partial \psi}{\partial \bar{M}.} \right)^2 \sigma_f^2 + \sigma_g^2$$

where the model variances are experimentally approximated by

$$\sigma_f^2 \approx \frac{1}{V-1} \sum_{v=1}^V [M_v(w) - \bar{M}.(w)]^2$$

$$\sigma_g^2 \approx \frac{1}{R-1} \sum_{r=1}^R [\Psi_r(w) - \bar{\Psi}.(w)]^2$$

and the derivative is experimentally approximated by

$$\frac{\partial \psi}{\partial \bar{M}.} \approx \frac{\psi_{\text{MCL}} - \psi_{\text{LOW}}}{M - M_{\text{LOW}}}$$

where the LOW current $M_{\text{LOW}} = S + 0.75(M - S)$ for the REF waveform.

For the mean $\bar{\Psi}.(w)$ of all $R = 5$ replications, the variance due to β is reduced by a factor of R , but the error due to α is not reduced further because all R replicates of Ψ use the same value of $\bar{M}.(w)$. Therefore,

$$\text{Var}(\bar{\Psi}) = \frac{1}{V} \left(\frac{\partial \psi}{\partial \bar{M}} \right)^2 \sigma_f^2 + \frac{1}{R} \sigma_g^2 \quad (7)$$

and the standard errors in Table 6.1 are the square root of this quantity.

To use ANOVA for testing the significance of Ψ effects, $MSTr$ is calculated similarly to Eq. (5). However, MSE must be carefully constructed for a valid f test. Based on the model in Eq. (6), it can be shown that the expected value of $MSTr$ is

$$E[MSTr] = \frac{R}{K-1} \sum_{k=1}^K \left(g(k) - \frac{1}{K} \sum_{k=1}^K g(k) \right)^2 + \frac{R}{V} \left(\frac{\partial \psi}{\partial \bar{M}} \right)^2 \sigma_f^2 + \sigma_g^2.$$

If the null hypothesis H_0 is true (there is no effect of waveform k on Ψ , i.e. $\Psi(1) = \Psi(2) = \dots = \Psi(K)$), then the first term (the real effect) is zero. Therefore, we construct MSE so that $f = MSTr/MSE = 1$ when H_0 is true:

$$MSE = \frac{R}{V} \left(\frac{\partial \psi}{\partial \bar{M}} \right)^2 \sigma_f^2 + \sigma_g^2$$

There are $K - 1 = 9$ dof for $MSTr$ and between $K(V - 1) = 20$ and $K(R - 1) = 40$ dof for MSE . We use 20 dof for a conservative test.

Scale 1, Scale 2, and Scale 3: Magnitude scale

Scale 1: Figure 6.7 shows the relationship between $\bar{\psi}(I)$ (mean of 5 replications) and I for the seven chosen Os who performed **Scale 1** (the results from three other Os were less repeatable). With individual variations, this relationship is an approximately linear function rather than a power function. The difference between this finding and the results of others [14], [15], [16] is because **Scale 1** defines two standard intensities: $\psi(S) = 0$ (sensation threshold) and $\psi(I_{REF}) = 20$ (reference). The

experiment therefore more closely defines a category scale than a true magnitude scale [23], [30]. This is adequate for our purposes because the main objective of this study was to maximize the dynamic range Ψ .

The data frequently show a nonuniformity in O's use of the magnitude scale. In particular, some O's (O1, O5, and O6) tended to cluster magnitude estimates near the REF level, causing a lower slope in this region. Other O's (O4, O7) showed a similar preference for the lower end of the scale. These end effects are expected because ψ is easier to estimate near the standard levels than in the middle of the scale [30].

Occasionally, the ψ vs. I relationship is nonmonotonic in one or more regions. This effect is not likely artifactual; it frequently exceeds the standard error SE of the ψ estimations, and it occurs in three Os (O2, O4, and O7). One possible explanation is that O mentally constructs two (or more) different scales depending on the approximate magnitude of the test stimulus. Low-level stimuli are therefore compared to zero, and high-level stimuli are compared to REF. The two scales may not coincide at intermediate levels, causing confusion and inaccurate ψ estimations. Fortunately, because the Ψ optimization experiments present stimuli mostly near REF, this occasional nonmonotonicity should not bias the optimization results.

Scale 2 explores the upper range of the ψ vs I relationship in more detail; eleven current levels span the upper half of the range from sensation threshold current S to maximal current without discomfort M . Figure 6.8 shows that the many closely-spaced currents increase O confusion at midrange levels. Again, however, the ψ estimates near $\psi(I_{\text{REF}})$ are reliable. *Scale 2* places $I_{\text{REF}} < M$ to extend the useful artifact-free range of the magnitude scale. Some Os were initially reluctant to specify test stimulus magnitudes above $\psi = 20$; they mistakenly identified $\psi(I_{\text{REF}}) = 20$ as

$\psi(M)$. A simple verbal clarification and one repeat of the experiment corrected this situation.

Scale 3: Except for O1, the seven Os each completed **Scale 3** twice; the results are called **Scale 3a** and **Scale 3b**. Figures 6.9 and 6.10 show that the artifact-free range of $\psi(I)$ is the upper 40% of the I scale for most Os.

Averages: Figure 6.11 shows the mean ψ of all seven Os for the four sessions of scaling experiments. To facilitate comparison of the three different experiments, the current scale is normalized so that 0 represents sensation threshold current S and 1 represents the reference current I_{REF} , regardless of M . The $\psi(I)$ function is similar for all of the experiments. In particular, the nonmonotonicities disappear in the mean, suggesting that there is no systematic error in the scale for this group of Os. Also note the expected, slightly higher, slope for the **Scale 2** experiment because of its closely-spaced currents [30]. Finally, Fig. 6.12 shows that the mean of the SE s for all seven Os is minimized near the standard magnitudes (0 and 20). This supports the earlier assumption that magnitude estimation is easier near the standard levels.

MagNPBscreen

Figure 6.13 shows $\Psi(NPB)$ for the 7 selected Os (the results from 3 other Os were more scattered, but similar in shape). All Os but O3 show a low Ψ at low levels of NPB , confirming earlier results. O3 continued as an O because the small Ψ variations were statistically significant ($p < 0.05$). Table 6.1 shows the mean over all waveforms w of the standard error $SE(\bar{\Psi}_w)$ for **Search** and all of the **Mag** experiments.

Gradient and Search: Finding Baseline 2 optimum

Table 6.3 shows the effects of the four waveform variables for the factorial experiment where $a_1 - a_4$ are the single-variable effects for NPB , PRR , W , and IPI , respectively. The single-variable effect a_1 is the change in Ψ resulting from changing NPB from NPB_L to NPB_H . These effects, along with the mean Ψ of all conditions a_0 and the variable interaction effects (changes in Ψ which result only from changing two or more variables at a time) form the following model which exactly describes the observed mean responses in the four-dimensional experiment:

$$\begin{aligned}\bar{\Psi}.(w) = & a_0 \\ & + (a_1x_1 + a_2x_2 + a_3x_3 + a_4x_4)/2 \\ & + (a_{12}x_1x_2 + a_{13}x_1x_3 + a_{14}x_1x_4 + a_{23}x_2x_3 + a_{24}x_2x_4 + a_{34}x_3x_4)/2 \\ & + (a_{123}x_1x_2x_3 + a_{124}x_1x_2x_4 + a_{134}x_1x_3x_4 + a_{234}x_2x_3x_4)/2 \\ & + (a_{1234}x_1x_2x_3x_4)/2\end{aligned}$$

where $x_1 - x_4$ are linearly-scaled versions of NPB , PRR , W , and IPI and take on values of only -1 and 1 [26]. The standard errors of the effects a are

$$SE(a) = \left\{ \frac{1}{4K} \sum_{k=1}^K \text{Var}[\bar{\Psi}.(k)] \right\}^{1/2}$$

where $K = 2^4 = 16$ waveforms and $\text{Var}[\bar{\Psi}.(k)]$ is given by Eq. (7).

The boldface entries in Table 6.3 denote variable effects which exceed $2 \cdot SE(a)$, i.e. have less than 5% chance of occurring due to experimental error. While effects due to NPB , PRR , and W usually dominate, two and three-factor interactions are present, suggesting a complex response surface. Such strong interactions could potentially undermine the gradient search for the maximal Ψ .

We found out that this was not the case, although the response for $\Psi(k)$ was somewhat scattered. Figure 6.14 shows Ψ along the gradient path (Fig. 6.4 and Eq. 2) for each O who completed **Search**. A second-order polynomial fit for each O's data shows that Ψ increases and peaks at $3 \leq k \leq 10$, confirming the correct gradient direction for all but O4. However, rather than using the peak of this polynomial model, we used the value of k which maximized the actual data Ψ to determine the new optimal w . *Baseline 2* (*Type* = B+, $F = 15$ Hz, $PRR = 400$ Hz, $W = 120$ μ s, $IPI = 100$ μ s, and $NPB = 7$) is approximately the mean of the waveform variable values which maximized Ψ for each of the 7 Os.

Single-variable effects

Figures 6.15 – 6.18 respectively show how $\bar{\Psi}_{.,}(k)$ varies with the 10 levels k of the scalar independent variables NPB , PRR , W , and IPI for each of the seven Os. Figures 6.19 – 6.22 show the mean $\bar{\Psi}_{.,}(k)$ and $\bar{\mathcal{R}}_{.,}(k)$ over all 6 or 7 Os (O1 did not complete **MagNPB** or **MagPRR**). Note that the mean $\bar{\mathcal{R}}_{.,}(k)$ value is averaged *geometrically* over the O observers o

$$\bar{\mathcal{R}}_{.,}(k) = \left[\prod_{o=1}^O \mathcal{R}_{.,o}(k) \right]^{1/O} \quad (8)$$

because while their trends are similar, their absolute levels are quite different; the means $\bar{\mathcal{R}}_{.,o}(\cdot)$ over all values of PRR vary over a 3:1 range. The error bars in Figs. 6.19 – 6.22 show the SE of the mean over all 6 or 7 Os, 10 waveforms k , and replications:

$$SE[\bar{\Psi}_{.,(\cdot)}] = \left(\frac{\frac{1}{K} \sum_{k=1}^K \left(\frac{1}{O} \sum_{o=1}^O \text{Var}[\bar{\Psi}_{.,o}(k)] + \frac{1}{O-1} \sum_{o=1}^O [\bar{\Psi}_{.,(k)} - \bar{\Psi}_{.,o}(k)]^2 \right)}{O} \right)^{1/2} \quad (9)$$

where the Var term is given by Eq. (7); a similar expression combined with Eq. (3) calculates $SE[\bar{\mathcal{R}}_{.,(\cdot)}]$. The addition of variances in the numerator is justified by the assumption that the errors due to Os and errors due to replications are independent.

Finally, Table 6.4 shows the p -values from the ANOVA test (in *Error analysis* section) for each O performing each of the four single-variable experiments. These results are not without bias. Os with low overall M/S ratios (e.g. O2 in Table 6.1) tend to show high (insignificant) p -values because the narrow current range causes small errors in determining M to translate into large effective errors in Ψ by Eq. (7) — a narrow current range necessarily expands the magnitude scale to fit the current scale. Some Os (e.g. O3 in Figs. 6.15 – 6.18) have low p -values because they do not show strong reactions to different waveforms for any experiment. Conversely, some very experienced observers, (e.g. O6) can easily distinguish between waveforms even when presented in different random orders, leading to several highly-significant effects. We will therefore concentrate on the mean plots in Figs. 6.19 – 6.22 rather than on the statistical results.

MagNPB: Figures 6.15 and 6.19 and Table 6.1 show that the increase in Ψ with increasing NPB is clearly the most important effect. The large increase in Ψ with NPB is not accompanied by a corresponding increase in \mathcal{R} . In fact, the maximal value of \mathcal{R} occurs at $NPB = 2$, far from providing the most intense comfortable stimulus at $NPB = 6$.

We speculate that the mechanism for the large Ψ increase from $NPB = 1$ to $NPB = 6$ may be due to an increased proportion of afferent touch (α) fibers being stimulated by the repetitive pulses compared with the pain (γ) fibers. Considering that $PRR = 400$ Hz, this is consistent with the high sensitivity of normal touch to vibration in the 100 – 600 Hz range [31].

The drop in Ψ at higher NPB may be attributable to a change in percept quality; the stimulation at $NPB \geq 15$ feels higher in "frequency" than stimulation at lower NPB . While Os might be expected to interpret this percept as stronger than one which feels lower in frequency [27], it takes on a character more of pressure than vibration. Some Os noted that such variations in percept quality between trials made magnitude comparisons difficult. This higher-frequency percept is expected because long bursts span a large portion of the overall waveform period T , and the waveform begins to look like a continuous train of pulses at a high frequency. (The definitions of the waveform variables allow for this redundancy. For example, a waveform defined by $Type = B+$, $W = IPI = 50 \mu s$, $NPB = 1$, $F = 400$ Hz is identical to a waveform with $Type = B+$, $W = IPI = 50 \mu s$, $NPB = 10$, $F = 40$ Hz, $PRR = 400$ Hz.)

MagPRR: Figure 6.20 shows that PRR has little consistent effect on Ψ or \mathfrak{R} . The observed effects are likely due more to changes in percept *quality* than magnitude. One O who in an informal experiment continuously varied PRR noted that for high values of PRR (> 700 Hz), the percept was more vibratory in nature (desirable), but stinging sensations occurred at lower vibratory magnitudes (undesirable) than at lower PRR . This is consistent with [11]. Lower values of PRR (< 350 Hz) produced a percept of "higher frequency," and the six Os interpreted this differently (Fig. 6.16).

The sharp dip at $PRR = 400$ Hz for most Os may be caused by the reference stimulus having the same PRR ; the Os may note that the reference and test waveform qualities are similar and thus bias their magnitude estimates. This is supported by the low spread in magnitude estimates at 400 Hz compared to other values of PRR . We conclude that any PRR value between 200 and 800 Hz is suitable; different Os may prefer different values. The average $\bar{\Psi}_{.,}(PRR)$ is maximized by $PRR = 350$ Hz (Fig. 6.20).

MagW: The small effect of phase width W on Ψ separates the Os into two groups. Fig. 6.17 shows that for O1, O2 and O6, Ψ increases with W whereas for O3, O4, O5, and O7, Ψ decreases with W . Because we did not repeat this experiment at different skin locations on the same O, this effect may rather represent two groups of skin sites with different tactile afferent innervations, because shifts of electrode position as small as 1 mm can result in different electrotactile percepts [1]. The mean Ψ for all seven Os (Fig. 6.21) peaks at $W = 150$ μ s, but values between 150 and 260 μ s result in a similar Ψ . \mathfrak{R} increases slightly with W up to 220 μ s and then falls, approximately following the variation in Ψ . Both \mathfrak{R} and Ψ continue to fall at increasing values of W ; the uncomfortable stinging sensation produced by waveforms with $W > 500$ μ s is well-known [15], [32]. We did not explore the region $W < 10$ μ s where \mathfrak{R} is reported to decrease substantially [24].

MagIPI: Interphase interval IPI has no apparent effect on \mathfrak{R} or Ψ . Figure 6.18 shows no consistent changes in Ψ with IPI ; the relatively large effect in O2's data is not statistically significant ($p > 0.05$) due to the large error. O2's unrepresentative data are not included in the mean $\bar{\Psi}_{.,}(IPI)$ or $\bar{\mathfrak{R}}_{.,}(IPI)$ plots (Fig. 6.22).

Sensation threshold and maximal current without discomfort

Figures 6.23 — 6.26 show the geometric means (Eq. 8) of all Os of the sensation threshold current S and the maximal current without discomfort M as they vary with NPB , PRR , W , and IPI , respectively. Both M and S data are corrected for drift using Eq. (1).

The drop in S and M with increasing NPB (Fig. 6.23) describes temporal summation of the pulses. These effects are significant ($p < 0.05$) for data from almost all Os. Because peripheral afferent neurons integrate single pulses with a time constant $\tau \approx 100 \mu s$, this summation of multiple pulses must take place at a higher level [15].

Fig. 6.24 shows that PRR does not substantially affect S or M . However, the small observed drops in S and M with increasing PRR are significant ($p < 0.05$) for some O's. We might expect a drop in S and M because the total burst energy is concentrated in a smaller time at high PRR values, allowing slightly greater temporal summation.

Figure 6.25 shows the usual strength–duration curve for threshold (S or M) vs. phase width W . This describes temporal summation at the peripheral neural level [15].

Others have observed the slight increase in S at low values of IPI [2], due to partial cancellation of charge by the nearly-adjacent positive and negative phases. We observed the effect for M as well (Fig. 6.26). As before, O2's data are not included in the average.

CONCLUSIONS

The sensation produced by electrotactile stimulation has comfortable (vibratory) and uncomfortable (stinging) percepts. The level of the stinging percept limits the stimulation current and hence the useful dynamic range. A waveform with the number of pulses/burst $NPB = 6$, pulse repetition rate $PRR = 350$ Hz, and phase width $W =$

150 μ s maximizes the intensity (magnitude) of the vibratory percept compared with the stinging percept. In particular, waveforms with $1 \leq NPB < 6$ substantially reduce the intensity of the vibratory percept while largely maintaining the sting. The interphase interval *IPI* between positive and negative phases of a balanced-biphasic waveform has no effect on dynamic range.

These experiments maximized the electrotactile dynamic range for one electrode geometry (5.5-mm-diameter-active coaxial) at one skin site (abdomen) with the balanced-biphasic pulse bursts delivered at one rate (15 Hz). The effects of *W* and *PRR* may be dependent on skin site or observer.

Measuring stimulation intensity at a predetermined maximal current without discomfort (for each waveform) provides a measure of electrotactile intensity dynamic range which is more relevant to the overall comfort of the stimulation percept than the ratio of pain threshold to sensation threshold. In most cases, the two measures yield different information.

ACKNOWLEDGEMENTS

We thank Dr. James Dannemiller (Dept. of Psychology), Dr. Murray Clayton (Dept. of Statistics), and Kurt Neuwirth (Academic Computing Center) for their assistance in psychophysical and statistical methods.

REFERENCES

- [1] K. A. Kaczmarek, J. G. Webster, P. Bach-y-Rita and W. J. Tompkins, "Electrotactile and vibrotactile displays for sensory substitution systems," *IEEE Trans. Biomed. Eng.*, vol. 38, pp. 1–16, 1991.
- [2] A. Y. J. Szeto and F. A. Saunders, "Electrocutaneous stimulation for sensory communication in rehabilitation engineering," *IEEE Trans. Biomed. Eng.*, vol. BME-29, pp. 300–308, 1982.
- [3] P. Bach-y-Rita, *Brain Mechanisms in Sensory Substitution*. New York: Academic, 1972.
- [4] C. C. Collins, "On mobility aids for the blind," in *Electronic Spatial Sensing for the Blind*, D. H. Warren and E. R. Strelow, Eds. Dordrecht, The Netherlands: Martinus Nijhoff, 1985, pp. 35–64.
- [5] C. M. Reed, N. I. Durlach and L. D. Bradia, "Research on tactile communication of speech: A review," *AHSA Monographs*, vol. 20, pp. 1–23, 1982.
- [6] C. E. Sherrick, "Basic and applied research on tactile aids for deaf people: Progress and prospects," *J. Acoust. Soc. Am.*, vol. 75, pp. 1325–1342, 1984.
- [7] A. Y. J. Szeto and K. M. Christensen, "Technological devices for deaf-blind children: Needs and potential impact," *IEEE Eng. Med. Biol. Mag.*, vol. 7, no. 3, pp. 25–29, 1988.
- [8] C. C. Collins and J. M. J. Madey, "Tactile sensory replacement," in *Proc. San Diego Biomed. Symp.*, vol. 13, 1974, pp. 15–26.

- [9] C. A. Phillips, "Sensory feedback control of upper- and lower-extremity motor prostheses," *CRC Crit. Rev. Biomed. Eng.*, vol. 16, pp. 105–140, 1988.
- [10] R. R. Riso, "Sensory augmentation for enhanced control of FNS systems," in *Ergonomics in Rehabilitation*, A. Mital, Ed. New York: Taylor and Francis, 1988, pp. 253–271.
- [11] F. A. Saunders, "Information transmission across the skin: High-resolution tactile sensory aids for the deaf and the blind," *Int. J. Neurosci.*, vol. 19, pp. 21–28, 1983.
- [12] A. Y. J. Szeto and R. R. Riso, "Sensory feedback using electrical stimulation of the tactile sense," in *Rehabilitation Engineering*, R. V. Smith and J. H. Leslie Jr., Eds. Boca Raton, FL: CRC Press, 1990, pp. 29–78.
- [13] F. A. Saunders, "Electrocutaneous displays," in *Proc. Conf. Cutan. Comm. Sys. Dev.*, F. A. Geldard, Ed., Psychonomic Society, 1973, pp. 20–26.
- [14] S. S. Stevens, "The psychophysics of sensory function," in *Sensory Communication*, W. Rosenblith, Ed. Cambridge: M.I.T. Press, 1962, pp. 1–33.
- [15] G. B. Rollman, "Electrocutaneous stimulation," in *Proc. Conf. Cutan. Comm. Sys. Dev.*, F. A. Geldard, Ed., Psychonomic Society, 1973, pp. 38–51.
- [16] D. V. Cross, B. Tursky and M. Lodge, "The role of regression and range effects in determination of the power function for electric shock," *Percept. Psychophys.*, vol. 18, pp. 9–14, 1975.
- [17] R. M. Sachs, J. D. Miller and K. W. Grant, "Perceived magnitude of multiple electrocutaneous pulses," *Percept. Psychophys.*, vol. 28, pp. 255–262, 1980.

- [18] P. McCallum and H. Goldberg, "Magnitude scales for electrocutaneous stimulation," *Percept. Psychophys.*, vol. 17, pp. 75–78, 1975.
- [19] K. A. Kaczmarek, K. M. Kramer, J. G. Webster and R. G. Radwin, "A 16-channel 8-parameter waveform electrotactile stimulation system," *IEEE Trans. Biomed. Eng.*, vol. 38, no. 10, 1991 (in press).
- [20] M. P. Lynch, R. E. Eilers, D. K. Oller and L. Lavoie, "Speech perception by congenitally deaf subjects using an electrocutaneous vocoder," *J. Rehab. Res. Dev.*, vol. 25, pp. 41–50, 1988.
- [21] F. A. Saunders, *Tacticon 1600 Electrotactile Sensory Aid for the Deaf: User's Guide*. San Rafael, CA: Tacticon Corporation, 1986.
- [22] D. V. Cross, "On judgements of magnitude," in *Social Attitudes and Psychophysical Measurement*, B. Wegener, Ed. Hillsdale, NJ: Lawrence Erlbaum Assoc., 1982, pp. 73–88.
- [23] M. Lodge, "Magnitude scaling: Quantitative measurement of opinions," in *Sage University Paper series on Quantitative Applications in the Social Sciences*, J. L. Sullivan and R. G. Niemi, Eds. Beverly Hills, CA: Sage Publications, 1984, pp. 1–87.
- [24] C. C. Collins, "Tactile television — mechanical and electrical image projection," *IEEE Trans. Man-Mach. Sys.*, vol. MMS-11, pp. 65–71, 1970.
- [25] C. C. Collins and F. A. Saunders, "Pictorial display by direct electrical stimulation of the skin," *J. Biomed. Sys.*, vol. 1, pp. 3–16, 1970.
- [26] G. E. P. Box, W. G. Hunter and J. S. Hunter, *Statistics for experimenters*. New York: Wiley, 1978.

- [27] A. Y. J. Szeto, "Relationship between pulse rate and pulse width for a constant-intensity level of electrocutaneous stimulation," *Ann. Biomed. Eng.*, vol. 13, pp. 373–383, 1985.
- [28] J. P. Girvin, L. E. Marks, J. L. Antunes, D. O. Quest, M. D. O'Keefe, P. Ning and W. H. Dobelle, "Electrocutaneous stimulation I. The effects of stimulus parameters on absolute threshold," *Percept. Psychophys.*, vol. 32, pp. 524–528, 1982.
- [29] W. Volk, *Applied Statistics for Engineers*. New York: McGraw-Hill, 1958.
- [30] L. E. Marks, "Psychophysical measurement: procedures, tasks, scales," in *Social Attitudes and Psychophysical Measurement*, B. Wegener, Ed. Hillsdale, NJ: Lawrence Erlbaum Assoc., 1982, pp. 43–71.
- [31] R. T. Verrillo, "Psychophysics of vibrotactile stimulation," *J. Acoust. Soc. Am.*, vol. 77, pp. 225–232, 1985.
- [32] R. H. Gibson, "Electrical stimulation of pain and touch," in *The Skin Senses*, D. R. Kenshalo, Ed. Springfield, IL: Charles C. Thomas, 1968, pp. 223–260.

Table 6.1

Mean values of sensation threshold current S and maximal current without discomfort M .
Drift of S and M over 30 trials.

Standard errors of means $\bar{S}(\omega)$, $\bar{M}(\omega)$, $\bar{\mathcal{R}}(\omega)$, and $\bar{\Psi}(\omega)$ (replication error).

Experiment	Observer	Mean $\bar{S}(\omega)$ (mA)	Mean $\bar{M}(\omega)$ (mA)	S Drift (%)	M Drift (%)	SE $\bar{S}(\omega)$	SE $\bar{M}(\omega)$	SE $\bar{\mathcal{R}}(\omega)$	SE $\bar{\Psi}(\omega)$
MagNPB screen	O1	1.85	5.72	6.3	25.1	0.066	0.15	0.13	0.92
	O2	1.72	3.80	11.7	-5.5	0.044	0.18	0.11	4.67
	O3	1.43	5.38	3.8	15.7	0.031	0.13	0.12	0.80
	O4	0.98	5.59	-2.9	33.0	0.087	0.65	1.19	1.76
	O5	1.14	7.35	-4.7	4.7	0.029	0.28	0.29	1.32
	O6	3.80	16.40	-3.3	7.5	0.082	0.31	0.12	0.73
	O7	1.97	4.83	2.8	34.9	0.106	0.15	0.15	1.42
Search	O1	1.82	8.74	6.9	27.0	0.056	0.35	0.24	0.83
	O2	1.51	3.17	-4.7	15.4	0.061	0.10	0.11	2.23
	O3	1.10	3.30	3.3	18.2	0.032	0.22	0.22	1.63
	O4	1.34	3.45	8.8	22.0	0.055	0.11	0.11	0.90
	O5	1.63	5.85	-6.9	24.3	0.099	0.27	0.27	1.32
	O6	2.25	14.55	8.6	12.4	0.060	0.13	0.18	0.40
	O7	3.05	8.39	-10.9	33.7	0.118	0.43	0.17	0.82
MagNPB	O1	—	—	—	—	—	—	—	—
	O2	1.56	2.89	-3.0	-7.2	0.086	0.10	0.11	3.84
	O3	1.22	5.51	9.3	37.0	0.033	0.30	0.28	1.29
	O4	1.97	8.21	7.9	83.5	0.027	0.29	0.15	0.69
	O5	1.73	8.01	-3.6	-0.4	0.040	0.20	0.16	1.58
	O6	1.76	9.72	4.9	22.9	0.049	0.35	0.25	0.59
	O7	2.06	4.66	-5.3	23.0	0.076	0.14	0.10	1.17
MagPRR	O1	—	—	—	—	—	—	—	—
	O2	3.00	5.60	-12.3	3.4	0.099	0.12	0.08	1.70
	O3	1.65	4.69	0.0	12.8	0.020	0.10	0.07	0.39
	O4	2.05	6.78	10.0	14.0	0.069	0.20	0.16	0.31
	O5	1.67	8.50	-5.6	8.8	0.018	0.16	0.11	0.72
	O6	2.46	12.18	-10.1	26.4	0.126	0.26	0.30	0.43
	O7	1.82	7.27	46.8	38.4	0.237	0.33	0.52	0.92
MagW	O1	1.63	5.54	0.9	0.3	0.022	0.19	0.12	0.51
	O2	1.28	2.81	0.4	-5.3	0.013	0.15	0.10	2.87
	O3	1.30	5.72	4.6	23.0	0.040	0.37	0.27	1.40
	O4	2.46	6.35	10.7	37.2	0.067	0.32	0.16	1.18
	O5	1.55	7.48	-0.8	18.1	0.041	0.30	0.19	2.26
	O6	2.57	12.60	11.8	7.9	0.112	0.22	0.22	0.50
	O7	0.97	6.60	-4.0	51.3	0.064	0.34	0.60	1.46
MagIPI	O1	1.59	7.06	-1.0	13.8	0.017	0.14	0.10	0.42
	O2	3.21	5.19	20.8	8.3	0.120	0.15	0.08	2.22
	O3	1.54	4.90	4.4	29.5	0.033	0.16	0.13	0.49
	O4	2.25	6.43	25.0	10.5	0.122	0.22	0.20	0.92
	O5	1.82	8.74	-3.7	7.1	0.038	0.17	0.13	0.70
	O6	1.80	9.79	-2.6	6.3	0.033	0.43	0.26	0.66
	O7	2.81	5.00	34.3	35.4	0.086	0.21	0.09	1.04

Table 6.2

Independent variable settings for
Gradient experiment.

Waveform <i>w</i>	<i>NPB</i>	<i>PRR</i> (Hz)	<i>W</i> (μ s)	<i>IPI</i> (μ s)
1	4	300	75	75
2	8	300	75	75
3	4	500	75	75
4	8	500	75	75
5	4	300	125	75
6	8	300	125	75
7	4	500	125	75
8	8	500	125	75
9	4	300	75	125
10	8	300	75	125
11	4	500	75	125
12	8	500	75	125
13	4	300	125	125
14	8	300	125	125
15	4	500	125	125
16	8	500	125	125
17	6	400	100	100
18	6	400	100	100

Table 6.3

Variable effects for **Gradient** experiment.
 Boldface type denotes effects $a \geq 2 \cdot \text{SE}(a)$ i.e. $p \leq 0.05$.

Effect	O1	O2	O3	O4	O5	O6	O7
a_1 (NPB)	-0.57	0.85	-0.27	0.82	0.93	2.33	0.93
a_2 (PRR)	-0.43	0.40	1.22	0.33	2.33	0.43	-0.48
a_3 (W)	-0.07	3.75	0.97	1.53	-0.58	0.38	0.32
a_4 (IP1)	-0.13	0.45	-0.58	0.22	0.47	-0.27	-0.07
a_{12}	-1.17	2.55	0.83	-0.58	-0.27	0.47	0.37
a_{13}	-0.33	1.10	-0.23	0.22	-0.47	-0.28	0.48
a_{14}	-0.08	-0.60	0.32	0.13	-1.03	-0.23	0.58
a_{23}	0.62	-0.95	-0.32	0.73	-0.47	0.33	0.27
a_{24}	1.28	1.35	0.22	0.12	0.18	0.57	0.68
a_{34}	0.92	0.60	0.77	-0.28	-0.43	1.03	-0.53
a_{123}	-0.33	-2.20	-0.33	-0.77	0.72	-0.92	0.12
a_{124}	-0.18	0.70	-0.47	0.02	0.38	0.43	-0.57
a_{134}	-1.63	-1.25	0.28	-0.58	2.68	-0.13	0.12
a_{234}	-0.47	-0.30	-0.63	-0.17	-0.13	-0.02	-0.98
a_{1234}	-0.32	-2.15	-0.13	0.33	-1.93	0.33	0.58
a_0 (Mean)	20.84	17.05	19.56	19.36	20.01	19.84	20.09
SE(a)	0.64	1.15	0.46	0.26	1.00	0.24	0.40
scale	0.22	0.15	0.25	0.25	0.20	0.13	0.15

Table 6.4

ANOVA p -values for **MagNPB**, **MagPRR**, **MagW**, and **MagIPI** experiments.
 Boldface type denotes $p \leq 0.05$.

Indep. Var.	Expt.	O1	O2	O3	O4	O5	O6	O7
\mathcal{X}	<i>NPB</i>	—	0.376	0.005	0.087	0.226	0.028	0.072
\mathcal{X}	<i>PRR</i>	—	0.218	0.342	0.020	0.843	0.499	0.661
\mathcal{X}	<i>W</i>	0.000	0.000	0.759	0.283	0.302	0.018	0.458
\mathcal{X}	<i>IPI</i>	0.019	0.597	0.536	0.734	0.108	0.828	0.412
Ψ	<i>NPB</i>	—	0.283	0.265	0.000	0.000	0.000	0.026
Ψ	<i>PRR</i>	—	0.828	0.121	0.000	0.471	0.000	0.011
Ψ	<i>W</i>	0.000	0.903	0.322	0.208	0.884	0.000	0.582
Ψ	<i>IPI</i>	0.066	0.915	0.661	0.297	0.843	0.850	0.903

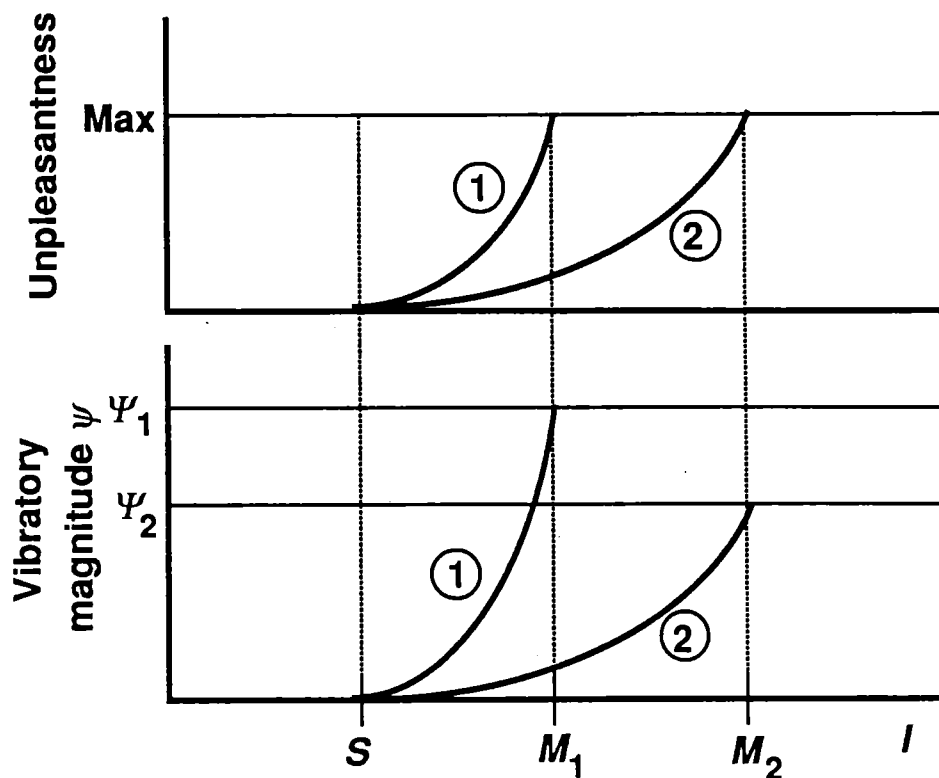


Fig. 6.1. Two qualities of electro tactile stimulation are vibratory magnitude ψ and unpleasantness. Condition 1 has a greater dynamic range than condition 2 because $\psi_1 > \psi_2$, even if $M_1/S < M_2/S$. The maximal current without discomfort M for each case is limited by the maximal acceptable unpleasantness in the electro tactile percept.

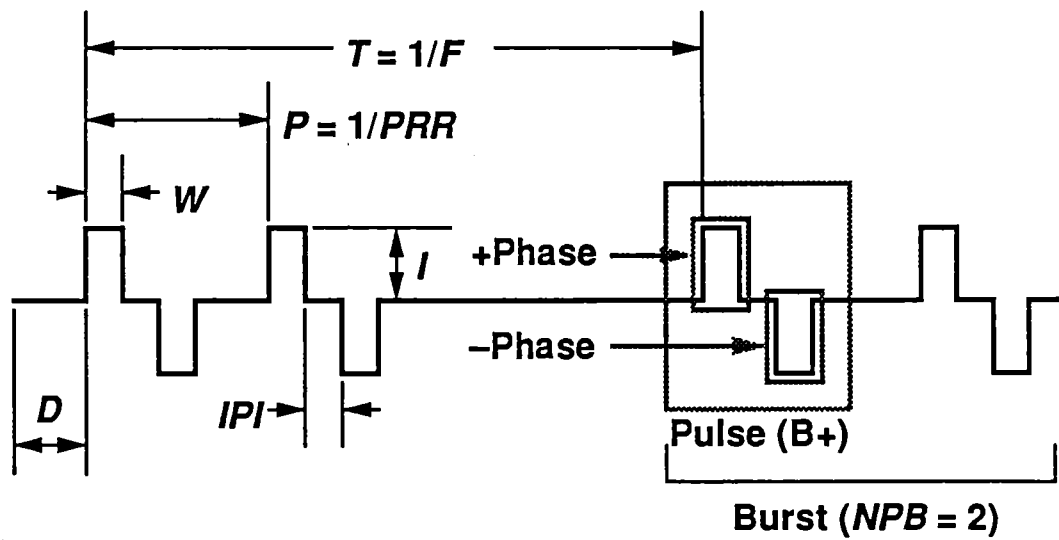


Fig. 6.2. Electrotactile waveform variables: D , delay; W , width; IPI , interphase interval; I , current; T , time between bursts; F , frequency of burst repetition; P , period of pulse repetition; PRR , pulse repetition rate; NPB , number of pulses per burst.

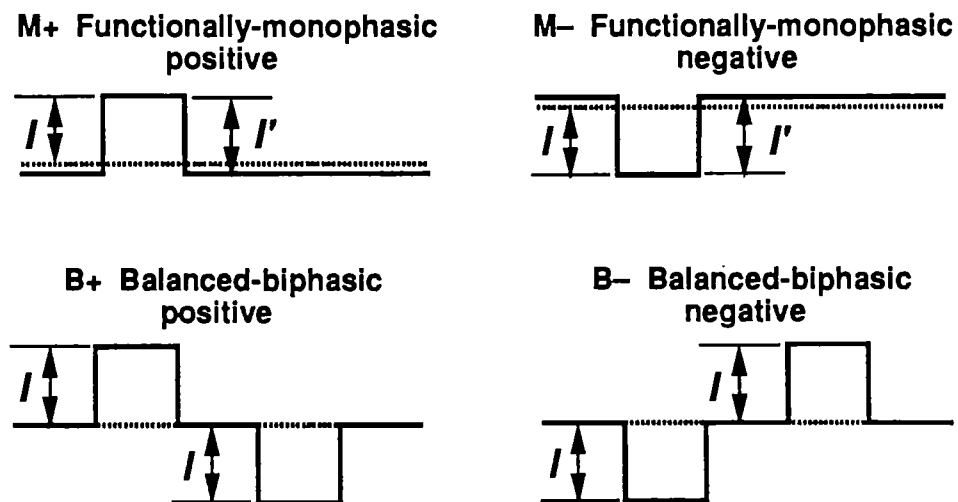


Fig. 6.3. Electrotactile waveform pulse types. Average current is zero for all types. The dotted line is the zero-current reference.

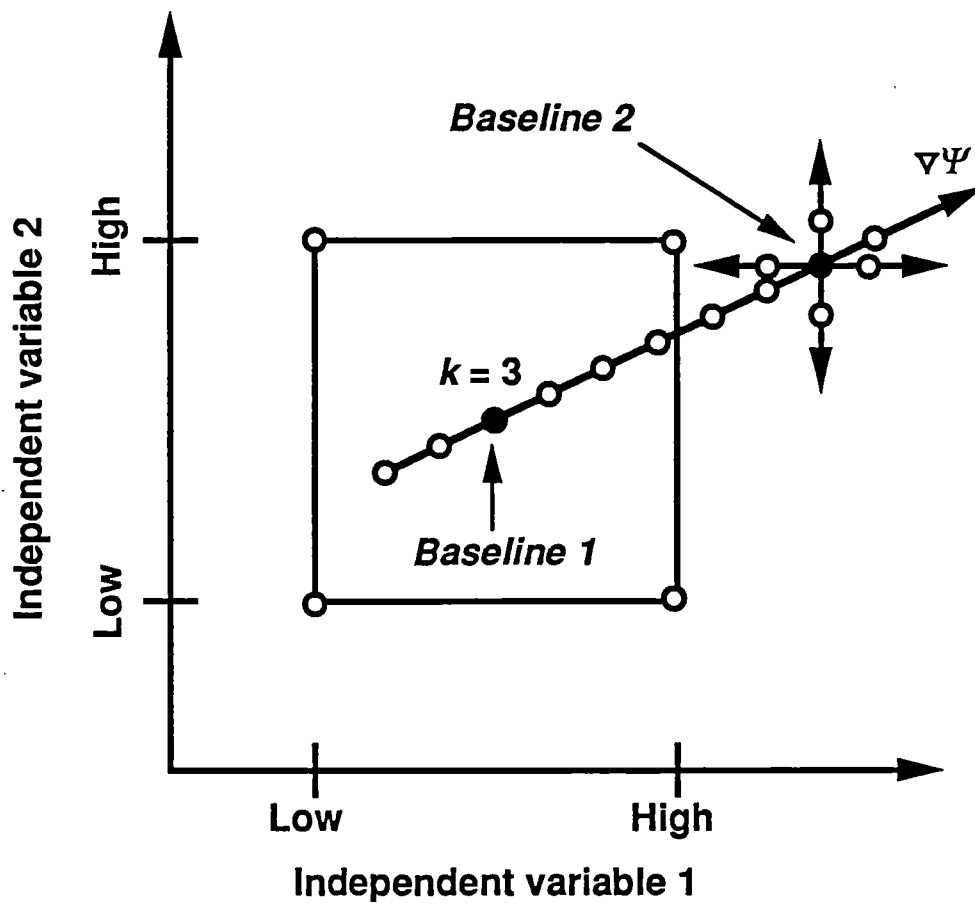


Fig. 6.4. The optimization procedure finds the waveform w which maximizes the dynamic range $\Psi(w)$. We show 2 of the 4 dimensions in the space of independent variables (NPB , PRR , W , IPI). The procedure starts by finding the gradient $\nabla\Psi(w)$ at the first approximation of the optimal $w = \text{Baseline 1}$. $\Psi(k)$ is measured along the gradient path (a 1-dimensional subspace). The value of k which maximizes $\Psi(k)$ defines $w = \text{Baseline 2}$. The four independent variables are then varied one-at-a-time around *Baseline 2* to explore this region and determine the final optimum. With fixed waveform values of $Type = B+$ and $F = 15$ Hz, *Baseline 1* = (6 pulses/burst, 400 Hz, 100 μ s, 100 μ s). With the same units, *Baseline 2* = (7, 400, 120, 100) and the final optimal waveform is (6, 350, 150, IPI) where IPI has no effect on Ψ .

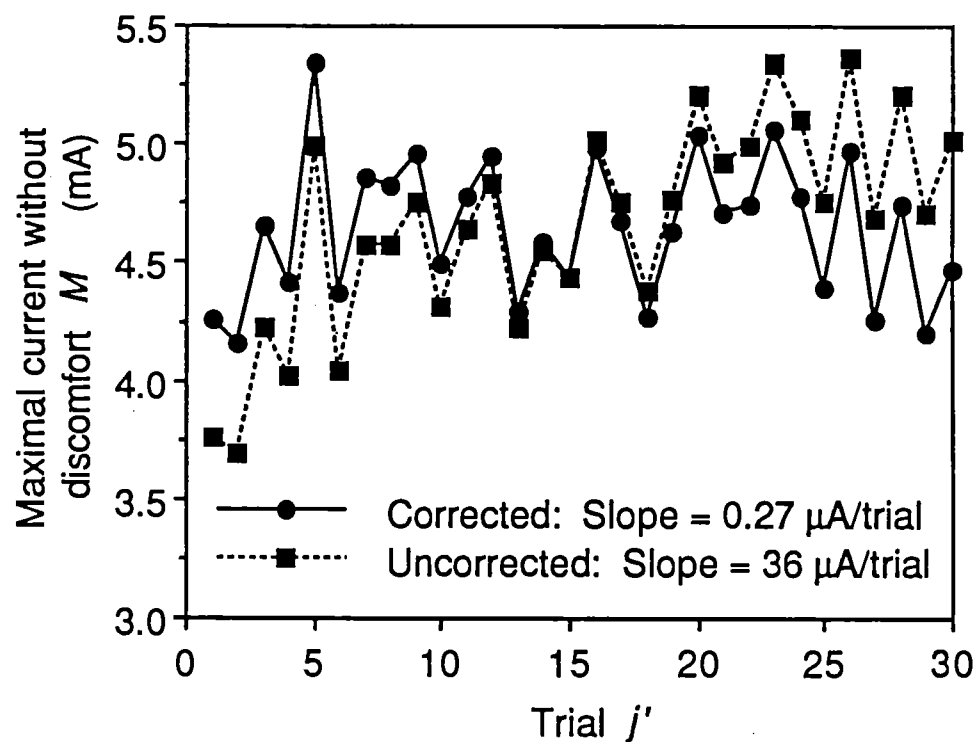


Fig. 6.5. A linear correction compensates for the typical upward drift in the maximal current without discomfort M with time. Trials are monotonic with time. (Data from experiment **MagNPB**, observer O7.)

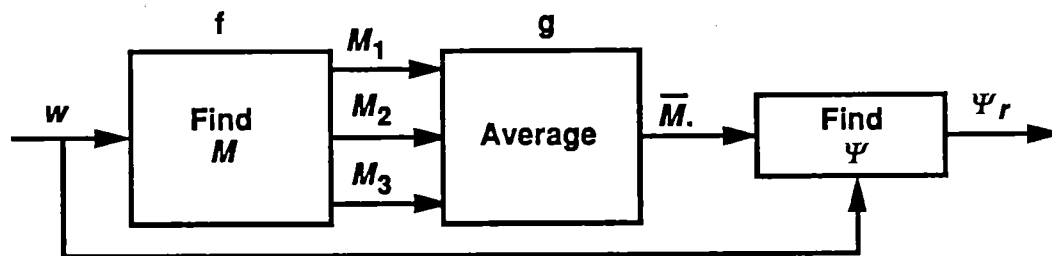


Fig. 6.6. The estimated dynamic range Ψ contains two sources of experimental error: (1) nonrepeatability in finding the maximal current without discomfort M and (2) nonrepeatability in finding the magnitude Ψ at current M . Ψ depends on both the current M and the waveform w .

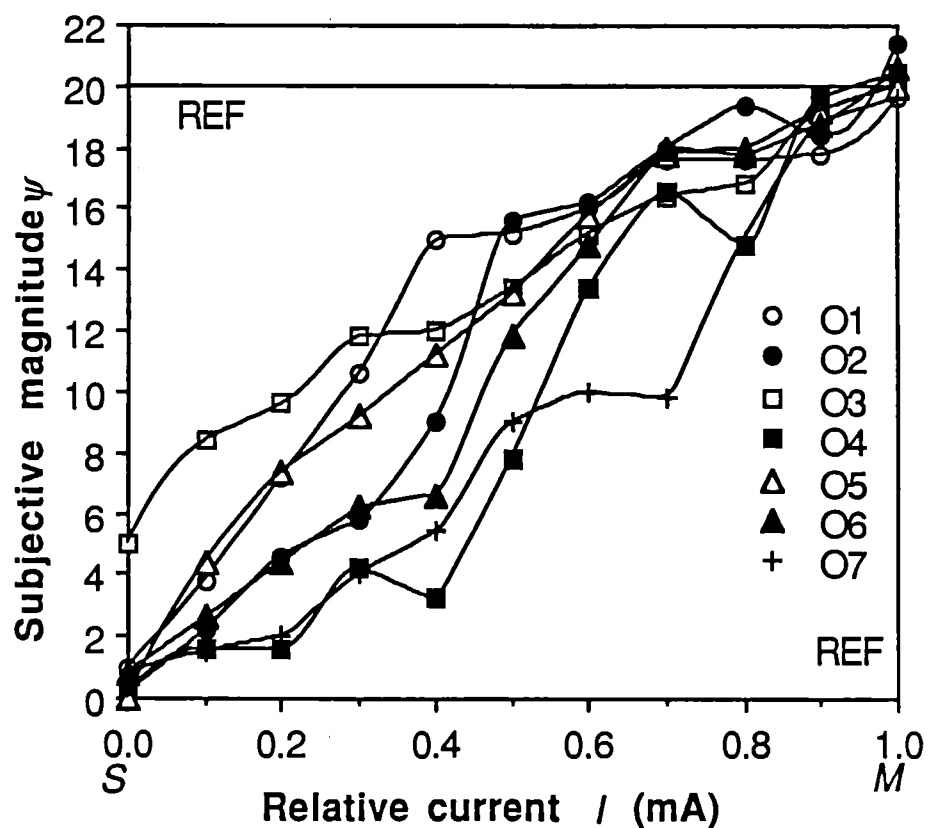


Fig. 6.7. **Scale 1:** Subjective magnitude ψ increases approximately linearly with stimulation current I for 7 observers. S is the sensation threshold current and M is the maximal current without discomfort. A reference current $I_{\text{REF}} = M$ (magnitude 20) is presented to the observer before each estimation.

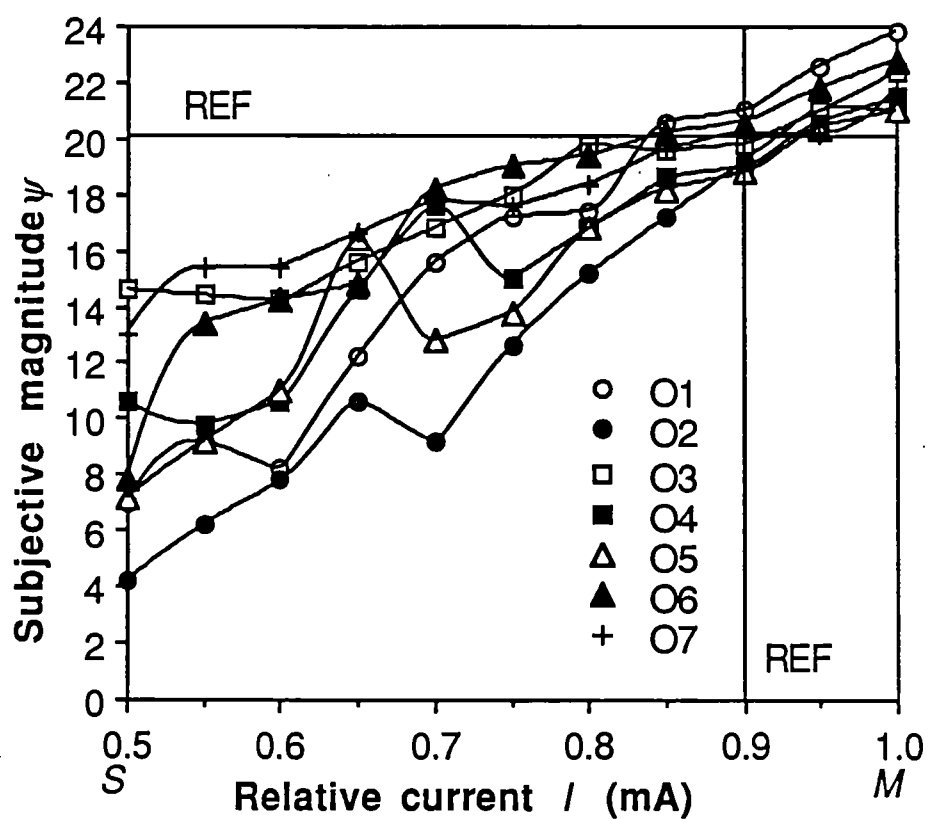


Fig. 6.8. **Scale 2:** The magnitude is more difficult to determine over a narrow range of currents from $S + 0.5(M - S)$ to M . A lower $I_{\text{REF}} = S + 0.9(M - S)$ reduces this error near the reference magnitude of 20.

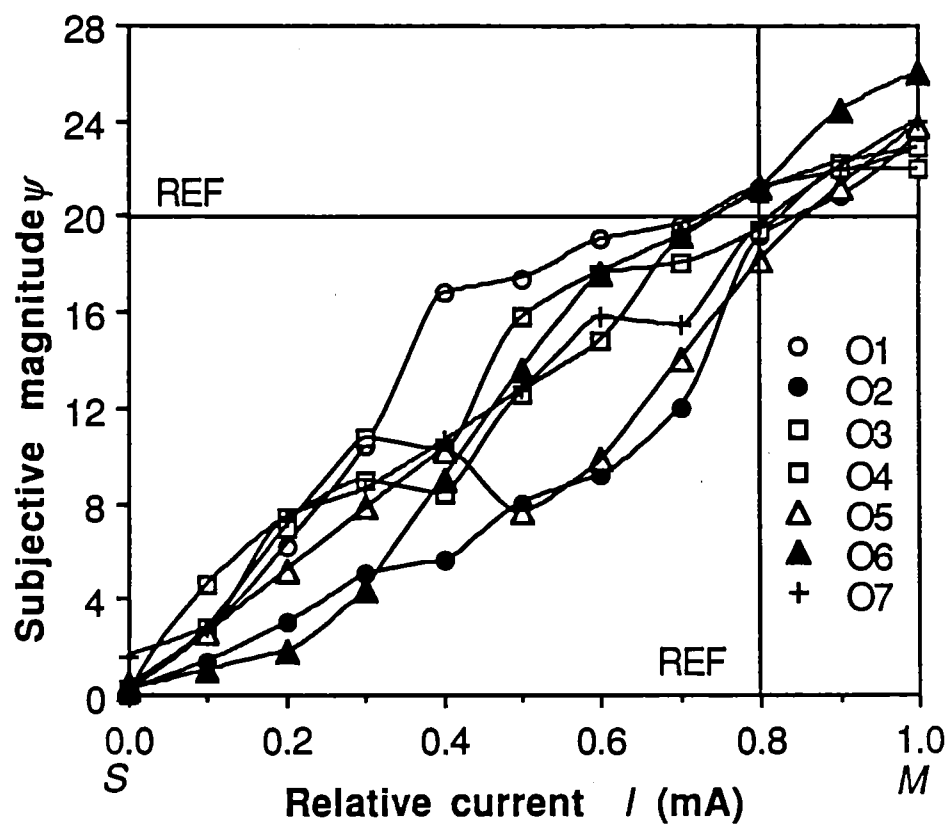


Fig. 6.9. Scale 3a: Magnitude vs. current over the full current range S to M with $I_{\text{REF}} = \dot{S} + 0.8(M - S)$.

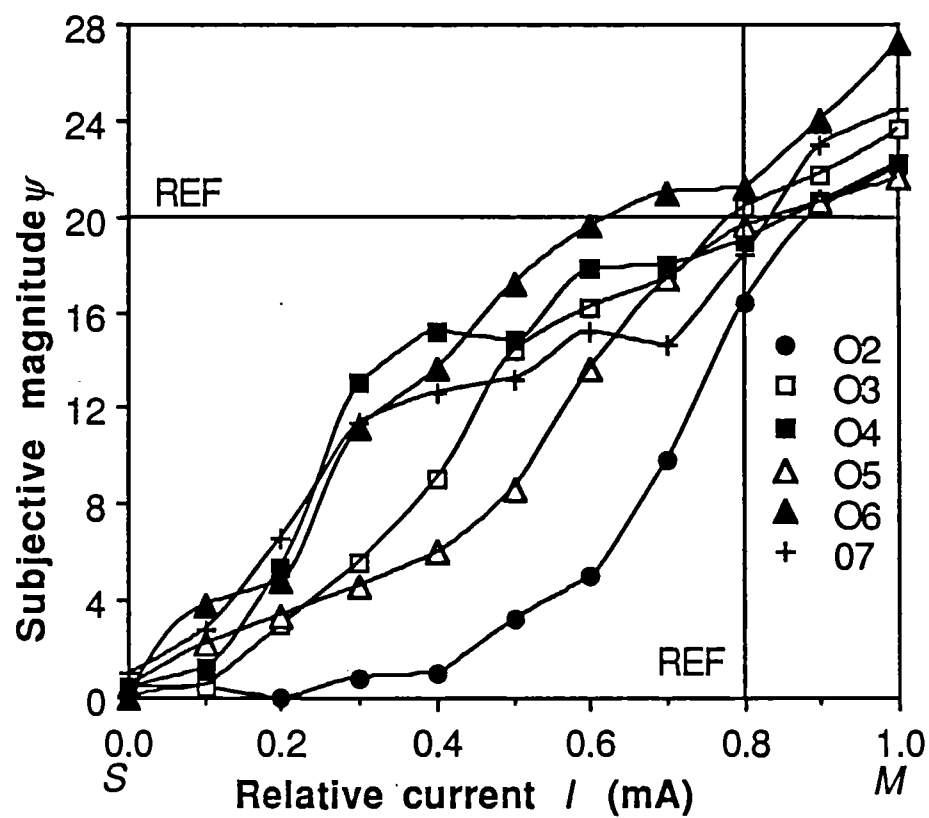


Fig. 6.10. Scale 3b: Magnitude vs. current over the full current range S to M with $I_{\text{REF}} = S + 0.8(M - S)$.

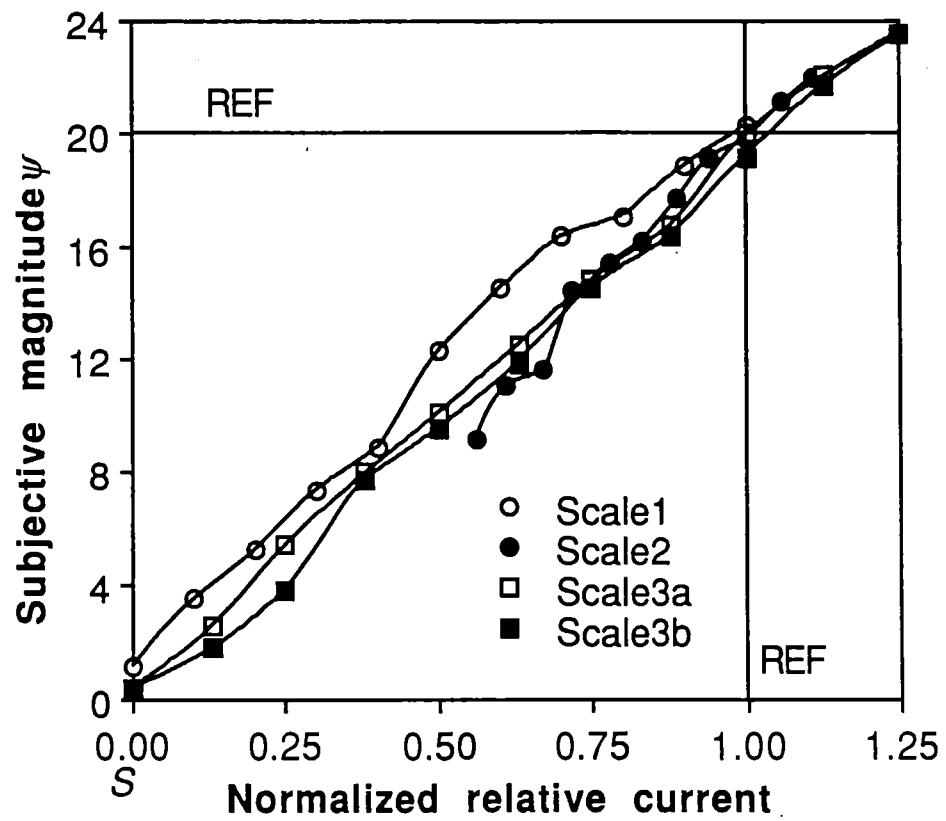


Fig. 6.11. The average magnitude vs. current relationship for all observers is nearly linear regardless of current range or reference current (Scale 1, 2, 3a, 3b). This current scale is normalized so that the reference current is 1.

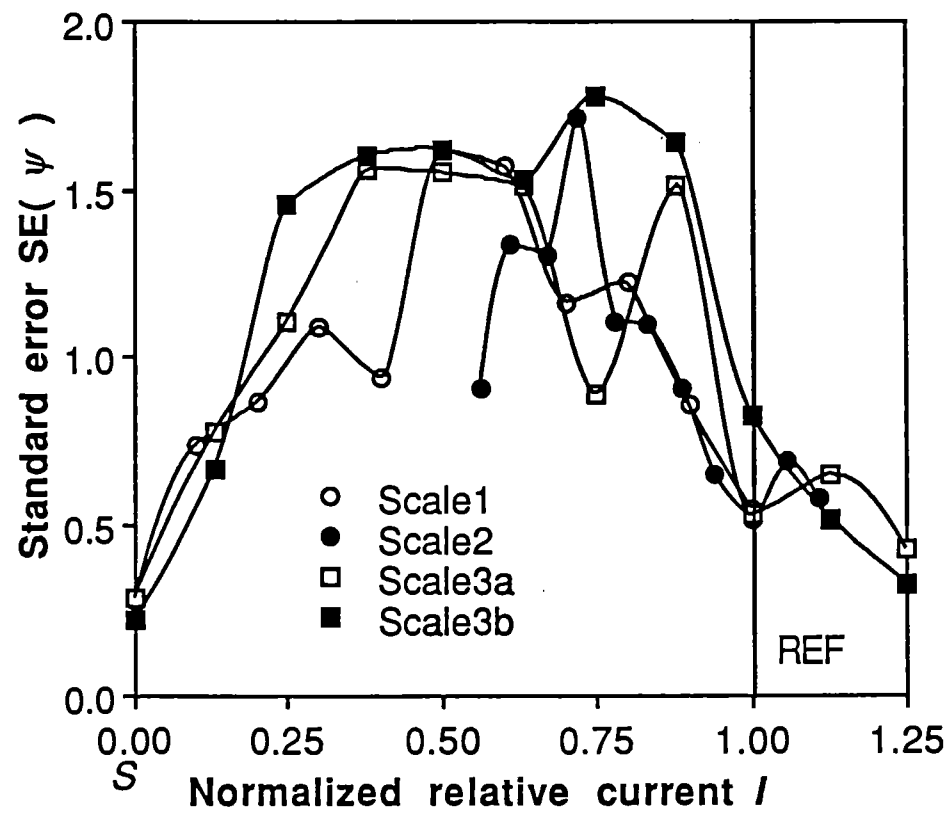


Fig. 6.12. The error in estimating magnitude is minimized near sensation threshold and reference level (Scale 1, 2, 3a, 3b).

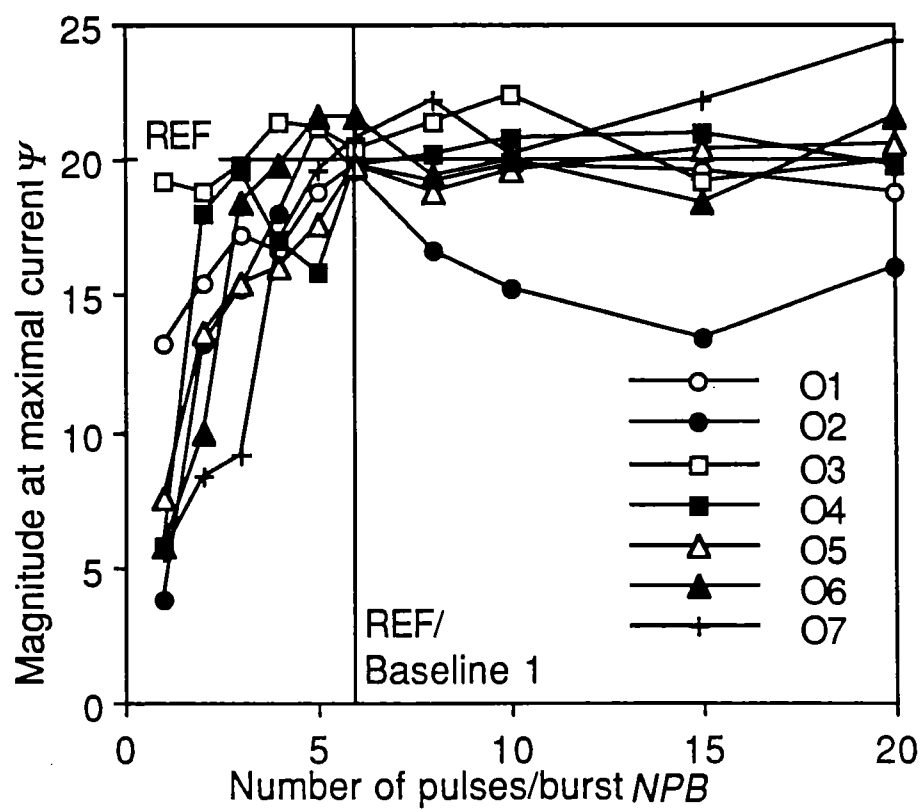


Fig. 6.13. MagNPBscreen screened observers by verifying that they could reliably detect the large increase in dynamic range with increasing NPB . Three observers with similar but more scattered results are not shown.

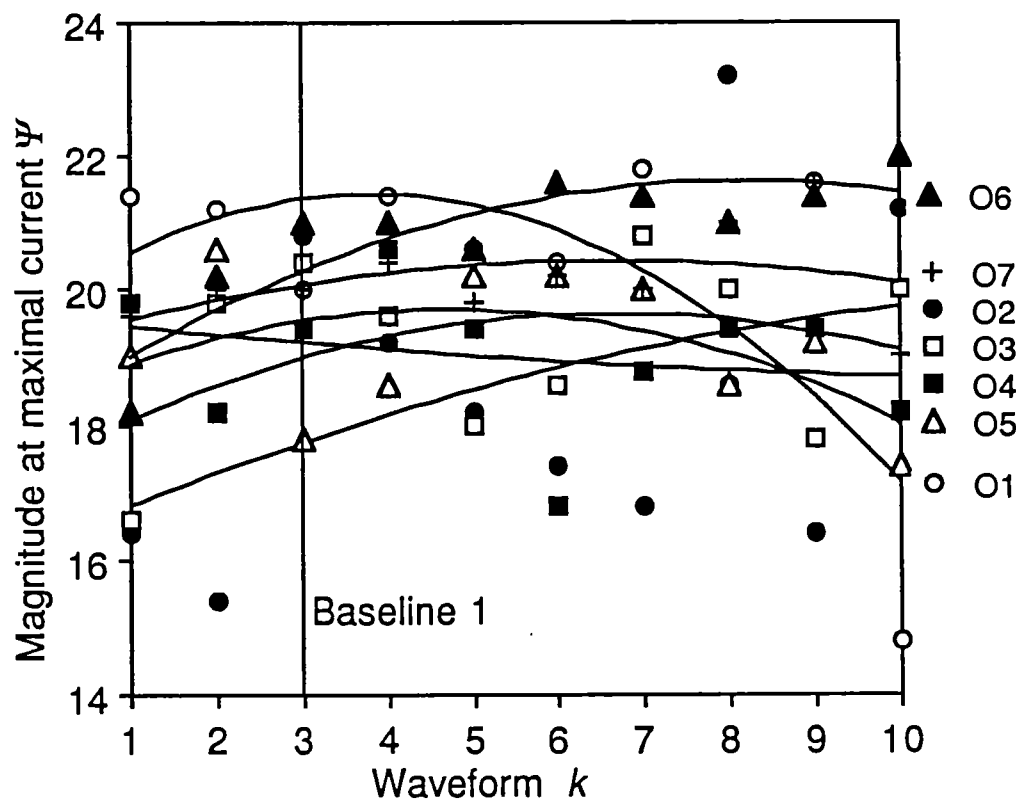


Fig. 6.14. **Search:** The dynamic range Ψ typically increases, peaks, and then decreases as the waveform w advances along the gradient $\nabla\Psi(w)$. A second-order polynomial fit (curved lines) shows this more clearly than the raw data.

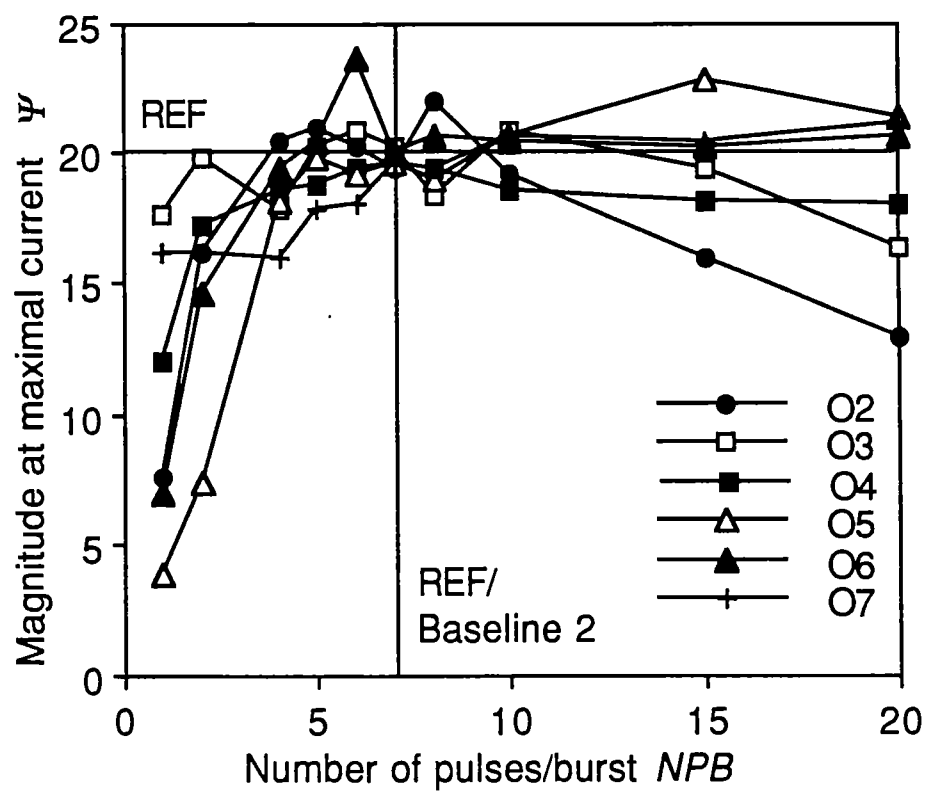


Fig. 6.15. **MagNPB**: Dynamic range increases greatly from $NPB = 1$ to $NPB = 6$ for most observers.

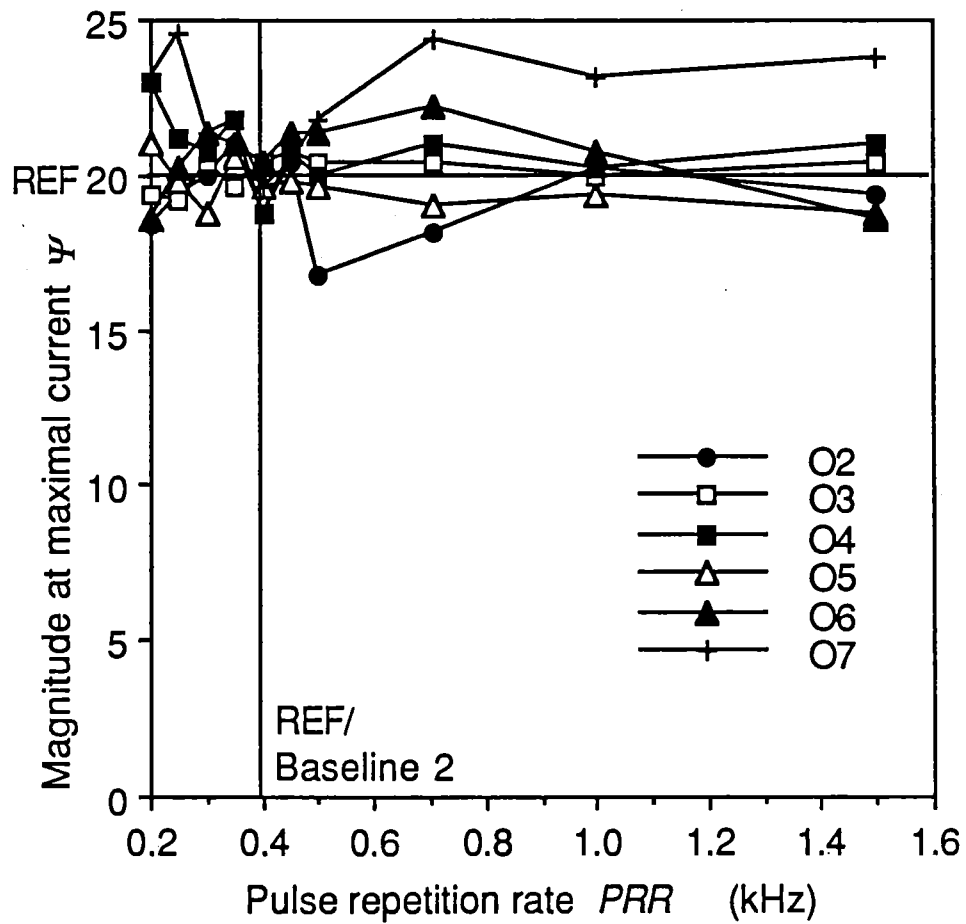


Fig. 6.16. **MagPRR**: Dynamic range changes differently with PRR for different observers.

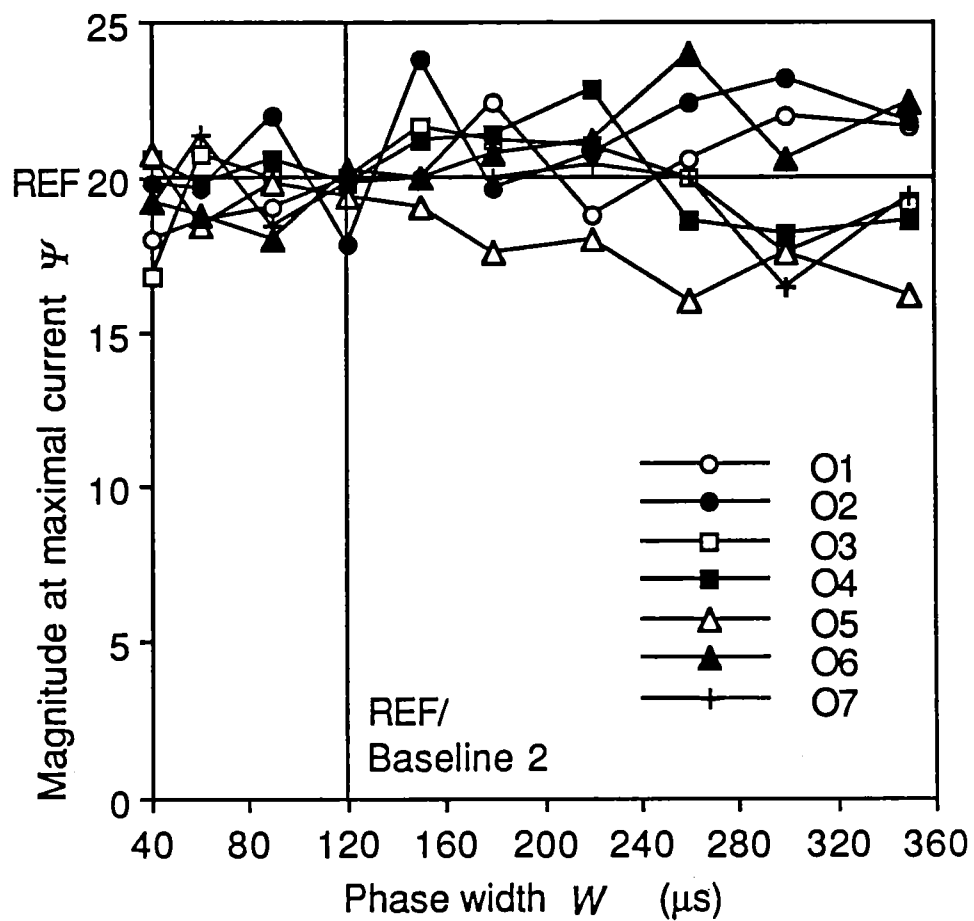


Fig. 6.17. **MagW**: Dynamic range increases with W for some observers and decreases for others, suggesting two groups of skin stimulation sites.

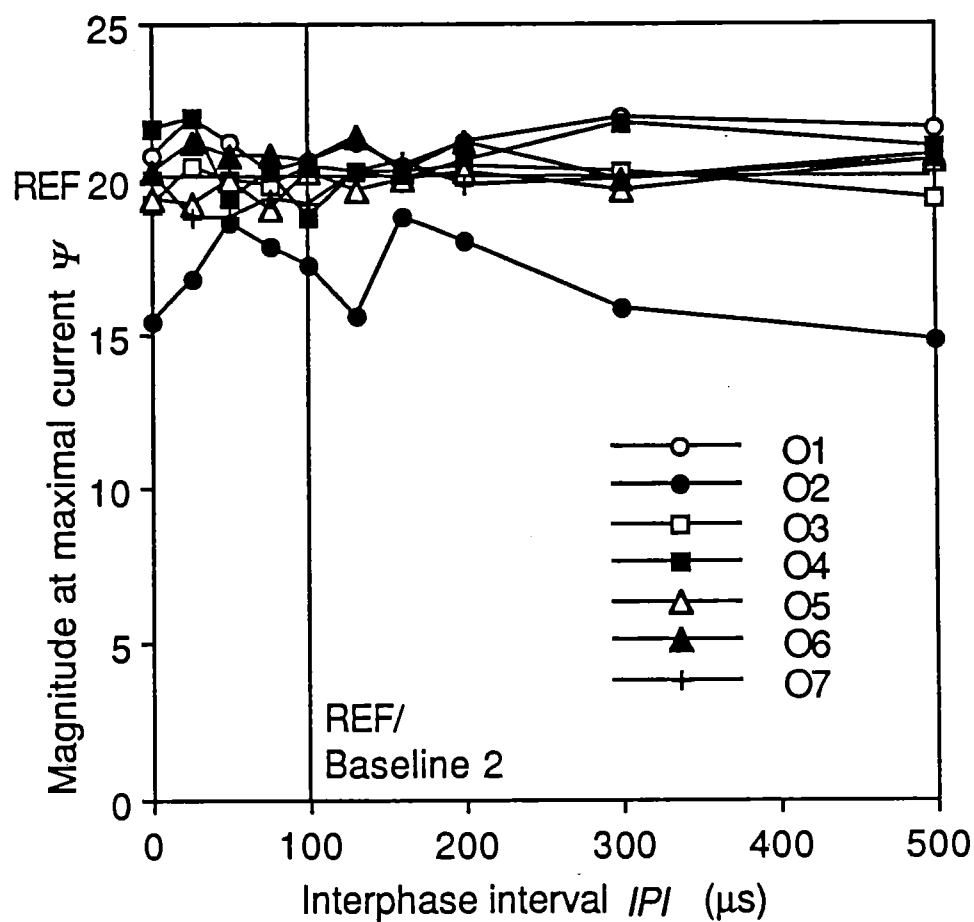


Fig. 6.18. **MagIPI**: Dynamic range does not change with IPI . O2's unrepresentative large variations are not statistically significant due to large experimental error (Table 6.1).

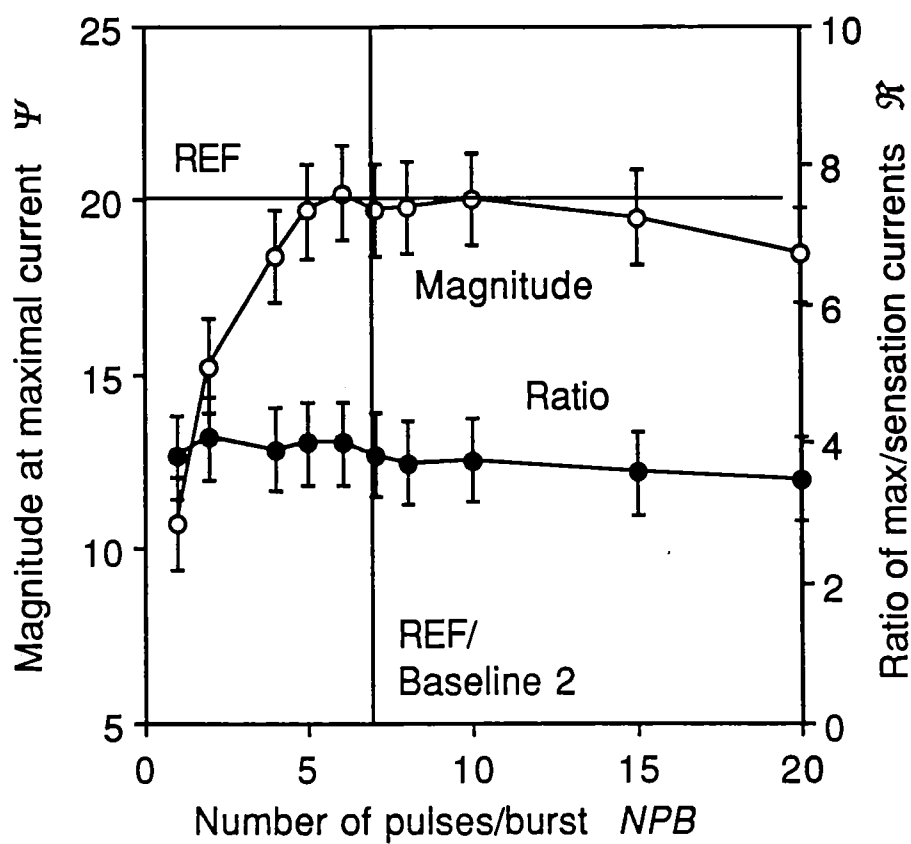


Fig. 6.19. The average dynamic range for 6 observers is maximized when $NPB = 6$ (**MagNPB**). The ratio \mathcal{R} of maximal current without discomfort to sensation threshold current is maximized when the magnitude dynamic range is low.

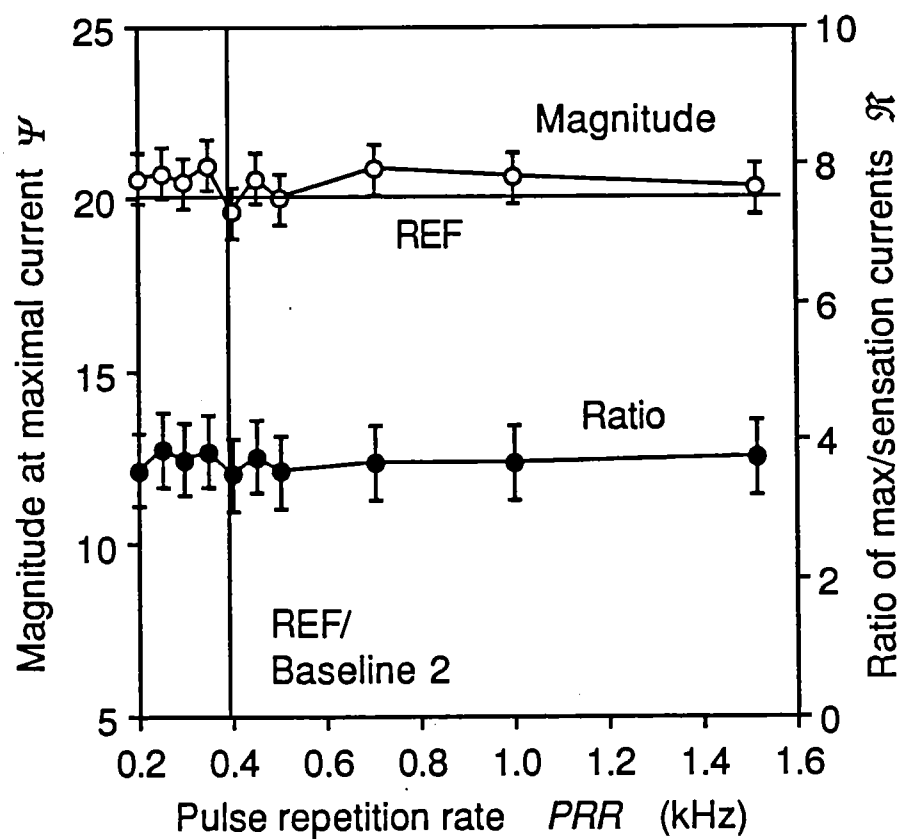


Fig. 6.20. The average dynamic range for 6 observers is maximized when $PRR = 350$ Hz, but the effect is small ($MagPRR$).

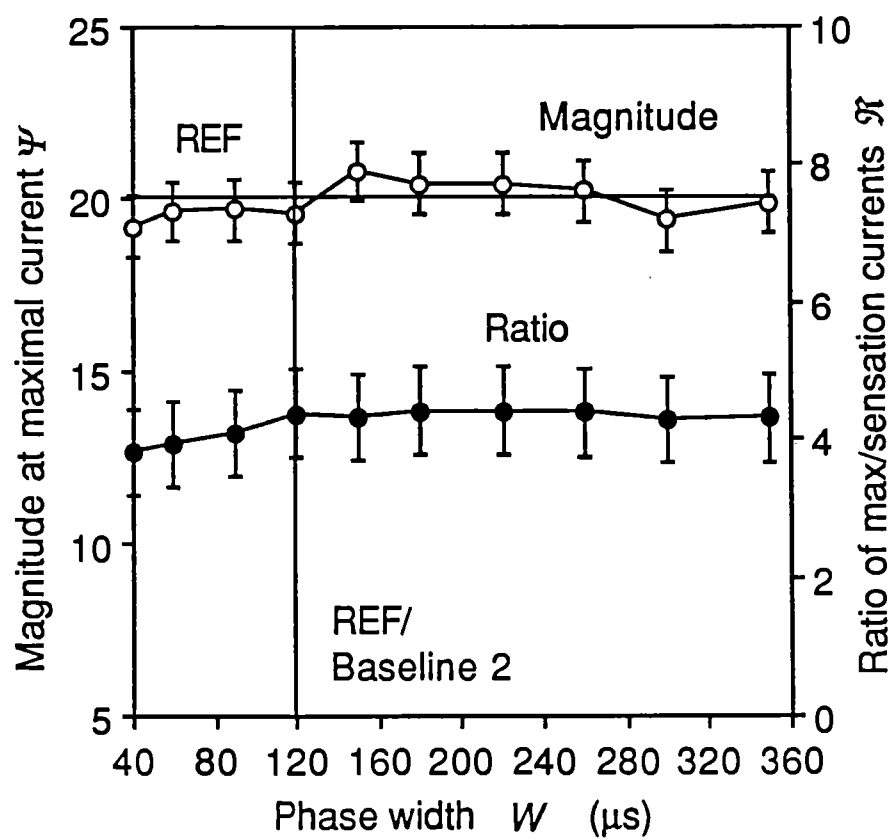


Fig. 6.21. The average dynamic range for 7 observers is maximized when $W = 150 \mu\text{s}$, but the effect is small (MagW).

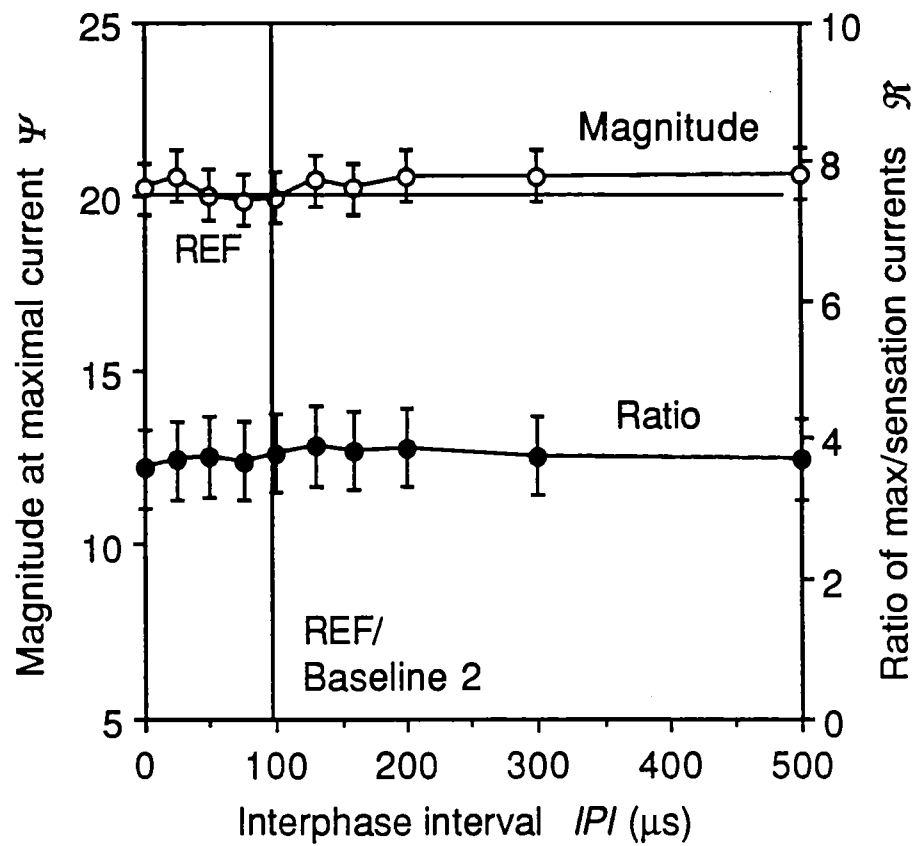


Fig. 6.22. The average dynamic range for 7 observers is not affected by IPI (MagIPI).

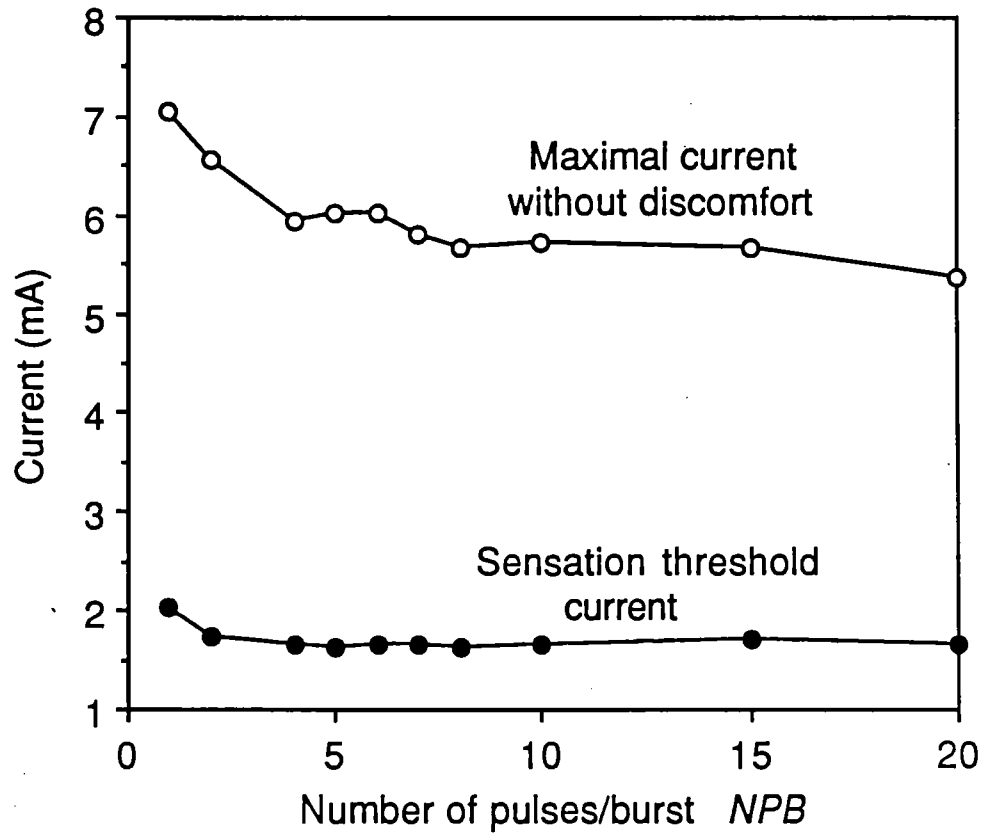


Fig. 6.23. The sensation threshold current S and the maximal current without discomfort M decrease with NPB due to temporal integration in the central nervous system (MagNPB).

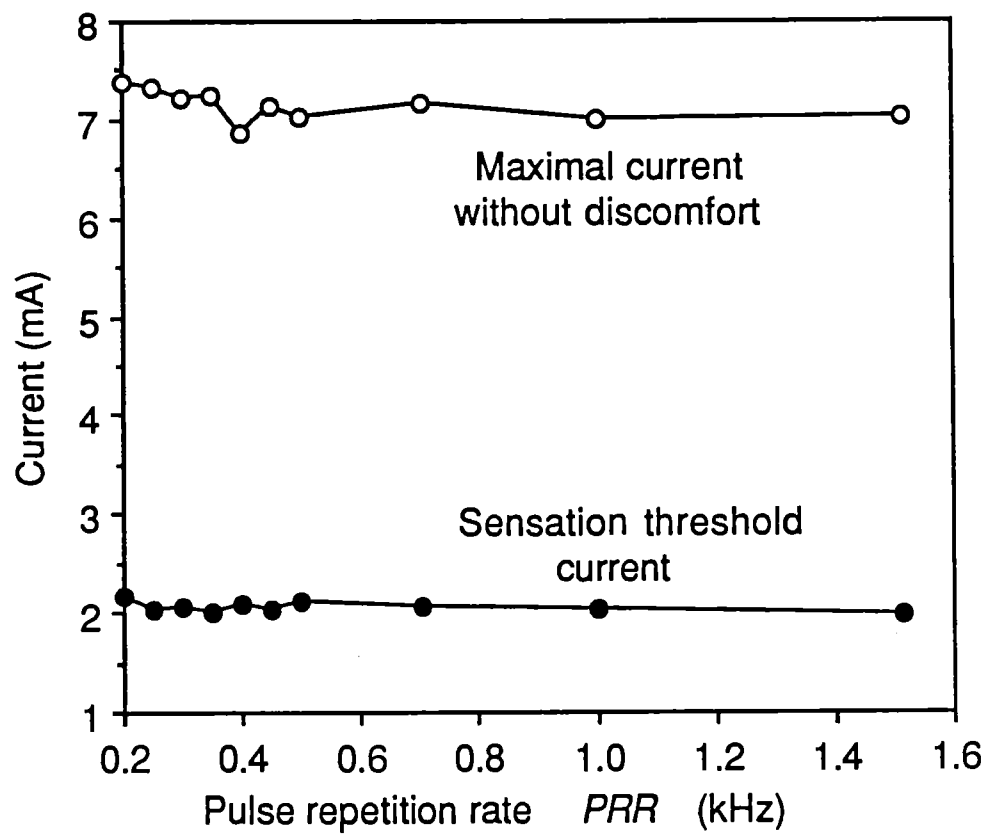


Fig. 6.24. S and M do not change much with PRR (Mag PRR).

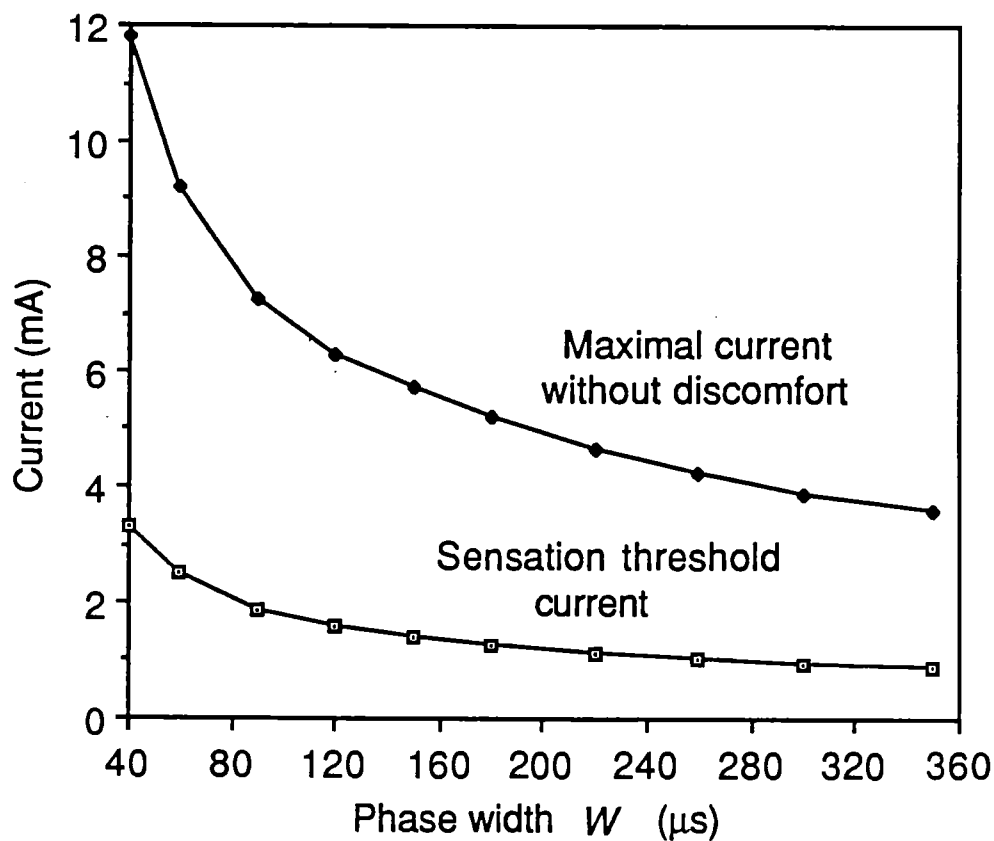


Fig. 6.25. S and M decrease markedly with W . This is the classical strength-duration curve due to temporal integration at the peripheral neural level ($\text{Mag}W$).

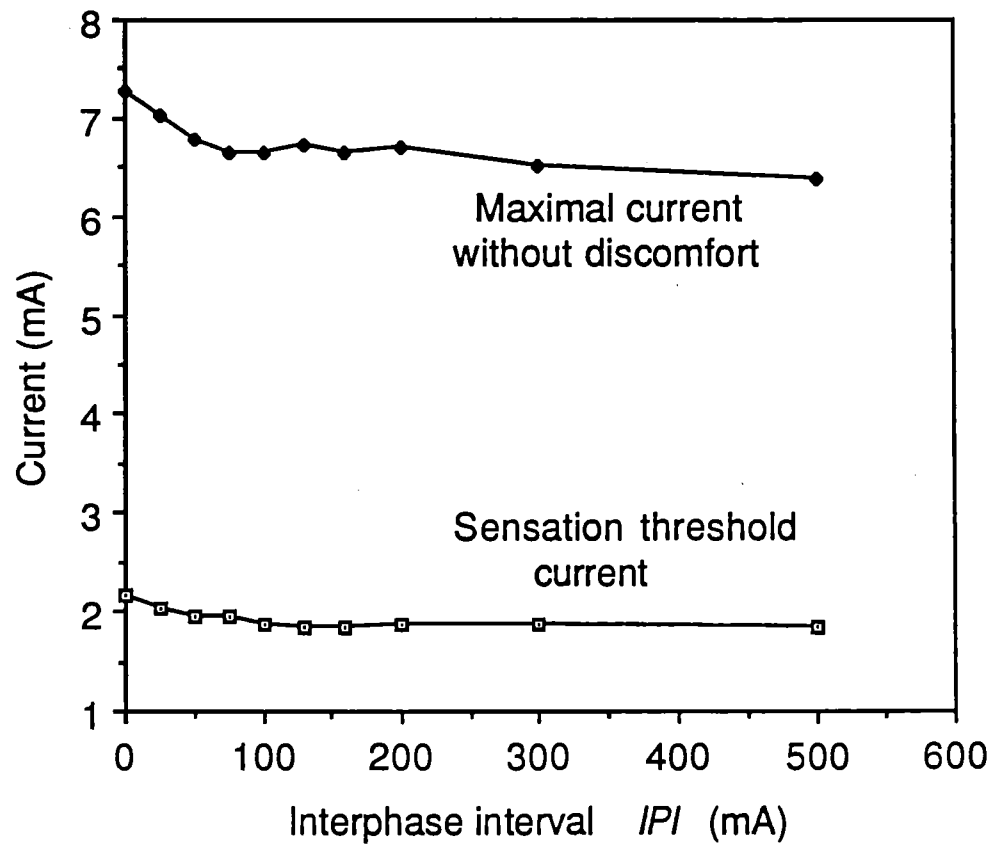


Fig. 6.26. S and M decrease slightly with IPI due to a reduction in the cancellation of charge by closely-spaced positive and negative phases in a biphasic pulse (**MagIPI**).

Chapter 7

ELECTROTACTILE ADAPTATION: EFFECTS OF STIMULATION WAVEFORM CURRENT, FREQUENCY, AND NUMBER OF PULSES PER BURST

Original Experiments

A similar version of this chapter coauthored by K. A. Kaczmarek and J. G. Webster is submitted to *IEEE Transactions on Biomedical Engineering*.

ABSTRACT

Electrotactile (electrocutaneous) stimulation at currents higher than sensation threshold causes sensory adaptation (accommodation) which temporarily raises the sensation threshold current and reduces the perceived magnitude of stimulation. The elevation (rise) of the threshold current during the adapting stimulus follows a first-order exponential function with a time constant of 0.3 – 1.2 min summed with a slower continuing rise until at least 15 min total adaptation time. Threshold recovery after the adapting stimulus is turned off behaves similarly, returning to approximately the original threshold within 15 min.

The threshold rise in 15 min is approximately 0.43 times the difference between the adapting current and the initial threshold when the adapting stimulus is presented for 10 s out of each 20-s interval. The threshold elevation increases sevenfold as the frequency (burst repetition rate) increases from 5 Hz to 45 Hz. Waveforms with 6 pulses/burst adapt twice as much as waveforms with either 1 or 2 pulses/burst (burst rate 15 Hz, with pulse repetition rate in a burst 350 Hz). The rate of threshold elevation is maximized with waveforms that cause the greatest 15-min threshold elevation.

INTRODUCTION

Background

Electrotactile stimulation evokes tactile (touch) sensations within the skin at the location of the electrode by passing a local electric current through the skin. Sensory substitution is the use of one human sense (in this case, touch) to receive environmental information normally received by another sense (often vision or hearing). For the

sense of touch, sensory substitution is the use of one area of skin to receive tactile information normally received at another location. Several articles review technology and devices for electrotactile stimulation [1] (Chapter 2), [2], visual substitution [3], [4], auditory substitution [5], [6], [7], and other applications [2], [8], [9], [10], [11], [12].

Waveform nomenclature

Eight stimulation waveform variables influence the electrotactile sensation. Figure 7.1 defines the pulse timing relationships; Figure 7.2 defines the four pulse types. The eight waveform variables define a generalized stimulation waveform; proper choice of variables can describe any rectangular electrotactile stimulation waveform previously described.

The literature contains inconsistent waveform terminology [13] (Chapter 5). Frequently, M+ and M– waveforms are called "biphasic" because they have positive and negative parts. We will use the terms "functionally-monophasic" for M+ and M– and "balanced-biphasic" for B+ and B– to avoid ambiguity. The two *phases* of a *balanced-biphasic* waveform pulse (Fig. 7.1) are often called *pulses* (with the result that interphase interval IPI is called "interpulse interval"). Introducing the term "phase" avoids the above ambiguity, and uniquely specifies the waveform timing relationships.

Adaptation

In its most general sense, "adaptation" can describe almost any time-dependent feature of a psychophysiological response to a stimulus [14]. For this study, we specifically define adaptation as one of the following effects during or shortly after a period of stimulation (adapting or conditioning stimulus) as compared with before the adapting stimulus: (1) an increase in the minimal stimulation current of a second test

stimulus required to achieve sensation threshold, or (2) a decrease in the subjective magnitude (intensity, strength) of the adapting stimulus or of a second test stimulus. We specifically exclude the effect usually called temporal integration, which is an increase in the subjective magnitude of a constant-level stimulus over the first second or so of stimulation (or the reduction in sensation threshold with increasing stimulus presentation time up to approximately 1 s) [15]. We also exclude the very rapid decrease in the firing rate of some cutaneous mechanoreceptors responding to static touch stimuli [16], [17]. This effect is probably not important for electrotactile stimulation anyway, because the afferent peripheral nerves are probably stimulated directly [2], [18], [19], but also see [20].

Although we are not aware of any published study specifically dealing with electrotactile adaptation, several anecdotal comments appear in the literature. The subjective magnitude of a 60-Hz steady train of pulses decreases within seconds, but can be brought back to full strength by switching to another electrode [21]. Little adaptation occurs if the frequency F is below 10 Hz; adaptation is very rapid (the sensation almost disappears after several seconds) above 1000 Hz. Furthermore, if the pulses are gated into bursts with $NPB = 4$ pulses/burst with a pulse repetition rate $PRR = 400$ Hz and a frequency $F = 25$ Hz, much less adaptation occurs [22]. Monophasic stimulation pulses result in less adaptation than biphasic pulses [23]. Subjects described as "sensitive" to electrotactile stimulation experience faster adaptation than other subjects [24]. The percept produced by stimulation of subdermal electrodes adapts less than that for surface electrodes [25].

The psychophysics of vibrotactile adaptation has been much more thoroughly investigated [14], [26], [27], [28], [29], [30], [31], [32]. Depending on methodology,

the vibrotactile sensation threshold increases gradually during approximately the first 5 – 25 min of stimulation and returns to normal within 2 – 15 min after the adapting stimulus is turned off. While the tactile system is adapted, the magnitude of a fixed-magnitude test stimulus is lower than in the unadapted state but the rate of magnitude growth with increasing vibration magnitude is increased [28].

Neurophysiological data shows that perceptual vibrotactile adaptation cannot be accounted for by the response of the cutaneous mechanoreceptors. For example, using the modern nomenclature in [17], FA I receptors [33] and FA II receptors [34] in the glabrous skin of the monkey foot complete their “adaptation” to repetitive stimuli in 300 ms and 30 ms, respectively. During these time periods of repetitive stimulation, the stimulation amplitude must be increased by 3 – 4 times to maintain the same afferent fiber response.

Finally, the adaptation properties of the four human glabrous skin mechanoreceptor systems [17] are independent of each other. A 10-Hz adapting stimulus which excites primarily the “nonPacinian” system (probably FA I and possibly SA I and SA II systems) does not affect the sensory threshold of the Pacinian (FA II) system [32]. Further studies [35], [36] showed that all four systems could be selectively adapted. The differential excitation of the four receptor systems by electrotactile stimuli has not been characterized, although this will be likely be necessary to make full use of electrotactile (or vibrotactile) stimulation for sensory substitution [36].

MATERIALS AND METHODS

Instrumentation

Waveform generator: A computer-controlled electrotactile stimulation system (ETSS) [13] (Chapter 5) automatically delivered the desired stimulation, prompted the observer (O) for responses, and then logged O's responses. For determination of the sensation threshold current S and the maximal current without discomfort M , a knob manipulated by O's left hand controlled the stimulation current according to:

$$I = (x - rnd)A$$

where I is the stimulation current in mA (clamped so that $I \geq 0$), x is the knob rotation where 0 is fully counter-clockwise (CCW) and 1 is fully clockwise (CW) (approximately 355° rotation from zero), rnd is a random number between 0 and 0.2, and A is a scaling factor which causes $0.2 < x < 0.8$ for all S and M determinations. Subtracting the knob offset rnd prevents O from using the knob rotation x as a cue for determining S and M .

Electrode: The current-controlled pulses were delivered to O's tapwater-premoistened abdomen by the twelfth electrode from the left (cable side) in the elasticized-belt linear electrode array from a Tacticon™ auditory prosthesis for the deaf [11], [37], [38]. The 5.5-mm-diameter gold-plated electrodes are surrounded by the conductive rubber base material of the belt, which serves as a ground plane. The electrode site was approximately 2 cm above and 7 cm right of the navel. For Os with dense hair or bony protuberances at this location which prevented proper electrode contact (as evidenced by sharp, prickly electrotactile sensations), we relocated the electrode laterally to a smoother location. Occasionally the chosen site would yield prickly sensations or muscle contractions for no apparent reason; this was readily

corrected by moving the electrode a few mm in any direction and re-wetting the skin. Insufficient skin hydration causes prickly sensations, probably because of nonuniform current density at the electrode-skin interface [1] (Chapter 1). The electrode location was constant for all three main experiments within a session; adjustments were made only during practice.

Waveform: Previous research [39] (Chapter 6) determined that the waveform which delivers the most intense stimulation percept that is not uncomfortable is defined by *Baseline*: ($PRR = 350$ Hz, $W = 150$ μ s, $IPI = 100$ μ s, and $NPB = 6$) where $Type = B+$, and $F = 15$ Hz.

Order of experiments by observers

Seven Os (2 female and 5 male, aged 23 – 46 with varied ethnic backgrounds) participated in this study. Os received \$5.00/h payment, and were recruited by personal contact and posters in University buildings.

Table 7.1 shows how the Os each completed 3 experimental sessions. (Two different persons served as O2; one for session 1 and another for sessions 2 and 3.) Each session consisted of a short practice experiment to teach or review the procedure followed by 3 similar main experiments with different levels of one of the three independent variables which earlier results had shown to strongly influence adaptation. The first session varied the adapting stimulus current I_A , the second session varied F , and the third session varied NPB . The experimental order in Table 7.1 guaranteed execution of all possible orders of the three main experiments within a session, thus minimizing possible effects caused by experiment order (such as fatigue and practice).

Procedure

At the beginning of each experimental session, O waited 5 min for the electrode-skin interface to stabilize after placing the electrode belt on moistened skin. During this time we explained the experimental procedure. First, O performed a practice experiment, which was a short version of the main experiments (identical procedures). Each of the three main experiments in a session consisted of (1) determination of the stimulation current range from S to M , (2) measurement of sensation threshold current I_S during adaptation, and (3) measurement of I_S during recovery. (We use I_S to distinguish the time-dependent sensation threshold during adaptation/recovery from the initial sensation threshold S measured at the beginning of the experiment.)

Determination of stimulation current range: O first determined the initial sensation threshold current S by a modified method of limits. Upon prompt by the ETSS, O turned a knob CW, starting at the zero (fully CCW) position, until s/he perceived a distinct but very weak tingling sensation at the electrode site. We instructed O to readjust the knob CW and CCW until s/he could just barely feel the stimulus, and then press the ENTER (RETURN) key on the keyboard, causing S to be logged to a result file and saved in memory for future use. Then O returned the knob to zero. (Os were carefully instructed to press ENTER *before* turning the knob to zero; the natural tendency was to press and turn simultaneously, which would yield an incorrect measurement.) This procedure was then repeated two more times. The computer averaged the three results to obtain \bar{S} .

Next, O determined the maximal current without discomfort M . Starting at zero, O turned the knob CW until the stimulus was as strong as possible without feeling uncomfortable as manifest by sharp, prickly, or burning sensations. O logged the response by pressing ENTER and then returned the knob to zero. As for the sensation

threshold, the computer calculated the mean \bar{M} of three trials. A 10-s separation between M trials allowed O's somatosensory system to partially recover from adaptation.

Normalization of currents: To facilitate comparison of data from Os with widely-different S to M current ranges, we normalized all measured currents I' :

$$I = \frac{I' - \bar{S}'}{\bar{M}' - \bar{S}'}$$

where the prime (') denotes the measured (nonnormalized) value and the overbar denotes a mean of three measurements. The normalized sensation threshold and maximal currents are therefore $\bar{S} = 0$ and $\bar{M} = 1$. The nonnormalized values \bar{S}' and \bar{M}' for all Os appear in Tables 7.2 and 7.3, respectively.

Adaptation: Figure 7.3 shows how O determined I_S every 20 s for 15 min upon prompt by the ETSS (46 determinations). After logging each I_S with the ENTER key as described above, the ETSS delivered the adapting stimulus at current I_A for 10 s. O then waited for the next instruction to determine I_S . Os required 5 – 10 s to determine I_S .

Recovery: After 15 minutes of adaptation, the adapting stimulus was turned off ($I_A = 0$). O continued to determine I_S every 20 s for another 15 min (45 determinations).

Session 1 — variation of adapting current I_A : The 3 (normalized) levels of the adapting stimulus current I_A for the 3 experiments in session 1 were 0.5, 0.7, and 0.9. All of the other waveform variables were at *Baseline*. Preliminary experiments showed

that when $I_A < 0.5$, the threshold elevation due to adaptation was difficult to measure, due primarily to periodic variations in the sensation threshold of unknown origin [40] (Chapter 4). $I_A > 0.9$ sometimes caused sensation threshold I_S elevations that would not readily recover within 15 min.

Session 2 — variation of frequency F : F had values of 5, 15, and 45 Hz for the three experiments in this session. All other waveform variables were at *Baseline*, and $I_A = 0.7$. $F < 5$ Hz is so slow that little real-time information can be delivered to O due to the 0.2-s time lag. Waveforms with $F > 45$ Hz adapt so quickly they would likely be unsuitable for a practical system.

Session 3 — variation of number of pulses/burst NPB : NPB had values of 1, 2, and 6 pulses/burst for the three experiments in this session. All other waveform variables were at *Baseline*, and $I_A = 0.7$. We chose $NPB = 1$ because it is a commonly-cited waveform, although it provides a weak vibratory percept (low magnitude dynamic range). $NPB = 6$ provides the strongest vibratory percept without discomfort [39], while $NPB = 2$ is a midpoint on the magnitude dynamic range scale.

RESULTS AND DISCUSSION

Data correction

The tedious nature of these experiments caused some Os to lapse in concentration and (1) press ENTER without turning the knob to determine I_S , (2) begin to return the knob to zero before pressing ENTER after finding I_S , or (3) turn the knob too high, overestimating I_S . Manual scanning of the data revealed I_S values which were substantially low or high compared with adjacent points. We replaced each such datum with the average value of the 2 points immediately before and after the suspect

point. No single experiment required more than two corrections; 47 of the 54 experiments required none.

Threshold and maximal currents

Tables 7.2 and 7.3 show the *nonnormalized* values \bar{S}' and \bar{M}' for all of the 54 main experiments. \bar{S}' and \bar{M}' for an individual O can change by a factor of 2 between sessions, due mostly to differences in skin location — even a shift of a few millimeters can substantially change the threshold as well as the subjective nature of the percept [1]. However, the means \bar{S}' and \bar{M}' over all Os do not change by more than a factor of 1.3; this is much smaller than the interobserver variations.

Exponential model

Figure 7.4 shows $I_S(t)$ from a typical adaptation/recovery experiment (observer O2, session 3, $NPB = 6$). Data from other experiments showed more and less scatter, outliers, and periodicity [40]. Figures 7.5, 7.6, and 7.7 show $I_S(t)$ averaged over all six Os for all values of I_A , F , and NPB . For clarity, a 3-point moving average smoothed these data:

$$I_A(k) = \frac{1}{3} [I_A(k-1) + I_A(k) + I_A(k+1)]$$

where k is the trial (0.. 90) and time $t = k \cdot 20$ s. To avoid bias at the endpoints and at the transition of adaptation to recovery, data at $k = 0, 45$, and 90 were not averaged.

The sensation threshold $I_S(t)$ elevation during adaptation can be approximately described by a first-order exponential function summed with a linear rise:

$$I_S(t) = a_A(1 - e^{-t/\tau_A}) + \frac{b_A t}{15}$$

where a_A is the final exponential rise in sensation threshold, τ_A is the time constant (min) for the exponential rise ($0 \leq t \leq 15$), and b_A is the rate of linear rise (normalized current/15 min), and t is time (min). Similarly,

$$I_S(t - 15) = I_F - a_R(1 - e^{-(t - 15)/\tau_R}) - \frac{b_R(t - 15)}{15}$$

describes the decrease in sensation threshold during recovery from adaptation ($15 \leq t \leq 30$). $I_F = I_S(t = 15)$ is the total elevation in sensation threshold at the end of the adaptation part of the experiment, and is approximately $a_A + b_A$ because usually $\tau_A \ll 15$ min. a_R is the final exponential drop, τ_R is the time constant, and b_R is the linear drop during recovery.

For each experiment, the SYSTAT statistical analysis program performed a least-squares nonlinear regression to determine a_A , b_A , τ_A , a_R , b_R , and τ_R . Except for a few outliers, the range of τ_A was 0.3 – 2.6 min and the range of τ_R was 0.1 – 2.0 min. For the adaptation part of 3 of the 54 experiments, the data were too scattered for a successful regression, so we estimated the model by eye. Other models, such a simple exponential rise (fall) and a second-order underdamped system did not fit the data as well for the 30-min experiments. Over a longer period of time, however, the linear rise must break down as $I_S(t)$ approaches an asymptotic maximal elevation during adaptation and $I_S(t - 15)$ asymptotically approaches S during recovery. A more intuitive model is the sum of two first-order exponential functions:

$$I_S(t) = a_1(1 - e^{-t/\tau_1}) + a_2(1 - e^{-t/\tau_2})$$

for adaptation and

$$I_S(t - 15) = I_F - a_3(1 - e^{-(t-15)/\tau_3}) - a_4(1 - e^{-(t-15)/\tau_4})$$

for recovery. Figure 7.8 shows how the double-exponential model fits the data from session 1, *Baseline* condition, mean of all Os. An eyeball fit provided the following parameter values (τ in min): $a_1 = 0.15$, $a_2 = 0.19$, $\tau_1 = 0.50$, $\tau_2 = 9.0$, $a_3 = 0.155$, $a_4 = 0.145$, $\tau_3 = 0.40$, $\tau_4 = 15.0$. In determining these values, we assumed that $I_S(t \rightarrow \infty) = 0$, therefore causing $a_3 + a_4 = I_F$. For some stimulation conditions (see below) this assumption may not be true.

The added degree of freedom in the double-exponential model and the lack of closely-spaced data near the beginning of adaptation and recovery prevented use of a least-squares fit. The single-exponential plus linear model does not have these numerical problems, and therefore provides the basis for the following discussion.

Effect of adapting current I_A

Figure 7.5 shows the mean sensation threshold I_S for all six Os during adaptation and recovery at the three levels of I_A . The maximal elevation after 15 min I_F was approximately $0.43 \cdot I_A$. This result was different for the six Os (Fig. 7.9); sometimes the relationship was even slightly nonmonotonic. One possible source of this nonmonotonicity is a change in O characteristics from the first to the third main experiment in a session due to fatigue or practice effects. However, the mean \pm standard error of the mean for all of the first, second, and third experiments (for all Os

and conditions) were respectively 0.241 ± 0.045 , 0.274 ± 0.047 , and 0.252 ± 0.042 .

Thus, there is no evidence for these proposed effects.

Both the exponential rise a_A and the linear rise b_A increased with increasing I_A . The linear part accounted for from one-third to one-half of the total rise, increasing with I_A . The average time constant for adaptation τ_A decreased from 1.2 to 0.5 min with increasing I_A . The average recovery time constant τ_R also decreased slightly, from 0.4 to 0.3 min.

Effect of frequency F

Figure 7.6 shows the mean sensation threshold I_S for all six Os during adaptation and recovery at the three levels of F . Very little adaptation occurred at 5 Hz; I_S recovered even to below the initial S for an unknown reason, for all six Os. In contrast, at 45 Hz the 15-min threshold rise I_F was large (Fig. 7.9) and very fast; the average $\tau_R = 0.3$ min compared with 2.2 min at 5 Hz. The linear part of the total rise was almost absent at 5 Hz and contributed one-third of the total rise at 45 Hz.

Effect of number of pulses/burst NPB

Figure 7.7 shows a more complex behavior of adaptation to changes in NPB . (The apparently-periodic behavior for $NPB = 1$ is an additive combination of several unusually-high data points from O4 and O6. The other four Os did not exhibit this behavior.) While the results for I_A and F suggest the hypothesis that increasing the total charge to the skin (with subsequent greater activity at higher neural levels) increases the adaptation amount and rate, 2 pulses/burst caused less adaptation than 1 pulse/burst for four of the six Os. However, a paired t -test comparing $I_F(NPB = 1)$ to $I_F(NPB = 2)$ yields $p = 0.31$ — not a significant difference. (The differences between 6 pulses/burst and 1 or 2 pulses/burst are significant; $p < 0.05$.) If it exists, the inflated

adaptation at 1 pulse/burst may be related to the low magnitude dynamic range of this waveform. The desirable tingling/vibratory sensation is not very strong at the maximal current without (stinging) discomfort M compared to waveforms with higher NPB [39]; different cutaneous or pain receptor systems may be excited. However, 6 pulses/burst produced the greatest and fastest adaptation, supporting the charge hypothesis.

Impact on sensory substitution

The dramatic increase in adaptation with F has important ramifications for the design of sensory substitution systems. Information transfer at 5 Hz is slow; an O detects a noticeable lag between turning a knob to control stimulation current and feeling the effect in the stimulus. Visual substitution systems have used frame update rates from 25 Hz [22] to 230 Hz [41]. Auditory substitution systems require even faster update rates to follow the rapidity of speech envelopes; frequencies of up to 1 kHz are used in the Tacticon™ auditory prosthesis [38]. Unpublished tests in our lab show that touch substitution for the perception of texture similarly to [8], [42] is enhanced at frequencies as high as 500 Hz, although 30 Hz is adequate for providing grip force feedback to persons using functional neuromuscular stimulation to restore hand grasp [43]. Frequencies of 10 – 15 Hz or even lower are adequate for force feedback from telerobotic manipulators [44]. The increase in adaptation at high levels of NPB is also important; waveforms with $NPB = 6$ are the most comfortable at high subjective intensities.

Fortunately, most application-oriented electrotactile feedback is dynamic rather than static in nature, so recovery occurs between periods of intense stimulation. Furthermore, adaptation is not necessarily undesirable; our normal senses of touch,

vision, and hearing use adaptation as a first-level filter to discard useless information. Therefore, the question for system design is not whether adaptation can be eliminated or at least reduced through compensatory signal processing — it can. The issue is what system adaptation characteristics (due to human perception plus signal processing) will maximize task performance. We hope that the information presented here will aid in this effort or at least provide a framework within which electrotactile adaptation can be discussed, quantified, and further explored. In particular, the change in perceived magnitude due to adaptation and recovery warrants detailed experimentation; suprathreshold levels are where real information is conveyed.

CONCLUSIONS

These experiments measured electrotactile adaptation and recovery for one electrode geometry (5.5-mm-diameter-active coaxial) at one skin site (abdomen) with balanced-biphasic pulse bursts. Waveforms with the highest current, frequency (burst repetition rate), and number of pulses/burst caused the largest and the fastest rise in sensation threshold. Recovery was generally faster than adaptation, at least in the initial exponential phase, although both adaptation and recovery appear to continue beyond the 15-min experimental limit on both.

REFERENCES

- [1] K. A. Kaczmarek, J. G. Webster, P. Bach-y-Rita and W. J. Tompkins, "Electrotactile and vibrotactile displays for sensory substitution systems," *IEEE Trans. Biomed. Eng.*, vol. 38, pp. 1–16, 1991.
- [2] A. Y. J. Szeto and F. A. Saunders, "Electrocutaneous stimulation for sensory communication in rehabilitation engineering," *IEEE Trans. Biomed. Eng.*, vol. BME-29, pp. 300–308, 1982.
- [3] P. Bach-y-Rita, *Brain Mechanisms in Sensory Substitution*. New York: Academic, 1972.
- [4] C. C. Collins, "On mobility aids for the blind," in *Electronic Spatial Sensing for the Blind*, D. H. Warren and E. R. Strelow, Eds. Dordrecht, The Netherlands: Martinus Nijhoff, 1985, pp. 35–64.
- [5] C. M. Reed, N. I. Durlach and L. D. Bradia, "Research on tactile communication of speech: A review," *AHSA Monographs*, vol. 20, pp. 1–23, 1982.
- [6] C. E. Sherrick, "Basic and applied research on tactile aids for deaf people: Progress and prospects," *J. Acoust. Soc. Am.*, vol. 75, pp. 1325–1342, 1984.
- [7] A. Y. J. Szeto, "Technological devices for deaf-blind children: Needs and potential impact," *IEEE Eng. Med. Biol. Mag.*, vol. 7, no. 3, pp. 25–29, 1988.
- [8] C. C. Collins and J. M. J. Madey, "Tactile sensory replacement," in *Proc. San Diego Biomed. Symp.*, vol. 13, 1974, pp. 15–26.
- [9] C. A. Phillips, "Sensory feedback control of upper- and lower-extremity motor prostheses," *CRC Crit. Rev. Biomed. Eng.*, vol. 16, pp. 105–140, 1988.

- [10] R. R. Riso, "Sensory augmentation for enhanced control of FNS systems," in *Ergonomics in rehabilitation*, A. Mital, Ed. New York: Taylor and Francis, 1988, pp. 253–271.
- [11] F. A. Saunders, "Information transmission across the skin: High-resolution tactile sensory aids for the deaf and the blind," *Intern. J. Neurosci.*, vol. 19, pp. 21–28, 1983.
- [12] A. Y. J. Szeto and R. R. Riso, "Sensory feedback using electrical stimulation of the tactile sense," in *Rehabilitation Engineering*, R. V. Smith and J. H. Leslie Jr., Eds. Boca Raton, FL: CRC Press, 1990, pp. 29–78.
- [13] K. A. Kaczmarek, K. M. Kramer, J. G. Webster and R. G. Radwin, "A 16-channel 8-parameter waveform electrotactile stimulation system," *IEEE Trans. Biomed. Eng.*, vol. 38, no. 10, 1991 (in press).
- [14] J. F. Hahn, "Tactile adaptation," in *The Skin Senses*, D. R. Kenshalo, Ed. Springfield, IL: Charles C. Thomas, 1968, pp. 322–326.
- [15] R. T. Verrillo, "Temporal summation in vibrotactile sensitivity," *J. Acoust. Soc. Am.*, vol. 37, pp. 843–846, 1965.
- [16] J. R. Phillips and K. O. Johnson, "Neural mechanisms of scanned and stationary touch," *J. Acoust. Soc. Am.*, vol. 77, pp. 220–224, 1985.
- [17] A. B. Vallbo and R. S. Johansson, "Properties of cutaneous mechanoreceptors in the human hand related to touch sensation," *Human Neurobiol.*, vol. 3, pp. 3–14, 1984.
- [18] R. Butikofer and P. D. Lawrence, "Electrocutaneous nerve stimulation - I: Model and experiment," *IEEE Trans. Biomed. Eng.*, vol. BME-25, pp. 526–531, 1978.

- [19] G. B. Rollman, "Electrocutaneous stimulation," in *Proc. Conf. Cutan. Comm. Sys. Dev.*, F. A. Geldard, Ed., Psychonomic Society, 1973, pp. 38–51.
- [20] E. A. Pfeiffer, "Electrical stimulation of sensory nerves with skin electrodes for research, diagnosis, communication and behavioral conditioning: A survey," *Med. & Biol. Eng.*, vol. 6, pp. 637–651, 1968.
- [21] C. C. Collins and F. A. Saunders, "Pictorial display by direct electrical stimulation of the skin," *J. Biomed. Sys.*, vol. 1, pp. 3–16, 1970.
- [22] C. C. Collins, "Tactile television — mechanical and electrical image projection," *IEEE Trans. Man-Mach. Sys.*, vol. MMS-11, pp. 65–71, 1970.
- [23] A. Y. J. Szeto and J. Lyman, "Comparison of codes for sensory feedback using electrocutaneous tracking," *Ann. Biomed. Eng.*, vol. 5, pp. 367–383, 1977.
- [24] A. Y. J. Szeto and Y. Chung, "Effects of training on human tracking of electrocutaneous signals," *Ann. Biomed. Eng.*, vol. 14, pp. 369–381, 1986.
- [25] R. R. Riso, A. Y. J. Szeto and M. W. Keith, "Comparison of subdermal versus surface electrocutaneous stimulation," in *Proc. IEEE Frontiers of Engineering in Health Care Conf.*, IEEE, 1982, pp. 343–347.
- [26] G. v. Békésy, "Synchronism of neural discharges and their demultiplication in pitch perception on the skin and in hearing," *J. Acoust. Soc. Am.*, vol. 31, pp. 338–349, 1959.
- [27] U. Berglund and B. Berglund, "Adaptation and recovery in vibrotactile perception," *Percept. Motor Skills*, vol. 30, pp. 843–853, 1970.

- [28] G. A. Gescheider and J. H. Wright, "Effects of sensory adaptation on the form of the psychophysical magnitude function for cutaneous vibration," *J. Exp. Psychol.*, vol. 77, pp. 308–313, 1968.
- [29] G. A. Gescheider and J. H. Wright, "Effects of vibrotactile adaptation on the perception of stimuli of varied intensity," *J. Exp. Psychol.*, vol. 81, pp. 449–453, 1969.
- [30] J. F. Hahn, "Vibrotactile adaptation and recovery measured by two methods," *J. Exp. Psychol.*, vol. 71, pp. 655–658, 1966.
- [31] J. F. Hahn, "Vibratory adaptation," in *Proc. Conf. Cutan. Comm. Sys. Dev.*, F. A. Geldard, Ed., Psychonomic Society, 1973, pp. 6–8.
- [32] R. T. Verrillo, "Psychophysics of vibrotactile stimulation," *J. Acoust. Soc. Am.*, vol. 77, pp. 225–232, 1985.
- [33] U. Lindblom, "Properties of touch receptors in distal glabrous skin of the monkey," *J. Neurophysiol.*, vol. 28, pp. 966–985, 1965.
- [34] U. Lindblom and L. Lund, "The discharge from vibration-sensitive receptors in the monkey foot," *Exp. Neurol.*, vol. 15, pp. 401–417, 1966.
- [35] G. A. Gescheider, B. F. Sklar, C. L. V. Doren and R. T. Verrillo, "Vibrotactile forward masking: Psychophysical evidence for a triplex theory of cutaneous mechanoreception," *J. Acoust. Soc. Am.*, vol. 78, pp. 534–543, 1985.
- [36] S. J. Bolanowski, G. A. Gescheider, R. T. Verrillo and C. M. Checkosky, "Four channels mediate the mechanical aspects of touch," *J. Acoust. Soc. Am.*, vol. 84, pp. 1680–1694, 1988.

- [37] M. P. Lynch, R. E. Eilers, D. K. Oller and L. Lavoie, "Speech perception by congenitally deaf subjects using an electrocutaneous vocoder," *J. Rehab. Res. Dev.*, vol. 25, pp. 41–50, 1988.
- [38] F. A. Saunders, *Tacticon 1600 Electrotactile Sensory Aid for the Deaf: User's Guide*. San Rafael, CA: Tacticon Corporation, 1986.
- [39] K. A. Kaczmarek, "Optimal Electrotactile Stimulation Waveforms," Ph. D. Thesis, Electrical Engineering, Univ. of Wisconsin-Madison, 1991.
- [40] K. A. Kaczmarek, J. G. Webster and R. G. Radwin, "Periodic variations in the electrotactile sensation threshold," in *Proc. Annu. Int. Conf. IEEE Eng. Med. Biol. Soc.*, Philadelphia, PA, P. C. Pedersen and B. Onaral, Eds., vol. 12, IEEE, 1990, pp. 1060–1061.
- [41] J. C. Bliss, M. H. Katcher, C. H. Rogers and R. P. Shepard, "Optical-to-tactile image conversion for the blind," *IEEE Trans. Man-Mach. Sys.*, vol. MMS-11, pp. 58–65, 1970.
- [42] P. Bach-y-Rita, J. G. Webster, W. J. Tompkins and T. Crabb, "Sensory substitution for space gloves and for space robots," in *Proc. Workshop on Space Telerobotics*, vol. 2, Jet Propulsion Laboratory, 1987, pp. 51–57.
- [43] M. R. Neuman, "Prosthetic Sensory Transducers: Quarterly Progress Report", Applied Neural Control Laboratory, Electronics Design Center, and Department of Obstetrics and Gynecology, Case Western Reserve University, Jan. 15, 1990.
- [44] S. F. Wiker, Personal Communication, June 24, 1991.

Table 7.1

Order of adaptation experiments
 Adapting current I_A normalized; Frequency F in Hz;
 Number of pulses/burst NPB

Session Independent var. Experiment	1 I_A			2 F			3 NPB		
	1	2	3	1	2	3	1	2	3
Observer 1	0.5	0.7	0.9	15	5	45	6	1	2
Observer 2	0.5	0.9	0.7	15	45	5	6	2	1
Observer 3	0.7	0.5	0.9	45	5	15	1	2	6
Observer 4	0.7	0.9	0.5	45	15	5	1	6	2
Observer 5	0.9	0.5	0.7	5	15	45	2	1	6
Observer 6	0.9	0.7	0.5	5	45	15	2	6	1

Table 7.2

Sensation threshold current \bar{S}' (mA nonnormalized)IV = independent variable; boldface denotes *Baseline* waveform I_A normalized current; F in Hz

Session (IV)	IV level	O1	O2	O3	O4	O5	O6
1 (I_A)	0.5	0.93	1.70	1.57	1.90	1.04	2.15
	0.7	1.02	1.72	1.58	1.84	1.05	1.86
	0.9	1.11	1.65	1.75	1.87	1.05	2.09
2 (F)	5	2.21	1.66	1.57	2.31	1.89	2.19
	15	2.07	1.28	1.20	1.80	1.78	2.14
	45	1.62	1.30	1.30	2.00	1.33	2.08
3 (NPB)	1	1.75	1.41	1.75	2.46	1.02	1.89
	2	1.64	0.96	1.33	2.32	0.83	1.49
	6	1.62	1.01	1.24	2.16	0.84	1.14

Table 7.3

Maximal current without discomfort \bar{M}' (mA nonnormalized)
 IV = independent variable; boldface denotes *Baseline* waveform
 I_A normalized current; F in Hz

Session (IV)	IV level	O1	O2	O3	O4	O5	O6
1 (I_A)	0.5	5.74	6.16	9.54	7.05	4.73	4.51
	0.7	4.97	4.79	6.64	6.59	5.10	3.54
	0.9	4.89	4.98	10.10	7.84	4.62	3.92
2 (F)	5	4.97	3.83	8.75	7.47	6.13	5.26
	15	6.25	4.01	7.97	7.14	4.12	6.07
	45	3.80	4.27	10.21	6.96	5.22	5.55
3 (NPB)	1	6.50	5.00	10.09	6.50	5.92	7.20
	2	5.84	4.24	9.56	6.76	5.57	6.52
	6	6.86	3.72	7.74	6.75	4.32	5.45

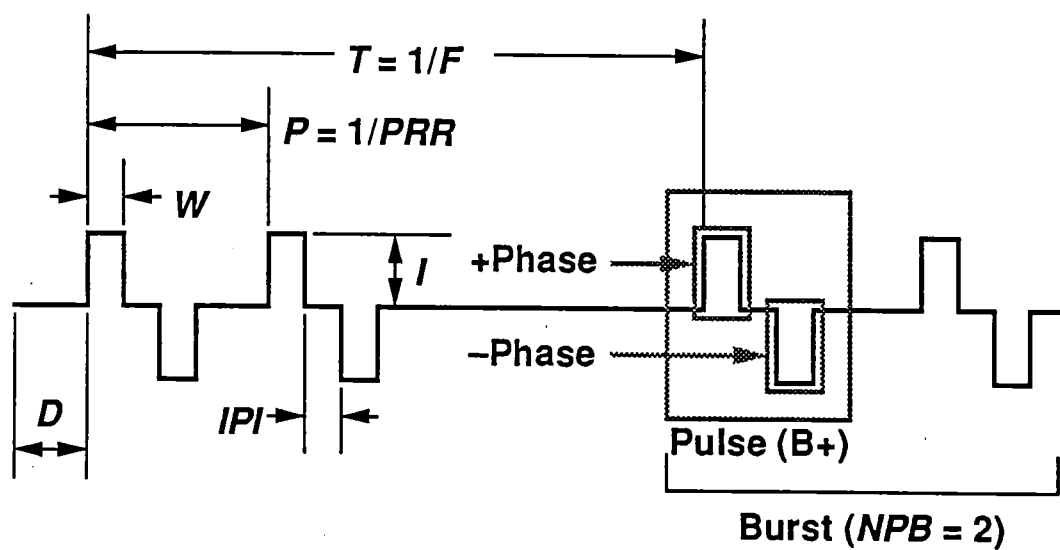


Fig. 7.1. Electrotactile waveform variables: D , delay; W , width; IPI , interphase interval; I , current; T , time between bursts; F , frequency of burst repetition; P , period of pulse repetition; PRR , pulse repetition rate; NPB , number of pulses per burst.

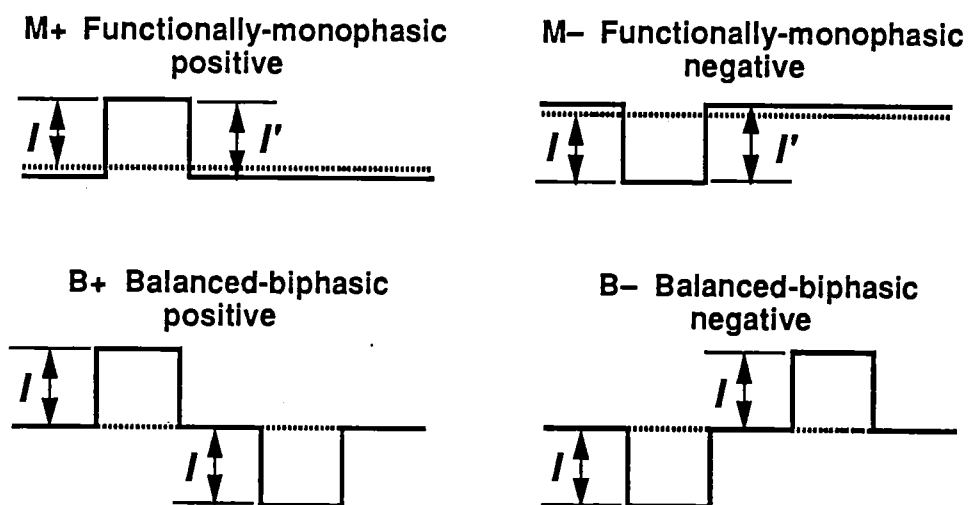


Fig. 7.2. Electrotactile waveform pulse types. Average current is zero for all types.

The dotted line is the zero-current reference.

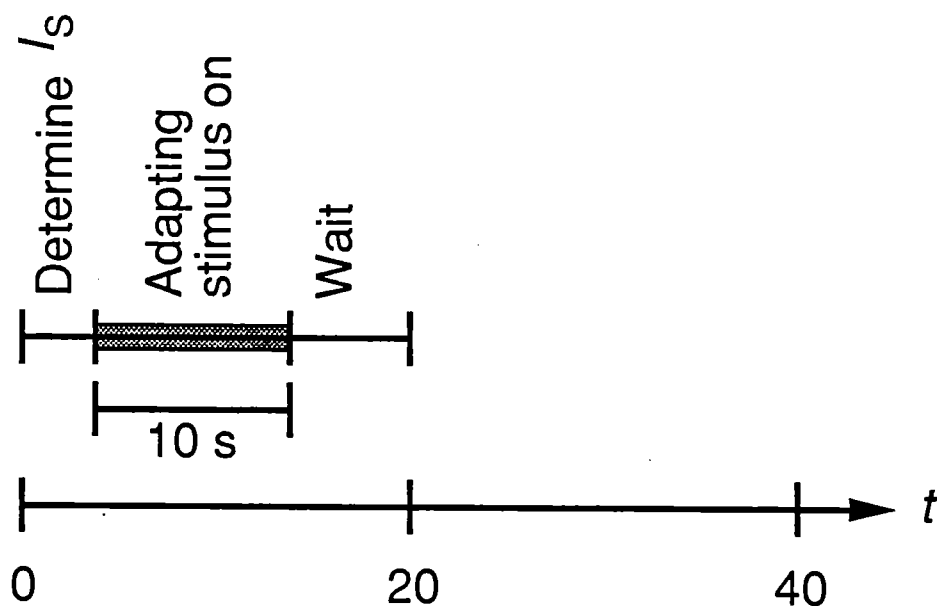


Fig. 7.3. Timing for adaptation experiment. Every 20 s, the computer prompts the observer to determine sensation threshold, which takes 5 – 10 s. After O presses ENTER to log this response, the system delivers a strong adapting stimulus for 10 s. The observer then waits until the next 20-s prompt. After 15 min, the recovery phase of the experiment continues for another 15 min with the same procedure but without the adapting stimulus.

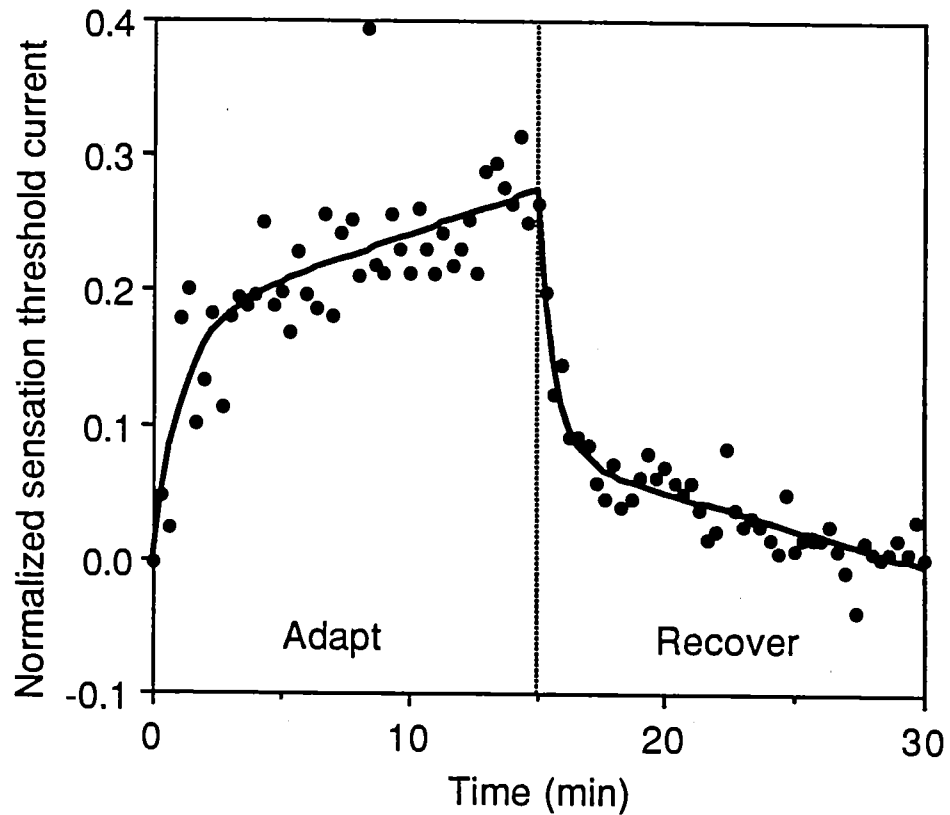


Fig. 7.4. Typical adaptation/recovery data and exponential-plus-linear model. During adaptation, the sensation threshold I_S quickly rises exponentially and then continues to rise slowly for at least 15 min total adaptation time. During recovery, I_S returns to close to normal in approximately 15 min. Data are from observer O2, session 3, $NPB = 6$.

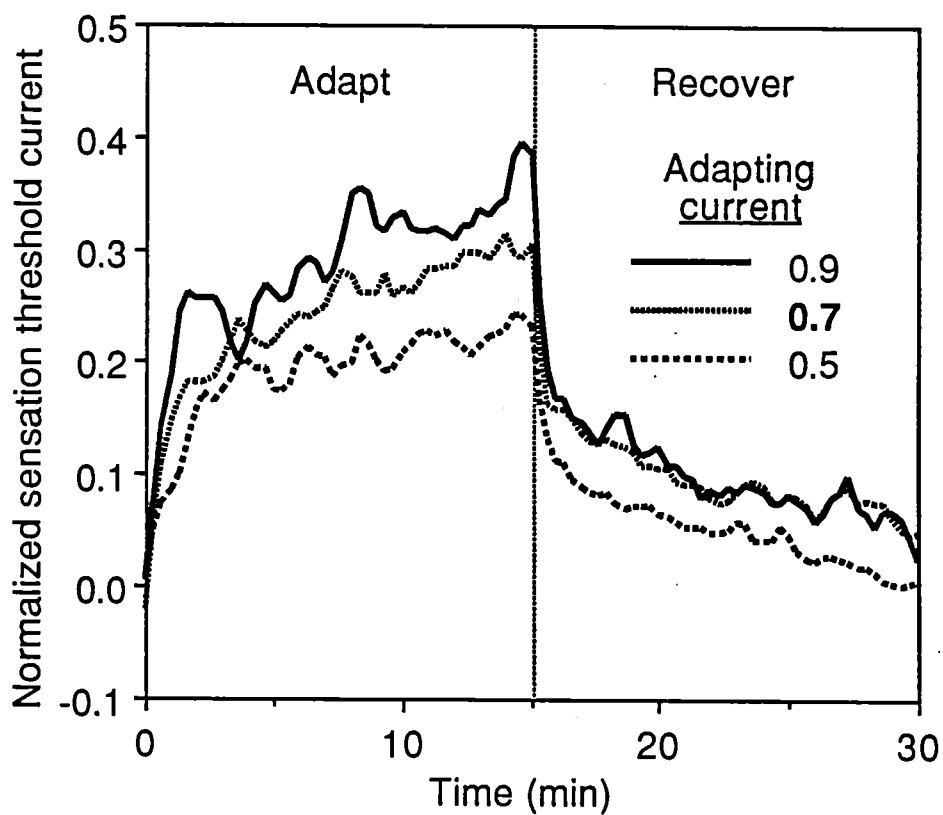


Fig. 7.5. Adaptation/recovery mean for six observers. A higher adapting current I_A causes faster and greater adaptation. The adapted sensation threshold $I_S(15 \text{ min}) = I_H$ is approximately $0.43 \cdot I_A$ (normalized current).

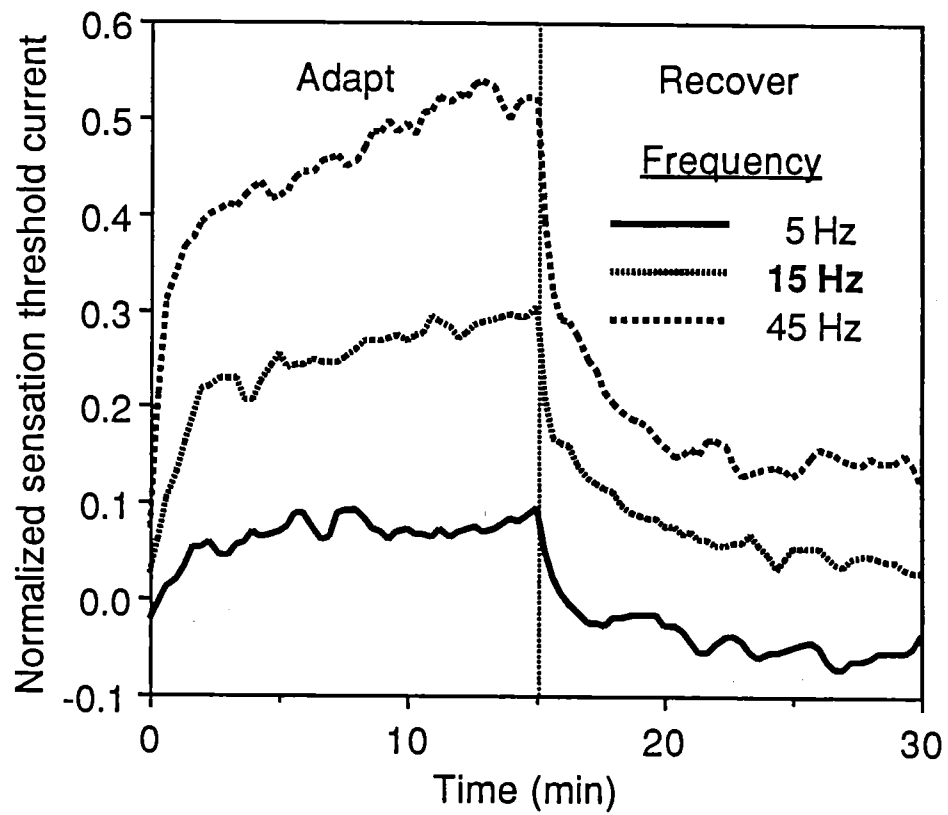


Fig. 7.6. Adaptation/recovery mean for six observers. A higher frequency F causes much faster and greater adaptation.

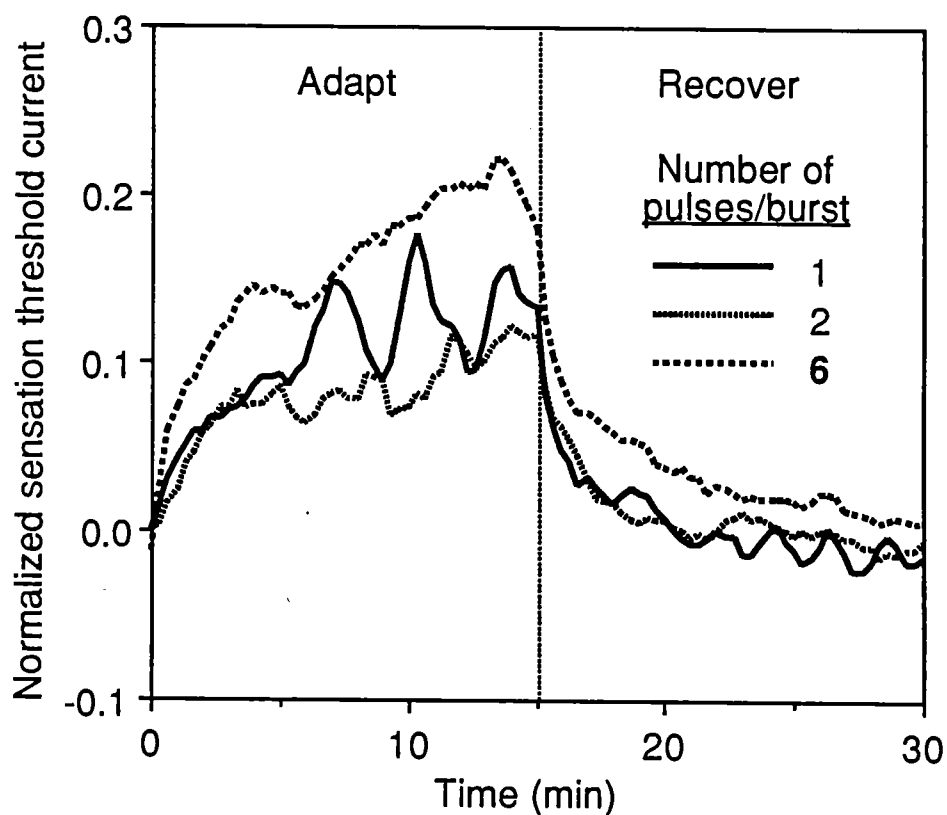


Fig. 7.7. Adaptation/recovery mean for six observers. Six pulses/burst *NPB* causes the fastest and greatest adaptation. The difference in sensation threshold elevation $I_S(15 \text{ min}) = I_F$ between 1 and 2 pulses/burst is not statistically significant (see text).

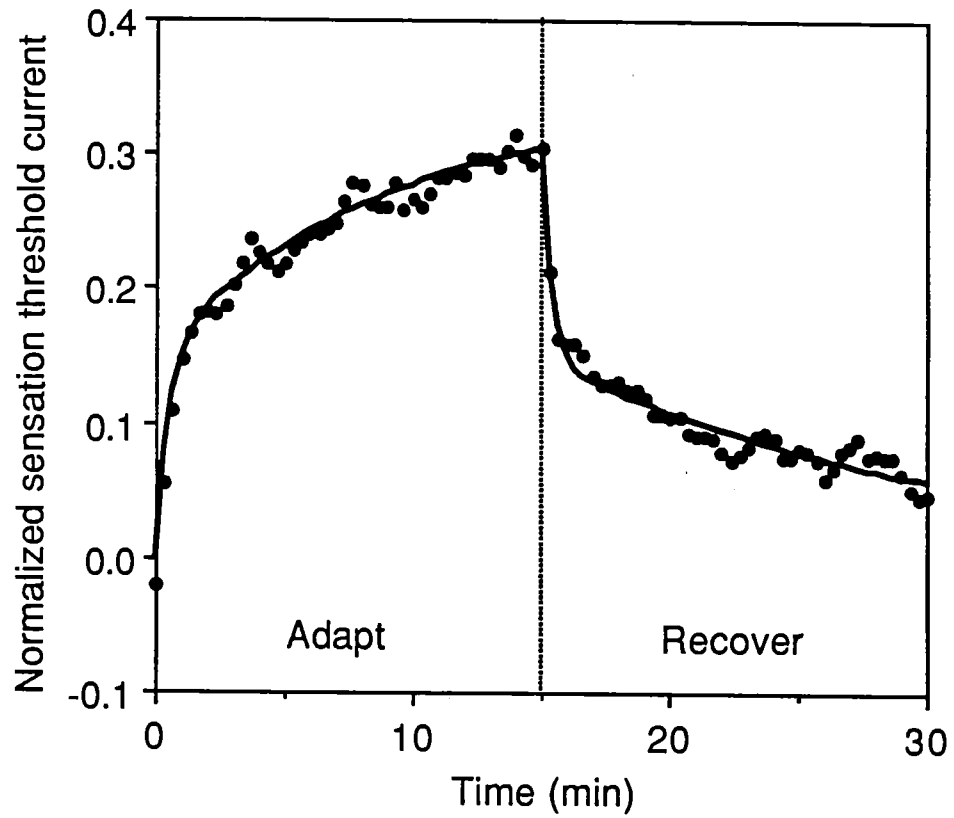


Fig. 7.8. A double exponential model predicts that $I_S(t)$ approaches zero (normalized sensation threshold) as t becomes large. Data are mean of all six observers, session 1, *Baseline* condition.

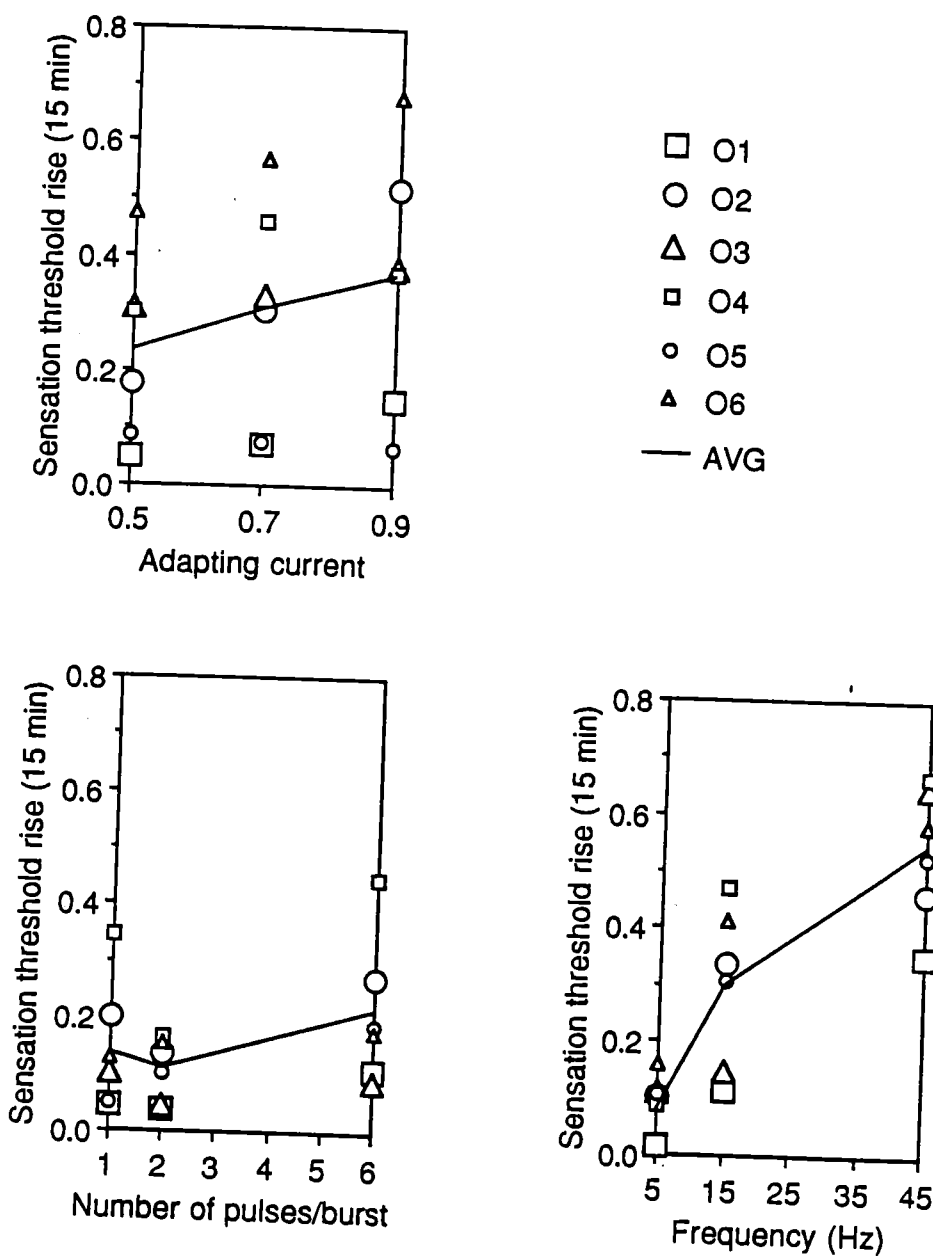


Fig. 7.9. Sensation threshold elevation after 15 min adaptation $I_S(15) = I_F$ vs. adapting current I_A , (normalized current) frequency F , and number of pulses/burst NPB . F has the greatest effect on the threshold elevation, followed by I_A and NPB .

Chapter 8

ELECTROTACTILE SKIN IRRITATION: INTRADERMAL DC CURRENT FLOW CAUSED BY ASYMMETRIC STIMULATION WAVEFORMS AND NONLINEAR ELECTRODE–SKIN VOLTAGE– CURRENT CHARACTERISTICS

Original Experiments and Model

A similar version of this chapter coauthored by K. A. Kaczmarek and J. G. Webster is submitted to *IEEE Transactions on Biomedical Engineering*.

ABSTRACT

Electrotactile (electrocutaneous) stimulation causes localized skin reddening under the stimulation electrode. Although most severe when a dc current flows across the electrode–skin interface, poststimulation redness is often greater if asymmetric stimulation waveforms are used, even with zero dc current across the interface. We speculate that this is caused by a circulating dc current which flows between structures in the electrode–skin interface and we propose a four-element nonlinear electrical model of the electrode–skin interface which predicts the magnitude of this current flow and also describes the voltage–current characteristics of the electrode–skin interface. We furthermore recommend that if a (symmetric) balanced-biphasic stimulation waveform cannot be used, that the dc current path at the output of the stimulator be as high as possible (at least 1 M Ω) to prevent a dc current through the electrode.

INTRODUCTION

Background

Electrotactile stimulation evokes tactile (touch) sensations within the skin at the location of the electrode by passing a local electric current through the skin. Sensory substitution is the use of one human sense (in this case, touch) to receive environmental information normally received by another sense (often vision or hearing). For the sense of touch, sensory substitution is the use of one area of skin to receive tactile information normally received at another location. Several articles review technology and devices for electrotactile stimulation [1], [2], visual substitution [3], [4], auditory substitution [5], [6], [7], and other applications [2], [8], [9], [10], [11], [12].

Waveform nomenclature

Figure 8.1 defines two commonly-used electrotactile stimulation waveforms. Both B+ (balanced-biphasic positive-leading) and M– (functionally-monophasic negative) waveforms have zero dc current to prevent rapid skin irritation due to a net electrochemical reaction at the electrode–skin interface. Reversing the phases of a B+ waveform (B–) causes little or no perceptual difference. A functionally-monophasic positive waveform (M+) requires more current than M– to achieve sensation threshold [13] and thus is not often used.

The stimulation current amplitude I of a B+ waveform is the value of either phase, i.e. $I = I_+ = -I_-$; for a M– waveform, I is the value of the negative phase with respect to zero, i.e. $I = -I_-$. To cause the dc current for M– to be zero, the current between negative phases I_+ must be positive:

$$I_+ = I \frac{D}{1 - D} \quad (1)$$

where $D = W/T$ is the duty cycle of the waveform. For waveforms with the pulses gated into bursts, desirable for higher dynamic range [14], W is replaced by W times the number of pulses/burst.

The literature contains inconsistent waveform terminology [15]. Frequently, M+ and M– waveforms are called "biphasic" because they have positive and negative parts (Fig. 8.1). We use the terms "functionally-monophasic" for M+ and M– and "balanced-biphasic" for B+ and B– to avoid ambiguity. The two *phases* of a *balanced-biphasic* waveform pulse are often called *pulses* (with the result that interphase interval

IPI is called "interpulse interval"). Introducing the term "phase" avoids the above ambiguity, and uniquely specifies the waveform timing relationships.

Skin irritation and dc current

It is well-known that rapid skin irritation, manifest by a red spot directly under and surrounding the stimulation electrode by up to 2 cm, occurs when the dc current across the electrode–skin interface \bar{i} is nonzero; \bar{i} as small as 10 μA can accelerate the reddening. However, we and others [16] have observed that the asymmetric M– waveform often causes more redness than the symmetric B+ waveform, even though both have zero \bar{i} . (However, see also [17], [18].) The cause may be related to the accumulation of charge in the capacitive elements of the dermis during a stimulation pulse; this charge does not readily dissipate unless a symmetric waveform is used [16], [19].

An alternate explanation is that because the voltage–current characteristic of the electrode–skin interface is highly nonlinear [16], [20], [21], [22], [23], $\bar{i} = 0$ does not guarantee that the dc voltage across the electrode–skin interface \bar{v} is also zero. In fact, \bar{v} can reach +2 V with M– stimulation at $I = 10 \text{ mA}$. We speculate that this dc potential may cause (or be the result of) an *internal* circulating dc current flow through some skin structure(s), causing skin irritation. We will present a simple electrical model which predicts \bar{i} and \bar{v} , as well as the static and dynamic electrical characteristics of the electrotactile electrode–skin interface. The calculations for \bar{i} and \bar{v} include, but are not fundamentally dependent on, the presence of the dermal capacitance.

DYNAMIC VOLTAGE–TIME CHARACTERISTICS

Experiment

A Tektronix model 2620 stimulus isolator driven by a Pulsar model 6i pulse generator delivered $I = 1$ mA, $W = 400$ μ s, B+ current pulses at a rate of 10 Hz ($T = 100$ ms) to a subject's tapwater-premoistened abdomen by an electrode in the elasticized-belt linear electrode array from a TacticonTM auditory prosthesis for the deaf [11], [24], [25]. The 5.5-mm-diameter gold-plated electrodes are surrounded by the conductive rubber base material of the belt, which serves as a ground plane. (We previously determined that the ground plane impedance is 1.3% of the active electrode impedance and is assumed to be negligible.) The electrode site was approximately 2 cm above and 7 cm right of the navel.

A 330-k Ω resistor directly across the stimulus isolator output provided a pathway for residual dc at the isolator output due to any slight waveform asymmetry. A 100- Ω resistor in series with the ground plane provided for stimulus current i measurement. The cursors on a Tektronix 2230 digital oscilloscope (in the averaging mode for noise reduction) measured i and the voltage v (with a 10-M Ω probe) between the active electrode and the ground plane. Figure 8.2 shows the voltage v recorded for the positive phase of the pulse. Very similar waveforms result for the negative phase, for functionally-monophasic waveforms, and at different skin locations on the abdomen (< 10% variation).

Single-exponential model

A casual glance at Fig. 8.2 suggests that the voltage response to a constant-current pulse is a simple exponential rise and fall modeled by the classical electrode model in Fig. 8.3a. The Fig. 8.3a electrode-skin voltage is:

$$\text{Rise: } v(t) = V_M(1 - e^{-t/\tau}) \quad (2)$$

$$\text{Fall: } v(t) = V_M e^{-t/\tau} \quad (3)$$

where $\tau = R_P C$ and $V_M = I \cdot R_P$. Note that t in the fall phase is normalized so that $t = 0$ corresponds to the end of the current pulse. We will also ignore the series resistor R_S in Fig. 8.3a; its value of 200 – 900 Ω is small compared to the total electrode–skin resistance. It likely represents the electrolyte–electrode resistance. We measured a resistance of approximately 600 Ω for the electrode applied to a saline-soaked (34 mM) paper towel for pulsatile currents of 0.1, 1, and 10 mA.

Figure 8.2 shows the voltage predicted by (2) and (3) where V_M and τ are chosen for a least-squares fit. ($V_M = 27.7$ V and $\tau = 46.7$ μ s.) While the rising phase is modeled quite well by (2), the falling phase is not modeled by (3). Not only are the model parameters changing between the rise and fall phases, but the model itself is changing or is inadequate.

Double exponential model

Since the skin is a multilayer structure, we might assume the double exponential model in Fig. 8.3b, which is described by:

$$\text{Rise: } v(t) = V_{M1}(1 - e^{-t/\tau_1}) + V_{M2}(1 - e^{-t/\tau_2}) \quad (4)$$

$$\text{Fall: } v(t) = V_{M1}e^{-t/\tau_1} + V_{M2}e^{-t/\tau_2} \quad (5)$$

The Systat™ least-squares nonlinear regression algorithm was not able to find parameters for Eq. (4) using the data in Fig. 8.2; V_{M1} and τ_1 approached V_M and τ in

the simple model, V_{M2} approached 0, and τ_2 approached infinity. We conclude that for the rise phase, a double exponential model is not necessary. However, Fig. 8.2 shows that Eq. (5) models the falling phase much better than Eq. (3). ($V_{M1} = 19.6$ V, $V_{M2} = 7.8$ V, $\tau_1 = 52.8$ μ s and $\tau_2 = 643$ μ s).

Using two different models for rise and fall seems unphysiological. It is likely that a better model might have time-varying parameters. In particular, the similarity of the time constants for the rise phase and early fall phase suggests that some parameter in Eq. (3) changes with time. The following section will develop this idea further.

STATIC VOLTAGE-CURRENT CHARACTERISTICS

It has been long known that the steady state resistance (after capacitive transients decay) of a current-carrying electrode-skin interface decreases substantially with increasing current [16], [20], [21], [23]. This section elaborates on our previous voltage-current model [22], extending its useful current range of 1 – 25 mA down to 0.4 μ A.

Experiment

A computer-controlled electrotactile stimulation system (ETSS) [15] delivered M- current pulses at a rate of 15 Hz to the subject through the electrode and monitoring circuit described above (without the 330-k Ω parallel resistor). The current amplitude I varied 0.2 – 20 mA; the phase width W inversely varied 1000 – 35 μ s to keep the sensation tolerable at high currents and to ensure that the voltage waveform v in Fig. 8.2 reached its maximal value V_M at low currents. We recorded only the current amplitude I and the maximal voltage V_M .

Excessive noise in the automated system prevented measurement of I and V_M below 0.2 mA. We hence adopted a method described by Boxtel [20] in which a 20-

Hz square-wave *voltage* waveform excited the electrode. In this case V is the zero-to-peak voltage. The resulting current is also a square wave with a large leading spike I_M at the voltage transitions ($I_M = V/R_S$ from Fig. 8.3a) and a long plateau region after the spike ($I = V/R_P$). V varied 0.1 – 7.0 V, below sensation threshold and below the point of current runaway [21]. The resulting $R_S = 833 \Omega$ was constant over this range. The measured current range was 0.4 – 33 μA , complementing the current-pulse method. Figure 8.4 shows the composite static voltage–current relationship.

Static nonlinear model

Figure 8.5 shows a nonlinear equivalent circuit model which yields the solid line in Fig. 8.4. The parallel resistances $R_V(i)$ and R_F replace $R_P(i)$ in Fig. 8.3a. In the steady state, where v and i are constant, Fig. 8.5 is described by

$$v(I) = i \cdot R(i) \quad (6)$$

where

$$\begin{aligned} R(i) &= R_S + R_P(i) \\ &= R_S + \frac{R_F R_V(i)}{R_F + R_V(i)} \\ R_V(i) &= \frac{R_F I_0}{|i|} \end{aligned}$$

and $R_S = 1.6 \text{ k}\Omega$, $R_F = 400 \text{ k}\Omega$, $C = 2 \text{ nF}$, and $I_0 = 60 \mu\text{A}$ are constants; $R_V(i)$ varies with current i . Figure 8.4 shows that Eq. (6) fits the data over nearly five orders of

magnitude in current i . These values are substantially different from our earlier estimates [22]: $R_S = 0.895 \text{ k}\Omega$, $R_F = 60.1 \text{ k}\Omega$, and $I_0 = 0.585 \text{ mA}$. (Note that before, we used R_0 for R_S and R_P for R_F — the present notation provides better consistency with the literature.) The new parameters allow the model to extend to much lower currents and still provide a reasonable fit over the whole range — the old parameters allowed a better fit for 1 – 25 mA (the useful range for electrotactile stimulation).

The correspondence of the elements of Fig. 8.5 to the electrode–skin interface is partly known. Removing the stratum corneum by abrasion [20] or drilling [23] reveals that R_P (the parallel combination of R_F and R_V), C , and part of R_S are located there. The mechanism that causes R_V to vary with i is not known. Sweat ducts carry most of the current across the skin [26], [27], so the current density in these ducts may be high enough to heat the sweat. However, the conductance of 0.017 – 0.051 mM NaCl solution (the approximate ionic content of sweat) only increases 100% from 40°C to 100°C. Therefore, heating of sweat in the sweat ducts cannot account for the 30-fold change in $R(i)$. Furthermore, the decrease in R_V with increasing i is virtually instantaneous [20], which probably precludes a heat-driven model. Another possible mechanism is electrically-driven filling of sweat ducts [21]. The observed V – I relationship due to the variation of R_V is independent of polarity.

Dynamic switched exponential model

A further observation by Boxtel [20] was that R_P (and hence R_V) decrease “instantaneously” with a step increase in i — or at least quickly enough that its change is obscured by the charging of C (recall that $\tau = 46.7 \text{ }\mu\text{s}$ for $i = 1 \text{ mA}$). However, a step decrease in i causes R_P to increase linearly with $\log(t)$ for $t \geq 2 \text{ ms}$. Although full recovery of R_P sometimes took as long as 100 s, only 10 ms were required for nearly-

complete recovery for large step decreases in i , e.g., a factor of 100. Boxtel did not characterize the recovery of R_P for $t < 2$ ms, presumably because the discharge of C obscured the measurement. However, it is clear that R_P rises rapidly in this time region.

This time-dependent recovery of R_P explains the inadequacy of the single-exponential model in Eq. (3). For the stimulation current $I_+ = 1$ mA in the rising phase of Fig. 8.2, Eq. (6) predicts that $R_P(I_+) = 22.6$ k Ω . With $C = 2$ nF, this predicts $\tau = R_P C = 45.2$ μ s. We observed $\tau = 46.7$ μ s, close to the predicted value. Also, we observed the time constant for the falling phase $\tau_1 = 52.8$ μ s, which is consistent with the assumption that R_P has not yet recovered much from the current pulse. The fully-recovered value of R_P predicted by Eq. (6) is 400 k Ω , because $i = 0$ between phases of a B+ pulse. This predicts $\tau_2 = 800$ μ s, while we observe 643 μ s in Fig. 8.2, indicating nearly complete recovery of R_P from the 1-mA current pulse. We therefore conclude that the single-exponential model in Eqs. (2) and (3) is adequate to explain the observed voltage on an electrode stimulated by a constant-current pulse, assuming that R_P is allowed to vary with current i in Eq. (6) and that R_P decreases in value very quickly with increasing i but increases in value more slowly with decreasing i .

DC CHARACTERISTICS

When the nonlinear electrode-skin interface is stimulated with an asymmetric waveform, a dc voltage \bar{v} appears even if the dc stimulation current $\bar{i} = 0$. We will show that \bar{v} can be largely explained by Eqs. (2), (3), and (6). This nonzero \bar{v} may be related to the increased skin redness caused by M- waveforms over B+ waveforms.

Experiment I — dc voltage

The apparatus in the last section [15] stimulated the electrode–skin interface with M -, $W = 150\text{-}\mu\text{s}$ pulses at a rate of 15 Hz ($T = 66.7\text{ ms}$) with current amplitude I ranging 0 – 13 mA. We measured \bar{v} by using a single-stage RC low-pass filter ($f_c = 0.14\text{ Hz}$) at the oscilloscope input to remove the pulsatile component of v . Figure 8.6 shows for two skin locations that \bar{v} increases with increasing I , but appears to be limited to 2 V. A 0.1 – 0.15-V negative dc offset is present with no stimulation.

Dc voltage-and-current model

The electrode–skin model in Fig. 8.5 is the basis for predicting \bar{v} . We will make the simplifying assumptions (1) R_S cannot contribute to \bar{v} because it is linear and because $\bar{i} = 0$ and (2) the value of R_V recovers instantly from the current pulse; this is reasonable because the interval $T - W$ between pulses (66.3 ms) is much longer than the R_P recovery time ($< 10\text{ ms}$), and therefore R_V is mostly recovered during this interval. Using the stimulation waveform in Fig. 8.1a, we then have

$$\frac{dv(t)}{dt} = \frac{1}{C} \left[i(t) - \frac{v(t)}{R_F} - \frac{v(t)}{R_V[i(t)]} \right] \quad (7)$$

If we let $R_P(i)$ represent the parallel combination of R_F and $R_V(i)$ and assume that $i(t)$ is piecewise constant, the solution to Eq. (7) is

$$v(t) = v(t_0) + \left[i \cdot R_P(i) - v(t_0) \right] \left[1 - e^{-(t - t_0)/R_P(i)C} \right] \quad (8)$$

We can apply Eq. (8) to the I_- (stimulating) part of the waveform, and let $t_0 = 0$ and $t = W$. We can also apply Eq. (8) to the I_+ (recovering) part of the waveform and let $t_0 =$

W and $t = T$. We now have two equations in the two unknowns $v(0) = v(T)$ and $v(W)$, which can be solved simultaneously to find the initial conditions for Eq. (8):

$$v(0) = \frac{\left(I_+ R_+ + I_- R_- e^{-\frac{W}{\tau_-}}\right) \left(1 - e^{-\frac{T-W}{\tau_+}}\right)}{1 - e^{-\left(\frac{W}{\tau_-} + \frac{T-W}{\tau_+}\right)}} \quad (9)$$

$$v(W) = \frac{\left(I_- R_- + I_+ R_+ e^{-\frac{T-W}{\tau_+}}\right) \left(1 - e^{-\frac{W}{\tau_-}}\right)}{1 - e^{-\left(\frac{W}{\tau_-} + \frac{T-W}{\tau_+}\right)}}$$

where $R_+ = R_P(I_+)$ and $R_- = R_P(I_-)$ from Eq. (6); I_+ and I_- are known from Eq. (1); $\tau_+ = R_+ C$, and $\tau_- = R_- C$. For calculation purposes, the denominator of these expressions is very close to 1. Knowing these initial conditions, Eq. (8) specifies $v(t)$ for the entire waveform in two sections, $0 - W$ and $W - T$. Finally, we can use the definition of average (dc) value to find \bar{v} :

$$\bar{v} = \frac{1}{T} \int_0^T v(t) dt \quad (10)$$

$$= \frac{1}{T} \int_0^W v(t) dt + \frac{1}{T} \int_W^T v(t) dt$$

Therefore,

$$\begin{aligned} \bar{v} = \frac{1}{T} & \left\{ v(0)W + [I_- R_- - v(0)] \left[W + \tau_- \left(e^{-\frac{W}{\tau_-}} - 1 \right) \right] \right\} \\ & + \frac{1}{T} \left\{ v(W)(T - W) + [I_+ R_+ - v(W)] \left[(T - W) + \tau_+ \left(e^{-\frac{T-W}{\tau_+}} - 1 \right) \right] \right\} \end{aligned} \quad (11)$$

where \bar{v} is a function of the waveform parameters I , W , and T , and the electrode-skin interface parameters R_F and I_0 .

Figure 8.6 shows that the predicted \bar{v} as a function of I (solid line) follows the data up to approximately 2 mA but then overestimates the data; the electrode-skin interface appears to clamp \bar{v} to approximately 2 V. This effect is not predicted by the model. Based on the result of the next experiment, we suspected that an *additional* voltage-sensitive dc current pathway not included in Fig. 8.5 clamps \bar{v} .

Because $\bar{i} = 0$, the only nonzero dc currents in Fig. 8.5 are through R_F and R_V ; in fact $\bar{i}_F = -\bar{i}_V$. Because R_F is constant,

$$\bar{i}_F = \frac{\bar{v}}{R_F} \quad (12)$$

where \bar{v} can be calculated with Eq. (11). This current, which we propose circulates only in the electrode-skin interface, should not be sensitive to the proposed dc-voltage-clamping element. The following experiment indirectly measures \bar{i}_F to confirm the validity of Eq. (11).

Experiment II — dc current

We modified the output circuit of the electrotactile stimulator [15] by adding an additional feedback loop to keep the dc voltage across the electrode \bar{v} at zero. This causes $\bar{i}_F = 0$, and therefore $\bar{i}_V = \bar{i}$, (i.e., the *circulating* dc current is channeled through the electrode). Then, $\bar{i}_V = \bar{i}$ is easily measured with the aid of a low-pass filter ($f_c = 0.05$ Hz). Because \bar{i}_F is less than 0.2% of I , this measurement technique does not disturb the value of R_V for either I_+ or I_- , and therefore does not disturb the system to be measured. The solid line in Fig. 8.7 shows the predicted [Eqs. (11) and (12)] and measured values of $\bar{i}_V = \bar{i}$ for stimulation currents corresponding to those in Fig. 8.6. We noted greater skin reddening with this zero- \bar{v} configuration than with the usual zero- \bar{i} configuration.

The close fit of data to model in Fig. 8.7 confirms that Eq. (11) accurately predicts \bar{v} as long as it does not exceed 1 V ($I < 2$ mA) and accurately predicts \bar{i}_V for stimulation currents 0 – 13 mA. It is likely that the return path for \bar{i}_V is R_F when $\bar{v} < 1$ V and a combination of R_F plus an *alternative* dc pathway when $\bar{v} > 1$ V. In either case, we propose that if the stimulation waveform is asymmetric, a circulating dc current exists in the electrode–skin system, even if the stimulation waveform has no net dc current flow. Such a circulating current, whatever the pathway, may be expected to cause net electrochemical reactions producing skin irritation at the electrode site.

Because \bar{v} exists, the dc output resistance of the stimulator should be as high as possible (> 1 M Ω) to minimize dc current through the electrode. In particular, transformer-output coupling should be accompanied by a dc-blocking coupling capacitor in series with the electrode.

DIODE MODEL

The preceding model depends on a current-sensitive resistor that may be difficult to link with any physiological structure. A more intuitive nonlinear element that has a similarly-shaped voltage–current characteristic is a forward-biased diode. Most of the current that flows through a sweat duct enters the dermis through the duct wall rather than through the secretory part of the gland [28]. Furthermore, a (semipermeable) cell membrane has layers of mobile charges on either side of a barrier, much like a P–N junction, and in fact often behaves electrically like a diode [29].

Figure 8.8 (the “diode model”) therefore shows an alternative to the current-sensitive resistor model in Fig. 8.5. Back-to-back diodes are used because the skin–electrode voltage–current characteristic is independent of polarity except for dry electrodes at very low frequencies [21]. The equivalent resistance of a forward-biased diode R_D is

$$R_D = \frac{a \ln\left(\frac{i_V}{I_S} + 1\right)}{i_V}$$

The dashed lines in Figs. 8.4, 8.6, and 8.7 show how the diode model predicts V_M , \bar{v} , and \bar{i} , respectively, where $a = 5.3$ V, $I_S = 0.012$ mA, $R_F = \infty$, and $R_S = 600$ Ω . The analysis proceeds similarly to Eqs. (7) – (12) but a closed-form solution is not possible; we show an approximation assuming that $C = 0$. While the diode model predicts V_M very well, it is less accurate for \bar{v} and \bar{i} than the current-sensitive resistor model.

CONCLUSIONS

A simple four-element model with only one current-and-time-dependent element predicts three electrical characteristics of the electrotactile electrode–skin interface: (1)

the electrode voltage waveform resulting from a constant-current stimulation pulse, (2) the variation of the asymptotic voltage with pulsed stimulation current from $0.4\ \mu\text{A}$ to $20\ \text{mA}$, and (3) the existence and magnitude of a circulating dc current in the electrode-skin system and related dc voltage on the electrode when the stimulation current waveform is asymmetric. The correspondence between the elements in the model and the electrode-skin system, and the nature of the limit on the dc voltage warrant further investigation. An alternate equivalent circuit based on the similarity of a cell membrane to a P-N junction may be more physiological and predicts the asymptotic voltage more accurately, but is presently inadequate for predicting circulating dc current flow.

These findings suggest two recommendations for the design of electrotactile stimulation systems. The first is that symmetric stimulation waveforms (such as balanced-biphasic) are desirable to reduce skin irritation. The second is that if an asymmetric waveform is used, the output resistance of the stimulator to dc current should be as high as possible, preferably capacitor-coupled. Otherwise, the electrode-skin interface itself can cause a dc current through the electrode.

REFERENCES

- [1] K. A. Kaczmarek, J. G. Webster, P. Bach-y-Rita and W. J. Tompkins, "Electrotactile and vibrotactile displays for sensory substitution," *IEEE Trans. Biomed. Eng.*, vol. 38, pp. 1–16, 1991.
- [2] A. Y. J. Szeto and F. A. Saunders, "Electrocutaneous stimulation for sensory communication in rehabilitation engineering," *IEEE Trans. Biomed. Eng.*, vol. BME-29, pp. 300–308, 1982.
- [3] P. Bach-y-Rita, *Brain Mechanisms in Sensory Substitution*. New York: Academic, 1972.
- [4] C. C. Collins, "On mobility aids for the blind," in *Electronic Spatial Sensing for the Blind*, D. H. Warren and E. R. Strelow, Eds. Dordrecht, The Netherlands: Martinus Nijhoff, 1985, pp. 35–64.
- [5] C. M. Reed, N. I. Durlach and L. D. Bradia, "Research on tactile communication of speech: A review," *AHSA Monographs*, vol. 20, pp. 1–23, 1982.
- [6] C. E. Sherrick, "Basic and applied research on tactile aids for deaf people: Progress and prospects," *J. Acoust. Soc. Am.*, vol. 75, pp. 1325–1342, 1984.
- [7] A. Y. J. Szeto and K. M. Christensen, "Technological devices for deaf-blind children: Needs and potential impact," *IEEE Eng. Med. Biol. Mag.*, vol. 7, no. 3, pp. 25–29, 1988.
- [8] C. C. Collins and J. M. J. Madey, "Tactile sensory replacement," in *Proc. San Diego Biomed. Symp.*, vol. 13, 1974, pp. 15–26.

- [9] C. A. Phillips, "Sensory feedback control of upper- and lower-extremity motor prostheses," *CRC Crit. Rev. Biomed. Eng.*, vol. 16, pp. 105–140, 1988.
- [10] R. R. Riso, "Sensory augmentation for enhanced control of FNS systems," in *Ergonomics in rehabilitation*, A. Mital, Ed. New York: Taylor and Francis, 1988, pp. 253–271.
- [11] F. A. Saunders, "Information transmission across the skin: High-resolution tactile sensory aids for the deaf and the blind," *Int. J. Neurosci.*, vol. 19, pp. 21–28, 1983.
- [12] A. Y. J. Szeto and R. R. Riso, "Sensory feedback using electrical stimulation of the tactile sense," in *Rehabilitation Engineering*, R. V. Smith and J. H. Leslie Jr., Eds. Boca Raton, FL: CRC Press, 1990, pp. 29–78.
- [13] J. P. Girvin, L. E. Marks, J. L. Antunes, D. O. Quest, M. D. O'Keefe, P. Ning and W. H. Dobbelle, "Electrocutaneous stimulation I. The effects of stimulus parameters on absolute threshold," *Percept. Psychophys.*, vol. 32, pp. 524–528, 1982.
- [14] K. A. Kaczmarek, "Optimal Electrotactile Stimulation Waveforms for Human Information Display," Ph. D. Thesis, Dept. Electrical and Computer Engineering, Univ. of Wisconsin-Madison, 1991.
- [15] K. A. Kaczmarek, K. M. Kramer, J. G. Webster and R. G. Radwin, "A 16-channel 8-parameter waveform electrotactile stimulation system," *IEEE Trans. Biomed. Eng.*, vol. 38, 1991 (in press).
- [16] F. A. Saunders, "Recommended procedures for electrocutaneous displays," in *Functional Electrical Stimulation: Applications in Neural Prostheses*, F. T.

- Hambrecht and J. B. Reswick, Eds. New York: Marcel Dekker, 1977, pp. 303–309.
- [17] A. Y. J. Szeto and L. Mao, "Dermal response to extended electrocutaneous stimulation," in *Proc. 34th Annu. Conf. Eng. Med. Biol.*, vol. 23, IEEE, 1981, p. 305.
 - [18] A. Y. J. Szeto and L. Mao, "Dermal effects of electrocutaneous stimulation," in *Proc. First Southern Biomed. Eng. Conf.*, S. Saha, Ed., Pergamon Press, 1982, pp. 121–124.
 - [19] F. A. Saunders and V. F. Saunders, "Intradermal recording during electrocutaneous stimulation," *Fed. Proc.*, vol. 33, I, p. 312, 1974.
 - [20] A. v. Boxtel, "Skin resistance during square-wave electrical pulses of 1 to 10 mA," *Med. Biol. Eng. Comput.*, vol. 15, pp. 679–687, 1977.
 - [21] S. Grimnes, "Skin impedance and electro-osmosis in the human epidermis," *Med. Biol. Eng. Comput.*, vol. 21, pp. 739–749, 1983.
 - [22] K. A. Kaczmarek and J. G. Webster, "Voltage–current characteristics of the electrotactile skin–electrode interface," in *Proc. Annu. Int. Conf. IEEE Eng. Med. Biol. Soc.*, Seattle, WA, Y. Kim and F. A. Spelman, Eds., vol. 11, IEEE, 1989, pp. 1526–1527.
 - [23] D. T. Lykken, "Square-wave analysis of skin impedance," *Psychophysiol.*, vol. 7, pp. 262–275, 1971.
 - [24] M. P. Lynch, R. E. Eilers, D. K. Oller and L. Lavoie, "Speech perception by congenitally deaf subjects using an electrocutaneous vocoder," *J. Rehab. Res. Dev.*, vol. 25, pp. 41–50, 1988.

- [25] F. A. Saunders, *Tacticon 1600 Electrotactile Sensory Aid for the Deaf: User's Guide*. San Rafael, CA: Tacticon Corporation, 1986.
- [26] F. A. Saunders, "Electrocutaneous displays," in *Proc. Conf. Cutan. Comm. Sys. Dev.*, F. A. Geldard, Ed., Psychonomic Society, 1973, pp. 20–26.
- [27] S. Grimnes, "Pathways of ionic flow through human skin in vivo," *Acta. Derm. Venerol. (Stockh)*, vol. 64, pp. 93–98, 1984.
- [28] D. C. Fowles, "Mechanisms of electrodermal activity," in *Bioelectric Recording Techniques: Part C. Receptor and Effector Processes*, R. F. Thompson and M. M. Patterson, Eds. New York: Academic, 1974, pp. 231–271.
- [29] J. J. B. Jack, D. Noble and R. W. Tsien, *Electric current flow in excitable cells*. Oxford: Clarendon, 1975.

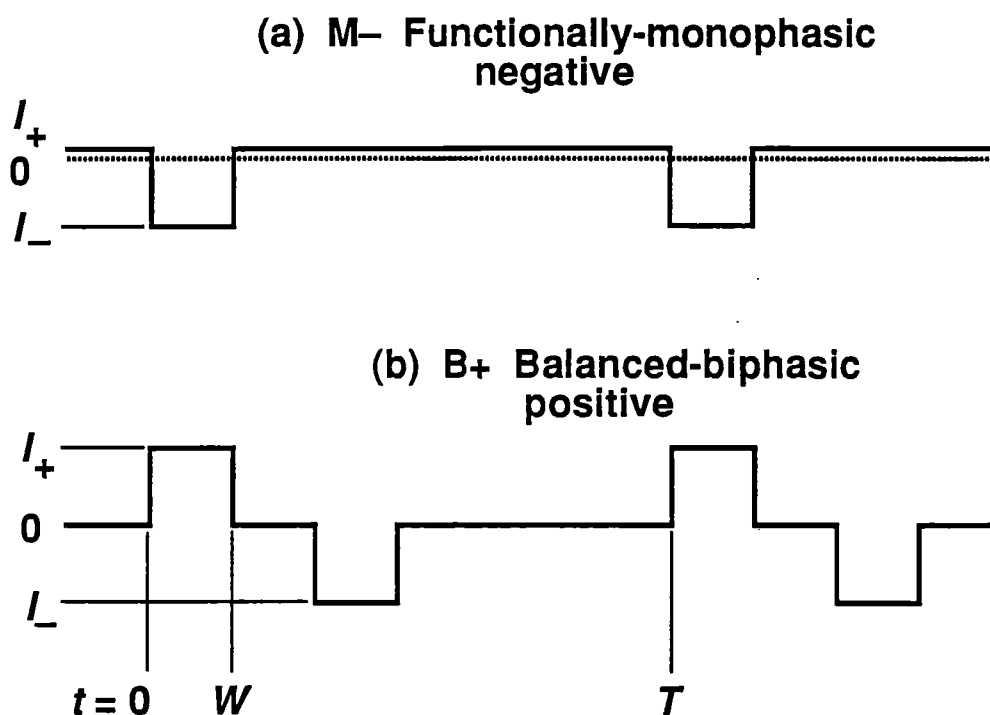


Fig. 8.1. Electrotactile current stimulation waveforms. (a) A functionally-monophasic negative (M-) waveform has positive (I_+) and negative (I_-) phases but zero dc current \bar{i} . (b) A balanced-biphasic positive-leading (B+) waveform is symmetric. For both waveforms, W is the phase width and $T = 1/F$ is the period.

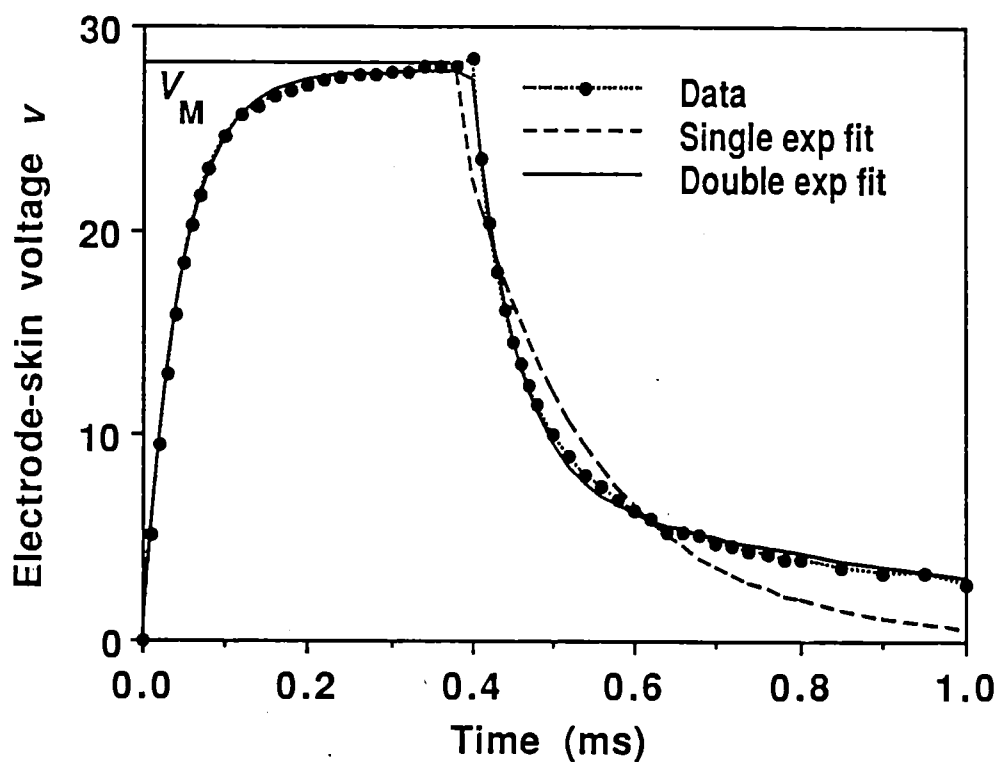


Fig. 8.2. The voltage v across the electrode–skin interface in response to a constant-current stimulation pulse i rises exponentially and falls as a time-varying exponential function. A double-exponential model approximates the time-varying exponential. V_M is the asymptotic maximal voltage reached during a long current pulse.

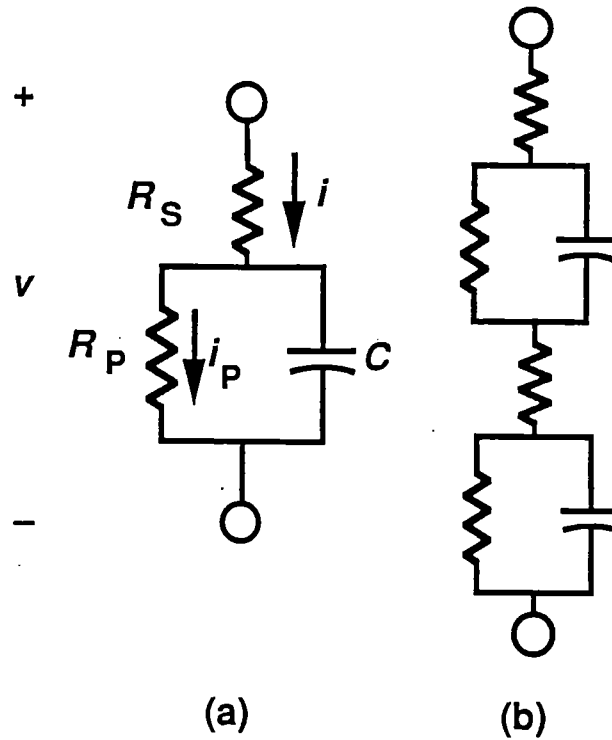


Fig. 8.3. The simple electrode-skin model (a) can explain the rising part of the voltage waveform v resulting from a constant-current stimulation pulse i . A two-stage model (b) more accurately describes the falling voltage, but seems unphysiological because the form of the model must change between rising and falling.

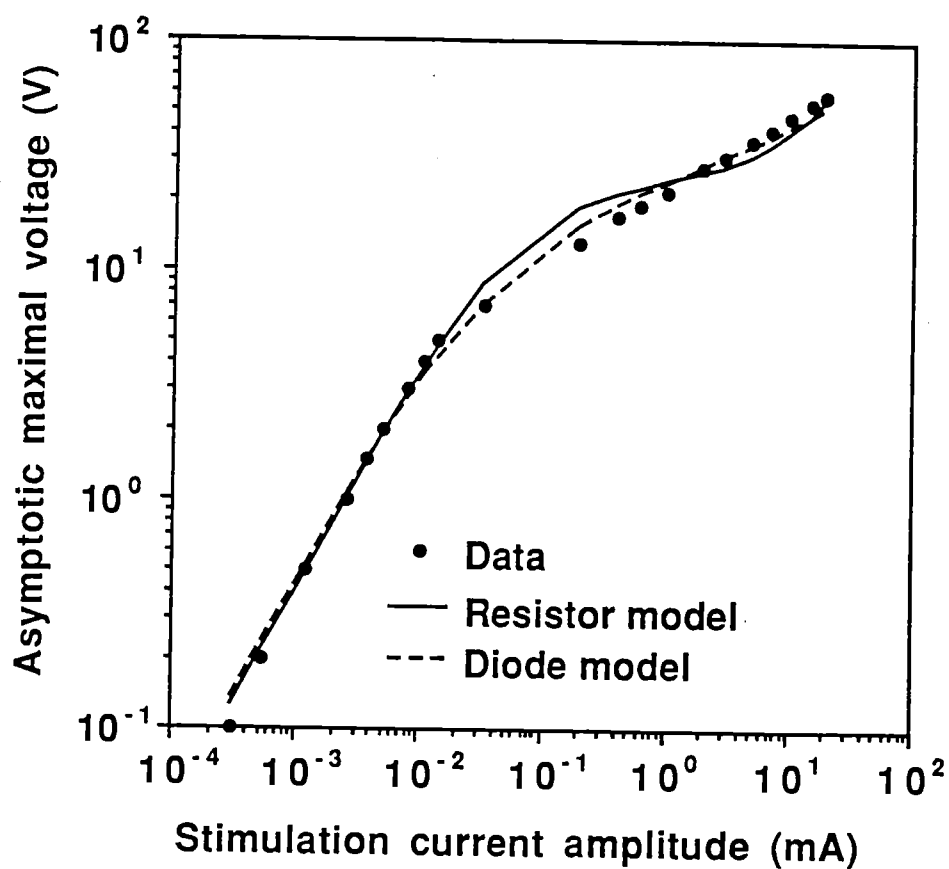


Fig. 8.4. The asymptotic maximal voltage V_M in response to a constant-current stimulation pulse becomes nonlinear for stimulation current amplitude I greater than $10 \mu\text{A}$. The text discusses a current-sensitive resistor model (solid line) and a diode model (dashed line) that predict V_M .

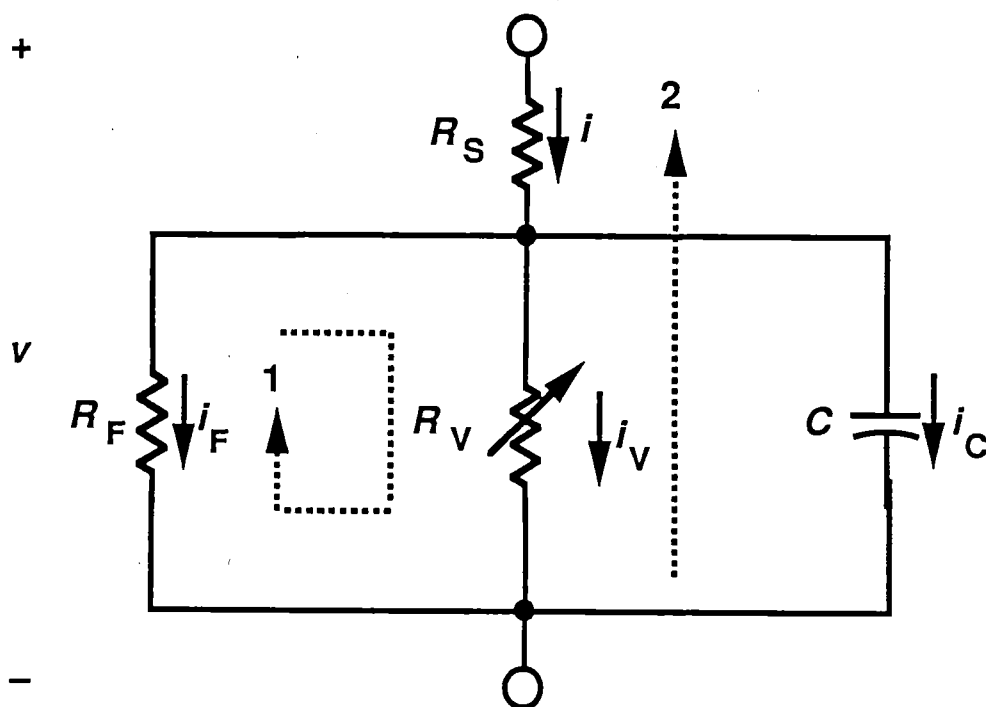


Fig. 8.5. A current-and-time-varying resistor $R_V(i)$ is the most important part of the nonlinear model which explains a number of the electrical characteristics of the electrode-skin interface. $R_V(i)$ varies inversely with current i ; its value decreases very quickly and increases more slowly. The dotted line 1 shows a circulating dc-current path even if the electrode dc current \bar{i} is zero. The dotted line 2 shows how \bar{i}_V is channeled to flow through the electrode so that it can be measured by an experiment in which \bar{v} is clamped to zero.

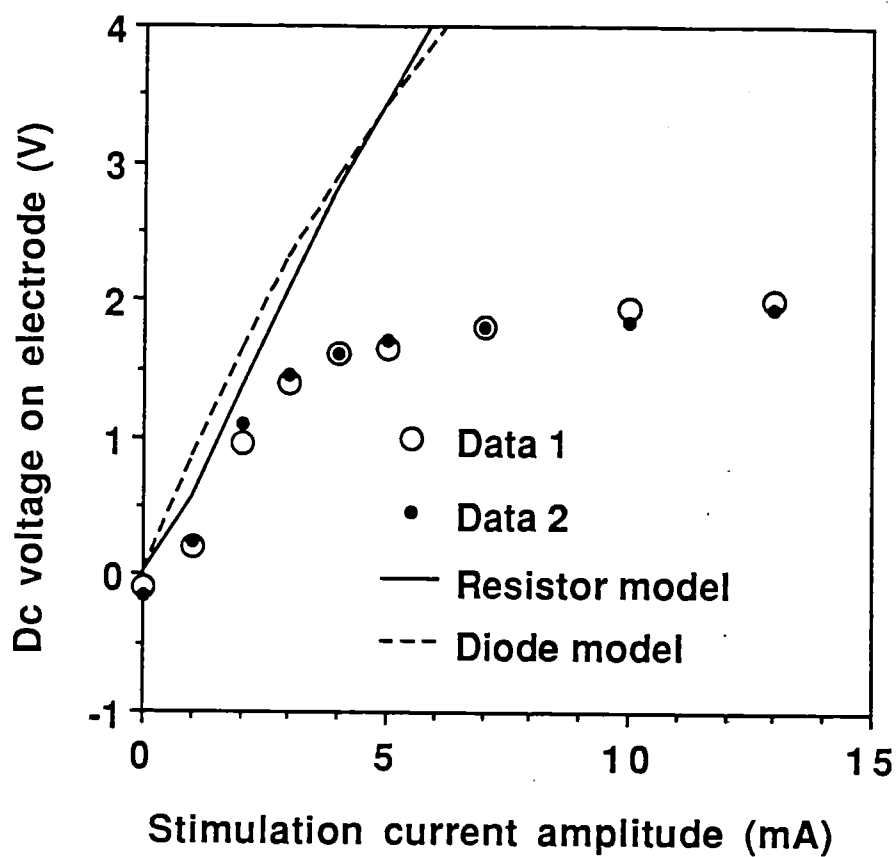


Fig. 8.6. A dc voltage \bar{v} appears on an electrode stimulated by an asymmetric current waveform, even if the dc current \bar{i} is zero. The value of \bar{v} increases with stimulation current amplitude I , but appears to be limited to approximately 2 V by some additional element not accounted for by either the current-sensitive resistor model (solid line) or the diode model (dashed line).

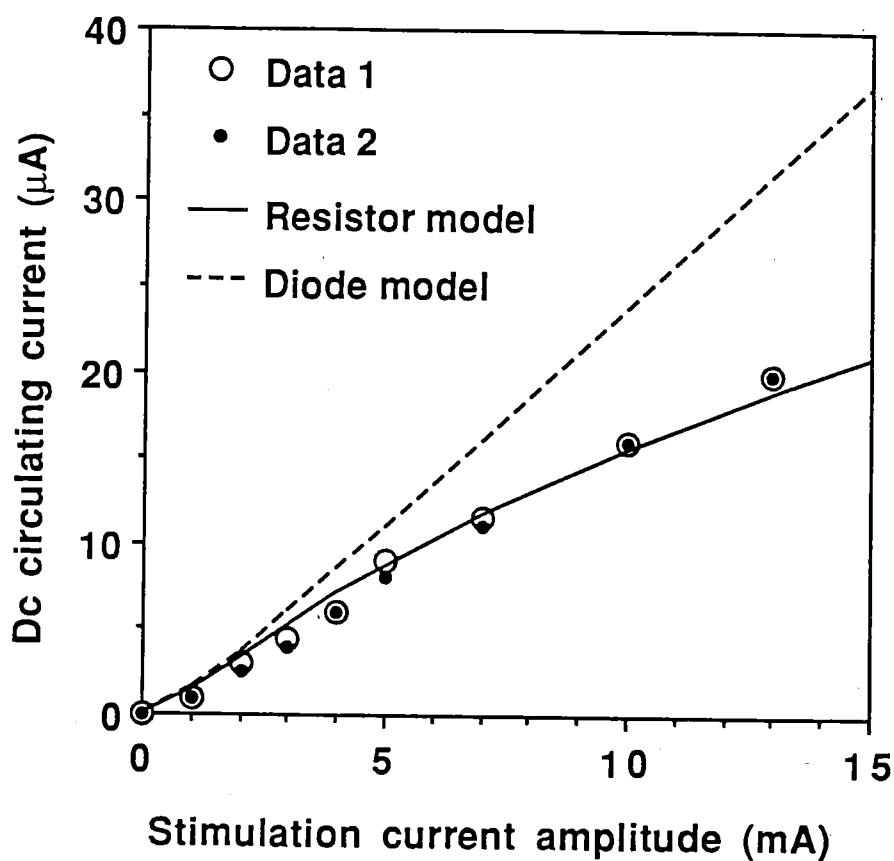


Fig. 8.7. If the dc voltage \bar{v} on an electrode is held fixed at zero, the internal circulating current in the nonlinear model \bar{i}_F is forced to flow through the electrode and is therefore easily measured. The circulating current is not subject to the additional voltage-limiting element (2-V dc limit). The current-sensitive resistor model predicts \bar{i}_F better than the diode model.

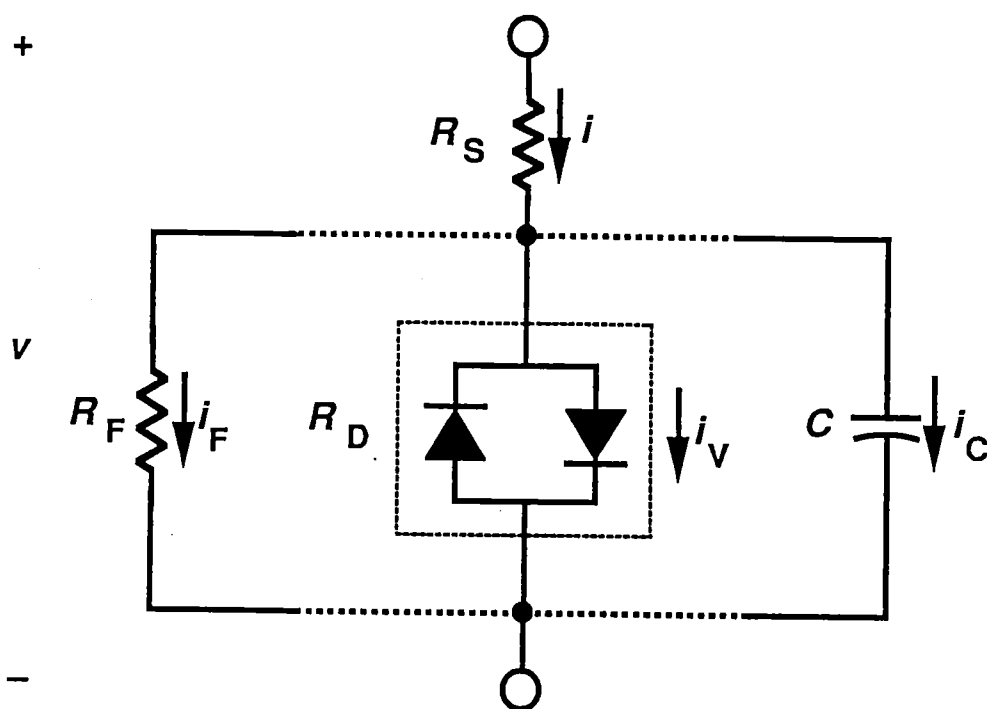


Fig. 8.8. Back-to-back diodes have a voltage-current characteristic similar to that for the electrode-skin interface, although the electrode-skin voltage is much higher.